UNIVERSITI TEKNOLOGI MARA

ELDERLY FALL CLASSIFICATION USING PASSIVE WI-FI RADAR AND MACHINE LEARNING

MUHAMMAD NAZRIN FARHAN BIN NASARUDIN

PhD

November 2024

UNIVERSITI TEKNOLOGI MARA

ELDERLY FALL CLASSIFICATION USING PASSIVE WI-FI RADAR AND MACHINE LEARNING

MUHAMMAD NAZRIN FARHAN BIN NASARUDIN

Thesis submitted in fulfilment
of the requirements for the degree of
Doctor of Philosophy
(Electrical Engineering)

College of Engineering

November 2024

CONFIRMATION BY PANEL OF EXAMINERS

I certify that a Panel of Examiners has met on 7 October 2024 to conduct the final examination of Muhammad Nazrin Farhan Bin Nasarudin on his **Doctor of Philosophy** thesis entitled "Elderly Fall Classification using Passive Wi-Fi Radar and Machine Learning" in accordance with Universiti Teknologi MARA Act 1976 (Akta 173). The Panel of Examiner recommends that the student be awarded the relevant degree. The Panel of Examiners was as follows:

Nofri Yenita Binti Dahlan, PhD
Professor
College of Engineering
Universiti Teknologi MARA
(Chairman)

Khairul Khaizi Bin Mohd Shariff, PhD
Senior Lecturer
College of Engineering
Universiti Teknologi MARA
(Internal Examiner)

Mardeni Bin Roslee, PhD
Senior Lecturer
Faculty of Engineering
Multimedia University
(External Examiner)

PROF IR DR ZUHAINA HAJI ZAKARIA
Dean
Institute of Postgraduates Studies
Universiti Teknologi MARA

Date: 19 November 2024

AUTHOR’S DECLARATION

I declare that the work in this thesis was carried out in accordance with the regulations of Universiti Teknologi MARA. It is original and is the results of my own work, unless otherwise indicated or acknowledged as referenced work. This thesis has not been submitted to any other academic institution or non-academic institution for any degree or qualification.

I, hereby, acknowledge that I have been supplied with the Academic Rules and Regulations for Post Graduate, Universiti Teknologi MARA, regulating the conduct of my study and research.

Name of Student	:	Muhammad Nazrin Farhan Bin Nasarudin
Student ID. No.	:	2021637824
Programme	:	Doctor of Philosophy (Electrical Engineering) – CEEE950
Faculty	:	College of Engineering
Thesis Title	:	Elderly Fall Classification using Passive Wi-Fi Radar and Machine Learning
Signature of Student	:	………………………………………………..
Date	:	November 2024

ABSTRACT

In the context of Malaysia's changing demographic landscape, the increasing elderly population necessitates innovative solutions for their healthcare and safety. Fall incidents among the elderly significantly affect their health, prompting a focus on assistive living technologies aimed at fall detection. This study aims to enhance fall detection by developing a system using Passive Wi-Fi Radar, addressing limitations of previous approaches. This method alleviates issues related to the comfort of wearable devices, privacy concerns of vision-based devices, and detection limitations of other ambient sensors. Passive Wi-Fi Radar, initially intended for communication, presents challenges in detecting human falls and movements. To address this, an enveloping algorithm is introduced to mitigate the influence of beacon signals carrying trajectory information. Additionally, four signal transformations which are Fourier spectrum, power spectrum, scalogram, and spectrogram are employed to analyse and extract Amplitude modulation signatures related to falls and movements. Feature extraction and selection are then applied to identify points that distinguish various fall types and fall-like movements. For Fourier and power spectrum features, extraction and selection are performed using Principal Component Analysis, followed by classification tasks utilizing Support Vector Machine, Random Forest, and Feed Forward Neural Network. Spectrogram and scalogram features are fed into the AlexNet Convolutional Neural Network. This study also explores combining AlexNet feature layers with traditional machine learning techniques to create hybrid classifiers, improving the performance of traditional algorithms. Results show that the Hybrid Random Forest classifier, using spectrogram images, performs exceptionally in single person scenarios, achieving an accuracy of 97.5%, recall of 0.9684, precision of 0.9872, and an F1-score of 0.981. In multiple person scenarios, the classifier attains an accuracy of 98.51%, recall of 0.9786, precision of 0.9914, and an F1-score of 0.9888. These findings highlight the effectiveness of the proposed fall detection system in addressing the challenges posed by the elderly population, marking a significant advancement in assistive living technologies. In conclusion, this study demonstrates the feasibility of using Passive Wi-Fi radar to detect falls, even high-speed falls. The introduction of hybrid classifiers has notably enhanced the model's overall performance, representing a valuable improvement for utilizing Passive Wi-Fi radar in fall detection. This research provides important insights and advancements in fall detection technologies, paving the way for more effective and accurate solutions to address the healthcare and safety concerns of the growing elderly population.

ACKNOWLEDGEMENT

Completing this PhD thesis has been a long, challenging, and rewarding journey, and it would not have been possible without the support and encouragement of many individuals and institutions. I am deeply grateful to everyone who has contributed to this accomplishment.

First and foremost, I would like to express my sincere gratitude to my supervisors, Assoc. Prof. Dr. Megat Syahirul Amin Megat Ali, Prof. Ir. Dr. Emileen Abd Rashid, and Dr. Norayu Zalina Zakaria. Your expertise, guidance, and unwavering support have been invaluable throughout my research journey. Your insightful feedback, encouragement, and patience have significantly shaped my academic and professional growth. I am profoundly grateful for the countless hours you dedicated to reviewing my work and providing constructive criticism that enhanced the quality of this thesis.

I am also thankful to the funding bodies that supported my research financially. The Ministry of Science, Technology and Innovation Malaysia, through the Technology Development 1 (TeD1), provided the necessary resources that allowed me to focus on my studies and pursue my research goals without financial concerns. Your support has been crucial in making this work possible.

I would like to extend my heartfelt gratitude to all those who directly and indirectly contributed to the data collection process for this research. To the participants who generously shared their time and insights, your contributions are the foundation of this thesis. Special thanks to the stuntmen and volunteers for their exceptional commitment in organizing and facilitating data collection sessions, ensuring everything ran smoothly.

On a personal note, I would like to express my deepest appreciation to my family. Your unwavering love, encouragement, and belief in my abilities have been my foundation throughout this journey. Your sacrifices and support have made my academic pursuits possible.

Finally, I would like to acknowledge all the participants and contributors to my research. Without their willingness to engage and share their experiences, this thesis would not have been possible. Your contributions have been invaluable, and I hope this work does justice to your input. In conclusion, this thesis is a testament to the collective effort, support, and encouragement of a wonderful community of individuals. To all who have contributed in one way or another, I extend my heartfelt thanks. This achievement is as much yours as it is mine.

TABLE OF CONTENTS

LIST OF TABLES

LIST OF FIGURES

LIST OF ABBREVIATIONS

Abbreviations

ADAM	Adaptive Moment Estimation
AI	Artificial Intelligence
ALT	Assistive Living Technology
ANN	Artificial Neural Network
AP	Access Point
BDA	Big Dat Analysis
CAF	Cross Ambiguity Function
CCTV	Close-Circuit Television
CNN	Convolutional Neural Network
CoP	Centre of Pressure
CPU	Central Processing Unit
CSI	Channel State Information
CWT	Continuous Wavelet Transform
DFT	Discrete Fourier Transform
DL	Deep Learning
DOSM	Department of Statistics Malaysia
EM	Electromagnetic
EoA	Energy of Arrival
FFNN	Feed-Forward Neural Network

FFT	Fast Fourier Transform
FMCW	Frequency Modulation Continuous Wave
FPGA	Field Programmable Gate Array
FrFT	Fractional Fourier Transform
FSR	Forward Scattering Radar
FT	Fourier Transform
HMM	Hidden Markov Model
HOG	Histogram of Oriented Gradient
ICNIRP	International Commission on Non-Ionising Radiation Protection
IMU	Inertia Measurement Unit
Iot	Internet of Things
IR 4.0	Industry Revolution 4.0
IR-UWB	Infrared Ultra-Wide Band
KNN	K-Nearest Neighbour
LBP	Local Binary Pattern
LNA	Low Noise Amplifier
LPF	Low Pass Filter
LSTM	Long-Short Term Memory
MCMC	Malaysia Communications and Multimedia Commission
MFCC	Mel-Frequency Cepstral Coefficients
MIMO	Multiple Input Multiple Output

MLRT	Multi-task Learning Radar Transformer
NN	Neural Network
OAA	One Against Another
OAO	One Against One
OFDM	Orthogonal Frequency Division Multiplexing
PCA	Principal Component Analysis
PWR	Passive Wi-Fi Radar
QAM	Quadrature Amplitude Modulation
RAM	Random Access Memory
RBF	Radial Basis Function
RCS	Radar Cross Section
RF	Random Forest
RFT	Random Fast Time
RMK-12	12^{th} Malaysia Plan
RNN	Recurrent Neural Network
SGDM	Stochastic Gradient Descent with Momentum
SVM	Support Vector Machine
VGG	Visual Geometry Group
WHO	World Health Organization
Wi-Fi	Wireless Fidelity
WLAN	Wireless Local Area Networking

CHAPTER 1
INTRODUCTION

1.1 Background Study

The global demographic landscape is undergoing a rapid transformation, characterized by a substantial increase in the elderly population. In light of this societal aging phenomenon, there arises a mounting apprehension for the well-being and safety of the elderly, particularly in the context of accidental falls. Falls occurring among the elderly constitute a significant and pressing public health challenge due to their potential for inflicting severe injuries, diminishing overall quality of life, and escalating healthcare expenditures [1]. According to a 2007 report from the World Health Organization (WHO), falls rank as the second leading cause of accidental or unintentional injury-related fatalities on a global scale, with the age group of adults aged 65 and older being disproportionately affected [2]. Although the aforementioned report may not reflect the most current data, it is noteworthy that numerous countries have diligently deliberated this issue and actively pursued preventive measures to date [1], [3], [4]. This issue assumes particular importance in the context of Malaysia, as evidenced by statistics provided by the Department of Statistics Malaysia (DOSM), which reveal a consistent upward trend in the elderly population, surging from 10.3% in 2020 to 11.1% in 2022. Projections further indicate an anticipated increase to 15% by the year 2030 [5].

In order to address this pressing concern, the WHO has advocated the implementation of various technologies, including artificial intelligence (AI), to mitigate the issue of falls among the elderly [3]. This call has been widely resonated within the global biomedical engineering research community, with a shared objective of developing Assistive Living Technologies (ALT) focused on fall detection. Several alternatives have been explored in this endeavour, such as wearable devices utilizing Inertial Measurement Units (IMUs), which combine gyroscopes and accelerometers to gauge the acceleration and orientation of the subject [6]. Additionally, vision-based, radar-based, ambient sensors, including pressure and acoustic sensors, have been considered [7], [8]. Among these sensor technologies, radar-based sensors have emerged as the most promising within the field of ALT. This distinction arises from their ability to circumvent issues associated with wearables, such as discomfort, privacy concerns inherent to vision-based sensors, and potential for high installation costs associated with pressure-based sensors [9], [10]. Furthermore, it is noteworthy that radar technology operates independently of ambient lighting conditions, weather fluctuations, and potential obstructions, which significantly enhances its reliability and effectiveness in the context of fall detection [11].

Radar technology has found extensive applications in detecting both aerial targets, such as aircraft, and terrestrial targets, including vehicles and human movement [12], [13]. This technology operates by emitting electromagnetic (EM) waves and subsequently receiving the EM wave that interacts with human activity and the surrounding environment. Through this interaction, the radar system can effectively detect and measure various motion characteristics of the target, including range, direction, and velocity [14]. However, there have been valid concerns regarding safety and radiation issues associated with the transmission of EM wave. To ensure compliance with radiation guidelines established by the International Commission on Non-Ionising Radiation Protection [15], a subfield of radar technology has emerged, which leverages external signals called Passive Radar, such as television and radio broadcasts, mobile cellular signals, satellite signals, and Wireless Fidelity (Wi-Fi) signals. Among these signals, Wi-Fi signals have proven to be the most accessible option due to their widespread availability in households, as indicated by a survey conducted by the DOSM reporting a 92% usage and accessibility rate [16]. Furthermore, Wi-Fi signals benefit from fixed access points, predominantly home routers, which tend to offer greater stability and consistency when compared to other signals that may exhibit variability in terms of signal strength and quality. he utilization of Wi-Fi signals in passive radar technology is often referred to as "Passive Wi-Fi Radar" (PWR).

In response to the WHO recommendation [17] to integrate AI into elderly care, this study represents a notable milestone by incorporating AI classifiers into radar-based fall detection systems. This integration stands as a significant advancement, markedly enhancing the precision and reliability of fall event identification while simultaneously mitigating false alarms. In the context of classifying human movements for radar-based fall detection, the need for intelligent classifiers is imperative due to the inherent complexity of radar signal data and the wide spectrum of variations in human movement, including speed, direction, size, and shape. AI classifiers, such as Machine Learning (ML) and Deep Learning (DL), are adaptive mathematical algorithms that exhibit learning capabilities analogous to human cognition, encompassing comprehensive understanding, learning, and adaptability. ML, for instance, requires initial human input to provide substantial information for training, as exemplified by Support Vector Machine (SVM), which learns from the distinctive features of data to construct a hyperplane for class separation. Moreover, a group of decision tree which called a Random Forest (RF) work by taking the vote form each tree that deciding by a binary decision with a specific threshold value. In addition, there exists a ML variant structurally akin to the human brain, known as Feed-Forward Neural Network (FFNN), characterized by multiple interconnected layers of neurons that collectively make decisions based on mathematical algorithms applied to the input data and transferring the information in forward direction up to the output neurons [18]. In contrast to ML, DL typically requires less manual feature engineering for feature extraction and decision making, although human expertise is still involved in various aspects of the DL process. This autonomy is achieved through the automatic learning of relevant features from raw data. For instance, Convolutional Neural Network (CNN) employ multiple layers of convolutional algorithms to extract pertinent features from images, which are subsequently classified through fully connected layers, mirroring the operation of FFNN. Moreover, a hybrid algorithm which combining the DL algorithm for features extraction and ML for classification task for also seem feasible in achieving the aim for this. In summary, the selection of classifier algorithms methodologies in radar-based human detection is grounded in their capacity to effectively manage the intricacy and variability of real-world data, their adaptability, scalability, and generalization capabilities, and their consistent record of achieving heightened accuracy across a broad spectrum of applications.

1.2 Problem Statement

The elderly population faces a heightened vulnerability to fall events due to prevalent health concerns, including issues like gait instability, balance problems, and impaired vision. Their risk is further compounded by the muscle weakness and decreased bones density. In response to this pressing issue, numerous research and development efforts have been dedicated to the creation of fall alert detection systems in recent years. Despite these commendable endeavours, it is essential to acknowledge that the existing systems have exhibited imperfections in terms of functionality, practicality, and the robustness of their fall event classification tasks. This underscores the need for continued innovation and enhancement in the domain of fall detection systems to ensure the safety and well-being of the elderly.

Indeed, the advantages of the PWR system are evident. However, Wi-Fi signals are primarily intended for the transmission of data packets to receivers and are sent sequentially. These packets are composed of symbols, and the choice of modulation scheme, including techniques like combining two amplitude-modulated signals into a single channel to increase data transmission rates and divides a single channel into multiple smaller sub-channels to transmit data simultaneously, increasing efficiency and reducing interference, determines how many bits are conveyed by each symbol [19]. These modulation methods alter the amplitude and phase of the continuous carrier wave to represent binary data. This results in a pulse-based signal, where the essential information is concentrated at the peak of the signal. In contrast to traditional radar,, PWR needs to account for these characteristics when extracting information for detection and tracking purposes. However, it's noteworthy that many researchers, as evidenced in [20], have primarily concentrated on distinguishing falls from regular human movements such as walking and sitting, with limited focus on categorizing the specific types of falls that may occur. Understanding the type of fall is crucial, as it carries vital information that is pertinent to the subsequent care and medical attention provided. This information can guide healthcare professionals in comprehending the underlying causes of the fall and taking immediate action to address the body part most affected.

The present of multiple person which create a noisy environment is a critical component of radar-based fall detection systems, and this area has been notably underexplored. In radar systems, the capability to estimate the range, velocity, and azimuth angle in noisy environment is paramount. One of the key challenges was to detect specific target within multiple moving individuals scenario, as dynamic scene with a lot of motion leads to clutter and noise [21]. This capability is fundamental for accurately recognizing human behaviours and facilitating the early detection of fall incidents. The lack of standardized benchmarks for fair comparisons between different fall detection systems further underscores the need for robust and effective methods for multiple person scenario [22]. Radar sensing plays a pivotal role in the classification of activities and the detection of falls in elderly individuals. A comprehensive experimental study has been conducted to acquire Doppler radar signal's amplitude signature encompassing various types of falls and daily living activities. The application of radar technology in fall detection has garnered attention within the domain of smart healthcare. Therefore, the development of radar systems endowed with the capacity to detect and track human movement in realistic environment stands as a crucial endeavour, as it holds the potential to enhance the accuracy and reliability of fall detection systems, thereby ensuring the safety and well-being of individuals.

Comparing the capabilities of ML and DL algorithms is a critical aspect of this research. The problem lies in the current lack of comprehensive comparative analyses that take into account accuracy, efficiency, robustness, and adaptability to PWR for human fall detection system which presented in complex signal. The absence of standardised benchmarks makes it challenging to objectively compare the performance of different between ML and DL for fall detection, hindering progress in the field and potentially delaying the adoption of effective solutions. The choice between ML and DL approaches can significantly impact the success of fall detection systems, and addressing this problem is essential to make informed decisions. Moreover, different applications and scenarios may demand tailored solutions, and it is crucial to understand the strengths and weaknesses of each approach. By systematically evaluating these factors, researchers can provide valuable guidance to practitioners and developers, aiding them in selecting the most suitable algorithmic framework for their specific fall detection requirements. This comprehensive analysis ensures that fall detection systems are optimised to meet the unique challenges of different real-world scenarios.

1.3 Research Objectives

The aim of this thesis is to develop an indoor PWR fall detection system that enhances the daily activity monitoring of elderly individuals, with a specific focus on detecting any indications of fall events. This overarching goal will be achieved through the pursuit of the following key objectives:

a) To understand how commercial WI-FI signal is affected during human motions and falls through experimentation.
b) To develop an efficient processing chain to facilitate the detection of actual human fall using low-cost algorithms.
c) To Investigate the capability recent Deep learning models to classify human fall using WI-FI signals.

1.4 Significance of Study

This study is crucial as it addresses a major concern for the well-being of the elderly, focusing on the serious consequences of falls, including injuries, reduced quality of life, and higher healthcare expenses. Taking a comprehensive approach, it aims to improve fall detection in the elderly, a group vulnerable due to age-related health factors. The study outlines four specific objectives in Section 1.3, each playing a significant role in enhancing fall detection systems and positively impacting the lives of elderly individuals.

In fall detection, this technique is based on extracting Amplitude modulation signatures to estimate types of falls for example forward, backward and sideways fall. from PWR signals, revealing object speed and direction. This capability is crucial for detecting subtle movements, enhancing the PWR system's sensitivity beyond large motions. Accessible Wi-Fi signals make the technology cost-effective and less intrusive compared to solutions relying solely on wearables or cameras. Characterizing falls and similar movements goes beyond a simple fall and non-fall classification, addressing the risk of false alarms in detection systems. The study focuses on distinguishing various fall types, like walk and fall, sit and fall, slip and fall, stumble, and fainting. This differentiation offers insights for tailored medical interventions and guides healthcare providers in anticipating injuries and causes. Knowing the specific fall type aids in prioritizing assessments and interventions, leading to more targeted care and potentially reducing recovery times. Categorizing falls also informs customized rehabilitation plans, expediting recovery by addressing specific injuries and circumstances. Moreover, this detailed information enhances medical records, providing valuable insights for future reference and informed decision-making in patient care and preventive measures.

Intelligent classifiers play a crucial role in fall detection, providing automated, data-driven methods for classifying fall events. They excel in handling complex, high-dimensional data common in fall detection scenarios. In environments like nursing homes or hospitals, where multiple individuals may be monitored simultaneously, the ability to detect falls amidst other movements is essential. Classifier models effectively segregate fall events from other activities that having similar features as fall, contributing to the reduction of false alarms. By training them with multiple person scenario, the study enhances precision, ensuring resources are allocated where needed and improving overall system effectiveness. In complex environments with multiple persons, the classifier models excel in processing high-dimensional data, addressing signal complexities and accurately distinguishing fall events.

Comparing classification algorithms is crucial for informed decision-making in designing fall detection systems, considering factors like accuracy, efficiency, robustness, and adaptability to complex signal data. ML models, such as SVM, RF and FFNN are known for computational efficiency but may need extensive feature engineering. ML excels with domain-specific knowledge and is suitable for tasks requiring interpretable results through crafted features. In contrast, DL techniques, like CNN, are adept at handling unstructured or high-dimensional data, automatically learning complex patterns without extensive feature engineering. Meanwhile the hybrid classifier is a combination of DL feature learning algorithm together with traditional ML classifiers. This comparative analysis guides developers in choosing between each algorithm based on specific scenario requirements, ensuring optimized fall detection systems for diverse real-world challenges. This tailored approach enhances the safety and well-being of the elderly population.

1.5 Scope and Limitation

To fulfil the research objectives, the collection of a signal dataset necessitates human participation in executing movements. Therefore, this study secured ethical clearance from the Universiti Teknologi MARA Research Ethical Committee, under approval number REC/06/2022 (ST/FB/9), as outlined in Appendix A. Additionally, to effectively achieve the research objectives, it is crucial to comprehend the overarching approach and constraints that will influence this research, thereby aiding in the interpretation and generalization of its findings. Consequently, the scope and limitations of this study are listed as follows:

1. This study focusses on signal processing, feature extraction and classification algorithms
2. Utilized PWR system with Wi-Fi signal transmit on the 2.4GHz channel.
3. Data collection was conducted in a controlled indoor laboratory setting with minimal background noise.
4. Collected fall signal performed by two trained stunt performers engaged in simulated fall activities and
5. Collected fall-like signal performed by a group of ten volunteers with range of height and weight of 145 to 171 cm and 47 to 100 kg, respectively.
6. Signal data was collected in the presence of both single and multiple individuals.
7. The feature extraction focuses on utilizing signal transformation technique which yield a discernible Amplitude modulation signature such FFT, STFT and CWT.
8. The feature selection method focused on the application of PCA, while image feature processing was conducted using the feature layers of the AlexNet model.
9. The classifiers application focused on SVM, RF FFNN and AlexNet model.
10. The validation technique was focus on the model's accuracy, recall, precision and F1-score.

Despite the ten research scopes outlined above, this study has a few limitations that warrant consideration:

1. Limited in study ability to account for path loss and signal propagation effects, which are critical factors influencing the performance of wireless radar systems.
2. This study was trained and validated using controlled datasets, which may limit their ability to generalize effectively to entirely new or highly dynamic environments not reflected in the training data.

3. This study based on the collected data which may introduce latency in real-time scenarios, which could impact the system's responsiveness
4. This study limits the ability in real-world deployments, where the PWR system may encounter interference from other Wi-Fi sources.

1.6 Thesis Outline

This Thesis consist of a total of 5 chapter which begin with this introduction chapter. This chapter background study, motivation, problem statement, objective, significant and scope and limitation and contribution of this study. The rest of the chapter had the following organization.

Chapter 2 serves as the literature review, delving into an examination of past research efforts pertaining to fall detection systems, with a particular focus on radar and PWR systems. This chapter plays a pivotal role in identifying gaps in the existing body of knowledge and offering justification for the methodology employed in this study.

Moving on to Chapter 3, it encompasses the methodology section, wherein the theoretical foundations and practical applications of PWR systems, preprocessing techniques, signal transformation processes, feature extraction and selection and classification algorithms are applied in accordance with the suitability of the collected signal data.

Chapter 4 is dedicated to the discussion of preprocessing methods, with a primary focus on validating their efficacy in extracting the Amplitude modulation signature from pulse-based signals, signal transformation involves evaluating various domains and image representations to analyse the applicability of distinct feature sets in characterizing different types of movements.

Next, Chapter 5 delves into the examination of variable parameters and the performance assessment of classifiers algorithms in the context of single and multiple person scenario for the classification task.

Finally, Chapter 6 serves as the conclusion, consolidating all the findings derived from this study and exploring potential avenues for future research, with the overarching goal of advancing the development of PWR-based fall detection systems into uncharted territory.

CHAPTER 2
LITERATURE REVIEW

2.1 Introduction

Chapter 2 serves as a comprehensive literature review encompassing recent research conducted between 2019 and 2023. Comprising seven subchapters, the chapter begins with an introduction providing an overview of its contents. Subsequently, subchapter 2.2 delves into the imperative of fall detection systems for the elderly. This section extensively discusses the burgeoning elderly population, their requirements for enhancing quality of life, and the factors and consequences associated with elderly falls. In subchapter 2.3, various types of fall detection systems are scrutinized, including wearable, vision-based, ambient-based, and radar-based sensors. A detailed analysis of each study is undertaken to assess the strengths and limitations inherent in the respective approaches employed. Moving forward, subchapter 2.4 evaluates the PWR approach for fall detection systems, elucidating its advantages compared to sensors discussed in section 2.3. Additionally, a thorough examination of signal processing techniques from prior works on PWR is conducted, considering their applicability to fall detection systems. Subsequent to the PWR assessment, subchapter 2.5 addresses the application of ML in fall detection. This discussion encompasses various ML architectures, parameters, and input considerations, drawing parallels between the functioning algorithms of ML and the PWR. Similarly, subchapter 2.6 delves into DL algorithms, scrutinizing architectures, parameters, and input specifics. These sections collectively form the signal processing and classification algorithm segment, wherein the merits and drawbacks of each approach are meticulously analysed and considered in relation to the forthcoming research. Meanwhile, Subchapter 2.7 explores the applications of hybrid classifier algorithms, focusing on their organizational structure and architecture. This section elucidates how ML and DL algorithms are synergistically employed to create classifiers that exhibit enhanced performance when compared to conventional classifiers. Concluding the chapter, subchapter 2.8 provides a comprehensive summary of the analyses conducted on prior works and accentuates identified research gaps. This synthesis serves as a foundation for the subsequent research, aligning the study with existing knowledge while laying the groundwork for addressing pertinent gaps in the field.

2.2 Elderly and Risk of Fall

As Malaysia anticipates a significant increase in its elderly population, projected to rise by approximately 7% by the year 2030, the government has recognized the gravity of this demographic shift [5]. In response to this demographic change, the government has taken substantial measures to address the issue of elderly care. Notably, this commitment to elderly care is prominently highlighted in Chapter 4 of the 12th Malaysia Plan (RMK-12) [23]. Hence this chapter have given attention on elderly health, lifestyle and also quality of life. Besides, Chapter 3 had mentioned the technology development will align with direction of Industry Revolution 4.0 (IR 4.0) which adoption of Big Data Analysis (BDA), Internet of Things (IoT), AI and intensifying the use of drones, robotics and sensors. Besides the Government Policy, this study also shows a significant context of reducing elderly healthcare expenditures, which the Malaysian government currently allocates approximately RM900 million annually [24].

In order to answer the call from Malaysia's government on issue of elderly care, a study examined the quality of life for senior citizens residing in residential care facilities run by the public, private, and non-profit sectors in Malaysia [25]. This study aimed to determine the factors influencing the quality of life of elderly individuals in these facilities. The result of this study shows that satisfaction rate is high on private care centre because of their monitoring facilities and also the involvement of technologies in monitoring elderly such AI-integrated Close Circuit television (CCTV) for the aim of sensing the possibility of hazard. Besides, a study in [26] was focused on the role of Ageing Care Centres in Malaysia and their impact on the quality of care and proactive environment for the elderly. The study examines the relationship between perception of health and happiness, behavioural attitude, health promotion, education, quality care, monitoring technologies, proactive environment, and elderly care services in these centres. This study provides insights into the factors that contribute to the quality of life of the elderly in Malaysia and the most significant factors were quality care, monitoring technologies and proactive environment. Another study in [27] aims to determine the factors associated with the need for assistance in the daily living activities of Malaysia's elderly population. This study found out that a systematic monitoring system is one of the needs of the elderly and the factors that influence their quality of life.

These studies consistently converge on the idea that monitoring systems or technologies play a pivotal role in enhancing the quality of life for elderly individuals. The significance of monitoring the elderly is underscored by their health limitations, which can result in falls, a critical concern in the context of elder well-being. In Malaysia, for instance, 27% of the rural community-dwelling elderly experience falls annually, with a considerable portion encountering recurrent falls within the same year [28]. The prevalence of falls among the elderly is a global issue, not limited to Malasia only such studies conducted in different countries have reported varying rates of falls among the elderly. For example, falls were observed in 57.1% of elderly individuals who had fallen in one study conducted in North India [29]. In Bangkok, Thailand, falls among the elderly are a significant problem, leading to morbidity, mortality, and increased use of healthcare services [30]. Human falls are defined as instances in which individuals lose their balance or stumble, resulting in an abrupt descent to the ground. These falls are often characterized by sudden spikes in acceleration upon contact with the ground. Falls can occur in various circumstances, including falls while walking, stumbling leading to forward falls, slipping resulting in backward falls, and tripping or fainting leading to sideways falls [31], [32], [33].

Factors contributing to these types of falls among the elderly include health limitations, such as hip fractures, which are frequently fall-related and pose a significant health challenge in this demographic [33]. Medications also play a role in contributing to falls among elderly, with some studies highlighting the prevalence of medication-related falls in elderly patients with hip fractures [34]. Frailty and the fear of falling are additional factors that can contribute to falls in both hospital and community settings [35]. Moreover, specific health conditions are associated with an elevated risk of falls in the elderly population. For instance, hypertension has been identified as a risk factor for falls, with elderly suffering from hypertension being more susceptible to falling [36]. Visual and hearing impairments can also contribute to falls among the elderly. Additionally, depression, a psychological factor, has a strong association with falls in the elderly, as individuals exhibiting symptoms of depression are more likely to experience falls [37]. Chronic diseases, muscle weakness, balance impairments, cognitive and sensory impairments are further health conditions that can heighten the risk of falls among the elderly [38], [39].

Consequently, the implementation of an effective monitoring system holds significant importance as it can alleviate the suffering experienced by elderly individuals in the aftermath of falls. Falls among the elderly can result in a range of physical and psychological consequences. Research has demonstrated that falls can have direct psychological effects on the elderly, negatively impacting their mental well-being [37]. Notably, long-stay facilities for the elderly face particular concern, given their higher incidence of falls and the increased severity of resulting injuries, which can have a more pronounced adverse impact on the individuals' functionality [40]. The consequences of falls in the elderly can be substantial, with a significant number of individuals experiencing serious injuries. For example, in China, nearly 20% of elderly individuals who experience a fall incur serious injuries, even if they were previously in good health. Additionally, many of these individuals suffer secondary injuries due to delayed discovery and medical treatment, a situation that is common among elderly individuals living alone [41]. Falls can also lead to a decline in the quality of life among institutionalized elderly individuals, as they may develop a fear of falling and a reduced confidence in performing their daily activities [42].

The deterioration in quality of life is intricately linked to a reduction in physical functioning following a fall. Medical research suggests that each category of fall is associated with distinct physical factors, and the type of fall can serve as an indicator of the specific anatomical region bearing the most significant impact. For example, when analysing a fall event where a person falls suddenly while walking, this may indicate an underlying gait and balance problem. The knee often absorbs the highest impact in such instances, as it is the body part that initially responds to mitigate the impact on the upper body and head. This type of fall informs healthcare providers to prioritize an assessment of the knee and gait-related issues [43]. Similarly, analysing a fall event that occurs when an individual attempts to rise from a chair may suggest issues with the arm or shoulder joint, which result in a loss of control when pushing the body upward from the chair. In such cases, immediate attention may be required for the hand

and carpal bones [44]. Conversely, a slip-related fall, where an individual falls backward, is associated with the risk of injuries to the buttocks or the occipital bone at the back of the head. These details can guide the medical response to address the specific injuries sustained in these types of falls [45]. Stumbling events, typically observed among the elderly with visual impairments, are associated with a higher risk of falling. These falls occur due to the individual's impaired vision, making it challenging to perceive changes in the floor or step surfaces. Stumbling events are particularly concerning because they restrict leg movement and hinder the absorption of impact by the upper body. This, in turn, places significant stress on body parts such as the palms, torso, and the front portion of the head [46]. In contrast to other types of falls, fainting or blacking out results from a lack of brain function, leading to a loss of consciousness. These falls do not exhibit high impact, as they involve a cessation or slowing down of movement activity when the individual senses uncertainty in their brain function [47].

The implications of falls among the elderly extend beyond physical injuries. Falls can also have consequences for the environment and social aspects of their lives. Concerns about maintaining balance after a fall can hinder elderly individuals from adopting preventive measures and making changes to their living environment to prevent future falls. Economic and social limitations can also hinder their ability to take preventive measures [41]. The consequences of falls among the elderly extend beyond physical injuries alone. Falls can significantly impact the mental well-being and overall quality of life of elderly individuals. Falls have been associated with the emergence of anxiety, fear, and a decline in the quality of life among the elderly [48].

Preventive measures and interventions are crucial in reducing the risk of falls and mitigating the post-fall implications for the elderly. Various interventions have been studied, including exercise programs, balance training, and vitamin D supplementation. These interventions have shown promising results in reducing the risk of falls and improving the balance and quality of life of elderly individuals [49], [50], [51], [52], [53]. Nonetheless, it is important to note that these interventions may not place sufficient emphasis on enhancing the monitoring system, which is a vital requirement in the elderly community to enhance their quality of life. Researchers are currently diligently exploring and developing technologies aimed at monitoring the elderly, with a particular focus on detecting falls, as will be elaborated upon in the forthcoming subsection. The development of this kind of technologies holds significant societal implications, particularly in the context of enhancement of emergency response within society. In the event of a fall, these systems can automatically notify caregivers, family members, or emergency services, expediting assistance. This proves especially critical for individuals living alone or those with medical conditions that heighten their susceptibility to falls. Research conducted by [23] indicated a substantial reduction in the time taken to receive medical assistance following a fall, thereby improving outcomes for affected individuals. Furthermore, the integration of fall detection systems can yield an improved quality of life for individuals at risk of falls. By instilling a sense of security and reassurance, these systems empower individuals to maintain their independence and reside in their own homes. This positive impact on mental well-being and overall quality of life is particularly noteworthy for the elderly and those grappling with mobility limitations. The study conducted by [24] underscored the psychological benefits of fall detection systems, with users reporting heightened confidence and reduced anxiety regarding the risk of falling. Therefore, the core motivation driving this study lies in the aspiration to enhance the safety and well-being of older individuals. This impetus propels the researchers to explore and develop advanced algorithms and techniques.

2.3 Emerging Technology Toward Fall Detection

A fall detection technology is a device currently in development that employs a variety of sensors for the purpose of detecting falls includes IMU, vision-based, ambient-base such pressure and acoustic sensor and radar-based sensors. All these sensors are aimed to visualize and detect movement that occur in the detection area utilize the AI classifier for the classification task of the movement [54]. This field of development has exhibited notable growth over the past five years, from 2019 to December 2023, as evidenced by a Scopus database search revealing the publication of 842 articles. This indicates that the issue remains relevant and offers opportunities for further advancements and enhancements.

2.3.1 Wearable Devices

IMU is a sensor that widely used in attachable or wearable fall detection device such as smartwatch and smartphone [55], [56]. Typically, this sensor consists of accelerometers and gyroscopes that can measure the acceleration and angular velocity of an individual's movements [57]. The utilization of IMU sensors for fall detection systems is demonstrated in various studies. In [57], a wearable device is positioned on the subject's head to monitor abrupt changes in acceleration and head orientation, signalling accidental falls. Upon fall detection, the system transmits alarm messages to a data server via a wireless network. A complementary filter is implemented to address instability and drift in angular measurements from the accelerometer and gyroscope. Similarly, another study detailed in [58] deploys an IMU sensor on the front shin bone to develop a wireless, low-power medical device capable of detecting fall movements. This study utilizes 12 features from the IMU sensor, integrating an improved version of gyro and accelerometer sensors with a Field Programmable Gate Array (FPGA). In [59], devices incorporating built-in three-axis accelerometers and gyroscopes in a nine-axis inertial sensor are placed on the user's chest. The resultant force is calculated using three-axis acceleration, and the pitch angle is obtained through integration of three-axis acceleration and a three-axis gyroscope using the gradient descent algorithm. The height value, derived from a barometer, is integrated with the pitch angle to determine the user's behavioural state. Beyond body-placement devices, researchers have integrated IMU sensors with current technology. Besides, 2-D accelerometers and three-axis gyroscopes are integrated into a smartwatch, and a similar approach is implemented in smart glasses, as presented in [60].

In light of the aforementioned study, IMU sensors show promise for developing fall detection systems, particularly due to their suitability for capturing high-speed downward movements associated with falls. However, IMU sensors, primarily found in wearable devices, are constrained by their single-detection capacity. This limitation restricts fall monitoring to individual users and does not align with the needs of elderly care settings where multiple elderly individuals may reside in a single room. Furthermore, wearable devices may not be the optimal choice for the elderly population, as this age group may experience discomfort when required to wear such devices continually [61]. Additionally, there is a risk of these devices being misplaced due to the cognitive challenges associated with weakened working memory in elderly individuals [62].

2.3.2 Vision-based Sensor

The limitations associated with IMU sensors have compelled researchers to explore the integration of camera vision sensors in the context of fall detection. This sensor functions by capturing light and converting it into a sequence of pixelated images, known as frames. Each frame encapsulates colour or layered information, including details pertaining to angles and joints. The expeditious capture of these frames per second yields a series of dynamic, motion-like images [63]. In the field of human movement, this sensor type discerns alterations in human joints across consecutive frames, thereby facilitating the recognition and analysis of human motion [64].

The application of vision-based sensors in fall detection systems is exemplified in various studies. In [65], the utilization of a digital video camera is employed to capture RGB colour images, which are then processed into frames. The frames undergo resizing, augmentation, and min-max based normalization to enhance image quality and eliminate noise. The presented method is asserted to exhibit superior performance compared to recent methods. In another study [66], live footage from a monitoring surveillance camera is processed using a fine-tuned human segmentation model and image fusion technique as pre-processing. The system then classifies the footage with a 3D multi-stream CNN model (4S-3DCNN), achieving excellent accuracy results.

Additionally, in [67], a video fall detection network based on a spatial-temporal joint-point model is proposed. The model utilizes time-series joint-point features extracted from a pose extractor and a 3D pose estimation network, enhancing the accuracy of the system. Another approach presented in [68] utilizes recorded video data, extracting human silhouette regions in each frame using the codebook background subtraction technique. Convolutional Neural Network-based autoencoder (CNN-AE) is employed to extract low-dimensionality representative features from the extracted silhouettes. Combining these approaches, yields improved results in terms of significant features and classification accuracy.

Furthermore, studies focusing on extracting the human skeleton to analyse changes in posture in each frame are presented in [69]. To enhance the skeleton capturing algorithm, the research utilizes the SORT algorithm and the Media Pipe framework to extract skeletons and calculate physical characteristics. This approach is further explored in [70], demonstrating its effectiveness in detecting multiple people's activities in the same scene, especially those requiring more than one frame for accurate detection.

Derived from the aforementioned study, the camera-based fall detection system effectively recorded human movement and distinguished between fall and non-fall events, whether involving a single or multiple persons. Furthermore, given its non-contact nature, this sensor addresses the discomfort associated with wearable devices utilizing IMU sensors. However, this sensor has raised noteworthy privacy concerns among researchers, particularly in Malaysia. While the guidelines set forth by the Malaysia Communications and Multimedia Commission (MCMC) may influence these concerns by prohibiting public CCTV installations in private areas such as bedrooms or bathrooms, it is unlikely that individuals are entirely restricted from using CCTV in their own homes, which can still pose significant privacy issues [71]. The study referenced in [28] indicates a substantial number of reported cases of elderly falls occurring in bedrooms and bathrooms. Consequently, this sensor is constrained in fully accessing the high chance areas for elderly falls.

2.3.3 Ambient-based sensor

The ambient-based sensor refers to a device designed to identify alterations in environmental conditions, encompassing factors such as light intensity, pressure, and sound. This technology has found widespread application in detecting anomalies within indoor spaces or discerning the presence of individuals [72]. In the field of fall detection systems, certain researchers have explored the integration of ambient sensors, specifically acoustic and pressure sensors [73], as a strategic response to address privacy concerns associated with the use of vision-based sensors. The acoustic sensor functions analogously to the human ear, recording and analysing environmental sound patterns to discern deviations from established norms. This approach offers a non-intrusive means of fall detection by monitoring alterations in ambient acoustics. Simultaneously, the floor-based sensor, designed to monitor changes in floor often associated with an individual's interaction with the ground, provides an additional layer of data for comprehensive fall detection analysis. This nuanced utilization of ambient sensors reflects a judicious approach in mitigating privacy concerns while enhancing the efficacy of fall detection systems.

A fall detection system incorporating acoustic sensors is detailed in [74]. The researcher installed three aerial microphones and one-floor acoustic sensor in a room, monitoring the acoustic information received from these devices during a fall event. Acoustic features, such as energy, spectral centroid, spectral flux, zero-crossing rate, and Mel-frequency cepstral coefficients (MFCC), are extracted from the recorded acoustic signal. These features are then classified using ML algorithms. In a different approach presented in [75], an audio device emits a 20kHz continuous wave, and a microphone record reflected signals to capture the Doppler shift caused by a fall. The author addresses interferences by developing strategies for their removal, producing clean spectrograms. The power burst curve is then applied to locate time points at which human motions occur. Subsequently, feature extraction and classification algorithms are employed. Other studies focus on distinguishing between noise and fall-related acoustic signals using AI algorithms. In [76], a Siamese Neural Network is utilized for this purpose, while in [77], the Tiny ML algorithm is applied. Both methods successfully distinguish background noise captured in real-room scenarios with three different floor surfaces.

The utilization of ambient-based sensors for detecting human falls extends to ground-based pressure detection, as demonstrated in [78]. The researcher introduces a smart carpet, comprising a sensor pad placed beneath a carpet, and the electronics read walking activity to provide an automated health monitoring and alert system. The system's functionalities are extended to improve fall detection, measure gait, and count the number of people traversing the carpet for socializing purposes. In another study [79], an algorithm enhances pressure-based sensors by building time and frequency domain parameters based on the centre of pressure (CoP) values obtained from time-series data from a pressure monitoring floor sensor. Furthermore, in [80] employs a magnetic sensor array for detecting falls in fragile elderly individuals. The magnetic tactile sensor arrays, installed on intelligent floors along frequently walked paths like bedroom and toilet floors, successfully detect falls among elders.

In addition to pressure-based sensors, researchers in [81] utilize floor vibration as a recognition source, incorporating person identification through vibrations produced by footsteps. The system introduces a voting system among sensor nodes to improve person identification accuracy, making the system more robust in identifying falls amidst similar events like jumps, door closings, and object falls. Another study in [82] demonstrates the effective application of a floor vibration sensor for fall detection. The system decomposes falling modes and characterizes them with time-dependent floor vibration features, leveraging a classifier and a novel reconfirmation mechanism using Energy-of-Arrival (EoA) positioning to assist in detecting human falls. However, the vibration model in some cases lacks significant features related to the mass proportion of the human body, essential for distinguishing between object drops and human falls. Therefore, in [83], the mass proportion of a human body is meticulously studied. A scaled 3D-printed model with twelve fully adjustable joints simulating human body movement is built to generate human fall data for signature analysis.

Overall, the implementation of acoustic and pressure sensors demonstrates favourable outcomes in the detection and classification of fall events, offering distinct advantages in addressing concerns associated with wearable devices and vision-based sensors. However, current acoustic fall detection technologies work well under laboratory conditions, but it is still problematic to produce reliable results when these technologies are applied to real-life conditions because the presence of high background noise especially elderly who lives in urban [84]. Meanwhile, the pressure sensor may have challenges in accurately capturing fast variations of applied pressure, such as those from the morphological changing processes of a droplet falling onto the sensor. Additionally, the existing fall detection algorithms primarily focus on sudden falls and may not effectively address slow fall scenarios, which are typical for elderly fallers [85].

2.3.4 Radar based Sensor

Radar-based fall detection systems have gained interest due to their ability to operate in various environmental conditions, insensitivity to lighting conditions, and limited privacy concerns [11]. Radar is a favourable approach for fall detection as it can accurately monitor physiological signals and body movements without the need for attaching devices to the body, making it suitable for elderly care and healthcare applications [85]. Additionally, radar systems offer the potential for non-invasive fall and vital signs detection, making them suitable for indoor health monitoring [86]. The concept of the radar detection principle involves transmitting a radar signal that reflects off the surrounding environment and any targets within it, which is then received by a receiving panel. This reflection affects the power received at the panel, resulting in changes in amplitude over time that can be meaningful in analysing. Additionally, when a target is in motion, changes in the frequency and wavelength of the signal provide valuable information known as Doppler time-frequency signatures. These signatures are crucial for effectively detecting falls in assisted living environments [87]. These systems are designed to recognize human behaviours and accurately detect fall accidents, contributing to independence-assisting remote monitoring technologies for the elderly population [88]. The use of radar technology for fall detection is further supported by its ability to accurately recognize human behaviours and allow early detection of fall accidents in daily environments [89].

Various topologies of radar-based sensors, such as monostatic, have been studied in [90]. In this work, the author employed a Frequency Modulated Continuous Wave (FMCW) radar to detect human movement. The radar signals were used to calculate the range-velocity map, range-horizontal angle map, and range-vertical angle map. Three neural networks were created for these signal maps, and the stacking method of ensemble learning was applied to fuse the time-space-velocity features extracted by the three neural networks for fall identification. Similarly, in [91], the author utilized the pattern contour-confined Doppler-time maps on signals from FMCW radar. The proposed PCC-DT map aims to reduce redundant information and remove outlier points from Doppler-time maps, enhancing detection accuracy by mitigating errors caused by unnecessary information and outliers. In another study [87], an angle-Doppler radar point clouds-based learning model was introduced for human activity classification using FMCW radar. The human echoes were transformed into a series of 3-D point cloud cubes, integrating motion signatures in time-range, time-Doppler, and range-Doppler domains. These RPC cubes were processed by a newly developed two-layer convolutional multilinear principal component analysis (PCA) network for feature extraction and motion classification. Furthermore, in [92], a millimetre-wave FMCW radar-based fall detection method was employed using the pattern contour vector. The study focused on analysing soft fall motions to mitigate elderly falls. Motion attributes such as velocity, intensity, and trajectory were used to distinguish sudden and soft fall motions from non-fall ones. The PCVs of Doppler time map, regional Power Burst Curve , and PCVs of range time map served as inputs for two CNNs.

In another study [93], millimetre-wave radar was employed based on histogram of oriented gradient (HOG) features and ML. The manually extracted HOG features from time-range maps, time-velocity maps, and time-angle maps served as inputs to the classifier. Additionally, the use of HOG was also presented in [94]. The researcher encoded the HOG signature using nonparametric local transforms, such as census transform and local binary pattern. These transforms contained enhanced gradient information, leading to distinguishable HOG features for improved fall event detection.

Furthermore, in [95], the study emphasized the use of the Multi-task Learning Radar Transformer (MLRT), a network designed for personal identification and fall detection based on IR-UWB radar. The MLRT employs the attention mechanism of Transformer as its core to automatically extract features for both personal identification and fall detection from radar time-series signals. Multi-task learning is applied to leverage the correlation between the personal identification task and the fall detection task, enhancing discrimination performance for both tasks.

Furthermore, to enhance the localization of human falls, the researcher in [96] utilized a Multiple Input Multiple Output (MIMO) radar system. The received signal was segmented into a time sequence using a sliding window along slow time. Subsequently, the FFT and multiple signal classification (MUSIC) algorithms were applied to estimate the general trend of the human body's time-varying range and pitch angle information. This information was then fused with a geometrical relationship to describe height changes during fall motions using a height trajectory map. Two height-based features were extracted and used as input to the classifier. In a study on human activity recognition [97], a distributed MIMO radar configuration was employed, featuring multiple antennas of a millimetre-wave (mm-wave) MIMO radar system (Ancortek SDR-KIT 2400T2R4). The setup included two independent and identical monostatic radar subsystems that irradiated and captured multidirectional human movement from two perspectives. This allowed the computation of two distinct time-variant radial velocity distributions. The feature extraction network extracted numerous features from the measured TV radial velocity distributions, which were then fused by a multiclass classifier to detect five types of human activities. Additionally, in [98], a mmWave MIMO radar system was used with two separate monostatic radars placed orthogonal to each other in an indoor environment. These two radars illuminated the moving person from two different aspect angles, producing two time-variant micro-Doppler signatures. The study computed the mean Doppler shifts from the micro-Doppler signatures, extracted statistical and time- and frequency-domain features, and applied the future fusion technique for the feature extraction algorithm to be fed into the classifier.

However, the challenge of accurately classifying different types of falls is a drawback of radar-based sensor fall detection systems. Researcher in [99], highlighted the difficulty in classifying falls due to the similarity of Doppler signatures among different fall types, making it extremely challenging for classification. Additionally, the classification task of radar signal encounters challenges when there are signals exhibiting signatures that mimic those of a fall such as bending, kneeling, lying, prostrating, squatting, and sitting, involve movements that cause the body to move downward. These fall-like movements can potentially trigger false alarms in fall detection systems due to their resemblance to actual fall events [99], [100], [101]. In summary, while differentiating falls from normal human movements is essential, the categorization of specific fall types is equally crucial in providing accurate and targeted medical intervention. Understanding the nature of a fall event is instrumental in tailoring the response and care to the individual's unique circumstances.

Furthermore, in [102] pointed out that AI-based fall detection using contactless sensing has drawbacks and limitations that need to be addressed. These limitations may include the complexity of accurately differentiating between various activities and fall patterns, which can impact the reliability of radar-based fall detection systems. Besides, the potential health risks associated with chronic radiation exposure from radar fields have been a subject of investigation and concern [103]. While some studies have emphasized the safety and non-ionizing nature of radar technology for at-home healthcare and fall detection [104], concerns about potential health risks associated with radar radiation, especially for long-term exposure, have also been raised. This is particularly relevant as the elderly may be more susceptible to the effects of radiation due to factors such as aging-associated low-grade inflammation, which is a significant risk factor for morbidity and mortality in elderly people [105]. However, a notable branch of radar systems, discussed in detail in subchapter 2.4, utilizes an outsourced signal known as passive radar. This signal presents advantages in mitigating radiation concerns, as it leverages established and safe signals like Wi-Fi or radio communication signals, which have been employed for their intended purposes over an extended period.

2.4 Passive Wi-Fi Radar

Passive radar is a type of bistatic radar architecture where the transmitter and receiver are physically separated, utilizing the backscatter of radar signal from targets to infer their range, speed, and angular position. This configuration leverages the principles of time-of-flight and Doppler effect to enhance target detection and tracking capabilities, enabling improved signal-to-noise ratio and clutter rejection through the analysis of multi-path propagation effects and scattering characteristics. This type of radar been widely applied on in cooperative principles, using LTE signals, and in satellite-based radar, offering benefits such as wider accessibility, less sensitivity to multipath effects, and signals not being blocked by obstacles [106], [107], [108]. Furthermore, passive radar has been used in multi-static radar systems, target localization, and detection on moving platforms, including seaborne and airborne platforms [109], [110], [111]. Moreover, it has been applied in target localization, target recognition, and target detection based on micro-Doppler analysis in forward scattering radar (FSR) geometry [112], [113].

In the discourse on indoor fall detection systems, the Wi-Fi router signal emerges as the most accessible outsourced signal. This assertion finds support in the widespread availability of Wi-Fi routers in households, as underscored by a survey conducted by the DOSM, revealing a substantial 92% usage and accessibility rate [16]. Moreover, highlighted that Wi-Fi technology operating at 2.45GHz is a significant source of non-ionizing electromagnetic radiation [15]. It is important to note that despite concerns about the potential harm from Wi-Fi radiation, emphasized that typical Wi-Fi exposure levels in the everyday environment are several orders of magnitude below guideline values, raising questions about the actual risk posed by such exposure [15]. Furthermore, [114] found that the average value for Wi-Fi emissions was well below the safety limit established by the International Commission on Non-Ionizing Radiation Protection (ICNIRP). Thus, this evidence substantiates the safety of Wi-Fi router emissions in comparison to the emissions from self-developed radar systems.

Passive radar systems, including those utilizing Wi-Fi signals, are designed to detect and track objects using signals that were not intentionally developed for target detection. In the case of Wi-Fi signals, these signals are primarily intended for transferring packet data in wireless communication networks rather than for human movement or fall detection. Unlike intentional radar signals, Wi-Fi signals emit beacon signals to announce their presence, typically at a fixed rate of 10Hz [115]. This periodicity can be observed and treated similarly to pulse-based signals in radar systems. The unique characteristics of Wi-Fi signals, including their emission patterns and frequencies, provide a distinctive source for passive radar applications. Hence, the use of passive radar has extended to various signal processing techniques, such as reference signal extraction, interference-to-noise ratio estimation, and parameter estimation for coherent passive MIMO radar to tackle the preprocessing challenge for human movement or fall detection system.

In the traditional use of Wi-Fi signals for human detection systems, processing is typically done using Channel State Information (CSI), as demonstrated in a study presented in [116], [117]. However, it's crucial to note that this algorithm is not considered a PWR, as it relies on channel information from the connections between the receiver and transmitter. Another study focused on PWR algorithms with MIMO radar trajectory, as shown in [116]. The author deployed two receivers, one for surveillance and the other for reference signal purposes. The study applied Cross Ambiguity Function (CAF) to characterize the correlation between the received signal and a local code replica for every possible Doppler pair. The results showed that while the CSI system was slightly better in line of sight, the PWR system significantly outperformed in non-line-of-sight conditions. In another study [118], beamforming technology was used for two-dimensional scanning of the entire person's breathing perception. This approach aimed to overcome phase offset introduced by asynchronous transceiver devices. The study eliminated static clutter using the ratio of the channel frequency response between the antenna array and the reference channel. The proposed system demonstrated the ability to estimate the direction and respiration rate of multiple persons, as well as monitor abnormal respiration in multi-person scenarios.

However, it's important to consider drawbacks associated with the reference channel in PWR. One significant drawback is the potential for clutter caused by multipath signals in the reference channel, impacting the accuracy of radar signal processing and analysis. This clutter, known as multipath clutter, refers to unwanted signals that arise when radar waves reflect off multiple surfaces or objects before returning to the receiver. This phenomenon poses challenges in space-time adaptive processing and can affect the radar system's ability to accurately detect and track moving targets. Additionally, clutter from the reference channel can introduce interference in the range-Doppler map, affecting the overall performance of the radar system [119]. Moreover, the reference signal received from the line of sight may have a significantly larger amplitude than the target reflections received by the imaging channel, potentially leading to challenges in signal processing and interpretation. This difference in signal amplitudes can impact the accuracy and stability of radar system design, particularly in scenarios where achieving a high degree of radiometric resolution is essential. Radiometric resolution refers to the ability of a radar or imaging sensor to detect and differentiate between small variations in the intensity of the reflected electromagnetic signal. It determines the sensor's sensitivity to differences in the power of the received signal, often measured in bits, which defines how finely the sensor can represent the energy reflected from different surfaces. Higher radiometric resolution allows for more detailed discrimination of subtle differences in reflectivity or emissivity.

To surmount the identified limitations, prior investigations have explored the implementation of PWR configurations, abstaining from the utilization of any reference channel akin to that delineated in [120]. The researcher executed median and outlier removal methodologies to mitigate noise within the raw data. Despite these efforts, residual outliers persisted subsequent to the preliminary filtration process. In response, the author employed Hampel fill outlier filters, which substituted any remaining outliers with the preceding non-outlier values in the dataset. Furthermore, an article emanating from this study was disseminated in [121], elucidating a pioneering application of an enveloping algorithm on beam signals. The enveloping method strategically leveraged the inter-beam distances to ascertain the optimal peaks, subsequently considered as salient points for extracting time-domain signals. The findings of this research posited that the enveloped signals closely resembled the continuous signals specifically designed for detection purposes, thereby warranting equivalent treatment for subsequent feature extraction and classification endeavours.

While the PWR system has demonstrated applicability in normal human movement detection systems, a notable gap exists in its adaptation to fall detection systems. As outlined in section 2.3.4, the radar signal presents challenges in accurately differentiating among various activities and fall patterns. Consequently, the selection of an appropriate classifier algorithm and the optimization of its parameters emerge as critical components in the development of the radar-based fall detection system, as further elucidated in sections 2.5 and 2.6.

2.5 Machine Learning Application

ML is a classifier that requires human intervention to facilitate effective algorithmic performance. It constitutes a subfield of AI concentrating on the formulation of algorithms and statistical models that empower computer systems to enhance their proficiency in a designated task through iterative learning from data, without necessitating explicit programming [18]. In the context of human fall detection systems employing radar technology, ML is primarily applied to execute the classification task and also can be meaningful for other tasks such as feature extraction and anomaly detections. It is trained to discern patterns associated with typical human movement and identify anomalies or deviations indicative of fall events, a recognition task that may deviate significantly from routine activities [54]. Various types of ML, including SVM, FFNN, and RF, fall under the category of supervise ML, and these are commonly employed in radar-based sensor fall detection systems [122].

However, human intervention remains essential for the extraction of significant features from the input data, as ML algorithms are inherently designed for classification tasks and lack an inherent feature extraction capability. In the field of radar technology applications, signal processing assumes a paramount role in the extraction of valuable insights from received signals. Likewise, in the context of radar-based fall detection systems, signal processing is indispensable for enabling precise target detection and motion analysis. When examining human movement, the Fourier transform stands as the most fundamental and widely employed tool for the analysis of the frequency content within discrete-time signals. This transformative process dissects a signal into its constituent sinusoidal components, thereby rendering it useful in an array of applications, including filtering, spectral analysis, and signal compression. Within the context of radar-based fall detection, the Fourier Transform plays a crucial role in detecting anomalies in motion data. For instance, a sudden shift in the frequency content of motion data can serve as an indicator of a fall event. It is important to note that there exist various types of Fourier transforms, such as the Discrete Fourier Transform (DFT), and Short Time Fourier Transform (STFT) [17], [18]. These variants share a common transformation algorithm while differing in their specific approaches. DFT, for instance, operates on discrete-time signals, while Fast Fourier Transform (FFT), which is a more efficient method for computing DFT, employs either an efficient Decimation in Time or Decimation in Frequency structure. STFT, on the other hand, computes DFT with smaller window sizes, making it particularly useful for analysing how the frequency content of a signal evolves over time. Overall, this section will provide a detailed discussion on ML algorithms in conjunction with feature analysis, emphasizing their significance and applicability within the field of fall detection systems.

2.5.1 Feed-Forward Neural Network

FFNN are a type of Artificial Neural Network that process information in a unidirectional manner, from the input layer through hidden layers to the output layer, without forming any cycles or loops [123], [124]. These networks are trained using algorithms such as backpropagation to determine the kinetic parameters governing the performance of various processes, such as ozonation of oil-drilling cuttings [125]. The FFNN architecture, with proper weights, has been proven to be capable of approximating any input-output function, making it suitable for forecasting and classification purposes [126].

Moreover, in the developing of the FFNN algorithm there is some optimizable parameters that influence the performance of the FFNN algorithm encompass a wide range of factors. These include the network architecture, such as the number of hidden layers and neurons, which can significantly impact the network's ability to learn and generalize from the input data [127], [128]. Additionally, the choice of optimization algorithm, such as particle swarm optimization, can influence the training process and the network's convergence to an optimal solution [129]. The type of data preprocessing and feature selection techniques employed also play a crucial role in determining the network's performance, as demonstrated in the prediction of longitudinal and transverse profiles of pressure flushing cones using FFNN and cascade FFNN techniques [130]. Furthermore, the choice of activation functions, learning rates, and regularization techniques can greatly affect the network's ability to avoid overfitting and improve generalization to unseen data [130], [131]. In the field of classification, FFNN have demonstrated efficacy across diverse applications, as evidenced by their successful utilization in tasks such as determining the roasting level of coffee through Microwave Non-Destructive Testing in [132]. Notably, the researcher in this study demonstrated strategic acumen in devising an FFNN structure aimed at reducing complexity and mathematical computational costs while ensuring high accuracy. The researcher adeptly addressed the challenge of significant class segregation by opting for a judiciously chosen FFNN structure. Despite the substantial number of input neurons reaching up to 6400, the researcher opted for a parsimonious approach, employing only 5 hidden neurons. This streamlined architecture proved remarkably effective in achieving excellent classification of coffee roasting levels. This approach underscores the researcher's discerning consideration of model simplicity, computational efficiency, and robust performance in the classification task.

The application of FFNN algorithms in ML classification tasks for human motion or fall detection systems has been relatively limited, as recent research has predominantly focused on employing this classifier within DL frameworks. Nonetheless, a study presented in [133] underscores the significance of FFNN in a human identification system. The author employed the IWR6843 mmWave radar sensor to capture signals, applying FFT to extract range and velocity features. These features were then input into a classifier with 18 neurons in the hidden layer. The FFNN demonstrated accuracy levels above the acceptance threshold, although it did not outperform the DenseNet, a comparable algorithm in the study. Another study in [134], showcased the utilization of FFNN with a single hidden layer comprising six sigmoid neurons, comparing its performance with RF. The features for the classification task were derived from both the entire 43-dimensional feature set and a feature set generated through the genetic algorithm guided $\Gamma-$Test. The findings suggested that RF performed well compared to FFNN algorithms, albeit without a significant difference in accuracy and F1-score. An additional contribution to this line of inquiry, as presented in [121], also involved the application of FFNN. In this study, the FFNN was fed with inputs from the frequency domain obtained through FFT. Human movements such as walking, bending, sitting, and kneeling were collected for analysis. The results demonstrated that features extracted with 8 hidden nodes in the FFT's hidden layer could excellently classify human movements.

2.5.2 Support Vector Machine

SVM is a widely used supervised ML technique for classification and regression tasks [135]. In the context of classification, SVM works by finding the optimal hyperplane that best separates the data points of different classes in a high-dimensional space [136]. This hyperplane is determined by maximizing the margin, which is the distance between the hyperplane and the nearest data points, known as support vectors [137]. The classification process involves assigning new data points to different classes based on which side of the hyperplane they fall [138]. In the training phase, SVM aims to find the hyperplane that minimizes classification errors and maximizes the margin. This is achieved by solving an optimization problem, typically a convex quadratic programming problem, which involves minimizing the regularized hinge loss function [138]. The training process involves determining the support vectors and the associated weights, which define the hyperplane and the decision boundary [139]. The optimization problem is solved to obtain the parameters of the hyperplane, which are used for classification [140].

Moreover, there are parameters that influence the SVM algorithm play a crucial role in its performance and effectiveness. These parameters include the penalty parameter [141], [142], the kernel parameter (gamma), and the choice of kernel function. The penalty parameter C controls the trade-off between maximizing the margin and minimizing the classification error, thus influencing the regularization of the model [143]. The kernel parameter gamma is particularly relevant for radial basis function (RBF) kernels, as it defines the variance of the Gaussian and affects the radius of influence of a single training example [141], [144]. Additionally, the choice of kernel function, such as linear or Gaussian kernels, impacts the SVM's ability to handle linearly inseparable data and nonlinear relationships [141], [145]. The lack of elegance in parameter optimization by a researcher was evident in [146], where the classification of coffee roasting levels employed C and gamma set to 1, and the RBF kernel function was applied to the SVM algorithm. Despite this seemingly simplistic approach, the study demonstrated the efficacy of SVM in excellently classifying coffee roasting levels with the smart strategy by the author in optimizing the parameters.

Furthermore, the application of SVM in radar-based fall detection has been extensively explored in various articles, including those found in [147]. The author employed FSR for fall detection, utilizing FFT for feature extraction and applying the SVM algorithm with RBF as the kernel function. The study yielded noteworthy outcomes as the author successfully differentiated features associated with fall movements from those related to sitting movements, which exhibited a comparable signature to fall events, achieving an excellent classification accuracy. In another study documented in [148], RBF-SVM was employed for classifying sitting and lying-down activities. The researcher utilized a K-band 24 GHz continuous wave Doppler radar for data collection and manually extracted features, eschewing signal transformation methods. Extracted features encompassed entropy, power, durations, zero-crossing rate (ZCR), turn count, mobility, power fraction, and power ratio. The SVM demonstrated commendable performance, surpassing acceptance values in terms of accuracy, F1-score, and precision. Additionally, a study in [149] conducted a comparative analysis between SVM and K-Nearest Neighbours (KNN) algorithms. The researcher collected signals for walking and running activities, considering single and multiple detections at angles of 0, 45, and 90 degrees. STFT with a window size of 2 seconds and 100 samples of sliding steps generated image features. Enveloping algorithms were subsequently applied to derive significant features. The study employed PCA to reduce feature dimensions, and the comparative analysis indicated that PCA-SVM exhibited the highest accuracy and F1-score. Moreover, in [150], the author delved into a study on kernel algorithms for SVM. The accuracy of three kernel types: linear, polynomial, and

RBF was examined in the classification task of human presence using mmWave radar. The study revealed that the polynomial kernel function outperformed other kernels when fed with point cloud-based features.

However, it can be extended to handle multi-class classification problems. One common approach is the One Against All (OAA) or One Against One (OAO) technique, where multiple binary SVM classifiers are trained to distinguish between different classes [151]. The OAA strategy involves training a single classifier per class, making it suitable for multi-class classification tasks, while OAO involves training multiple binary classifiers [152]. The OAA strategy is often preferred over OAO in radar-based human movement analysis when using SVM algorithms due to its simplicity and efficiency in handling multi-class classification tasks [152]. The OAA approach simplifies the classification process by training a single classifier for each class, making it computationally efficient and easier to implement. This simplicity is advantageous in scenarios where real-time processing of radar data for human movement detection is crucial. Additionally, the OAA strategy has been shown to achieve high precision rates, making it a accessible choice for radar-based applications.

Moreover, the implementation of multi-class SVM has enhanced the fall detection algorithm. Whereas previously it could only discern between fall and non-fall incidents, the introduction of multi-class SVM enables the system to identify the direction or type of falls. The applications of OAO strategy were presented in a related study by [96], the FFT and Random Fast Time (RFT) were employed to extract numerical features. Feature selection involved analysing the localization of signal peaks, and the selected features were fed into SVM using the OAO strategy. The aim of this study was to classify types of falls, encompassing accident falls, falls associated with heart attacks, falls with hypotension, falls from chairs or beds, and fall-like movements such as stepping, bowing, sitting, squatting, and walking. The SVM exhibited commendable performance, achieving almost perfect accuracy in the classification task. In contrast the study documented in [153] showcases the implementation of a multi-class SVM using the OAA algorithm with RBF. The objective was to classify various human movements, encompassing walking, jumping, and bending, as captured by a FMCW radar. Initially, the researcher employed the STFT algorithm to convert the time-domain signal into image features. Furthermore, features such as texture, extracted using HOG and Local Binary Pattern (LBP), were incorporated, along with numerical features including Micro-Doppler shift, Doppler bandwidth, torso Doppler bandwidth, and torso mean Doppler frequency. Subsequently, these features were utilized as input for the RBF-SVM employing the OAA strategy.

2.5.3 Random Forest

RF is a powerful ML algorithm that operates by generating multiple decision trees through random sampling on the same dataset and then combining them to predict the target variable [154]. By training multiple decision trees with diverse data and feature subsampling, the resulting RF can lead to more stable and accessible predictions than a single decision tree [155]. It is a combined classification method belonging to ensemble learning, using decision trees as classifiers [156]. The algorithm has been widely used and has achieved excellent performance for classification and regression tasks [157]. RF is a successful method based on Bagging and Decision Trees [154]. It is known for its high classification intensity and wide application range [158]. The algorithm is highly capable of very precise generalization, proposes no requirements for training data attributes, and can meet the requirements of high parallel operation of big data processing [159].

The RF algorithm is influenced by various parameters that play a crucial role in its performance and effectiveness. These parameters include the number of observations drawn randomly for each tree, whether they are drawn with or without replacement, the number of variables drawn randomly for each split, the splitting rule, the minimum number of samples that a node must contain, and the number of trees [160]. Additionally, the number of decision trees and the maximum number of features for constructing the optimal model of decision trees have a significant influence on the accuracy of the RF classification results [161]. Furthermore, the selection of hyperparameters such as the maximum number of features used by a single decision tree and the number of sub-trees directly controls the tree structure of the model, impacting the performance of the classifier [162]. The RF algorithm also requires tuning of the hyperparameters to achieve optimal performance [163]. Moreover, the risk of deeply grown trees in RFs can lead to overfitting the training dataset, resulting in predictions with low bias but high variances [164].

The effectiveness of RF in a classification task was demonstrated in [165]. The author gathered data on various normal human movements, including drinking, sleeping, walking, and sitting, using UWB radar. Statistical analysis was applied to the time-domain signals to extract features such as minimum, maximum, mean, standard deviation, variance, skewness, kurtosis, signal length, mean absolute deviations, energy, cross-correlation, and mean crossing rate. These features were then utilized with both K-NN and RF, employing a random subset of attributes for the classification task. The results indicated that RF outperformed K-NN significantly in terms of accuracy and F1-score for the classification assignment. Another study presented in [166] compared two classifiers, namely XGBoost and RF. Synthetic hand gesture signals were transformed into spectrograms using STFT to extract angular, range, and velocity features. These features were fed into RF with specified parameters, and the results were compared with XGBoost. The findings revealed that RF exhibited excellent accuracy, whereas XGBoost performed below the acceptance level. Furthermore, in [167], a study focused on the placement of mmWave radar and the choice of a classifier algorithm. The radar was positioned on both the wall and the ceiling to assess their optimal locations. Both radars collected data on movements such as walking, sitting, and standing. The author applied statistical analysis to generate 29 numerical features, akin to previous articles, but applied separately to each axis. These features were then fed into RF, SVM, and K-NN. The results indicated that RF performed exceptionally well in both radar locations, whereas SVM exhibited satisfactory performance only when the radar was placed on the wall.

Prior research substantiates the efficacy of SVM, FFNN, and RF in the classification of human motion and fall events. Nonetheless, it is noteworthy that conventional ML algorithms necessitate explicit feature extraction guided by predefined rules. Feature extraction and selection is a crucial step in the process of classification, as it directly impacts the efficiency and accuracy of ML algorithms. The selection of relevant features is essential to ensure that the classifier is not influenced by irrelevant or redundant information, which could introduce bias into the classification process. Irrelevant features can significantly affect the classification efficiency of ML algorithms [168], [169]. Therefore, it is necessary to select features using appropriate methods to improve classification performance such in earlier studies, where researchers manually conducted feature extraction from signals employing signal transformations such as FFT and STFT. Moreover, researchers were engaged in the manual selection of features from the transformed domain, with some also employing unsupervised feature selection methods, including PCA to avoid human bias in features selection. Given this constraint, it becomes imperative to consider the integration of Deep Learning algorithms to fine-tune and optimize the selection of a compatible classifier algorithm.

2.6 Deep Learning Application

Diverging from ML, DL represents an AI algorithm that operates without the necessity of human intervention in feature extraction. DL is structured into two main components: the feature extraction part and the classification part. The classification part bears similarities to FFNN algorithms but entails a more profound neural network with multiple layers of hidden layers. Conversely, the feature extraction part in DL is uniquely designed, incorporating algorithms tailored for DL frameworks. These algorithms are specifically crafted to autonomously learn and adapt to raw data, discerning and selecting the most significant features, whether they manifest as images or numerical data. This intrinsic ability of DL to independently extract intricate features contributes to its effectiveness in complex tasks, requiring a high level of abstraction and representation learning. Two common types of DL architectures used for feature extraction are CNN and Long-short Term Memory (LSTM).

2.6.1 Long Short-Term Memory

LSTM is a type of ANN that is particularly effective in feature extraction, classification, and training in the context of radar detection. It is designed to capture long-term dependencies in sequential data, making it well-suited for processing radar signals and extracting relevant features for classification tasks [170]. The key insight in the design of LSTM is its ability to incorporate nonlinear, data-dependent controls into the RNN cell, which prevents the vanishing gradient problem and enables effective training of the network [170]. This is crucial for radar detection applications where the network needs to learn and capture complex patterns in the data. The LSTM has been shown to efficiently extract temporal features for classification tasks, making it suitable for radar-based applications [171]. Additionally, the use of LSTM in radar signal processing has been found to be effective in capturing the spatial-temporal characteristics of radar data, leading to improved recognition accuracy and relatively low complexity compared to other methods [172].

The parameters that influence the LSTM algorithm are crucial for its performance in various applications, including radar detection. The LSTM cell, as a fundamental component of the LSTM algorithm, is designed to address the vanishing gradient problem and introduce changes that make the system robust and versatile [170]. This is essential for capturing long-term dependencies in sequential data, which is particularly relevant in radar signal processing. Furthermore, the ability of LSTM-RNN to consider both current and previous input information enables it to effectively extract features from sequential data, such as crank speed in misfire detection applications [173]. Additionally, the classification accuracy of LSTM-RNN can be influenced by parameters such as the number of filters and LSTM units, which have been shown to impact the performance of the model [172]. Moreover, the LSTM-RNN model's performance can be affected by the choice of architecture and the number of hidden layers and nodes, as demonstrated in studies comparing different settings of LSTM-RNNs [174].

The application of Long Short-Term Memory (LSTM) networks in the context of radar-based human motion classification and fall detection has been extensively investigated, as evidenced by the work in [175]. In this study, researchers employed time domain signals, directing them into two stacked LSTM layers, each comprising 100 hidden units. Notably, only the initial layer possessed a depth of 10 units. The primary objective of this investigation was to undertake a comparative analysis of LSTM and CNN performance in discerning walking, ascending/descending stairs, and falling movements. The study revealed that a CNN, featuring two convolutional layers and utilizing a spectrogram with time-frequency analysis features, achieved notably high accuracy. In contrast, another research endeavour [176] addressed the inherent challenges associated with utilizing time series data as input for LSTM. The investigators gathered fall and non-fall activities through FMCW radar mounted on the ceiling. Subsequently, they applied a normalized greyscale spectrogram connected to a single LSTM layer with 128 hidden units. Results indicated superior performance of

LSTM over CNN, although the observed difference was not statistically significant. Furthermore, in the study presented in [177], researchers employed 1-D point cloud and Doppler velocity domain inputs fed into an LSTM layer with 512 hidden units to classify human slow fall motion in various room settings. This investigation asserted that employing a single-layer neural network before and after LSTM yielded excellent accuracy and F1-score values. Additionally, an innovative modification known as Bidirectional LSTM (Bi-LSTM), as introduced in [178], [179], involved the simultaneous consideration of forward and backward directions in LSTM layers. In this study, the authors developed two layers of Bi-LSTM using Micro Doppler signals, range time signals, and range trilateration signals to classify 12 human gait movements. The Bi-LSTM approach demonstrated improved classification accuracy compared to a standard single-layer LSTM.

Even though the application of LSTM had shown an outstanding performance in capture temporal dependencies and sequential patterns in movement data. LSTM's architecture, with its memory cell and gating mechanisms, allows it to retain and selectively forget information across long sequences, making it particularly well-suited for recognizing complex motion patterns, handling variable-length input sequences, and mitigating issues like vanishing gradients in deep learning models for the task of feature extracting and classification of human movement detection. This algorithm, holding few limitations that been detect its inability to effectively capture long-term dependencies in sequential data due to the vanishing/exploding gradient problem [180]. This limitation can impact the model's ability to accurately recognize and classify complex patterns in human movement data, especially in scenarios where long-term dependencies are crucial for accurate detection. Furthermore, the complexity and robustness of the LSTM model can be affected by the size of the dataset used for training and evaluation [181]. In the context of human movement or fall detection, the availability of comprehensive and diverse datasets is essential for training LSTM-RNN models to accurately recognize and classify different movement patterns and potential fall events. Limited or biased datasets may hinder the model's ability to generalize and accurately detect diverse human movements and potential fall scenarios. Moreover, the computational complexity and energy consumption associated with LSTM-RNN models can pose challenges, especially in real-time applications such as fall detection systems [182]. The high computational demands of LSTM-RNN models may limit their practical deployment in resource-constrained environments, impacting their suitability for real-time human movement and fall detection tasks. This limitation had influence researcher in applying the CNN algorithms on the radar-based fall detection system.

2.6.2 Convolutional Neural Network

CNNs work on images by employing convolutional layers to extract features, followed by classification and training processes. The feature extraction in CNNs involves the use of convolutional layers to detect patterns, edges, and textures within the input images [183]. These convolutional layers are designed to extract data such as lines, curves, edges, and structural orientation from images, enabling the network to learn hierarchical representations of the input data [184]. The feature extraction process can be enhanced by converting time-frequency signals into grayscale images using wavelet transform, which has been shown to make CNNs more effective in extracting feature information [183]. After feature extraction, CNNs utilize the extracted features for classification tasks. The local features of images are aggregated to form global features, which are then used for classification purposes [185]. Additionally, CNNs can be used for image segmentation, where the efficiency of extracting features corresponding to different layers in the CNN is evaluated, with different layers showing varying extraction efficiencies [186].

The performance of CNN algorithms is influenced by several crucial parameters. These parameters significantly impact the feature extraction, learning, and classification capabilities of CNNs. The key parameters that influence CNN algorithms include the number of convolutional layers, the network architecture, the choice of transfer learning, hyperparameter fine-tuning, and the optimization algorithms used for training. The number of convolutional layers in a CNN significantly impacts its performance. Utilizing a network with fewer convolutional layers can lead to a reduction in the number of parameters, thereby affecting the feature extraction network's strength [187]. Additionally, the architecture of the network, including the choice of transfer learning and the fine-tuning of hyperparameters, plays a crucial role in determining the CNN's performance [188].

Experiments that focused on the meticulous adjustment of CNN hyperparameters have revealed their pronounced impact on model performance, as illustrated in [189]. This particular investigation targeted fall detection, specifying a directional fall system employing an FMCW radar sensor. To accommodate the high-speed movements inherent in falls, the signal underwent transformation into a spectrogram via STFT with 0.5-second windows. The ensuing features were then fed into a Kernel-CNN architecture with varying numbers of convolutional layers, ranging from 1 to 5. The outcome highlighted that the algorithm with a singular convolutional layer exhibited superior accuracy, sensitivity, and specificity. Subsequently, a comparative analysis was undertaken between a CNN model featuring 2 convolutional layers and 2 fully connected layers, and the LSTM-RNN algorithm for the classification of five distinct human movements and fall events was presented in [190]. The CNN algorithm leveraged spectrogram images, while the LSTM algorithm processed time series signals. Results indicated that the CNN algorithm outperformed in terms of classification accuracy, recall, and precision.

However, there is a branch of CNN call transfer learning, which involves using knowledge gained from solving one problem to solve another related problem, is a key advantage of pretrained CNNs. By leveraging the knowledge acquired from a task-independent dataset, pretrained CNNs can effectively extract features and learn representations that are beneficial for various classification tasks [191]. This capability has been particularly advantageous in scenarios such as image classification, where pretrained CNNs have demonstrated excellence in feature extraction and retrieval optimization [191]. The CNN heavily rely on their architecture, influencing the number, significance, and adaptability of features. In the domain of human movement and fall detection systems, a prevalent approach involves leveraging transfer learning models such as AlexNet, Visual Geometry Group (VGG), and ResNet.

VGG presents two architectural variants, namely VGG-16 and VGG-19, with our discussion here focusing on VGG-16 due to its lower complexity while maintaining exceptional performance in radar-based human detection systems. The deployment of VGG-16, characterized by 13 convolution layers and 4 pooling layers, was delineated in [192]. This study employed three distinct CNN architectures which is 8-layer CNN, AlexNet, and VGG-16—to classify human activities such as walking, sitting down, standing up, bending, and falling. The signal was transformed into images using STFT with 1-second windows. The study yielded outcomes indicating that VGG-16 demonstrated optimal accuracy results, with AlexNet exhibiting excellent accuracy levels, albeit not significantly different from those achieved by the self-developed 8-layer CNN. In another study, as presented in [193], the focus was on comparing a self-developed 4D-CNN with the VGG-16 algorithm for micro-Doppler voice recognition. The received signals were translated into spectrogram images using a 0.005-second window with a sliding method, serving as inputs to the CNNs. The selection of the window size was grounded in the rapid vibrations associated with endoscopic projections of human sound. The results revealed that the VGG-16 approach performed superiorly, whether in free space or in the presence of barriers.

Meanwhile, there was a shallower CNN algorithm but had proven their ability which called AlexNet which its architectural composition encompasses five convolutional layers dedicated to feature extraction, complemented by three pooling layers designed for the purpose of either reducing layer depth or selecting features. The utilization of AlexNet in radar-based human movement and fall detection systems is expounded upon in [194]. The researcher collected data on five distinct human movements such sitting, bending, walking, getting up, and falling utilizing FMCW radar. The collected signals were transformed into images using STFT with a 1-second window size, after which the features layers within AlexNet were applied to each image. In the classification phase, while conventional AlexNet configurations consist of two fully connected layers with 4096 neurons, this study modified the classifier using the SVM algorithm. The results demonstrated that the features layers of AlexNet performed effectively in extracting features, significantly impacting classifier accuracy and achieving an excellent level of accuracy. Additionally, in [195], modifications to AlexNet were explored in terms of feature extraction layers for the purpose of classifying human gait conditions. The authors implemented two parallel branches of AlexNet's feature extraction layer, connected to a single classification fully connected layer or configured in the shape of a 'Y'. The results indicated that the accuracy level surpassed acceptable thresholds, particularly when the input was derived from a scalogram extracted via Continuous Wavelet Transform (CWT). Furthermore, another study presented in [196] employed the complete architecture of AlexNet for human movement classification. The authors utilized the AlexNet algorithm and compared its performance with GoogleNet when both networks were fed with pseudocolor images obtained through FFT. The results suggested that AlexNet exhibited superior accuracy and lower loss levels in comparison to GoogleNet.

Although possessing fewer layers compared to ResNet (50 to 152 layers), VGG (165 and 19 layers) and DenseNet (121 to 264 layers), AlexNet had demonstrated outstanding performance in radar-based human movement and fall detection systems. This suggests that transferred learning CNNs with a reduced number of layers can adeptly capture and extract significant features from intricate human movement signals, including fall events.

2.7 Hybrid Algorithm Applications

In light of the accomplishments in the application of ML and DL for classification tasks in human movement and fall detection systems, there has been an exploration into the field of hybrid algorithms for handling complex data classification. This hybrid approach involves the integration of DL features extraction components with ML algorithms to enhance performance in classification tasks.

The necessity for large volumes of labelled data for optimal performance in DL classifiers is a well-acknowledged constraint. In scenarios where labelled data is limited, traditional ML models may exhibit superior efficacy. Additionally, traditional ML models, including RF and SVM, often boast greater interpretability compared to deep neural networks. However, it is noteworthy that the performance of traditional ML models is contingent on expertly crafted features, whereas DL models excel in autonomously deriving hierarchical representations from raw input. Consequently, a hybrid model adeptly combines the strengths of both algorithmic approaches, potentially enhancing overall performance, especially in contexts with restricted data availability [197], [198], [199]. Moreover, a hybrid model combining CNN for feature extraction and ML for classification outperformed traditional ML methods, addressing the issue of overfitting [200].

Since in the SVM and RF were the ML that had shown a significant result in classification task of human movement or fall detection system, these two algorithms might have a potential in developing a hybrid algorithm together with AlexNet that performing well even though having a most shallow architecture of transfer learning CNN. The use AlexNet -SVM in radar human detection system were shown in [201], where extract image of spectrogram using AlexNet features extraction layers and supply the features into SVM. As a comparison the author run the same spectrogram image into full architecture of AlexNet and ResNet-18. The result shows that the AlexNet-SVM having the highest accuracy and F1 score. Besides, a researcher in [153] also compared a feature extract from AlexNet with other numerical features extracted from Doppler shift and total Doppler bandwidth. As result the feature from AlexNet, the fed to SVM shows an acceptable accuracy result. Moreover, a study in [202] had implement a more advance hybrid classifier architecture which the author combining the CNN with LSTM for feature extraction and utilized the SVM for classification task. The author had compared the result with the normal AlexNet and found that the CNN-LSTM-SVM hybrid version was outperform the AlexNet.

The literature is notably sparse on Hybrid classifiers algorithms as they represent a novel avenue for refining traditional ML and DL algorithms. Despite this scarcity, the discernible outstanding performance demonstrated by these hybrid models underscores their significance, rendering them a compelling subject of study that cannot be overlooked.

2.8 Summary

In conclusion, the phenomenon of falls among the elderly represents not only a national challenge but also an urgent international concern. This critical issue has garnered considerable attention from the Malaysian government, which anticipates a 7% increase in the elderly population by 2030. The RMK-12 underscores the imperative for advancements in healthcare technology tailored specifically for geriatric health, as elaborated in Chapters 3 and 4 of this thesis. In response to this pressing public health challenge, the government has earmarked an annual budget of RM900 million dedicated to enhancing healthcare services for the elderly. This focus on the elderly population is justified by their increased vulnerability to falls, stemming from a myriad of factors such as polypharmacy, fear of falling, hypertension, sensory impairments, chronic illnesses, muscle weakness, and balance deficits. Moreover, this demographic exhibits the highest risk, as post-fall complications can profoundly impact their mental health and overall quality of life, leading to increased morbidity and mortality rates, decline in quality of life, and disrupt both their environmental and social interactions.

Table 2.1
Comparative analysis toward fall detecting technologies

Technologies	Pros	cons
Wearable device technology	Can detect indoor and outdoor environment [55,56]	Single detection capacity, experience discomfort and potential of these devices being misplaced [61,62]
Vision-based technology	High accuracy and can be perform for multiple detection [65-68,70]	Privacy issue, limited detection area based on the line-of-sight [71]
Acoustic-based technology	Affectively in noise control environment [76]	Not proven in real environment situation especially in urban [84]
Floor pressure base technology	improve fall detection, measure gait, and count the number of people [79,80]	inaccurately capturing fast variations of applied pressure [85]
Floor vibration sensor	accuracy, making the system more robust in identifying falls amidst similar events like jumps [81]	lacks significant features related to the mass proportion of the human body [83]
Radar-based technology	Multiple detection and does not rise any privacy and discomfort issue [11,89]	Rise doubt about transmit signal especially the use of transmit frequency above 6GHz [15,103-105]

This critical issue has prompted extensive research into fall detection technologies, reflecting a commitment to ensuring the well-being of the elderly population, given the adverse health consequences that often follow a fall. Over the past five years, researchers have predominantly focused on the application of wearable devices, vision-based sensors, ambient sensors, and radar sensors such presented in Table 2.1. The findings presented indicate that the radar-based sensor approach has exhibited notable superiority over other methodologies. This is attributed to its ability to address issues inherent in alternative approaches, such as discomfort associated with wearable devices, privacy concerns with vision-based sensors, elevated background noise with acoustic-based sensors, and the potential for false alarms with pressure-based sensors. However, it is imperative to acknowledge that the radar-based sensor approach still contends with challenges related to signal complexity and the possibility of electromagnetic radiation.

Nonetheless, there exists a category of radar that addresses the concern regarding the possibility of EM radiation. PWR employs Wi-Fi signals, which have been proven safe from radiation even for the elderly population. Despite its safety, PWR has seen limited application in human movement and fall detection systems. This is attributed to the fact that the signal it utilizes is not explicitly designed for human detection algorithms, emitting beacon signals to announce presence at a fixed rate of 10Hz. Researchers applying this sensor face challenges in adapting this type of signal for fall detection. The majority of studies resort to using CSI and dual input approaches. However, this study takes a unique approach by applying the enveloping technique. This novel method, proven and published, preserves the Doppler signature and transforms the signal into a form akin to radar systems explicitly designed for human target detection. Thus, the signal can be treated similarly to other studies. It's important to note that while the PWR approach eliminates the Em radiation issue, it does not alleviate the signal complexity issue inherent in the classification task.

The inherent signal complexity, coupled with the synchronized nature of human movement, has directed the focus of this study towards signal processing and classification algorithms for the PWR approach. While various classifiers have demonstrated their capability to adapt and classify fall movements, both ML and DL approaches have been explored. In the ML domain, which requires human intervention for feature extraction, recent research trends, emphasize ML algorithms with learning abilities, including SVM, FFNN, and RF. These algorithms have exhibited commendable performance in the classification task of human movement and fall detection systems, particularly when features are extracted through signal transformation via FFT. Although the FFT domain has proven highly effective in providing features for classification tasks, an additional approach involves feature selection through PCA. PCA has demonstrated its efficacy in reducing feature dimensionality and complexity, facilitating the adaptability of features for classification. Consequently, the FFT-PCA approach, perceived as advantageous in extracting significant features, is applied in this study and will be tested on three supervised ML algorithms.

The challenge of signal complexity extends beyond the field of ML algorithms to also encompass DL algorithms. The success of DL algorithms, including LSTM, custom CNN, and transferred learning CNN models, in effectively classifying signals captured from radar in the context of human movement and falls. LSTM-RNN, a notable DL algorithm, demonstrates exceptional proficiency in autonomously extracting and classifying signals without human intervention. However, it is reported to face challenges related to the vanishing gradient problem, limiting its ability to effectively capture long-term dependencies in sequential data. Self-crafted CNNs, while effective, encounter challenges in designing architectures that ensure accurate feature extraction. As unsupervised classifiers, the convolutional layers play a pivotal role in providing valuable features. However, the lack of guidance regarding the optimal number of layers and their arrangement poses a challenge.

In response, researchers have increasingly turned to pretrained CNN models, the success of AlexNet in accurately classifying human falls with a shallow number of CNN layers. Given the proven efficacy of low complexity pretrained algorithms in classification tasks, this study incorporates these algorithms. Furthermore, the study explores the combination of Spectrogram from STFT with AlexNet and Scalogram from CWT with AlexNet, both of which exhibit impressive classification accuracy. This exploration is driven by the recognition that the combination of STFT-AlexNet and CWT-AlexNet may offer valuable insights and enhancements to the fall detection system.

Despite the established performance of both ML and DL in classification tasks, a noteworthy hybrid variant has emerged, integrating DL feature layers with ML classification algorithms. This hybrid approach has demonstrated substantial enhancements over traditional algorithms, particularly in terms of accuracy and mitigating overfitting issues. Notably, the amalgamation of CNN algorithms with SVM has received considerable attention in the literature. In this study, we aim to extend this exploration by employing the hybrid algorithm on AlexNet feature layers, coupled with both SVM and RF classifiers.

In conclusion, this chapter comprehensively covers various AI-based fall detection systems, detailing their accuracy, algorithmic complexity or mathematical cost, adaptability, specificity, and sensitivity of the classifiers. By systematically discussing these aspects for each classifier, this study aims to conduct a comparative analysis. The goal is to address existing gaps and identify the most suitable algorithm for application in the PWR system for elderly fall detection.

CHAPTER 3
RESEARCH METHODOLOGY

3.1 Introduction

This Chapter is a critical section that outlines the approach, techniques, and methods used to conduct the research. It serves as a roadmap explaining how the research was planned, executed, and analysed. Figure 3.1 illustrates the experimental flow diagram of this study. The research commences with data collection, encompassing human fall and fall-like signal data in both single and multiple person scenario, acquired through the use of PWR. A detailed exposition of the data collection process is provided in Section 3.2. Subsequently, the study advances to pre-processing steps in Section 3.3, involving the application of the enveloping algorithm to the raw signal to preserve the Doppler signature inherent in the beacon signal.

Following pre-processing, the enveloped signal undergoes signal transformation through FFT, STFT, and CWT in Sections 3.4. PCA was utilized on the frequency domain obtained through FFT, ensuring the meaningful representation of movement and differentiation across diverse classes within a low-dimensional feature space. Conversely, spectrograms and scalograms, acquired through STFT and CWT, respectively, are input into the feature extraction layers of AlexNet to capture significant features from each image in Section 3.5. Subsequently, the selected features are input into three distinct Intelligence classifier models, namely FFNN, SVM and RF, in Section 3.6. This step facilitates the analysis and comparison of each ML and DL model's performance with respect to the input features.

Ultimately, in Section 3.8, a comparative analysis is conducted on all ML and DL models. Each classifier is scrutinized in terms of accuracy, learning capabilities, and specificity, providing a comprehensive evaluation of their respective performances.

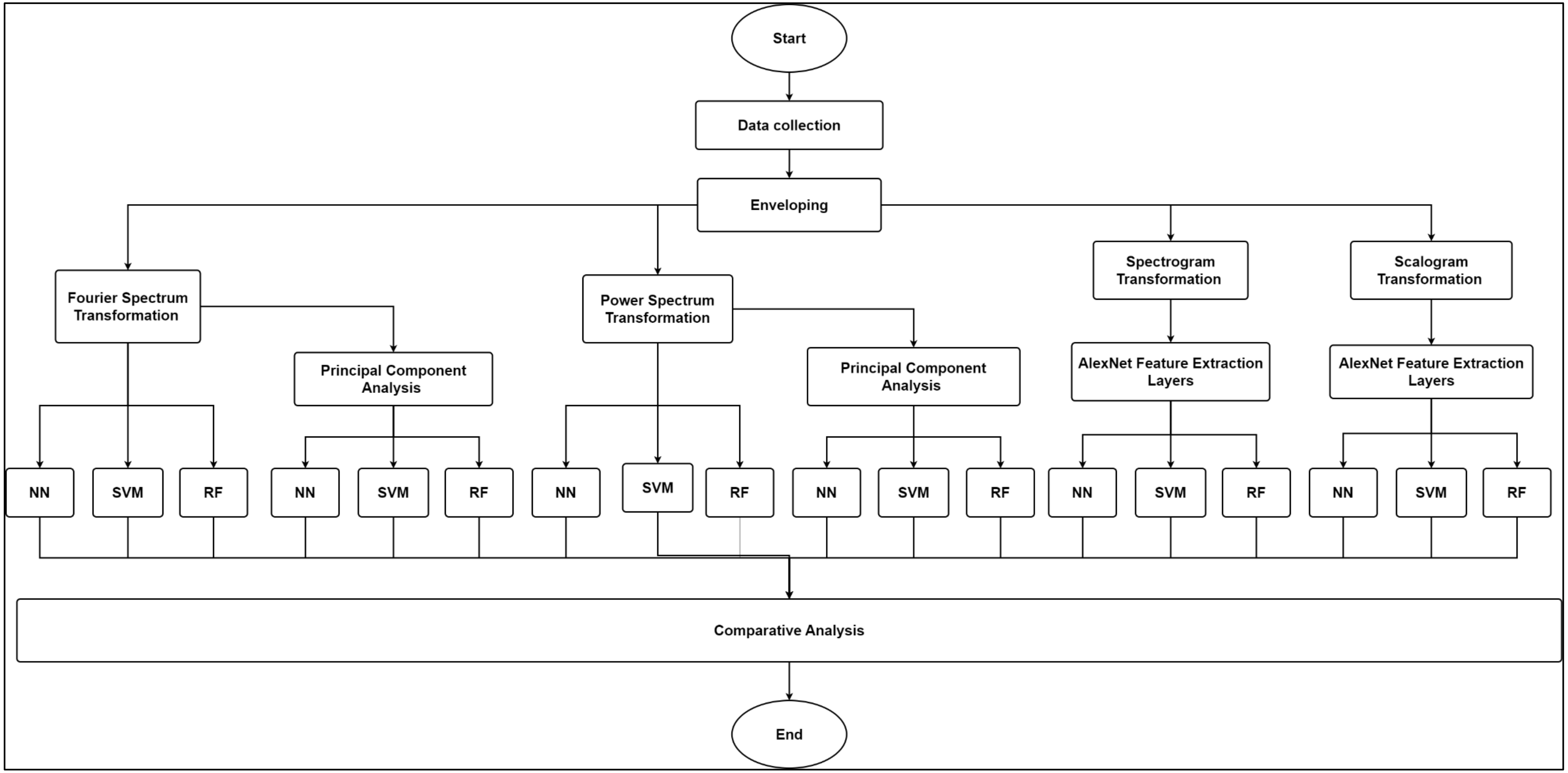

Figure 3.1 Experimental Flowchart for single and multiple person scenario

3.2 Data Collection

The data collection is a process of signal acquisition using the PWR system using the separate transmitter (Tx) and receiver (Rx) mentioned resulting in radar bistatic trajectory. PWR, a technology harnessing extant Wi-Fi signals for movement detection and environmental monitoring, relies significantly on hardware capabilities. The PWR system will works by transmit EM wave using the Wi-Fi router, which are a combination of electric and magnetic fields oscillating in space. However, the Wi-Fi router functions by transmitting beacon signals, which serve the purpose of frame management in wireless networking. These beacons are employed by access points (AP) to announce their presence and convey essential information about the network. Within the IEEE 802.11 standard, governing protocols for wireless local area networking (WLAN), beacons play a crucial role [203]. The beacon signal frames encompass several significant components, including frame control, addresses, and the Basic Service Set Identifier (BSSID). In the context of target detection, the primary components requiring analysis are the timestamp and beacon interval, providing information about when the beacon was transmitted. Similar to other wireless networks, the beacon signal transmission utilizes antennas, giving rise to electric and magnetic fields oscillating in space. Upon signal receiving, these signal trajectories manifest in observable changes in the beacon amplitudes.

3.2.1 Hardware Configuration

In this study, the designated transmitter for the passive Wi-Fi radar is exemplified by the Asus RT-N12+ B1 Wi-Fi router, as illustrated in Figure 3.2. Operating at a frequency of 2.4GHz, this router exhibits a power transmit capability of up to 200mW. Noteworthy features include the inclusion of two omni-directional antennas, affording a comprehensive coverage spanning 360-degree angles. Conversely, the principal hardware element constituting the Passive Wi-Fi Radar (PWR) is the receiver device as presented in Figure 3.3. Comprising an interconnected assembly of an omni-directional antenna, Low Noise Amplifier (LNA), diode detector, Low Pass Filter (LPF), and an oscilloscope, the receiver's components are detailed in Table 3.1.

This antenna, with an operational range of 2.4 to 2.41 GHz, aligns with IEEE 802.11b/g/n standards in the 2.4 GHz ISM band. Its 100 to 700 MHz bandwidth supports multiple Wi-Fi channels, improving resilience against drift and interference. The 2 dBi gain provides balanced coverage, while the omni-directional radiation ensures 360-degree reception, ideal for capturing signals from multiple access points without alignment. With a 10 W power rating, it performs reliably in consumer and industrial settings. The LNA's 20 MHz to 6 GHz range covers both 2.4 GHz and 5 GHz Wi-Fi bands, with 30 dB gain to boost weak signals, though care is needed to avoid saturation near strong sources. Its 17 dBm approximately 50mW power limit may require attenuation for the Wi-Fi output. A 2 dB noise figure minimizes degradation, maintaining SNR for stable communication. The diode detector's 0.1 to 3200 MHz range covers Wi-Fi and other RF signals, with sensitivity of -30 to -40 dBm suitable for low-power detection. It handles up to 20 dBm approximately 100 mW power, making it reliable for RF measurement, signal monitoring, and receiver applications.

Figure 3.2 Asus RT-N12+ B1 Wi-Fi router

Figure 3.3 Receiver device

Table 3.1
Receiver component specifications

Item	Specifications
Omni-Directional Antenna	Working frequency: 2.4 to 2.41GHz Bandwidth:100 to 700 MHz Gain: 2dBi Max Power: 10 W Radiation: Omni-Directional
Low-Noise Amplifier	Working frequency: 20 M to 6GHz Gain: 30dB Max Power: 17dBm Noise Figure: 2dB
Diode Detector	Working frequency: 0.1-3200 MHz Sensitivity: -30 to -40dBm Max Power: 20dBm
Low Pass Filter	Cut-off Frequency: 100hZ
Oscilloscope	Bandwidth: 10MHz Max Sampling Rate: 100MS/s

The receiving antenna of the radar system is designed to capture the scattered electromagnetic waves. As these waves interact with the antenna, they induce an electrical current in the antenna structure. The induced electrical current is then processed to form an electrical signal. This signal represents the variations in the received electromagnetic field over time [204], [205]. Hence, this combination was resulting in a pattern of time domain signal which projecting the signal variations in the electrical current induced in the receiving antenna in voltage (v) along the time or can be gain by mathematical expression as:

$$S(t) = \frac{P_{tx} \cdot G_{tx} \cdot G_{rx} \cdot \lambda^2 \cdot \sigma(\theta_b)}{(4\pi)^2 R_{tx}^2 \cdot R_{rx}^2} \tag{3.1}$$

Where the $S(t)$ is received signal voltage as a function of time, P_{tx} is the transmitted power, G_{tx} and G_{rx} are the antenna gains of the transmitter and receiver, respectively, λ is the wavelength, σ is the radar cross-section (RCS), θ_b is the bistatic angle and the R_{tx} and R_{rx} is the distance between the transmitter and receiver with the target, respectively. Furthermore, with regard to signal projection and acquisition, the oscilloscope was directly interfaced with a computer for visualization through the PicoScope 2204A software. Notably, this software facilitates high-resolution measurements, enabling the precise capture of detailed waveforms. This attribute holds particular significance in applications necessitating exacting data, as exemplified in electronics and control systems. Additionally, the software provides a spectrum of sampling rates, affording users the capacity to tailor the rate according to the specific requisites of their measurements. This adaptability ensures the oscilloscope's efficacy in accommodating diverse signal types and capturing swiftly evolving events.

3.2.2 Sample Selection

The data collection process engaged the expertise of 2 professional stuntmen for fall activities and involved the participation of 10 volunteers for fall-like movements. The participants were deliberately selected to encompass a range of physical sizes with the intent of introducing variability into the data collection process. The selection process for stuntmen demands careful consideration of both skill and health conditions, given the high-risk nature of fall-related activities. Therefore, specific criteria must be met by certified stuntmen, including the absence of physical disabilities, no history of severe health conditions, and no recent medical operations within the past six months. In contrast, volunteers who participate in low-risk activities do not require specific skills or stringent health conditions. However, these volunteers must have diverse body sizes, including variations in weight and height. Additionally, a mix of male and female volunteers (5 male and 5 female) is necessary to account for variability in the study.

Moreover, this study had design to elderly used, hence the data collected must have the elderly movement signature. An age simulation suit had been assessed it performance in order to mitigating the movement of elderly people when perform by middle-aged people. The Gert suit consist of 6 equipment such described in Table 3.2. To simulate elderly movements effectively, the volunteers were equipped with 7 elderly simulation suits. This strategic approach enhances the diversity of the collected data, considering the impact of different physical sizes and the tailored simulation suits for each movement type. Safety considerations dictated the choice of suits for each movement, with specific suits assigned to ensure participant safety and address the impact of the suit on the corresponding fall-like movement. For instance, the sitting movement involved the use of a hunchback simulator, as it does not entail heavy movements on the legs or knees. Conversely, the kneeling movement required volunteers to push their knees down to the ground, necessitating the use of a knee mobility restriction simulator, while avoiding the knee pain simulator due to potential safety risks associated with its iron spike. Additionally, safety concerns precluded the stuntmen from wearing any elderly simulator suits, given the potential risks associated with their performance while equipped with such simulation gear.

Table 3.2
Age Simulator Suit detail

Item	Image	Description
Unsteady gait simulator		• The supplemental soft sole introduces a cushioned sensation, diminishing the sensitivity to floor contact. • The ankle weights introduce additional resistance to movements of the lower extremities. • This combination provides a significantly improved understanding of the elderly walking experience.
Knee mobility restriction simulator		• Due to their reinforced construction with spring steel elements, it is able to simulate knee osteoarthritis even enhanced restrictions.
Knee pain simulator		• Utilizing in-built spring steel elements combined with integrated spiking steel, this system effectively replicates increased constraints on mobility. Furthermore, it employs internal stimulus elements that act on the skin's surface to simulate knee pain in a harmless yet highly effective manner.

Hunchback simulator		• By tightening the strap at the back, a posture mimicking a hunchback is induced. This is a result of the force exerted by the strap, which pushes the shoulders downward.
Walking stick		• Through the distribution of weight and the consequent reduction of strain on the legs and joints, notably the knees, the user will encounter heightened pressure on the palms while walking.

3.2.3 Trajectories

Human movement can affect the amplitude of a time-domain signal in various ways, such as through the change in RCS. As a person moves, different parts of their body present different RCS to the radar system. The RCS is a measure of how well the target reflects radar signals. Changes in the effective radar cross-section of the moving human can result in variations in the amplitude of the received signal. Besides, human movement in an environment with reflective surfaces can cause multipath reflections. These reflections can interfere constructively or destructively, leading to changes in the amplitude of the received signal [206], [207].

As a person moves, the positions of the reflecting surfaces and the path lengths of the multipath signals may change, causing fluctuations in amplitude. The utilization of PWR in indoor target detection offers distinct advantages, particularly evident in the FSR region such in Figure 3.4. In FSR, the scattering of radar signals primarily occurs in the forward direction, delineated as the path from the radar transmitter to the target and subsequently back to the radar receiver. This unique phenomenon results in a lowered RCS due to the minimal obstruction of the direct leakage signal between the transmitter and the receiver by the target. The efficacy of FSR is especially pronounced when the bistatic angle approaches 180 degrees, signifying close alignment between the transmitter, receiver, and the target. At this configuration, the RCS is notably diminished since the target allows the leakage signal to pass through unimpeded, minimizing the shadow power which defined as the power subtracted from the leakage signal by the target.

Consequently, when the bistatic angle is precisely 180 degrees, the target becomes aligned with both the transmitter and the receiver, resulting in shadow power and RCS approaching zero. However, as the bistatic angle deviates slightly from 180 degrees, the target begins to obstruct the leakage signal, leading to increased shadow power and RCS [208]. This effect is particularly pronounced within the FSR region, generating significantly higher shadow power and RCS values compared to regions outside this specific angle range. this phenomenon having a direct relationship with Δf where when the θ_b is equal to 180, the $\cos\theta_b$ will resulting in 0 value.

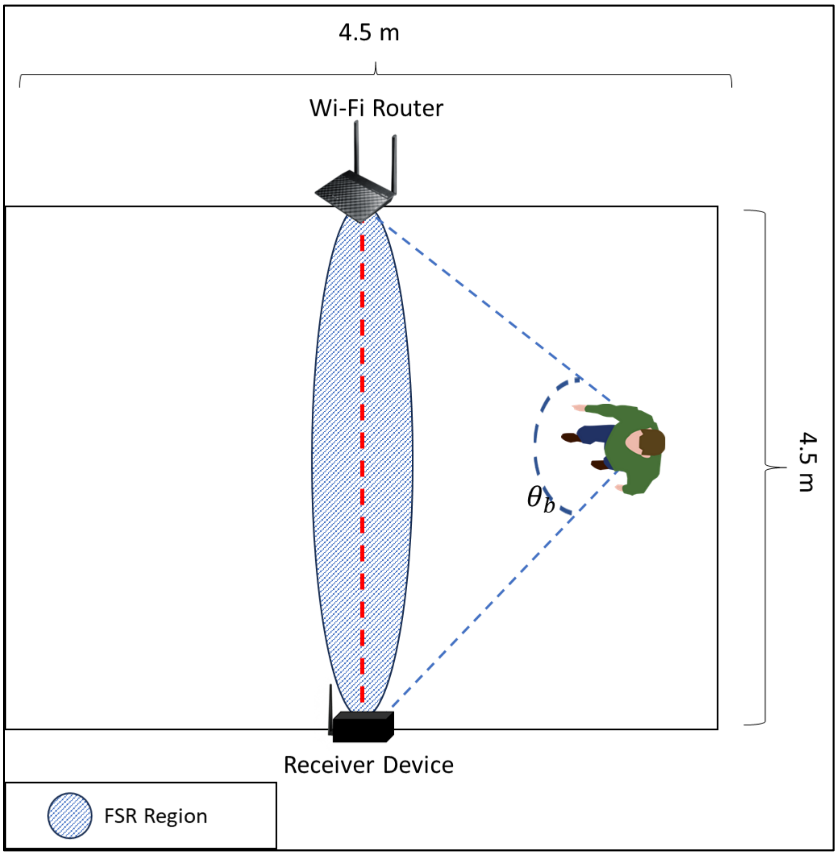

Figure 3.4 FSR Region in PWR

The signal transmission and reception configuration have been designed to facilitate the collection of signal propagation data within a confined space measuring 4.5m x 4.5m, as depicted in Figures 3.5. This spatial dimension aligns with standard room sizes [209] and is chosen to evaluate the signal's effectiveness throughout the designated area. The chosen of wooden tables at the same elevation for the placement of Tx and Rx is to minimize the impact on the collected data. Wood, as a dielectric material with low electromagnetic reflectivity, produces weak reflections that reduce multipath interference and clutter. However, some multipath propagation may still occur due to surrounding objects. Partial obstruction of the line of sight by the table or other objects can lead to attenuation or shadowing, especially for signals at low incidence angles. While consistent direct path alignment preserves phase coherence, careful positioning is essential to avoid obstructing the antennas' field of view. Overall, with thoughtful placement, the wooden table has a limited effect on data collection, but slight multipath effects and shadowing should be considered as a noise and does not impact the human movement amplitude modulation signatures.

As presented in Figure 3.6, single-target data were collected at three different angles within the same location to introduce multiple variations in the collected data. The variation of 45°, 90°, and 135° angles ensure comprehensive coverage of human movement. At 45°, partial frontal and side views capture transitions in motion. The 90° angle maximizes signal blockage enhancing sensitivity to human movements. The 135° angle provides rear-scatter data, capturing motion from behind. Together, these angles reduce blind spots, maximize scattering diversity, and improve movement detection and classification. This deliberate approach aims to enhance the classifier's ability for generalization and pattern learning, focusing on the significant features of the collected signals. Conversely, double-target data collection employed a distinct strategy where one individual performed a fall movement at location 1, while another individual executed fall-like movements at either location 2 or location 3, as illustrated in Figure 3.7. This approach introduces diversity in the dataset by incorporating different scenarios of fall-related movements. For triple-target detection, the fall movement was executed at location 1, while fall-like movements were simultaneously performed at locations 2 and 3. This setup aims to capture and analyse complex scenarios involving multiple persons within the defined space. The decision to confine the performing of fall-like movements exclusively to the right-hand side was based on the outcome of achieving identical values for θ_b, R_{tx} and R_{rx} which resulting in mirror effect. This can be observed on through Figure 3.8 where the same $\theta_b 1$, $R_{tx} 1$ and $R_{rx} 1$ was identical to the same $\theta_b 2$, $R_{tx} 2$ and $R_{rx} 2$, respectively.

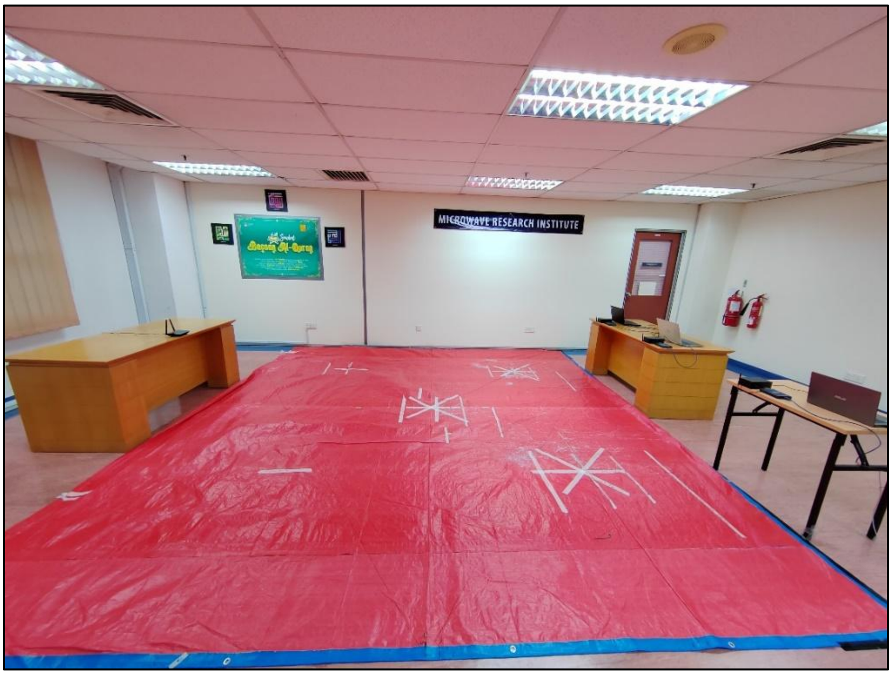

Figure 3.5 Data Collection location

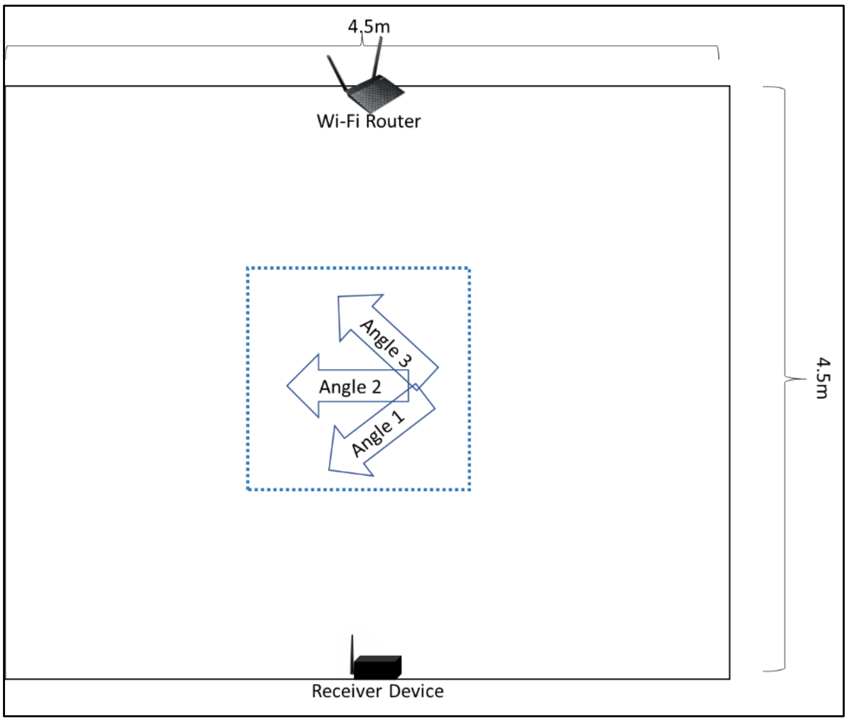

Figure 3.6 Data Collection configuration for single person scenario

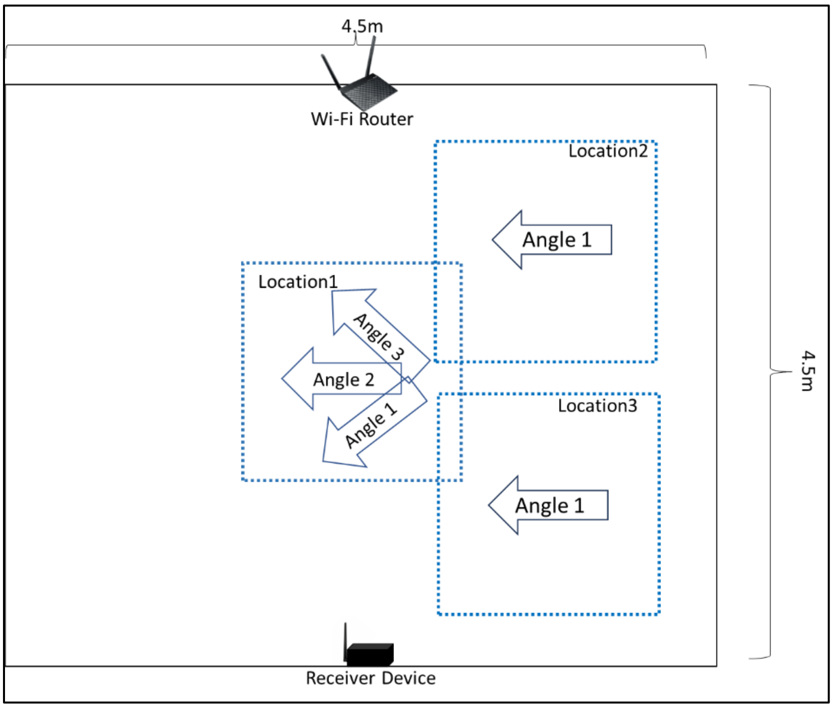

Figure 3.7 Data Collection configuration for multiple person scenario

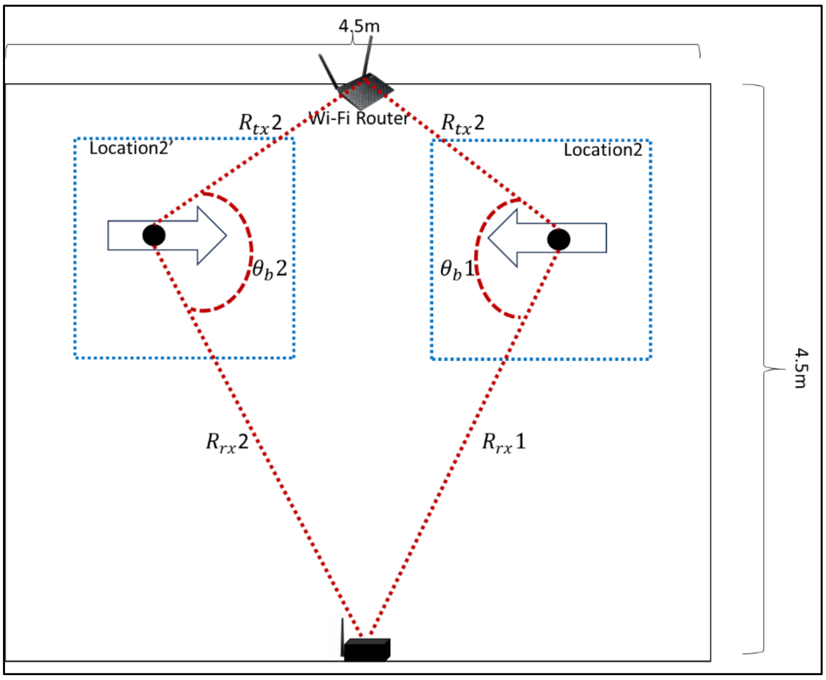

Figure 3.8 Symmetrical effect of right-hand side and left-hand side of bistatic radar.

3.2.4 Protocol

The data collection encompasses 11 distinct types of movements, with 5 of them corresponding to fall activities, including walking and falling, sitting and falling, slipping, stumbling, and fainting such illustrate in Figure 3.9. The remaining 6 movements involve sitting on a chair, bending, kneeling, lying on a bed, squatting, and prostrating as in Figure 3.10. For single-target detection, these movements are categorized into 6 classes, each representing a specific fall movement, and one class for fall-like movements defined as the movement that shared some characteristic of falls. The distribution of repetitions for each movement at various angles ensures a balanced dataset for single-target detection, as detailed in Table 3.3.

Moreover, in double-target detection, only 5 classes are considered, each denoting a fall class movement. Each class combines the fall movement with one fall-like movement, resulting in 6 distinct combinations for fall and fall-like movements, as outlined in Table 3.4. Meanwhile, triple-target detection introduces 15 different variants in each class, with each type of fall performed in conjunction with 2 distinct fall-like movements, as specified in Table 3.5. This configuration aims to capture diverse and complex scenarios involving multiple persons. All data were collected over a 20-second period, allowing sufficient time to capture slow movements typical of elderly individuals. A sampling rate F_s of 1000 samples per second was specifically selected to ensure precise detection of beacon signals occurring at f_{beacon} of 10 Hz. This sampling rate is critical for capturing the signal peaks, as a lower rate could risk missing these peaks and higher would also introduce unnecessary computational costs. By aligning F_s with the beacon signal frequency, we optimize data integrity while efficiently managing processing requirements. This meticulous approach is undertaken to facilitate an in-depth analysis of movements, especially those relevant to the elderly population, and to align with the characteristics of the beacon signals under consideration.

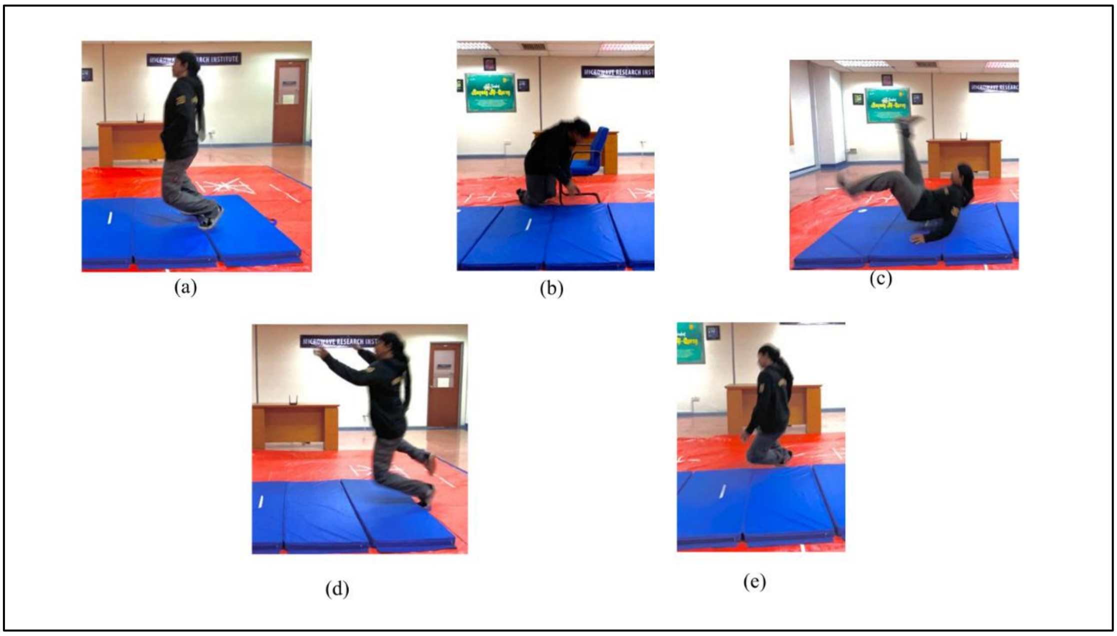

Figure 3.9 Fall Activities. (a) Walk and Fall (b) Sit and Fall (c) Slip and Fall (d) Stumble (e) Faint

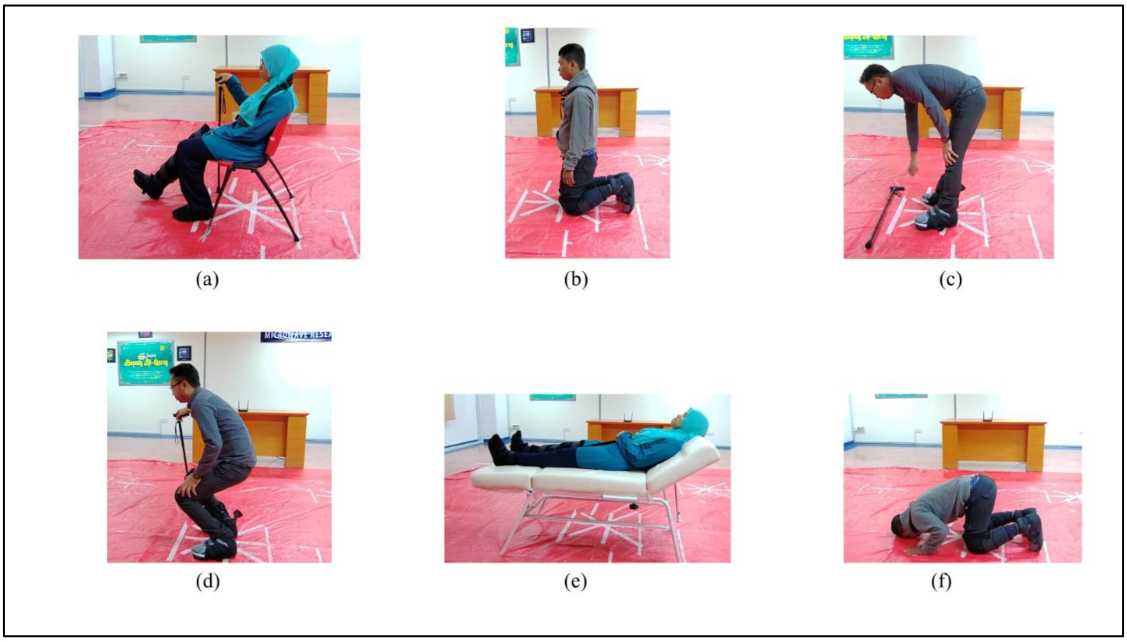

Figure 3.10 Fall-like Activities. (a) Sitting (b) Kneeling (c) Bending (d) Squatting (e) Laying (f) Prostrating

Table 3.3
Single person scenario data specification

Type of Activities	**Movement**	**Repetitions each angle**	**Cumulative signal**
Fall	Walk and fall	30	90

	Sit and fall	30	90
	Slip and fall	30	90
	Stumble	30	90
	Faint	30	90
Fall-Like	Sitting	5	15
	Kneeling	5	15
	Bending	5	15
	Squatting	5	15
	Laying	5	15
	Prostrating	5	15

Table 3.4
Double person scenario data specification

Type of Fall Movement	Type of Fall-like Movement	Repetitions each angle (Fall)	Cumulative signal
Walk and Fall/ Sit and fall/ Slip and fall/ Stumble/ Faint	Sitting	6	18
	Kneeling	6	18
	Bending	6	18
	Squatting	6	18
	Laying	6	18
	Prostrating	6	18
Cumulative signal for each Fall movement			108

Table 3.5
Triple person scenario data specification

Type of Fall Movement	Type of Fall-like Movement	Repetitions each angle (Fall)	Cumulative signal

	Sitting + Kneeling	2	6
	Sitting + Bending	2	6
	Sitting + Squatting	2	6
	Sitting + Laying	2	6
	Kneeling + Prostrating	2	6
	Kneeling + Bending	2	6
	Kneeling + Squatting	2	6
Walk and Fall/ Sit and fall/ Slip and fall/ Stumble/ Faint	Kneeling + Laying	2	6
	Kneeling + Prostrating	2	6
	Bending + Squatting	2	6
	Bending + Laying	2	6
	Bending + Prostrating	2	6
	Squatting + Laying	2	6
	Squatting + Prostrating	2	6
	Laying + Prostrating	2	6
Cumulative signal for each Fall movement			90

3.3 Enveloping Algorithm

Following the data collection phase, the acquired signals were expected to manifest in the form of beacon signals, necessitating preprocessing algorithms before being treated as continuous signals within the human target detection system, as elucidated in Sections 2.5 and 2.6. As discussed in Section 2.4, several methods have been successful in preprocessing beacon signals, with the enveloping algorithm emerging as the most efficient approach.

3.3.1 Noise reduction

The preprocessing procedure commenced with noise filtering utilizing a thresholding approach. This algorithm effectively eliminates noise below a specified threshold value, making the careful selection of this threshold paramount. Given that the sampling frequency, F_s, at 1 kHz, while f_{beacon} at 10 Hz, noise tends to appear more frequently compared to significant amplitudes. To address this, the threshold value was determined through a moving variance, $MV(k)$, which adapts to local changes in the signal, making it useful for signals with varying noise levels. Additionally, this algorithm is effective in detecting sudden changes in the data, which can indicate noise threshold levels. The algorithm was employed with a 0.1s window to optimally find the noise level for each beacon, expressed as:

$$MV(k) = \frac{1}{N-1}\sum_{i=1}^{N} |x(k-(i-1)\cdot\Delta t) - MA(k)|^2 \tag{3.1}$$

$$MA(k) = \frac{1}{N}\sum_{i=1}^{N} x(k-(i-1)\cdot\Delta k) \tag{3.2}$$

$MA(k)$ is defined as the mean at each particular window which can be expressed as the equation 3.2, the N was the number of data point in a window size, such in this case in 0.1s window, there were 500 data point and Δk was the time difference between consecutive data points.

3.3.2 Enveloping Algorithm

Following the noise removal process, the subsequent step involves the enveloping algorithm, crucial for ensuring accurate detection of signal signatures by mitigating the impact of any remaining noise. Before executing the enveloping algorithm, it is essential to identify key parameters, specifically for the used of PWR such the total number of peaks considered, N_{peak} and the distance between each peak, Δd_{peak}. Both the parameters can be obtained by the following mathematical expression.

$$N_{peak} = f_{beacon} * duration \tag{3.3}$$

$$\Delta d_{peak} = F_s * \frac{1}{f_{beacon}} \tag{3.4}$$

The original enveloping algorithm, $E(t)$ applied to a radar signal, represents the maximum signal strength, A_0 which governs the amplitude of the received signal as it completes one full oscillation. The period to complete one full oscillation called T which determines the frequency of these oscillations, while the phase shift, φ defines the initial starting point of the oscillation with respect to time, as expressed in Equation 3.5. With the applied conditions, the period has been replaced by Δd_{peak} corresponding to the distance between peaks, and the phase shift has been replaced by N_{peak} representing the number of peaks in the signal. This transforms the original algorithm to account for spatial peak distribution on discrete peaks were shown in Equation 3.6.

$$E(t) = A_0 \sin \frac{2\pi}{T} t + \varphi \tag{3.5}$$

$$E(n) = A_0 \sin \frac{2\pi n}{\Delta d_{peak}} \; for \; n = 0,1,2, \dots, N_{peak} - 1 \tag{3.6}$$

Hence by setting this criterion, the peak was being found the max amplitude in between until the total number of N_{peak} being selected. The peak detection algorithm works by detect a data point, x_i that the value is larger than the value of data point before, x_{i-1}, and after, x_{i+1}. By applying the established criteria, the peak identification process involves detecting the maximum amplitude within each interval of Δd_{peak} until the total number of N_{peak} peaks are identified. The peak detection mechanism operates by identifying a data point x_i where the value is greater than both the value of the data point before it, x_{i-1}, and the value of the data point after it, x_{i+1}. This algorithm of peak detection ensures that only significant peaks in the signal are considered, contributing to the signature of the signal that contains human signal's amplitude signature and shadow compression.

3.3.3 Comparative Analysis with Continuous Wave Radar

Given that the PWR radar was not originally designed for human target detection, it is essential to conduct a comparative analysis with an active radar to validate the collected Amplitude modulation signatures. The selected active radar for comparison was a bistatic CW radar, which shares similar signal propagation with the PWR, ensuring a more meaningful comparison but different formation of signal. The CW was constructed using components including an Arduino Nano, nRF24L01 module, and an omnidirectional antenna, which continuously transmitted signals at 2.4GHz as depicted in Figure 3.11. The choice of transmission frequency and antenna was deliberate to closely resemble Wi-Fi transmission signals, aimed at mitigating interference and achieving relevant comparisons with the PWR's signals.

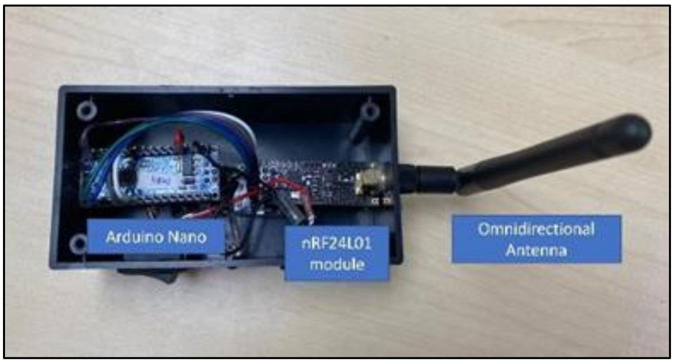

Figure 3.11 CW hardware configurations.

The signal collected using the CW was limited to three types of fall-like movements: sitting, bending, and kneeling, with 36 repetitions of each activity. The dataset size was relatively small due to the preliminary nature of this comparative analysis, which served as a pilot study to validate whether the enveloping algorithm could effectively capture human movement patterns. These data were not further analysed beyond this initial validation.

To compare the patterns of the PWR signal and the CW signal, both signals underwent preprocessing algorithms. For the CW signal, a smoothing algorithm was applied to generate a continuous form of the signal. Specifically, the Savitzky-Golay algorithm with a window size, N of 0.1 second was utilized on the raw signal. The Savitzky-Golay filter, y_i achieves smoothing by fitting a polynomial of degree m to the input signal within a sliding window of specified size, x_{i+j}. This smoothing process can be understood using the following equation:

$$y_i = \frac{1}{N}\sum_{j=0}^{m} c_j\, x_{i+j} \tag{3.7}$$

Here the c was the polynomial coefficients which was set to 1 or can be determined using least squares regression. The Savitzky-Golay algorithm effectively reduces noise and sharp variations in the signal, producing a smoother version suitable for the analysis and comparison.

3.4 Signal Transformation

After obtaining the enveloped signal, which encapsulates clean and significant information about human movement, the signal undergoes a signal transformation process to enhance and project it into a more informative domain. The transformation involves considering the Doppler effect, wherein the frequency of the reflected signal experiences changes when a human is in motion [206]. The Doppler effect does not directly affect the amplitude in the time domain, but it can influence the signal's frequency content. If the radar system is sensitive to Doppler shifts, Δf the moving human will cause periodic variations in the signal, potentially leading to changes in the amplitude of the signal over time. Assume the v is the velocity between the target and radar system, and the f_d can be express using a mathematical equation as:

$$f_d = \frac{2v}{\lambda}\cos\theta_b \tag{3.8}$$

However, the analysis of f_d cannot be conducted directly on the time-domain signal since it lacks frequency content information. Therefore, the signal must undergo a transformation into the frequency domain. Several widely used signal transformation methods are available, including FFT, STFT, and CWT. Each of these methods provides unique insights into the frequency characteristics of the signal, enabling a more comprehensive understanding of the variations induced by the Doppler effect during human motion.

3.4.1 Fast Fourier Transform

The FFT serves as a widely employed technique for extracting Doppler signatures' characteristics. Doppler signatures are obtained by evaluating the frequency shift displayed by a wave due to the relative motion between the source and the observer. FFT facilitates the transformation of time-domain Doppler signals into the frequency spectrum which can help in analyse in measuring the amplitude depth across the signal, akin to the application of DFT, expressed as:

$$X(k) = \sum_{n=0}^{N-1} x(n) e^{-j\frac{2\pi nk}{N}} \tag{3.9}$$

Where the $X(k)$ is the magnitude of frequency bin k, $x(n)$ is the signal at the sample bin n and N is the total number of samples. The FFT algorithm computes the same equation in more efficient way by decomposing into a multiplication of sparse factors, where the majority of the factors are zero. Indirectly it can reduce the operation and complexity from N^2 to $N \log_2 N$.

The mathematical equation of the DFT illustrates that the amplitude values are directly proportional to the actual magnitudes of the frequency components, expressed in volts. This representation offers a direct correlation between voltages and the energy distribution of the signal across the frequency spectrum. Such a mapping facilitates the identification and extraction of significant data related to the velocity, direction, and characteristics of mobile entities or phenomena. In the context of radar systems, the FFT is employed to analyse the Doppler signatures of objects in motion relative to the radar antenna. By scrutinizing the frequency components present in the received signal, it becomes possible to determine the velocity, direction, and size of the mobile target, providing valuable insights into the dynamics of the observed motion.

On the contrary, the dB scale is a logarithmic scale employed to represent magnitude or power ratios. Commonly utilized in signal processing applications, it aligns more closely with human perception of loudness and dynamic range. The dB scale offers a more concise and meaningful depiction of a broad spectrum of values. To transition from a linear scale to a dB scale in the context of FFT, amplitude values are converted to dB using a logarithmic function with a base of 10 [210]. This conversion compresses the dynamic range of amplitudes, facilitating more straightforward visualization and comparison of components with diverse magnitudes. The application of a dB scale yields several advantages. It improves the visibility of small or weak signals that might be obscured on a linear scale. Additionally, it simplifies the identification of significant frequency peaks and facilitates the assessment of relative differences in magnitude among various frequency components.

3.4.2 Short Time Fourier Transform

On the other hand, spectrogram is a time-frequency feature that visual representation of the frequency content of a signal over time. It is obtained by applying the STFT and calculating the magnitude and phase information of the resulting frequency components. The STFT is almost alike the FFT, but the Fourier transformation was segmented into a short period of time or called windowed instead transform the whole-time domain data at once which help in analysing modulation of amplitude frequency changes over time [211]. This transformation can avoid any misleading information that occurs in a short period of time. Therefore, the optimum window size is an important account in order to extract the accurate features for fall movement. Thus, the selection of the Gaussian function, characterized by its smooth and continuous bell-shaped curve, helps reduce spectral leakage, which is the spreading of spectral energy into adjacent frequency bins. Its small size aids in preserving the Doppler signature of fall movement. The Gaussian window has significantly lower sidelobe levels than the Hamming window, which is beneficial for reducing spectral leakage and interference from adjacent frequencies.

Additionally, the Gaussian window offers superior time-frequency localization, making it more suitable for analysing signals with varying frequency content, such as the human Doppler signature. For preserving the human Doppler signature in forward scattering radar using STFT, the Gaussian window is generally better than the Hamming window. Its superior frequency resolution, minimal sidelobe levels, and excellent time-frequency localization make it more effective in capturing the detailed variations of the amplitude modulation signature caused by human movement. This ensures that the nuances of the Doppler shifts, crucial for identifying and analysing human motion, are preserved more accurately [212]. The Gaussian function can be defined mathematically as:

$$w(n) = e^{-\pi\alpha n^2} \tag{3.10}$$

where $w(n)$ represents the value of the window at sample index n, and α is a parameter that determines the width or spread of the window. Furthermore, the size of the window in seconds can be translated into how many data point has involved in each window, N by multiple the window size in seconds with the sampling frequency.

Next, the movement of the window also must be considered in order to gain image features that have accurate information without missing any of them. The presence of high-speed movement, most of the researchers such as in [213] applied a sliding window which is the window will move continuously from one data point to the next data point. Hence the overlapping size of window can be obtained by $N - 1$. Afterwards, each segment of the signal needs to be multiplied with the corresponding window function to reduce spectral leakage effects. Denote the windowed segment as $xw(n)$, the mathematical expression as follows:

$$xw(n) = x(n)w(n) \tag{3.11}$$

Hereafter, the DFT will be applied to each of the $xw(n)$ and transform the DFT equation into a mathematical equation as follows:

$$x(k) = \sum_{n=0}^{N-1} xw(n)e^{-j\frac{2\pi nk}{N}} \tag{3.12}$$

As result, the STFT coefficients are represented in a complex-valued matrix, where the real part, $Re(x(k))$, represents the amplitude and the imaginary part, $Im(x(k))$, represent the phase of a particular frequency content at a particular time segment. To obtain the spectrogram, $p(k)$, the magnitude of each element in the STFT matrix must be computed and represented in terms of power. This is achieved by taking the absolute value of each complex number in the STFT matrix and squaring these absolute values, as expressed in equations 3.13 and 3.14, respectively.

$$|x(k)| = \sqrt{(Re(x(k)))^2 + (Im(x(k)))^2} \tag{3.13}$$

$$p(k) = |x(k)|^2 \tag{3.14}$$

The magnitude of the spectrogram shows the strength or amplitude of each frequency component in the signal at various time intervals. Brighter colours denote higher magnitudes on a colour scale, which is frequently used to illustrate it. By providing details about the energy distribution across various frequencies, the magnitude spectrum enables to pinpoint the key frequency components that evolve over time. In contrast, the spectrogram phase shows the phase connection between the signal's various frequency components.

3.4.3 Continuous Wavelet Transform

Same to the spectrogram, the product of the scalogram is projected in time-frequency features but the transformation used is the wavelet transform instead of Fourier transform. The CWT transformed the time-domain signal using mother wavelet function which typically used was Morse, Morlet and Bump wavelet such presented in [214], [215]. The Morlet wavelet is widely used due to its balance between time and frequency localization [216]. It provides both modulus and phase information, making it suitable for various signal processing applications [216]. However, the bump wavelet offers better frequency localization than the Morlet wavelet due to its bandlimited nature [217]. On the other hand, the Morse wavelet exhibits high oscillatory behaviour, which makes it well-suited for capturing and analysing signals with oscillatory components such the signal captured in this experiment. It provides excellent time-frequency localization for signals with sharp and rapidly varying features. Besides, it also has a high concentration of energy in both time and frequency domains, which means it provides excellent localization properties. It can accurately pinpoint the time and frequency information of localized features within a signal [218], [219].

The Morlet wavelet, despite being a common choice, has limitations such as leakage to negative frequencies when time resolution is increased [220]. In contrast, the Morse wavelets remain analytic even with highly time-localized parameter settings [220]. Additionally, the Morse wavelet family provides a systematic framework for selecting and generating wavelets for various applications [221]. In essence, while the Morlet wavelet is a popular choice for its versatility and widespread use, the Morse wavelet stands out for its improved time and frequency localization benefits, making it a favourable option for applications requiring precise feature extraction in the time-frequency domain.

The Morse wavelet's parameters, such as the bandwidth parameter σ and the shape parameter γ, provide additional flexibility in adapting the wavelet to different signal characteristics. These parameters allow customization of the wavelet to match the oscillatory behaviour of the signal being analysed. The Morse wavelet Function, $\psi(t)$ can be expressed mathematically as follows:

$$\psi(t) = \left(\frac{2\pi\sigma}{\gamma^{\gamma}}\right)^{\frac{1}{2}} * k^{\gamma-1} * \exp(-\pi\sigma k^2) * \exp\,(2\pi i\beta k) \qquad (3.15)$$

Where the i is the imaginary unit and the $\beta = \frac{\gamma}{\sigma}$. This mathematical representation of $\psi(t)$ shows that the γ and σ play a crucial role in the transformed signal. Since fall is a unique movement, hence the frequency resolution needs in extract the features must be in high resolution. The selection of $\sigma = 60$ is a sufficient to gain a high frequency resolution but it will cost at reduced time resolution. This parameter works same as the window size in the STFT algorithm where shorter windows provide better time resolution but poorer frequency resolution. Meanwhile, to avoid the wavelet transform captured the excessive oscillatory behaviour that might appear because of noise, the γ is set to 3. It is the moderate level of oscillatory behaviour, which can effectively capture signals with moderate oscillatory components.

However, this function been discretized for practical implementation to reduce the computational complexity compared to the continuous version. Computing the

CWT at all possible scales and translations in the continuous domain can be computationally expensive and impractical, especially for long signals or high-resolution analysis. Discretization allows us to focus computations only on the desired scales and translations, making it more efficient. Discretize the time axis from input signal into a set of discrete time points, typically denoted as n = 1, 2, ..., N.

Next, the discretized CWT perform by convolving the input signal $x(k)$ with the $\psi(k)$ across different scales, a and translations, b. This transformation is given by:

$$\mathrm{CWT}(a,b) = \sum_{n=1}^{N} x(k) * \psi\left(\frac{n-b}{a}\right) \tag{3.16}$$

In order for the aim to detailed frequency analysis across the signal, the number of wavelets used to cover each octave of frequency in the wavelet transform was used 10 per octave means that the frequency range of the signal is divided into 10 sub-bands for analysis, each covering one-tenth of the total frequency range.

As the CWT generates a scalogram, which can be visualized as an RGB image, each pixel having its own information such the dark colours typically represent low amplitude or small magnitude of CWT coefficients. These areas in the plot correspond to parts of the signal where the wavelet transform did not find a significant presence of the analysed frequency at that specific time and scale. Meanwhile, the bright colours representing the high amplitude or large magnitude of CWT coefficients. These regions correspond to points in the time-frequency plane where the analysed frequency is present with considerable strength. Besides, the colour intensity or saturation of the colours represents the magnitude of the CWT coefficients. More intense or saturated colours indicate higher magnitudes, while less intense or desaturated colours represent lower magnitude.

In summary, these signal transformation methods, including FFT, STFT, and CWT, play crucial roles in extracting and interpreting Doppler signatures from human movement signals, offering valuable insights for applications such as radar systems and motion analysis. The choice of the transformation method depends on the specific requirements of the analysis, including the need for time or frequency resolution and the characteristics of the signal under investigation.

3.5 Features Selection

The Feature selection involves choosing a subset of relevant features from a larger set of variables, aiming to enhance model performance, interpretability, and computational efficiency [222]. This process is crucial because not all features contribute equally to the predictive task at hand. Some features may be redundant, irrelevant, or even noisy, introducing unnecessary complexity and potentially hindering model generalization. Feature selection methods address this challenge by identifying and retaining the most informative attributes, allowing models to focus on the most discriminative aspects of the data.

The objectives of feature selection are diverse. Primarily, it helps address the challenge of dimensionality, a common issue when dealing with datasets containing a large number of features. By selecting only the most influential variables, feature selection aids in creating more parsimonious models that are less prone to overfitting and are better equipped to generalize to new, unseen data [223]. Moreover, feature selection contributes to model interpretability. Simplifying the input space by excluding irrelevant or redundant features facilitates a clearer understanding of the relationships between variables and the model's decision-making process. This interpretability is crucial in scenarios where transparency and explain ability are paramount.

As the landscape of data-driven applications continues to evolve, the significance of feature selection becomes increasingly evident. It not only contributes to the efficiency and interpretability of classification models but also holds the potential to unlock valuable insights from complex datasets, making it an indispensable step in the data preprocessing pipeline. This had introduction sets the stage for a deeper exploration of various feature selection techniques and their applications in improving the performance and interpretability of classification models such PCA where the features dimension being reduced. Meanwhile, for image-based features, feature extraction layers of AlexNet will process and transform the image into a set of significant numerical value that used as input to the classifiers [224].

3.5.1 Principal Component Analysis

Next, the PCA is a commonly employed method in the fields of data analysis and machine learning for the purpose of reducing the dimensionality of a dataset. This technique aims to convert a dataset with a high number of dimensions such in this experiment, deploy the Fourier and power spectrum features that contains $N/2$ frequency index according to Nyquist frequency in into a lower-dimensional space by referring to the number of principal components that give a cumulative variance of at least 95%. This threshold is considered significant as it ensures that the retained principal components capture a substantial portion of the variability present in the original dataset. When conducting PCA, the objective is to identify the principal components that explain the maximum variance in the data [225]. By retaining components that collectively account for 95% or more of the total variance, researchers can effectively summarize the dataset while minimizing information loss. This threshold ensures that the retained components capture the essential patterns and structures present in the data, facilitating meaningful interpretation and analysis [226].

The PCA performs by acquiring the eigenvalue and eigenvector of the covariance matrix. Denotes that the data that need to be observed are in row, x and the variable are in column, y and n is the total number of variables to be observed, hence the covariance matrix can be gained by repeating the following equation until each pair of variables in the dataset were considered to obtain a square matrix with sizes of the variables [227], or can be express as follows:

$$cov(x, y) = \frac{\sum_{i=1}^{n}(x - \bar{x})(y - \bar{y})}{n - 1} \tag{3.17}$$

The covariance matrix is a mathematical representation in a matrix format, that summarizes the relationships and covariations between all the variables in a dataset which provides valuable insights into the interdependencies and associations among the variables. Next, the eigenvalue, λ and its eigenvector, v can be gained by performing the eigen decomposition as the mathematical equations as follows:

$$\det(A - \lambda \mathrm{I}) = 0 \tag{3.18}$$

$$(A - \lambda \mathrm{I})v = 0 \tag{3.19}$$

Where A is the covariance matrix with size and I is the identity matrix with the same size as the covariance matrix. As the aim are to choose the PC that gives a sum of variance explaining 95% and above and also reduce the dimension of the features, the eigenvector was sorted according to the corresponding eigenvalue in descending order and then was chosen based on the PC that achieves the sum desired variance. Finally, to project the original data into a lower-dimensional space using PCA, multiply the data matrix by the transformation matrix. This produces the projected data, which has reduced dimensions. In the lower-dimensional space, each observation is represented by its coordinates based on the principal components. Up to this point, the study has introduced two additional sets of features, namely the PCA-Fourier spectrum and the PCA-power spectrum. These feature sets are derived through dimensionality reduction techniques, and their incorporation aims to explore the impact of reduced dimensions on the effectiveness of feature representation.

3.5.2 AlexNet Feature Extraction Layer

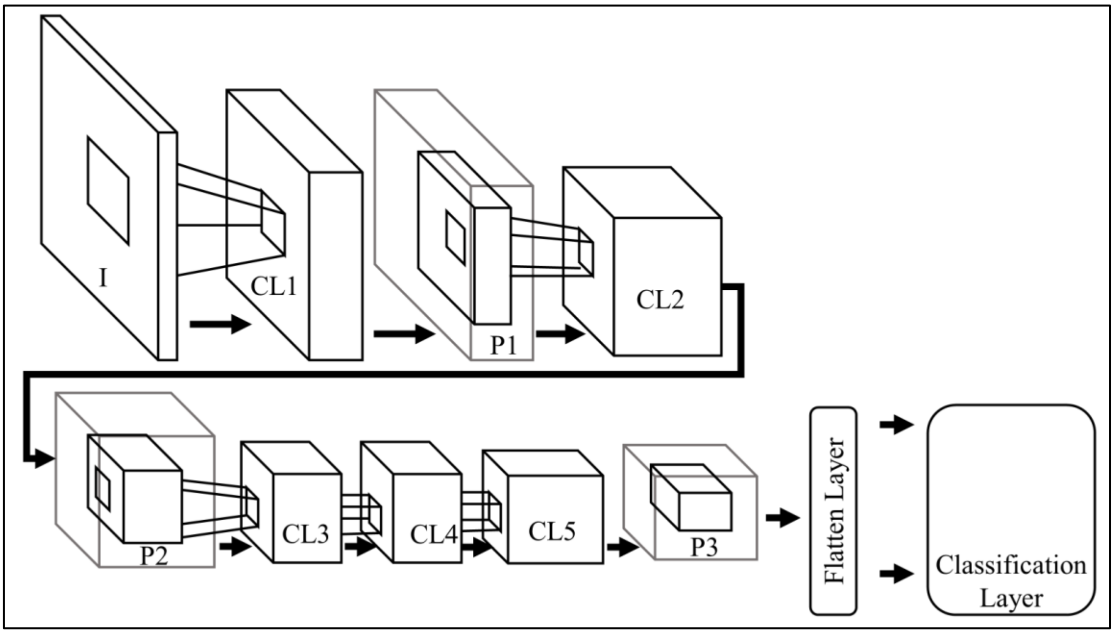

Figure 3.12 AlexNet feature extraction layers

Having completed the analysis of the Fourier and power spectrum, this phase involves feature extraction from the scalogram and spectrogram. This step is pivotal in deriving meaningful numerical features from the image-based representations of the data, providing a basis for further analysis and comparison with the previously examined feature sets. To extract and select the features from the images, the AlexNet features extraction layers that contain 5 convolutional layers with 3 max pooling layers located at in between first and second, second and third and after the fifth convolutional layer and also a flatten layers located at end of the structure such presented in Figures 3.12 and described in Table 3.6.

Table 3.6
AlexNet feature extraction layers specifications

Layers	Parameters	Value
Input Layer (I)	Input size	224x224x3
Convolutional Layer 1 (C1)	Filter size	11x11
	Number of filters	96
	Stride	4
	Output size	55x55x96
Max pooling 1 (P1)	Pooling size	3x3
	Stride	2
	Output size	27x27x96
Convolutional Layer 2 (C2)	Filter size	5x5
	Number of filters	256
	Stride	1
	Output size	27x27x96
Max pooling 2 (P2)	Pooling size	3x3
	Stride	2
	Output size	13x13x256
Convolutional Layer 3 (C3)	Filter size	3x3
	Number of filters	384
	Stride	1
	Output size	13x13x384
Convolutional Layer 4 (C4)	Filter size	3x3
	Number of filters	384
	Stride	1
	Output size	13x13x384
Convolutional Layer 5 (C5)	Filter size	3x3
	Number of filters	256
	Stride	1
	Output size	13x13x256
Max pooling 3 (P3)	Pooling size	3x3
	Stride	2
	Output size	6x6x256

In each convolutional layer, there exists a filter, also referred to as a weight, W, which undergoes optimization during the training process to become sensitive to specific patterns, edges, textures, or features present in the data. This filter is then convolved with the input features, resulting in the operation $conv(x, W)$. Additionally, another set of parameters optimized during training to enhance image feature extraction is the bias term, B. The bias term introduces a shift or offset to the output of the convolutional layer, enabling the model to capture information that may not be adequately represented by the weights alone. This bias term adds flexibility to the model, allowing it to learn and represent patterns that might have different baseline values, contributing to a more nuanced understanding of the data.

Next, before projecting the output of each convolutional layer, the sum of $conv(x, W)$ and B were transform with an activation function called Rectified Linear Unit (ReLU) and will have a full mathematical expression as:

$$Y = \text{ReLU}(conv(x, W) + B) \tag{3.20}$$

The ReLU serve as important functions in the context of image analysis that works by remap the input value, x to 0 if x is negative value and remain the input value if x is positive value or else can be expressed as:

$$\text{ReLu}(x) = \max(0, x) \tag{3.21}$$

Besides in AlexNet also have a layer that used in dimension reduction or feature selection which called as Max Pooling layer. It involves taking the maximum value from a group of values in a certain region of the input or can be in form of mathematical equation for as follows:

$$maxpool(x, W_{size}, S)_{i,j,k} = max_{a,b}(x_{i\times S+a}, x_{j\times S+b}, k) \tag{3.22}$$

The Max Pooling operation is applied independently to each depth slice of the input volume. The pooling window is moved across the input with a certain stride, and for each position, the maximum value within the window is taken. This operation helps in reducing the spatial dimensions of the input, making the network more robust to variations in object position within the input images and reducing the computation needed in subsequent layers.

The extracted and selected features to an input that sized of 227x227x3 were resulting in 6x6x256 which after being flatten it becomes 9215 total number of numerical features being extracted from the images [228], [229]. At this stage, another 2 set of features being extracted, one from the spectrogram and another one was from the scalogram. In total, the study introduced six sets of features, including raw Fourier spectra, PCA-transformed Fourier spectrum, PCA-transformed power spectrum, and features extracted from the scalogram and spectrogram using AlexNet. Each set of features aimed to capture distinct aspects of the signal, and their effectiveness was evaluated in terms of model performance.

The findings at this point contribute to the broader understanding of feature selection techniques in signal processing and image analysis, highlighting the importance of selecting relevant and informative features for classification tasks. The exploration of different feature representation methods provides valuable insights into the impact of dimensionality reduction and image-based feature extraction on model outcomes.

3.6 Classifier Algorithm

Intelligence Classifier, a subset of AI, is dedicated to developing algorithms and models that can learn from data, enabling them to make predictions or decisions without explicit programming. Rather than relying on explicit instructions or rules, classifier algorithms utilize statistical techniques to identify patterns, trends, and correlations within the features. These algorithms iteratively adjust their internal parameters during training to optimize their performance on the given task. The primary objective is to enable the model to generalize effectively, making accurate predictions and classifications on unseen or future data. This generalization is facilitated by dividing the collected data into two categories: the training set and the validation set. The training set is used to train the algorithm, aiming to optimize the values of W and B. Meanwhile, the validation set is employed to validate the training classification task and to detect signs of overfitting together with optimize the hyperparameter.

In the context of this experiment, various machine learning techniques were employed, including FFNN, AlexNet, SVM, AlexNet- SVM, RF and AlexNet-RF. The fundamental concept underlying machine learning is to empower computers to learn and enhance their performance during training on classification tasks. Specifically, in this experiment, the focus is on classifying five types of fall movements and distinguishing them from fall-like movements in single and multiple person scenario by leveraging patterns and relationships within the six different sets of extracted and selected features.

3.6.1 Feed Forward Neural Network

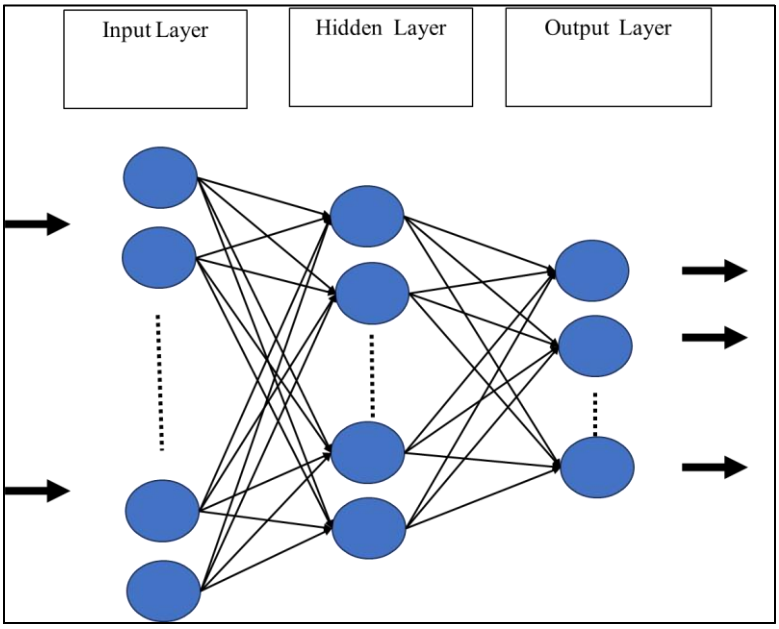

Figure 3.13 Neural Network Architecture

FFNN is a network that fully connected a set of input neurons, $x(k)$ called input layers to a set of output neurons, $y(k)$ through a set of hidden neurons such illustrate in Figure 3.13. The input layer represents the input variables or features. Each input neuron corresponds to each set of features, or it can be stated that the size of input neurons is the same as the size of each feature set. Meantime, the hidden layer, $h(k)$ which contains a weight and bias assigned serves as a connector that connects the input neurons and the output neurons [230]. The weights, W represent the strength or importance of the connections between neurons in different layers of a neural network. It determines how much each input contributes to the neuron's activation or output. In contrast, the bias, B is an additional parameter used to adjust the output of a neuron which are not dependent on any specific input but are added to the weighted sum of the inputs. They act as an offset or a baseline value that helps control the activation of the neuron.

Since this layer is a fully connector layer, there was transferring algorithms occur that involving neurons in each layer. This transfer algorithms involved a transfer function, $f()$, input from $x(k)$, W assigned and the B or can be express using a mathematical expression as follows:

$$fc(k) = f(B + \sum x(k)W) \tag{3.21}$$

Since there are 2 transfer algorithms involved which from input to hidden and hidden to output layer, therefore, there will have 2 different transfer function involve in this state for projecting the input neurons into a new form in order to introduce non-linearities enabling learning and generalization, adding robustness and stability, and facilitating gradient-based optimization [231]. From $x(k)$ to $h(k)$, the function used in the algorithm is the log-sigmoid transfer function which maps the input value into a range of 0 and 1 and distributes most of the input approaching 0 and approaching 1 in order to the vanishing gradient problem. This transfer function can mathematically express as:

$$f(x) = \frac{1}{1 + e^{-x}} \tag{3.23}$$

On the other hand, from $h(k)$ to $y(k)$ the transfer function involved is the linear transfer function where the input and the output are mapped equivalently or can be expressed as:

$$f(x) = x \tag{3.24}$$

The output layer consists of output neurons, corresponding to the number of classes to be classified. The output neurons take the weighted sum of the inputs from the hidden layer, apply an activation function to produce an output value, and serve as the final output of the network.

After the algorithm finishes in predict the output value in each epoch, y_{pred} the predicted output will be compared with the actual output, y in order to measure the losses. The losses can be calculated using Mean Square Error (MSE) algorithm which is mathematically expressed as follows:

$$Loss = \sum (\Delta y)^2 \tag{3.25}$$

Where n is the total number of outputs and the Δy is the difference between the y_{pred} and y. Next the gradient of the loss, ∇Loss, must be acknowledged in order to represent the derivative of the loss with respect to the represent W and B. The ∇Loss can be measure through a mathematical equation as follows:

$$\nabla \mathrm{Loss} = \frac{\partial Loss}{\partial a} \tag{3.26}$$

Here is where that training phase is significant where the w and b will be updated in each epoch via the Levenberg-Marquart (LM) algorithm until it achieves the aim of minimum losses approaching 0 losses or it detect the sign of overfitting were an increasing in $Loss$ value in 6 consecutive time. The LM is a modification of the Gauss-Newton method, which is a variant of the gradient descent algorithm. The Levenberg-Marquardt algorithm adjusts the weight and bias updates during training based on the second-order information of the error surface. Both W and B variables can be updated through a mathematical equation as follows, respectively:

$$W_{new} = W - (J^T * J + \lambda * I)^{-1} * J^T * \nabla \mathrm{Loss} \tag{3.27}$$

$$B_{new} = B - \alpha \left(\frac{\nabla \mathrm{Loss} * f'(z)}{B} \right) \tag{3.28}$$

Where the J^T is the transpose of the Jacobian matrix, J, the λ is the damping factor, I is the identity matrix and the $f'(z)$ represents the derivative of the activation function with respect to the weighted sum.

Recognizing that, among the three FFNN layers, the hidden layer plays the most crucial role in determining how effectively this algorithm can handle the classification task. Therefore, determining the number of neurons in this layer is a crucial part of the process. In order to achieve the best structure for the classification task of five types of falls and segregating fall-like movements collected from PWR, the FFNN structure will be tested with various numbers of neurons in the hidden layers. This study is designed to fine-tune the optimal number of hidden neurons, which will involve testing different numbers of hidden neurons ranging from 2 to 100 with a step size of 1. Each configuration of hidden neurons will be tested 10 times, and the average value will be calculated. The optimum number of hidden neurons will be determined based on the highest average validation set accuracy.

3.6.2 AlexNet

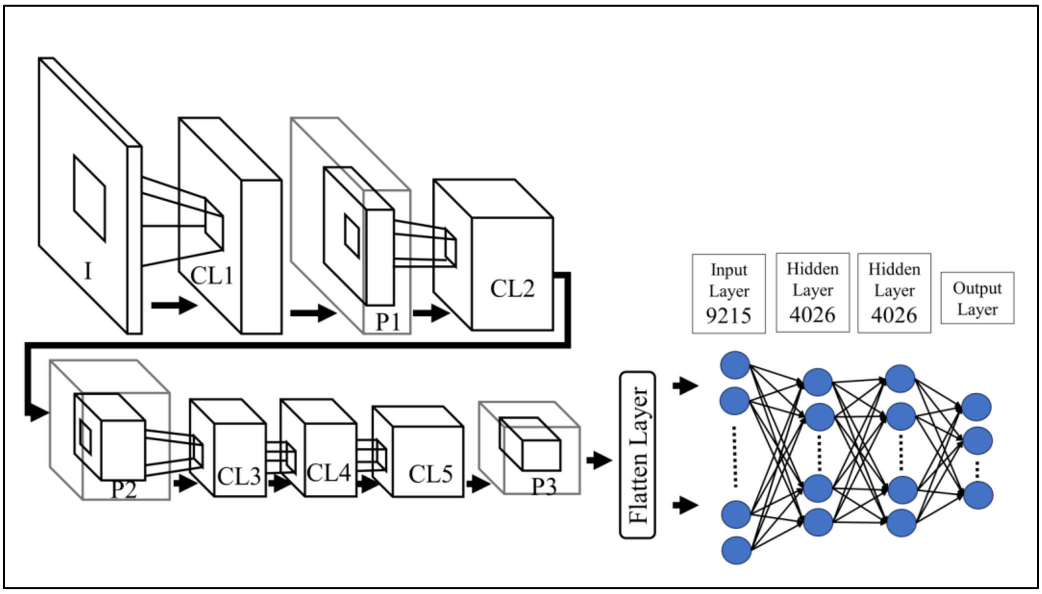

Figure 3.14 AlexNet architecture

On the other hand, the NN specifically designed with the AlexNet algorithm has been used on features extracted using the AlexNet features extraction layer, resulting in a complete AlexNet algorithm. In the classification layer, AlexNet has 2 hidden layers ($h_1(k)$ and $h_2(k)$) each consisting of 4096 hidden neurons, and then connected to the output layer [229] such shown in Figure 3.14. Similar to the FFNN, each transfer learning will have its own activation function. In AlexNet, ReLU is used in both transfer algorithms from $x(k)$ to $h_1(k)$ and $h_1(k)$ to $h_2(k)$. Meanwhile, from $h_2(k)$ to $y(k)$, the SoftMax activation function is used, where it takes a vector of real numbers as input, x, and outputs a probability distribution, p, representing the likelihood of each class. The SoftMax function normalizes the input vector, ensuring that the resulting values lie between 0 and 1 and sum up to 1. As this experiment aims to classify six classes, the output layer will also have six neurons. Hence, the input vector is $[x_1, x_2, x_3, x_4, x_5, x_6]$ and the probability vector will have $[p_1, p_2, p_3, p_4, p_5, p_6]$ and to compute each p, the mathematical expression as follows:

$$f(x_i) = \frac{\exp\,(x_i)}{\exp(x_1) + \exp(x_2) +..\exp(x_6)} \tag{3.29}$$

As an ascent to a NN algorithm, an optimizer algorithm will be utilized to update W and B the in each epoch such used in FFNN was the LM and the AlexNet was utilized the Stochastic Gradient Descent with Momentum (SGDM). SGDM enhances the traditional stochastic gradient descent (SGD) method by incorporating a momentum term. This momentum factor introduces a moving average of past gradients, allowing the optimizer to continue moving in the same direction as previous steps, which can help accelerate convergence and navigate through flat regions or small oscillations in the loss landscape. The update rule of SGDM can be expressed as follows:

$$m_t = \beta \cdot m_{t-1} + (1 - \beta) \cdot \nabla\text{Loss} \tag{3.30}$$

$$\theta_{t+1} = \theta_t - \alpha \cdot m_t \tag{3.31}$$

Here, θ_t represents the model parameters at time step t which contains a vector of updated W and B, α is the learning rate, and β is the momentum parameter. The momentum term, m_t, essentially becomes a weighted sum of past gradients, influencing the current update direction. The higher the momentum value, the more the past gradients contribute to the current update, making the optimization process more stable and potentially faster. The SGDM is effective in overcoming issues associated with plain SGD, such as slow convergence in the presence of complex or ill-conditioned surfaces. It provides a smoother and more persistent trajectory through the parameter space, often leading to faster convergence and improved generalization performance of the trained model.

Moreover, there was an optimizer that can handle sparse gradients effectively and known for its efficiency and effectiveness in practice, often converging faster than traditional optimization techniques called Adam (short for Adaptive Moment Estimation) which combines the benefits of two other popular optimization techniques: RMSprop and momentum. The core idea behind Adam is to maintain two moving averages for each parameter in the model which are a momentum term, akin to classical momentum optimization, and an exponentially decaying average of past squared gradients, inspired by RMSprop. These moving averages are then used to adaptively adjust the learning rates for each parameter during training.

The algorithm's update rule involves computing the moving average of past gradients (first moment, m_t) and the moving average of past squared gradients (second moment, v_t). The initial bias of these averages is corrected to account for their initialization at zero. The resulting values are then used to scale the learning rate for each parameter individually, enabling adaptive updates based on the historical behaviour of gradients. The mathematical equation for updating the m_t were the same as SGDM and the v_t can be express as:

$$v_t = \beta \cdot v_{t-1} + (1 - \beta) \cdot (\nabla \mathrm{Loss}. \nabla \mathrm{Loss}) \tag{3.32}$$

Let the hat symbol as the estimated value, then both momentum estimation, $\widehat{m_t}$ and $\widehat{v_t}$ will undergo bias-corrected estimation, which can be express as:

$$\widehat{m_t} = \frac{m_t}{1 - \beta^t} \tag{3.33}$$

$$\widehat{v_t} = \frac{v_t}{1 - \beta^t} \tag{3.34}$$

From here, the updated parameters will be gained after computation using the following mathematical expression:

$$\theta_{t+1} = \theta_t - \alpha \cdot \frac{\widehat{m_t}}{\sqrt{\widehat{v_t}} + \epsilon} \tag{3.35}$$

Where the ϵ is the small constant to prevent division by zero.

These two optimizers have demonstrated good performance in updating the parameters, with SGDM being the one used by the developers of AlexNet and the other being an improved and combined version. Therefore, this study was designed to find the optimum optimizer between these two algorithms using the same technique on SVM and RF which was the cross- validation k-fold technique with k=10. Additionally, keeping the number of mini-batch size to 512, which was the optimized value for a GPU with 8GB memory, this study also tested this algorithm with three different values of initial learning rates includes $1e^{-3}$, $1e^{-4}$ and $1e^{-5}$.

3.6.3 Support Vector Machine

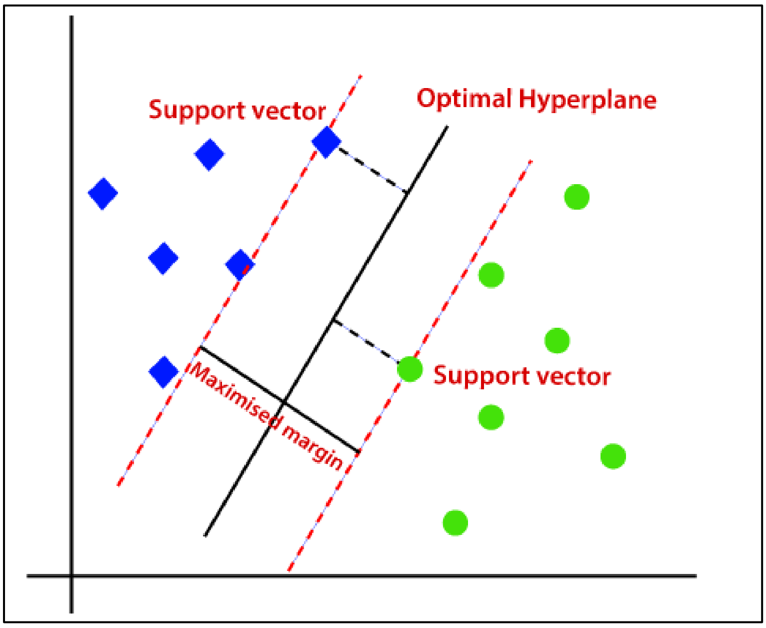

Figure 3.15 Support Vector Machine Algorithm

SVM is a binary classifier algorithm that aims to find the best decision boundary or call hyperplane that separates the input features belonging to its classes with a high margin as illustrate in Figure 3.15. Typically, in binary linear SVM, the hyperplane is defined by the equation:

$$Wx + B = 0 \tag{3.36}$$

Where it will determine on which side of the hyperplane the data point lies and the projection of input features will be defined as:

$$f(x) = Wx + B \tag{3.37}$$

If the result is positive, the point is classified as belonging to one class, and if it is negative, it belongs to the other class. However, since this experiment aims to classify six different classes, an approach called OAA is utilized, where it distinguishes one class from the rest of the classes [232]. The OAA strategy involves training multiple classifiers based on the number of classes, denoted as *N*; in this experiment, $N = 6$. Therefore, six SVM classifiers will be used in the training state, with each classifier trained to separate one class from the other five classes. During training, for a given class, the positive samples are from that class, and the negative samples are from all other classes. The SVM classifier learns a hyperplane that separates the positive samples from the negative samples. This process is repeated for each class, resulting in "N" binary classifiers. Hence, the decision function for each classifier is transformed into:

$$f_i(x) = W_i x_i + B_i \tag{3.38}$$

Where the i represent the classifier used to classify i_{th} class.

This experiment utilized multiple input features from the reduced dimension of the 2 frequencies domain; hence, the features must be transformed into a higher-dimensional feature space by using the kernel function. The kernel function will transform the W in the form of the Lagrange multipliers α_i with the combination of their class label, y_i [233]. The magnitude and sign of these Lagrange multipliers determine the influence of each support vector on the decision boundary. The kernel activation function transformed the decision function into:

$$f(x) = sign\left(\sum \alpha_i y_i K(x_i, x) + b\right) \tag{3.39}$$

Where the $sign()$ is the signum function and $K(x_i, x)$ is the type of kernel algorithm applied which computes the similarity or distance between the training sample x_i and the input sample x.

There are 3 types of kernel function that are being tested in this experiment in order to build an optimum SVM for this classification task which are Linear Function, RBF and Polynomial Function. In the case of a linear kernel, the decision boundary is simply a hyperplane in the original feature space, and the kernel function is defined as:

$$K(x_i, x) = x_i . x \tag{3.40}$$

Meanwhile, the RBF uses a Gaussian-like similarity function to measure the similarity or distance between two data points which is defined as:

$$K(x_i, x) = \exp\left(-\gamma \|x_i - x\|^2\right) \tag{3.41}$$

Where the γ is a hyperparameter that controls the width of the Gaussian kernel and $\|x_i - x\|^2$ represents the squared Euclidean distance between the training sample x_i and the input sample x in the original feature space. This kernel function can create decision boundaries that are more flexible and nonlinear. It allows SVMs to capture intricate patterns in the data, enabling effective classification in complex scenarios. On the other hand, the Polynomial kernel function uses a polynomial function to measure the similarity or distance between two data points which can be useful to capture polynomial relationships in the data. The polynomial kernel function is defined as:

$$(x_i, x) = (\gamma(x_i . x) + r)^d \tag{3.42}$$

Where the γ and r is the hyperparameter that control the dot product and constant term and the d is the degree of polynomial which controls the complexity of the decision boundary. Higher degrees allow for more complex decision boundaries, potentially capturing more intricate relationships in the data.

As the ascent of intelligence classifier model, it will go through and update of α_i and B in order to minimize the error, E gain. The E can be obtained by the equation as follows:

$$E = f(x) - y \tag{3.43}$$

During the training process, an optimization algorithm called Sequential Minimal Optimization (SMO) is used. These algorithms iteratively update the α_i and the b until an optimal solution is reached. Generally, the algorithm iteratively selects a pair of Lagrange multipliers (α_i, α_j) and updates their values to move towards the optimum, while satisfying the constraints imposed. Since α_i was selected in pairs for the update process during training thus the training samples, class label, bias and error also will be selected in pair and become (x_i, x_j), (y_i, y_j), (B_i, B_j), and (E_i, E_j) respectively. The update of $\alpha_i$and $\alpha_j$can be expressed mathematically as follows, respectively:

$$\alpha_{i_{new}} = \alpha_{i_{old}} + \frac{y_i(E_i - E_j)}{K(x_i, x) + K(x_j, x) - 2K(x_i, x_j)} \tag{3.44}$$

$$\alpha_{j_{new}} = \alpha_{j_{old}} + y_i y_j(\alpha_{i_{old}} - \alpha_{i_{new}}) \tag{3.45}$$

Moreover, the bias term (B_i, B_j) is also adjusted during the optimization process to ensure the correct classification of the training samples by the equations as follows:

$$\begin{aligned} B_{i_{new}} = E_i + y_i(\alpha_{i_{new}}) - \alpha_{i_{old}} K(x_i, x_j) + y_j(\alpha_{i_{new}}) \\ - \alpha_{j_{old}} K(x_i, x_j) + b_{old} \end{aligned} \tag{3.46}$$

$$\begin{aligned} B_{j_{new}} = E_j + y_i(\alpha_{i_{new}}) - \alpha_{i_{old}} K(x_i, x_j) + y_j(\alpha_{i_{new}}) \\ - \alpha_{j_{old}} K(x_i, x_j) + b_{old} \end{aligned} \tag{3.47}$$

After the training process, the trained SVM model consists of the optimized α_i and the B will undergo prediction on unseen data or validation set that been separated before. This step is important to analyse the capability of the algorithm captured and learn the features pattern together with analyse the overfitting sign. Moreover, the results with unseen data also open up space to optimize significant tenable parameters, such as the kernel function used, in SVM. In this study, 4 sets of features will be fed into the SVM classifier with a constant box constraint, kernel scale, and outlier fraction, as tabulated in Table 3.7. This will be done to find the optimized kernel function, either linear, polynomial, or RBF, that best suits the classification problem. To assess the efficacy of each kernel function, the training process were done for 10 times. This involved applying SVM with varying kernel functions to classify each feature, a process iterated 10 times to obtain a robust evaluation. The resulting performances were then averaged to derive a comprehensive assessment.

Table 3.7
SVM parameters

Parameter	Value
Box constraint	1
kernel scale	1
outlier fraction	0

3.6.4 AlexNet-SVM Hybrid Model

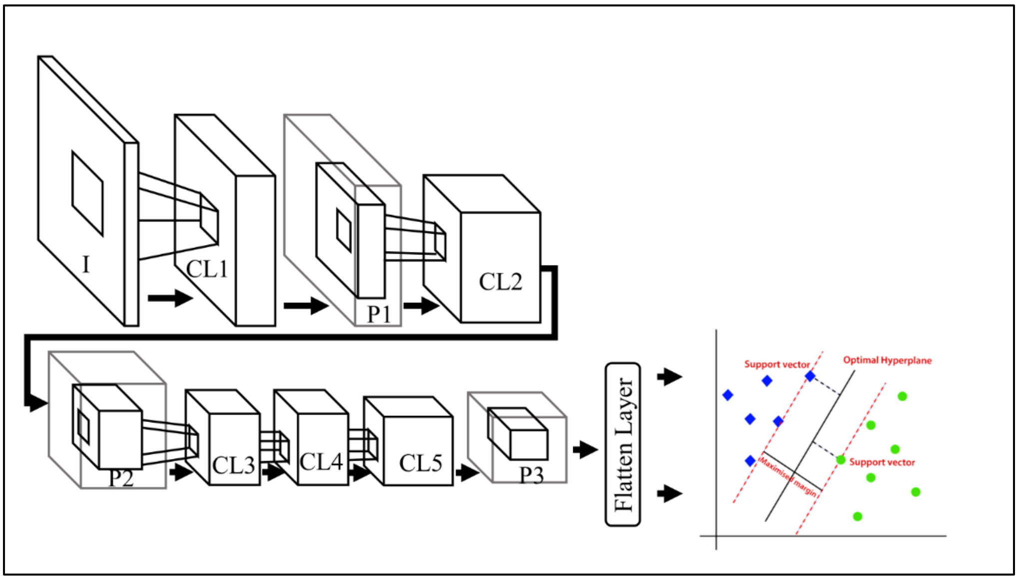

Figure 3.16 AlexNet-SVM architecture

Similar assessments conducted on the traditional SVM were also applied to the AlexNet-SVM hybrid model. The key difference in this hybrid model lies in the input data; specifically, the features used are unsupervised data extracted from the AlexNet feature layers and directly fed into SVM classifiers. The structural configuration of this hybrid model can be visualized as depicted in Figure 3.16.

3.6.5 Random Forest

RF consists of a collection of decision trees, with each tree grown using a subset of the training data and features. These algorithms involve three main steps: bootstrapping, tree construction, and voting. Bootstrapping is designed to create multiple subsets or bootstrap samples by randomly selecting N data points from the training dataset through sampling with replacement. This technique is crucial for introducing diversity into the training process, as it allows some data points to be repeated and others to be left out in each subset. The mathematical details of bootstrapping involve the concept of probability, including the probabilities of inclusion ($P_{include}$), exclusion ($P_{exclude}$) and absent (P_{absent}), expressed as:

$$P_{inclusion} = \frac{1}{N} \tag{3.48}$$

$$P_{exclusion} = 1 - \frac{1}{N} \tag{3.49}$$

$$P_{absent} = \left(1 - \frac{1}{N}\right)^N \tag{3.50}$$

By incorporating this algorithm before initiating the decision-making process using multiple decision trees, diversity is introduced into the training process by creating different subsets of the data for each tree. Some data points may be present in multiple subsets, while others may be excluded, leading to a variety of perspectives for each tree. Bootstrapping helps reduce overfitting by allowing some data points to be repeated and others to be left out in each subset. This prevents the model from memorizing the training data and promotes a more generalized understanding. It also enhances the stability of the model by reducing the impact of outliers or noise in individual subsets.

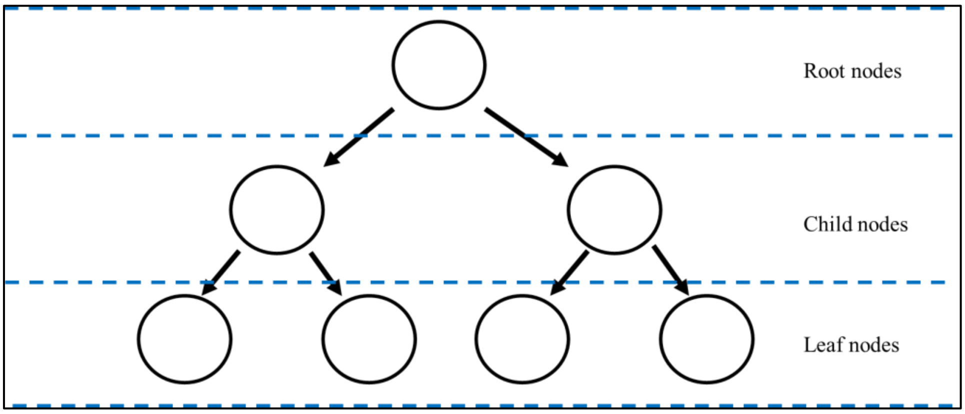

Figure 3.17 Decision Tree's Structure

Next, the tree construction process in Random Forest involves growing multiple decision trees, each trained on a different bootstrap sample of the dataset. The decision tree works such if-else function such illustrate in Figure 3.17 which having a root node which the whole dataset in in each bootstrap undergo evaluation with a threshold value with least Gini Impurity value ($Gini(D)$) that resulting in separating the dataset into 2 subsets. Then each subset will undergo another evaluation at the child nodes with same algorithm as root nodes.

$$Gini(D) = 1 - \sum_{i=1}^{number\ of\ class} p_i^2 \tag{3.51}$$

Where the p_i is the proportion of class i the D. This process is repeated recursively for each node until a stopping criterion is met. The goal is to find the best feature and threshold combination that minimizes the $Gini(D)$ of the resulting child nodes at each split. The recursive splitting continues until reaching the leaf nodes, which represents a class. Next, for the prediction part where the validation set were used to be classified using the trained algorithm, the prediction will be made by the mathematical expression as follows:

$$y = arg\ max_i(count(i, L)) \tag{3.52}$$

Where the $count(i, L)$ represents the number of data points in the leaf node L that belong to class i. It's essentially counting how many data points in the leaf node have the label i. Meanwhile, the $arg\ max_i()$ is the function used to finds the class label i for which the count is maximized. This expression signifies that the predicted class for a data point in a leaf node is determined by selecting the class that has the highest count among the data points in that leaf node.

Subsequently, the voting process will take over where the prediction from each decision tree will be take into account. Each tree "votes" for a class in a classification task or provides a prediction in a regression task. In classification, the class with the majority of votes becomes the final prediction. This voting mechanism helps mitigate the impact of individual errors or biases in a single tree, leading to a more robust and accurate model. In a regression task, the final prediction is often the average of the predictions from all the trees. This ensemble approach leverages the diversity and independence among the trees, enhancing the overall predictive performance of the Random Forest. Additionally, the voting process allows Random Forests to generalize well to new, unseen data by combining the knowledge captured by different trees during the training phase.

Furthermore, the optimization of the number of trees in a RF model stands as one of the pivotal areas of this study, with profound implications for model performance and generalization. The number of trees in a Random Forest plays a critical role in balancing the trade-off between bias and variance, ultimately influencing the model's predictive accuracy. A judiciously chosen number of trees can significantly enhance the model's robustness and resilience to overfitting, thereby ensuring better generalization to unseen data. To optimize the number of trees in a Random Forest, this study was deploying the technique same as the one used the SVM which training process were done in 10 times with various number of decision start from 1 to 200 with stepping size of 1. These methodologies enable systematic exploration of the hyperparameter space, allows to identify the optimal number of trees that maximizes predictive performance. Additionally, ensemble learning methods, which combine the strengths of multiple models, can further enhance the RF’s efficacy, offering a comprehensive and sophisticated means of achieving optimal model architecture.

3.6.6 AlexNet-RF Hybrid Model

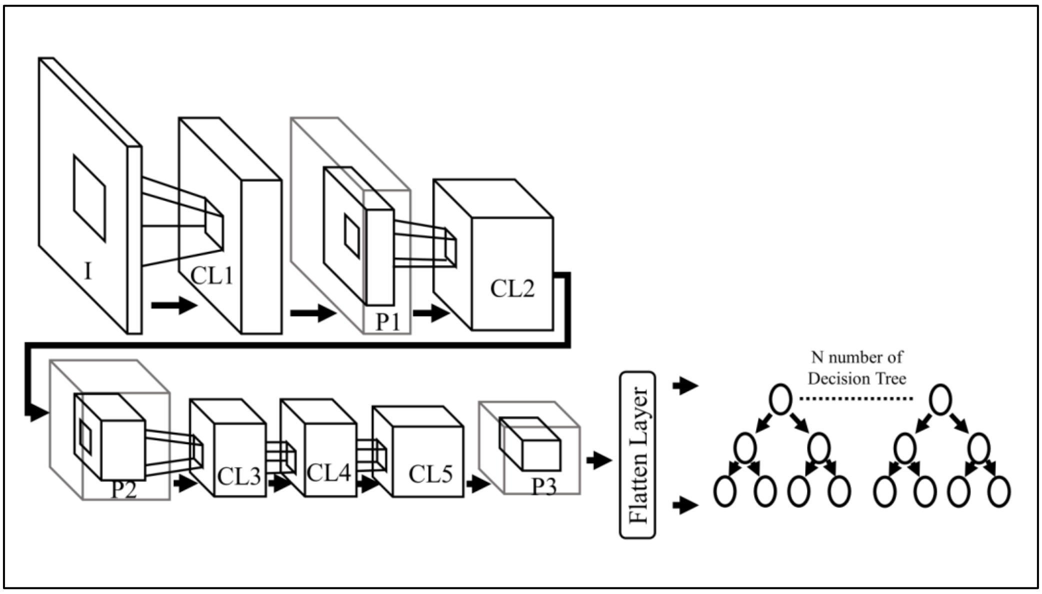

Figure 3.18 AlexNet-RF architecture

Similarly to the AlexNet-SVM hybrid model, the AlexNet-RF hybrid model underwent a comparable assessment to the traditional RF model, albeit with distinct input features. This hybrid model utilized input features extracted from the output of AlexNet feature layers applied to scalogram and spectrogram image features. The structural configuration of this model can be observed in Figure 3.18.

3.7 Comparative Analysis

The comparative analysis focused on evaluating the classifier's proficiency in categorizing the provided features. This analysis comprised two distinct stages: one conducted within the same category of classifiers and features, and the other executed across all types of classifiers and features. The one that made within same type of classifier and features actually was designed to find the optimum parameter for the classifier that been fed with specific set of features such tabulate in Table 3.8. This stage was involved the comparison on average accuracy of validation set upon performing the k-fold cross validation technique with k=10. The accuracy level can be gain by the mathematical expression as follows:

$$accuracy = \frac{TP + TN}{TP + TN + FP + FN} \tag{3.53}$$

Where the TP is the number of true positives (correctly predicted positive instances), TN is the number of true negatives (correctly predicted negative instances), FP is the number of false positives (incorrectly predicted positive instances), and FN is the number of false negatives (incorrectly predicted negative instances).

Table 3.8
List of features and classifier

Features	**Classifiers**
Fourier spectrum	FFNN
	SVM
	RF
Power spectrum	FFNN
	SVM
	RF
PCA-Fourier spectrum	FFNN
	SVM
	RF
PCA-Power spectrum	FFNN
	SVM
	RF
Spectrogram	AlexNet
	AlexNet-SVM Hybrid Model
	AlexNet-RF Hybrid Model
Scalogram	AlexNet
	AlexNet-SVM Hybrid Model
	AlexNet-RF Hybrid Model

Conversely, a pivotal aspect of this study involved conducting a comparative analysis among each optimized classifier algorithm and its corresponding feature set. During this phase, only the highest accuracy on each type of classifiers were underwent evaluation based on the recall, precision and F1-score. or can be express as:

$$recall = \frac{TP}{TP + TN} \tag{3.54}$$

$$precision = \frac{TP}{TP + FP} \tag{3.55}$$

$$F1 = \frac{2 \times TP}{2 \times TP + FP + FN} \tag{3.56}$$

The recall serves as a pivotal metric for assessing the effectiveness of a machine learning model, particularly in situations where correctly identifying all relevant instances of a specific class holds paramount importance. Also referred to as sensitivity or true positive rate, recall quantifies a model's ability to accurately identify all positive instances among the total actual positive instances. A higher recall value signifies that the model adeptly captures a larger proportion of true positive cases, thereby minimizing the likelihood of false negatives. In critical domains like medical diagnoses or fraud detection, where overlooking positive cases can bear significant consequences, prioritizing a high recall value is common practice. A model exhibiting high recall is more attuned to detecting pertinent information, delivering robust performance in scenarios where the comprehensive identification of instances within a particular class is imperative.

Meanwhile, the precision is a critical metric that significantly influences the overall performance of a machine learning model, particularly in scenarios where the cost of false positives is high. Precision, also known as positive predictive value, measures the accuracy of positive predictions by assessing the ratio of true positives to the total predicted positives. A high precision value indicates that the model is making fewer false positive predictions, providing confidence in the correctness of positive classifications. In applications where the consequences of misclassifying negative instances as positive are substantial, such as in medical diagnoses or spam email filtering, achieving a high precision is often prioritized. A model with high precision minimizes the occurrence of false alarms, contributing to a more accessible and trustworthy system.

Nevertheless, it is essential to recognize the inherent trade-off between precision and recall. Precision denotes the accuracy of positive predictions by measuring the ratio of true positives to the total predicted positives. As recall increases, precision may decrease, and vice versa. Striking an appropriate balance hinge on the specific requirements of the application. In situations where false positives carry severe consequences, achieving an equilibrium between precision and recall becomes crucial. Hence this trade-off can be analysed through the F1-score which computed as the harmonic mean of precision and recall, assigning equal importance to both metrics. Consequently, a high F1 score is attained when both precision and recall exhibit high values, striking a harmonious balance between the two. The F1 score proves particularly valuable in situations characterized by class imbalances or where substantial consequences are attached to both false positives and false negatives. This metric provides a comprehensive assessment by considering both precision and recall, making it particularly suitable for scenarios where a nuanced evaluation of model performance is essential.

This comparative analysis serves as a critical tool for evaluating the performance of each classifier within the context of the specific dataset under consideration. The varied design principles and assumptions underlying different classifiers can result in divergent effectiveness across datasets. Through this comparison, valuable insights are garnered, aiding in the determination of which classifier is most apt for the given feature sets. Secondly, the analysis contributes to discerning the impact of feature selection on classifier performance. Understanding how each classifier responds to these feature variations is imperative, elucidating the informativeness of specific features for each algorithm. Moreover, the comparison analysis offers valuable contributions to model interpretability and generalization. Some classifiers inherently exhibit greater interpretability, facilitating a more transparent comprehension of the model's decision-making processes. Concurrently, assessing generalization performance on unseen data is pivotal to prevent overfitting and ensure the model's robustness in real-world scenarios.

In conclusion, a comprehensive comparative analysis involving three distinct classifiers and six feature sets is indispensable for comprehending their respective strengths and weaknesses within the confines of the dataset. This analytical process informs decisions pertaining to model selection, feature engineering, and deployment, culminating in the development of a resilient and efficacious machine learning solution.

3.8 Summary

In summary, the methodology provides a comprehensive framework for studying the application of Passive Wireless Radio (PWR) technology in fall detection systems. The process commences with data collection, as detailed in Section 3.2, which outlines the hardware configuration employed for this purpose. The configuration includes the utilization of the RT-N12+ B1 Wi-Fi router as both the transmitter and receiver, complemented by an omni-directional antenna, LNA, diode detector, LPF, and an oscilloscope for data acquisition. This systematic approach not only facilitates effective data gathering but also enhances the reliability and accuracy of the fall detection system under investigation.

Subsequently, the sample selection for this study was meticulously designed to meet specific requirements. The selected stuntman was required to possess professional stuntman certification, while the volunteers were chosen based on variations in height and weight, ensuring a balanced representation of gender with 5 male and 5 female participants. Additionally, the volunteers were equipped with aging simulators to accurately mimic the movement patterns of the elderly. In total, five fall movements were executed for data collection: walking and falling, sitting and falling, slipping and falling, stumbling, and fainting. Additionally, six fall-like movements were performed, including sitting, bending, kneeling, squatting, lying down, and prostrating. For the single-person scenario, data were collected across 90 repetitions per class, while in the multiple-person scenario, 198 repetitions per class were recorded. This comprehensive approach to sample selection and data collection aims to ensure the robustness and validity of the findings in the context of fall detection systems.

Subsequently, the collected signals underwent an enveloping algorithm designed to preserve the amplitude modulation signatures inherent in the data. The enveloping process commenced with noise reduction, where a threshold for significant amplitude and noise levels was established using a moving variance algorithm. Following the removal of noise, the signal was subjected to enveloping under specific conditions, taking into account both the distance between peaks and the total number of peaks present in the signal. Once the significant amplitudes were identified, the enveloped signal was compared to a standard CW setup to analyse the similarities between the PWR and CW signals concerning their amplitude modulation signatures. This comparative analysis directly contributes to achieving Research Objective 1, which focuses on developing a preprocessing method for pulse-based PWR signals to effectively capture amplitude modulation signatures. This systematic approach not only enhances the integrity of the data but also facilitates a more nuanced understanding of the underlying signal characteristics essential for fall detection applications.

The enveloped signal subsequently underwent comprehensive signal processing, transforming it into both the Fourier spectrum and Power spectrum through the application of the FFT. This transformation facilitated the analysis of amplitude depth across the signal. Additionally, the signal was converted into a spectrogram by applying the STFT algorithm to examine the modulating frequency changes over time. Furthermore, the signal was transformed into a scalogram using CWT to analyse high-resolution transient changes, thereby enabling the capture of rapid fluctuations in amplitude modulation. Following these transformations, the features extracted from the Fourier and Power spectra, as well as the spectrogram and scalogram images, underwent a feature selection process. The dimensionality of the Fourier and Power spectra was reduced using PCA, ensuring that 95% of the cumulative variance was retained. Concurrently, features from the image data were selected using the AlexNet feature extraction layer, converting the images into a set of numerical features that encapsulate significant information for classification tasks. This systematic approach to feature extraction and selection is integral to achieving Research Objective 1, which aims to extract key features that characterize and differentiate fall movements from fall-like movements.

The methodology proceeds to the classification algorithms, which will incorporate FFNN, SVM, RF, AlexNet, and a hybrid classifier. The numerical features derived from the Fourier and Power spectra will be directly input into the machine learning classifiers, while the image features will be processed through AlexNet and the hybrid model. Each classifier will undergo an optimization process to identify the optimal values for hyperparameters. For the FFNN, assessments will be conducted with a varying number of hidden neurons ranging from 2 to 100. The SVM will be evaluated using three distinct kernel activation functions: linear, RBF, and polynomial. In the case of the RF model, the hyperparameter under consideration will be the number of DT, with a range of 1 to 200 trees being tested. Furthermore, AlexNet will be evaluated using two different optimizers such Adam and SGDM, alongside four different initial learning rates, specifically $1e^{-3}$, $1e^{-4}$ and $1e^{-5}$. The hybrid model will also undergo a fine-tuning process similar to that of the SVM and RF hyperparameters. Optimizing these parameters for each model is crucial in fulfilling the second research objective, which focuses on developing and evaluating various classifier algorithms based on the extracted features. This approach is aiming for develop and assess types of classifier algorithm based on extracted features for the task of classify each type of fall and segregate from fall-like in controlled and realistic environment which align with second objective.

Finally, all optimized models will be assessed using recall, precision, and F1-score metrics. Recall is essential for evaluating the effectiveness of a machine learning model, particularly in contexts where accurately identifying all relevant instances of a specific class is of utmost importance. Conversely, precision serves as a critical metric that significantly affects the overall performance of a machine learning model, especially in scenarios where the costs associated with false positives are substantial. The inherent trade-off between precision and recall is encapsulated in the F1-score, which provides a comprehensive assessment of model performance. These analyses will yield valuable insights, facilitating the identification of the most suitable classifier for the given feature sets, as well as illuminating the impact of feature selection on classifier performance. By implementing thorough evaluation and validation analyses to compare the capabilities of traditional machine learning, deep learning, and hybrid algorithms in adapting to complex signal data, this study directly addresses the third research objective. Through this rigorous assessment, it’s align third objective, evaluating and validating analysis for the capability between the traditional ML, DL and hybrid algorithm in term of accuracy, efficiency, robustness and capability of the algorithm to adapt on the high complex signal data.

CHAPTER 4
ENVELOPING ALGORITHM AND ACTIVITY CHARACTERIZATION RESULTS

4.1 Introduction

This chapter presents a comprehensive discussion of the outcomes derived from the applied methodologies, directly addressing research objectives 1. These objectives were accomplished through the implementation of the methodologies outlined in sections 3.3 and 3.4 following the completion of the data collection process.

In Section 4.1, a comprehensive exploration of the sample selection will be presented. This section will include samples of varying heights and weights, which will directly highlight the variation in signals collected. Such diversity in the data will enhance the system's robustness, ensuring reliable detection of humans across a wide range of body sizes and improving overall performance in real-world scenarios.

In Section 4.2, a comprehensive exploration of the enveloping algorithm will be presented. This entails a detailed examination of raw signal representations, the process of noise removal, and the intricacies of the enveloping algorithm. Throughout this section, particular emphasis will be placed on underscored the significance of extracting the signature of time-domain signals in the form of a continuous signal rather than beacon signal.

In Section 4.3, the focus shifts to conducting a comparative analysis on the time domain signals of PWR and CW to validate whether the envelope algorithm accurately extracts the correct patterns of human movement signals from Wi-Fi signals. This discussion will involve a side-by-side comparison of the patterns of these two different signals for the same activities.

Moving on to Section 4.4, the focus will be on the outcomes of signal transformation processes. A detailed discussion will ensue, elucidating how the translation of time domain information into various transform domains is executed for each movement class. Furthermore, this section will emphasize the characterization of each movement based on the transformed signals to confirm that the transformed signals accurately represent each collected movement.

4.2 Sample Selection

The data collection process involved the participation of 2 stuntmen and 10 volunteers, each varying in body size as detailed in Table 4.1. The variations in the height and weight of a human target affect the reflected signal through changes in several key parameters. These include RCS, amplitude modulation signature, and path loss. Taller individuals or those with larger body mass result in a higher RCS due to increased body surface area, leading to stronger reflected signals. Variations in weight can also impact amplitude modulation signatures by altering the biomechanics of walking, such as limb movement and gait frequency. Additionally, height differences can modify the elevation angle of the reflected wave, influencing path length and propagation characteristics, thereby causing slight changes in amplitude at the receiver.

Table 4.1
Data collection's Participant specification

Participant	**Gender**	**Height**	**Weight**
Stuntman 1	Male	165	74
Stuntman 2	Male	171	67
Volunteer 1	Male	170	69
Volunteer 2	Male	168	100
Volunteer 3	Male	170	86
Volunteer 4	Male	165	47
Volunteer 5	Male	176	58
Volunteer 6	Female	163	63
Volunteer 7	Female	154	51
Volunteer 8	Female	166	74
Volunteer 9	Female	168	59

Volunteer 10	Female	170	79

4.3 Enveloping Algorithm

Following the completion of the data collection process, a total of 990 signals were gathered. Among these, 540 signals pertained to single person scenario, encompassing six groups of classes that included five distinct types of falls and fall-like activities. The remaining signals, constituting double and triple target detection, comprised five classes featuring signals that were a mixture of falls and fall-like activities.

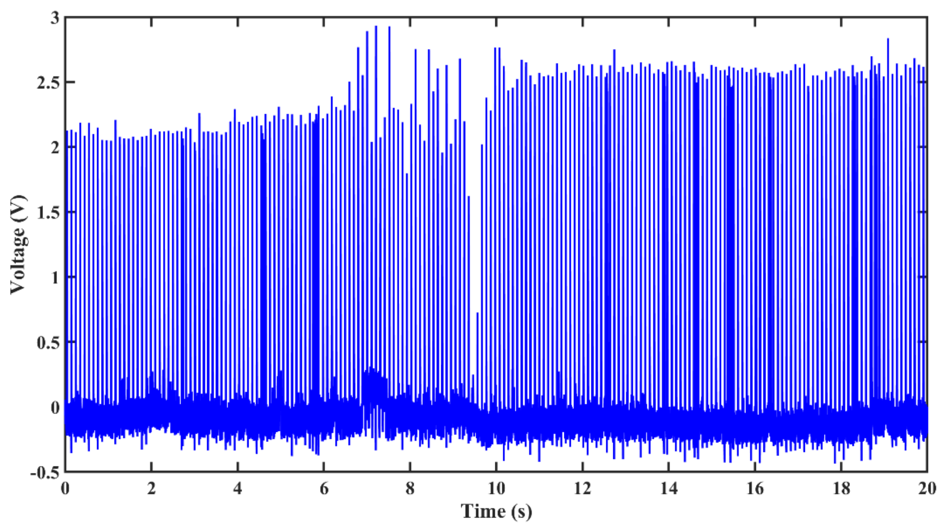

Figure 4.1 Raw Passive Wi-Fi Radar signal

Upon analysing each collected PWR signal, it was observed that the signal exhibited the expected beacon signal pattern with amplitude in the range of 0-3V, consistent with theoretical expectations as illustrated in Figure 4.1. Subsequent analysis revealed that the signal maintained a consistent signature, with the beacon appearing at 10Hz and exhibiting amplitude variations that projected signal patterns in the time domain. However, noise was observed in between each beacon signal, albeit with significantly lower amplitude compared to the beacon signal. To address both the noise and beacon signal appearance, the raw signal underwent pre-processing through noise removal and enveloping algorithms.

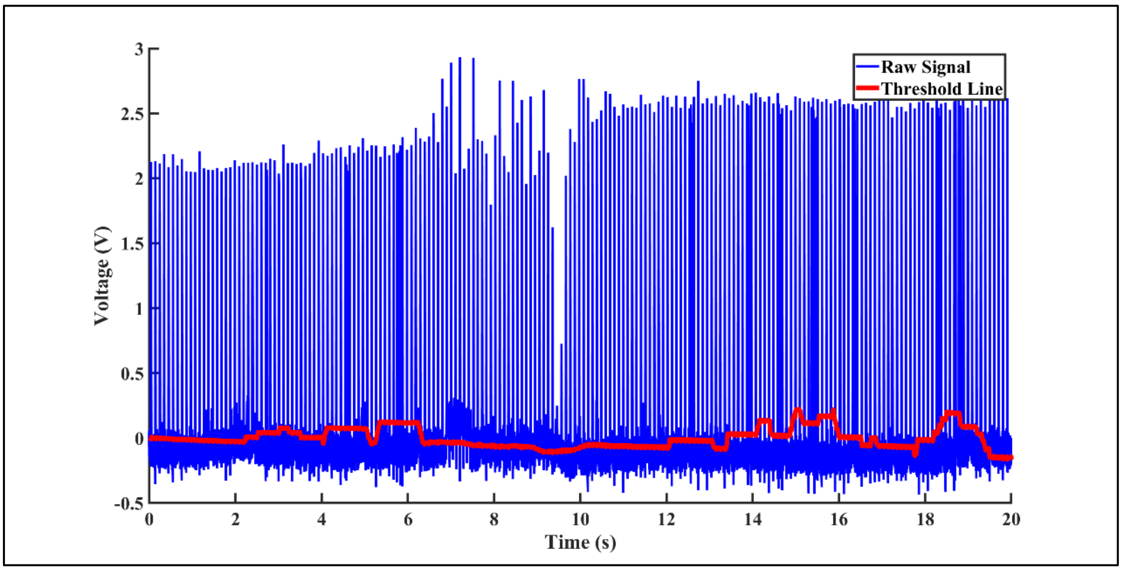

Figure 4.2 Raw Signal vs Noise threshold line

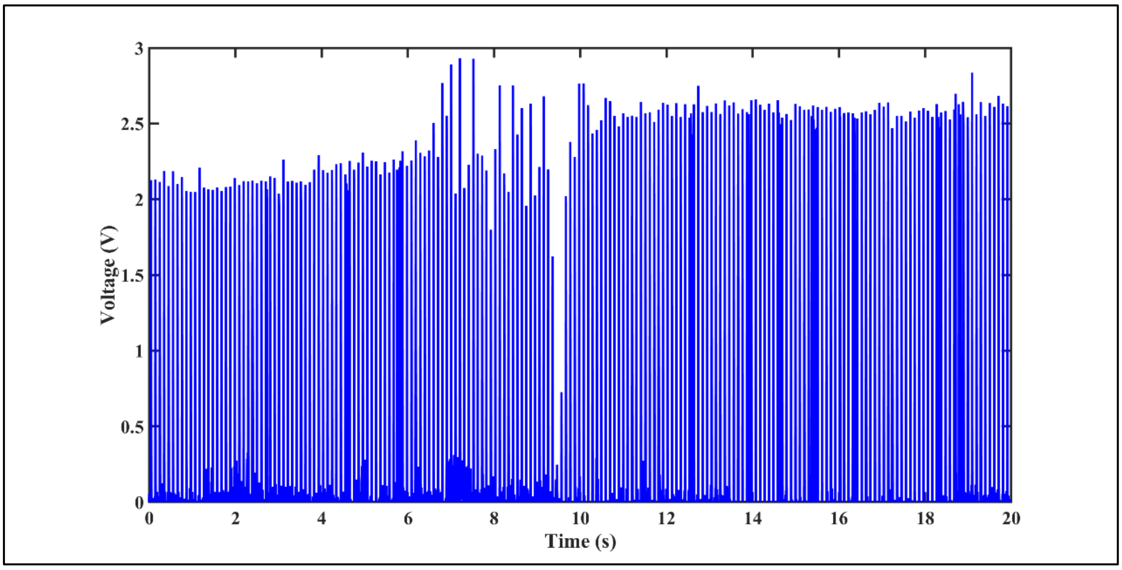

Figure 4.3 Noise removed signal

In the case of the PWR signal, the noise removal algorithm employed was the threshold algorithm. The threshold value was determined by applying the moving average algorithm with a window size of 0.5 seconds, as depicted in Figure 4.2. In the thresholding algorithm, each data point lower than the threshold value within the same number of data points was adjusted to 0V. Consequently, as illustrated in Figure 4.3, the noise removal algorithm resulted in a signal devoid of noise. This preprocessing step is crucial before applying the enveloping technique to prevent misspeaking of the beacon signal.

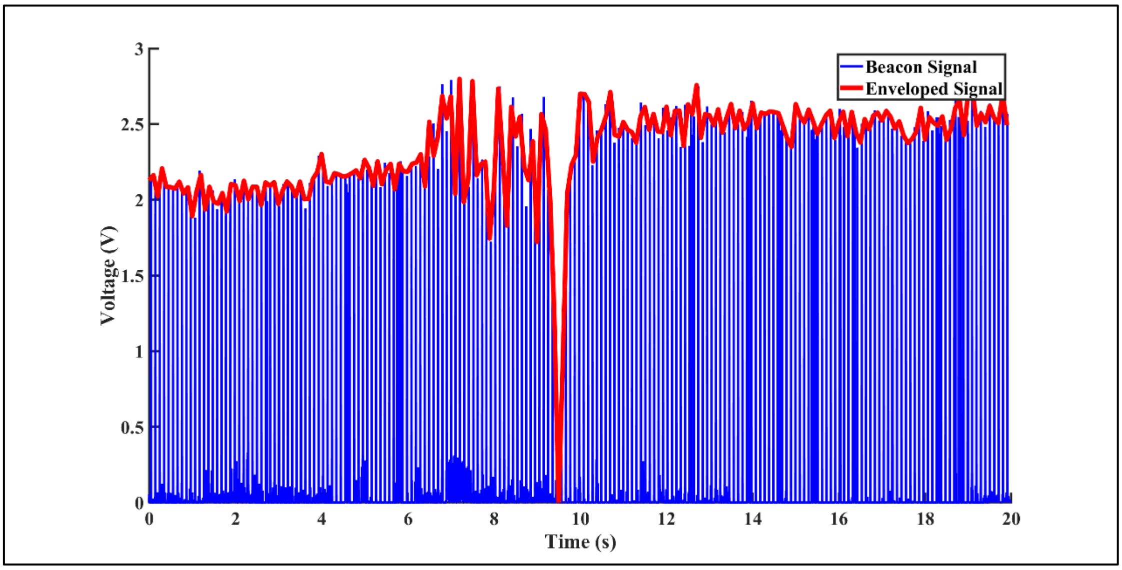

Figure 4.4 Beacon signal vs Enveloped signal

Subsequently, the signal underwent the enveloping algorithm, which involved selecting peaks based on predefined conditions. These conditions included stipulations such as ensuring that the distance between each peak is 100 data points and a total of 200 peaks are selected. This selection criterion aligns with the data being collected at a sampling frequency of 1000 Hz over a 20-second duration, where 10 consistent rhythmic peaks per second are deemed significant. Connecting all the selected peaks yielded the enveloped signal, as illustrated in Figure 4.4. At this stage, the enveloped signal assumes a continuous appearance, akin to other signals studied, facilitating the application of further analysis techniques without aberrations.

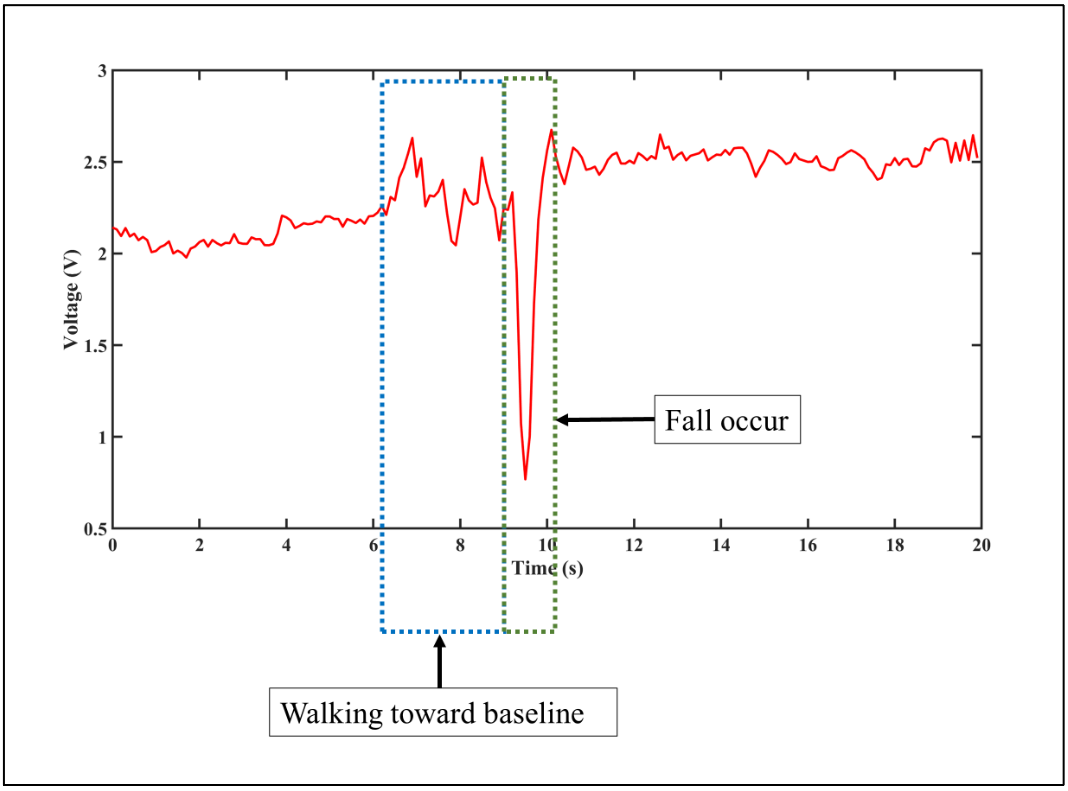

Figure 4.5 Enveloped signal for walk and fall activity

To ensure the efficacy of these algorithms in capturing the signature of human movement, an analysis of the enveloped signal becomes imperative. For instance, Figure 4.5 illustrates the enveloped signal of a scenario where an individual is walking and suddenly falls at the midpoint between the Wi-Fi router and the receiver device (baseline). In the signal, the rhythmic fluctuations indicative of human walking is discernible, characterized by the swinging of arms and torso movement. Notably, around the 10th second, an increase in the amplitude of fluctuations is observed, signifying the subject entering the FSR region without yet crossing the baseline. Subsequently, a sudden drop in amplitude occurs, denoting a substantial-sized subject crossing the baseline. This phenomenon transpires within a mere second, suggesting a high-speed movement associated with the act of falling which is a catastrophic event involving rapid downward motion of the entire body.

4.4 Comparative Analysis Between CW and PWR Signal

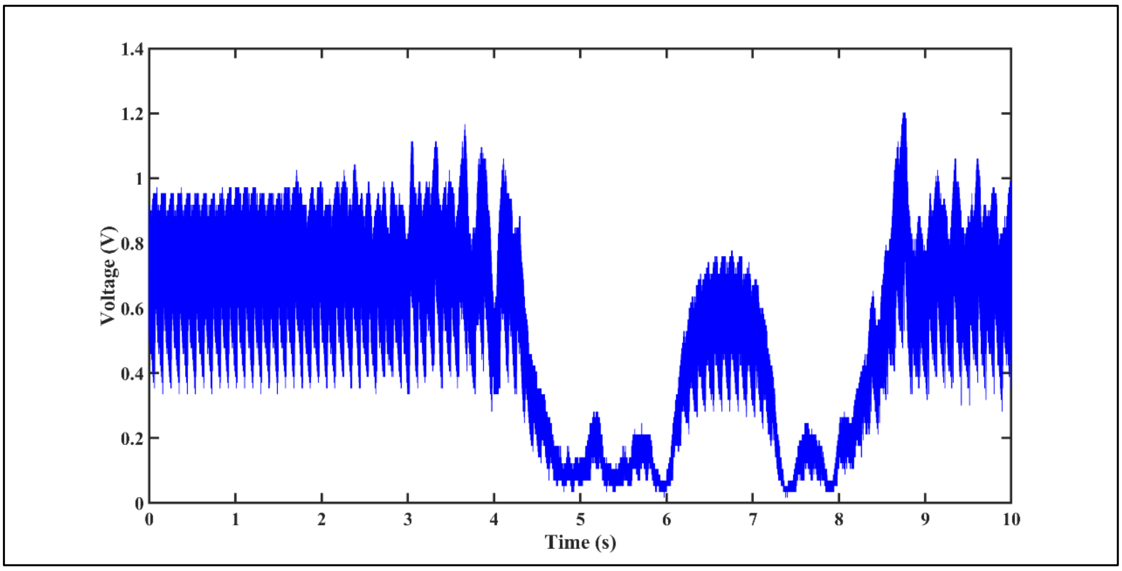

Figure 4.6 Raw CW signal

To validate the capability of Wi-Fi signals in capturing human movement signatures and assess the envelope algorithm's in preserving human movement patterns, signals from bistatic CW were collected and are depicted in continuous form as shown in Figure 4.6. These CW signals underwent a specific preprocessing procedure. Given that the characteristic of the signal is inherently continuous, the preprocessing involved a smoothing process using the Savitzky-Golay method, resulting in signals illustrated in Figure 4.7.

A high degree of similarity is observed between the pre-processed signals from both radar topologies. The signals exhibit oscillations before dropping close to zero as the subject blocks the RF wave at the baseline. Subsequently, the amplitude increases again as the subject moves away from the baseline. This consistency demonstrates the effectiveness of the envelope algorithm and highlights the potential of Wi-Fi signals in capturing and preserving human movement patterns.

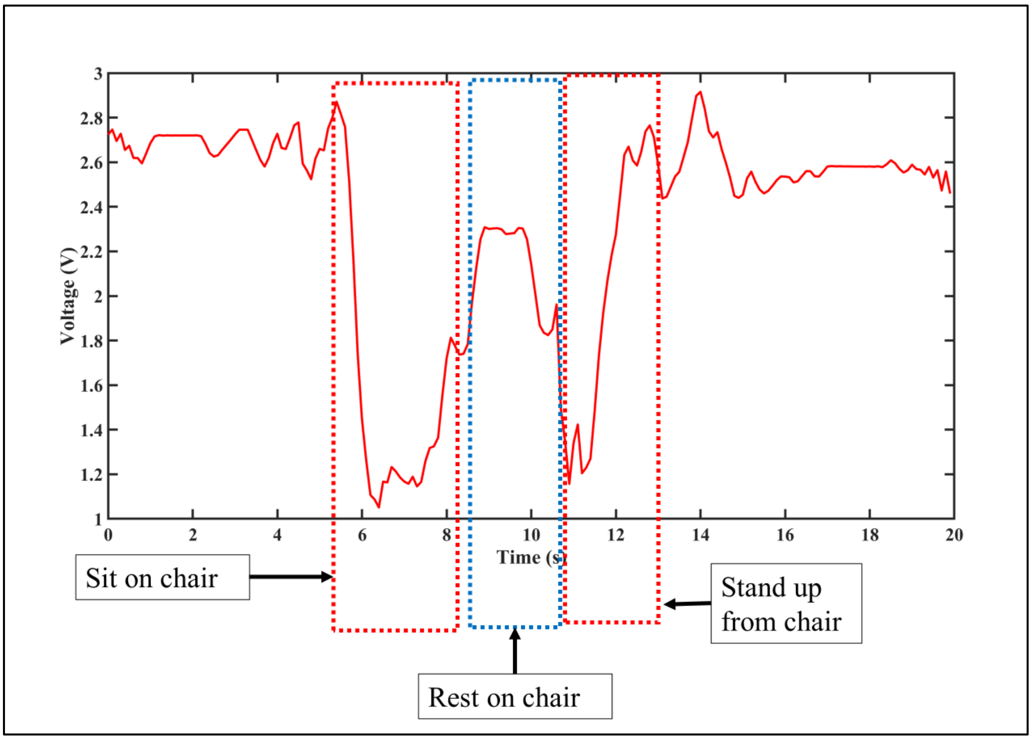

Figure 4.7 Envelope PWR signal for sitting Activity

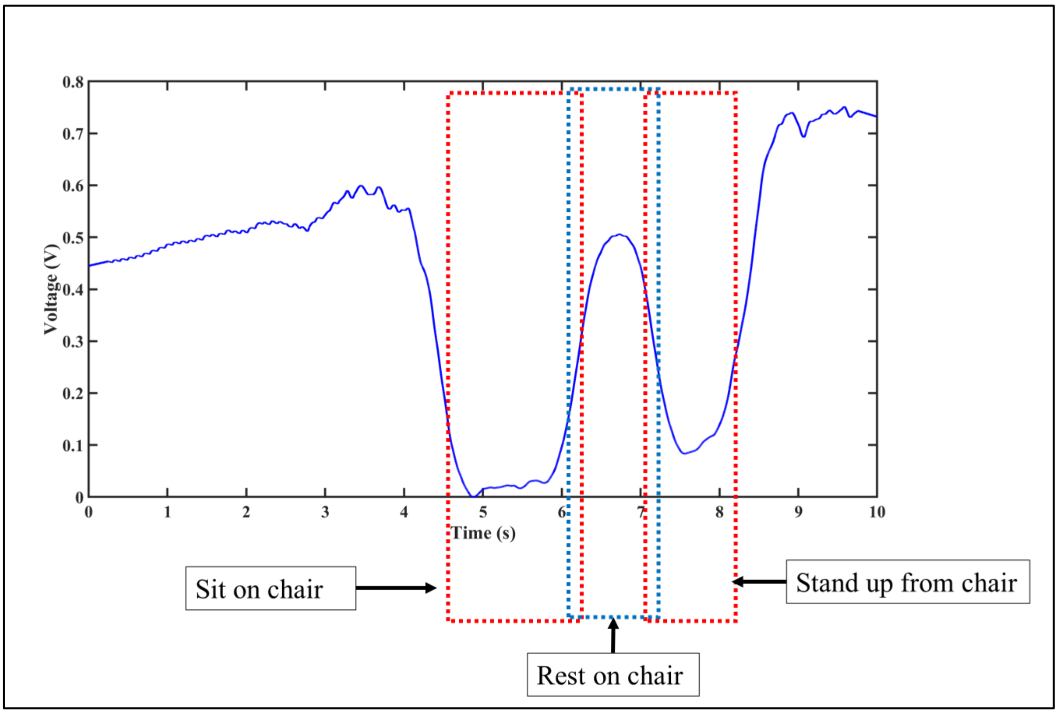

Figure 4.8 Smoothened CW signal for sitting activity

In Figure 4.7, the activity depicted involves a person walking and subsequently sitting on a chair positioned on the baseline. Similar to Figure 4.8, rhythmic fluctuations are evident, signifying the walking movement. However, distinctive voltage drops are observed when the person sits on the chair. The first drop occurs as the upper body crosses the baseline while placing the body on the chair. Another drop is observed as the person leans back, constituting a second crossing at the baseline. Meanwhile, the interval between sitting and leaning back showcases a notable increase in amplitude, indicating that the person is still in the FSR region but has not yet crossed the baseline. It is noteworthy that the second voltage drop is not as pronounced as the first, given that only the torso is involved in this action, in contrast to the first drop, which encompasses a larger body part crossing the baseline. Additionally, both drops occur over an extended time underscoring that the sitting movement is controlled and deliberate, unlike a fall, which is an uncontrolled and rapid movement.

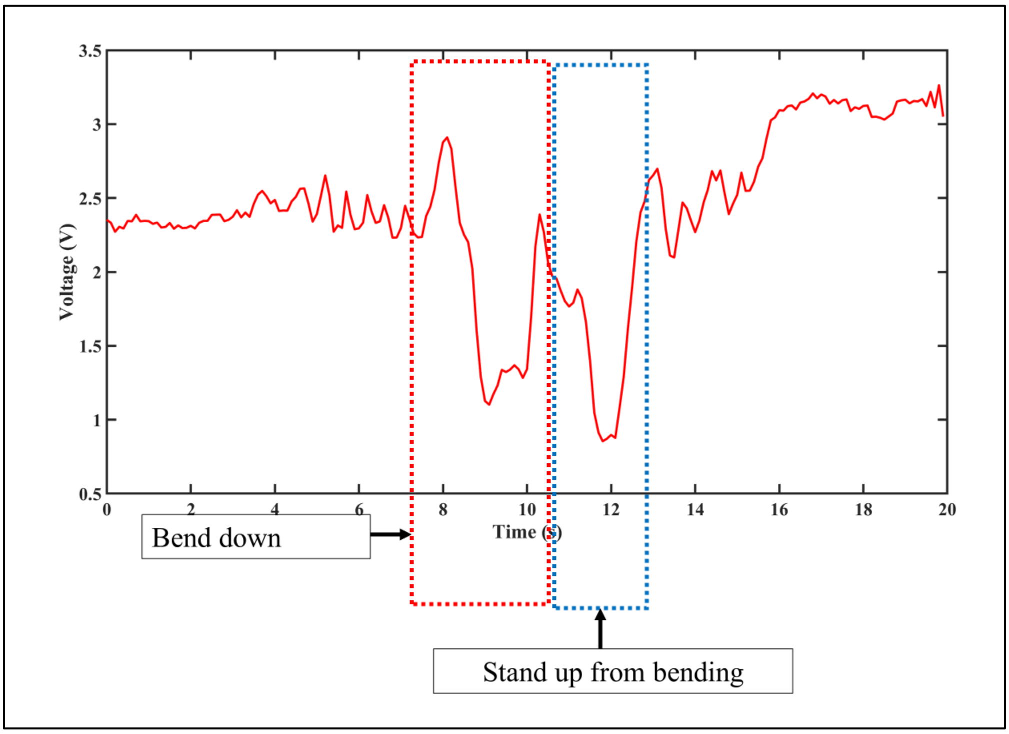

Figure 4.9 Envelope PWR signal for bending activity

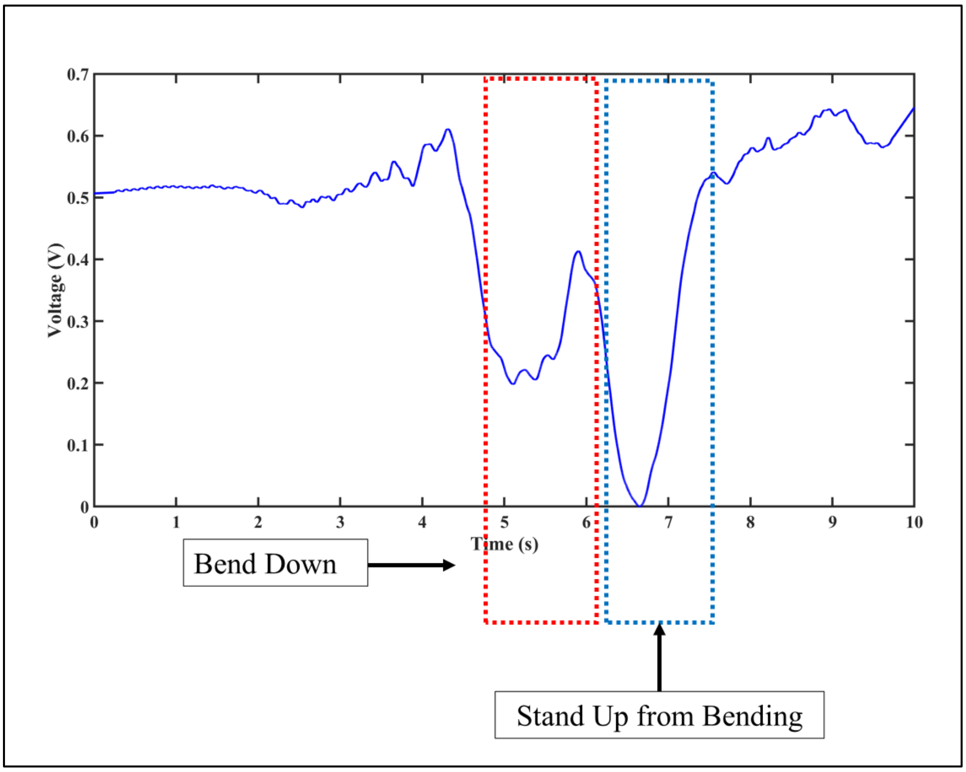

Figure 4.10 Smoothened CW signal for bending activity

Subsequently, the Doppler signature for bending is compared between both radar topologies. Figure 4.9 and Figure 4.10 each shows the enveloped signal from PWR, and pre-processed signal from CW, respectively. For bending, a two-stage amplitude depression has been observed for both radar topologies. The first indicates bending movement at the baseline. There is a slight elevation after that as the body in bent position does not fully block the transmitted RF wave. The second depression occurred as the subject stood back up and walked away from the baseline.

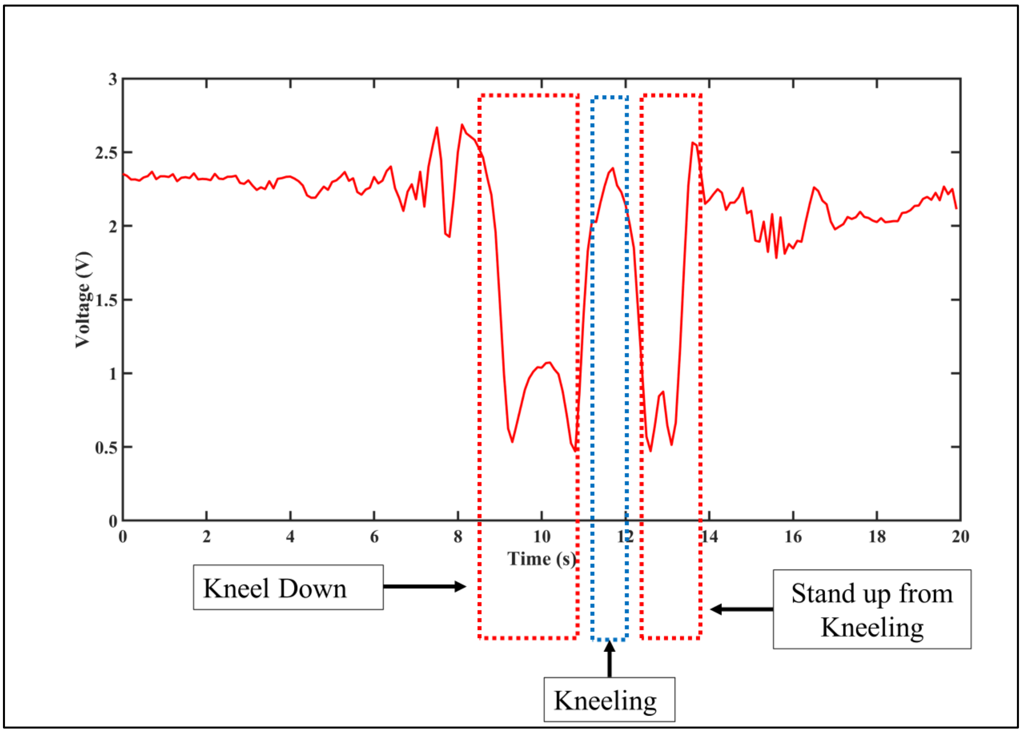

Figure 4.11 Envelope PWR signal for kneeling activity

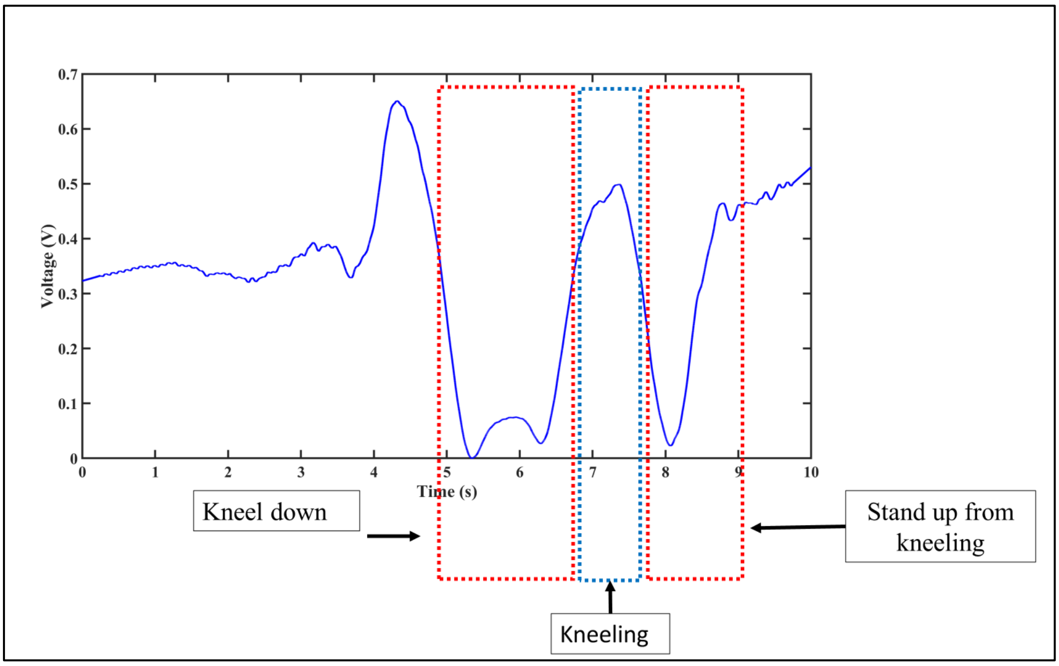

Figure 4.12 Smoothened CW signal for kneeling activity

Figure 4.11 shows a sample of Amplitude modulation signature for kneeling. The pre-processed signal was obtained using PWR. Comparatively, the sample shown in Figure 4.12 was acquired from CW. Similar to sitting, kneeling exhibits two-stage amplitude depression characteristics. The first indicates the subject going down to the kneeling position. In this position, the transmitted RF was not blocked as the subject is well below the height of Tx and Rx. Therefore, there is a rise in amplitude to its original state. Then, the amplitude was reduced back close to zero as the subject stood back up to walk away from the baseline.

Based on the presented analysis, it can be affirmed that the enveloping algorithm is successful in preserving the signature of the PWR time-domain signal for human movement same as the one that designed specifically for the aim of human target detection. Additionally, this algorithm effectively captures information related to size, speed, and type of movement via the amplitude modulation signatures.

4.5 Characterize Each Movement

Following the preservation of the time-domain signal signature, the signal underwent a series of four signal transformation processes resulting in Fourier spectrum, power spectrum, spectrogram, and scalogram. The Fourier and power spectrum can unveil the frequency components inherent in human movement. Various movements, such as walking, falling, or bending, exhibit characteristic frequency ranges specific to each motion type. Through the analysis of these frequency components, one can discern the underlying patterns and rhythms of different movements. This approach allows for the identification and differentiation of distinct movement patterns based on their frequency signatures.

Meanwhile. both time-frequency features (scalogram and spectrogram), represented as RGB images, convey information through the colour spectrum, where each colour indicates the magnitude power. Across all images, three main colours—red, yellow, and blue—play a crucial role in understanding each movement. The red colour signifies high energy or power in the time-frequency representation, often indicating strong or dominant frequency components in the signal. Yellow, on the other hand, highlights transient or impulsive events in the time-frequency representation, pointing to significant changes in the signal. Meanwhile, the blue colour may represent low energy or power in the time-frequency representation, indicating the surrounding reflection of the signal with weak frequency components.

The analysis of types of fall movements can be categorized into three groups: pre-fall, fall, and post-fall movements. Pre-fall and post-fall movements denote actions before and after the subject commits to falling, providing insights into the type of movement occurring. In contrast, fall movements create a unique signature that can be utilized to differentiate falls from fall-like movements.

4.5.1 Walk and Fall

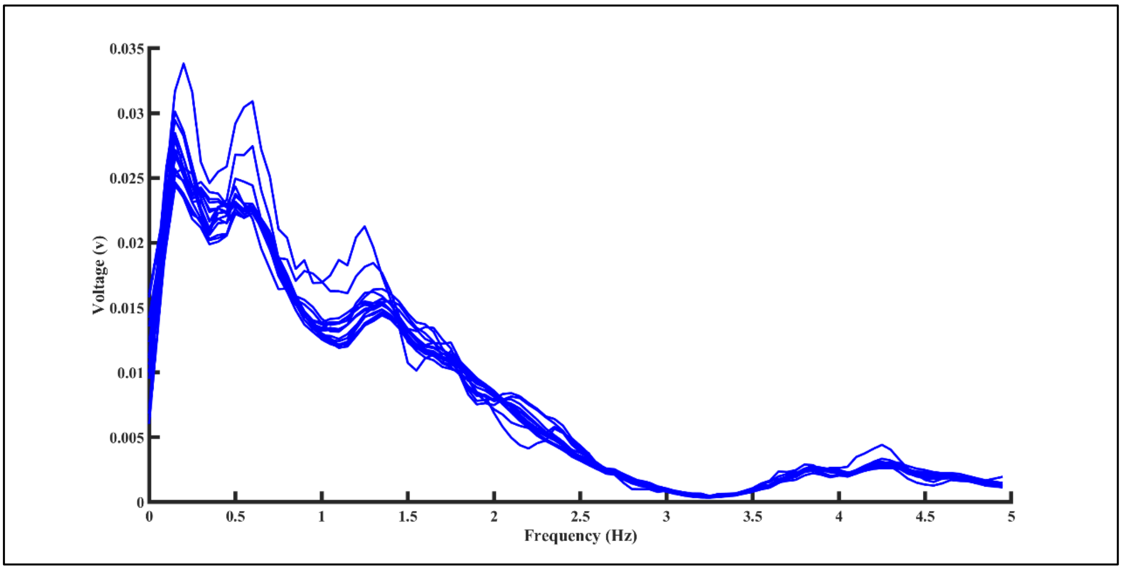

Figure 4.13 Fourier spectrum Walk and Fall for Single person scenario

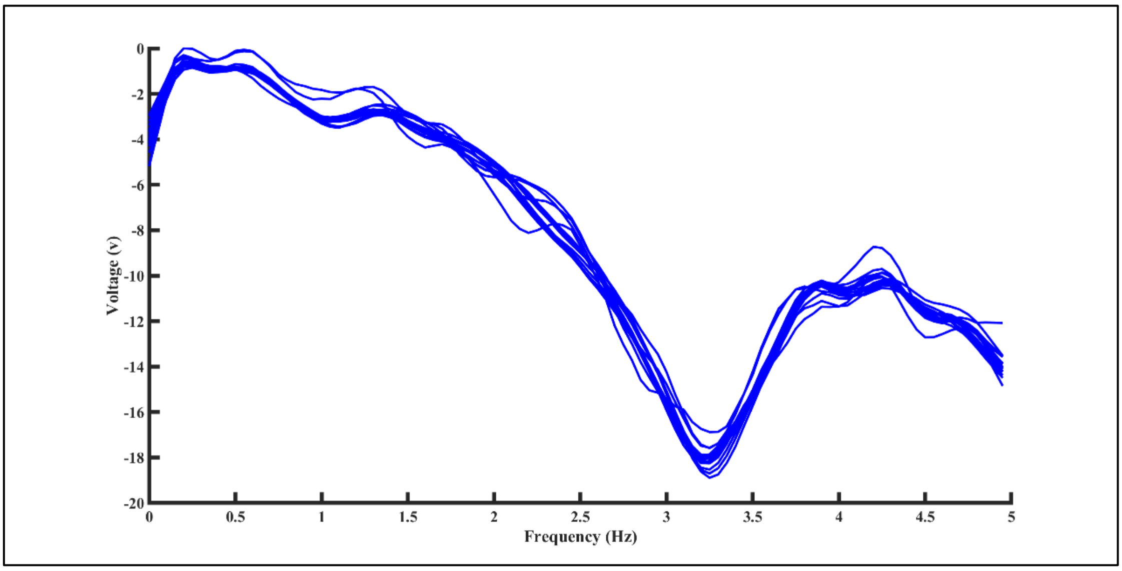

Figure 4.14 Power Spectrum Walk and Fall for Single person scenario

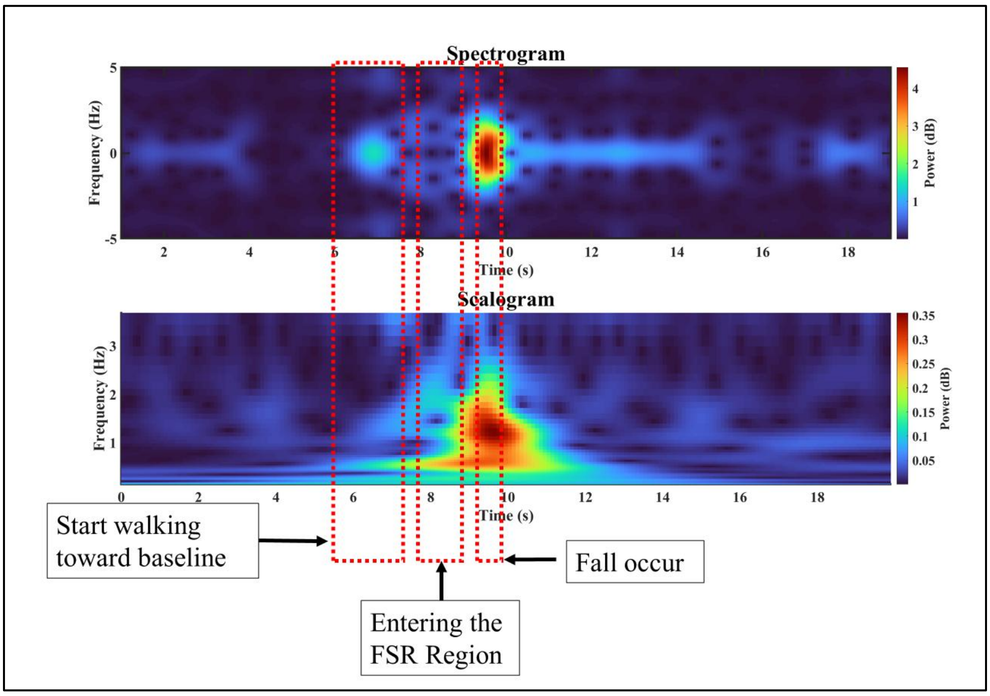

Figure 4.15 Walk and Fall image features (Single person scenario)

Figure 4.13 displays the Fourier spectrum of Walk and Fall activities, exhibiting three major peaks at frequencies of 0.2, 0.6, and 1.3 Hz with corresponding amplitudes of 0.03, 0.23, and 0.15 V, respectively. These findings offer intriguing insights into the biomechanics underlying both walking and falling movements. The distinct peaks observed provide valuable information regarding the rhythmic patterns inherent in these activities. The 0.2 Hz peak is considered noise because, when observed in the power spectrum (Figure 4.14), the power at this frequency component is approximately 0 dB, indicating negligible energy gain. This suggests a relatively low presence of significant rhythmic patterns or movements within this frequency range.

In contrast, the 0.6-0.8 Hz peak in both spectrums represent a higher-frequency component of walking dynamics, potentially associated with the swaying motion of the torso or the interaction between the limbs and the ground as the individual navigates their environment. This peak captures the cyclic nature of walking strides, reflecting the oscillatory motion of the limbs and body as they move in tandem during the gait cycle. Both walking trajectories are clearly illustrated in the example shown in [234]. The study demonstrates that gait cycle appears at 2 Hz, while in this study it is observed at 0.6-0.8 Hz. The difference arises from the walking trajectories; in the previous study, the walking movement was conducted at a speed of 1 m/s with the subject walking toward the transmitter. In contrast, this study aims to mitigate elderly walking, which is slower and has a θ_b closely to 180 degrees.

Lastly, the 1.3 Hz peak could reflect distinctive features of falling, such as sudden shifts in body weight or rapid movements made to regain balance. This higher-frequency component may be indicative of the abrupt and irregular nature of falling movements compared to the smoother, more regular motion observed during walking.

Furthermore, Figure 4.15 presents image features of walk and fall, showcasing both spectrogram and scalogram images. These images reveal three significant changes in power at specific frequency components over time. Firstly, as the walking movement begins, a mixture of low-intensity yellow and blue colours appears, indicating variations in frequency components corresponding to the swinging of arms and torso movement. Subsequently, when the subject enters the FSR region but has not exactly crossed the baseline, the signature of the walking subject becomes clearer. As the subject enters the FSR region, the fluctuation amplitude becomes more visible. Finally, the fall movement is observed, characterized by a high intensity of red colour, signifying a high-power density measured within a small-time frame. This crucial information contributes to visualizing the walk and fall activity, as the walking signature is clearly discernible before the occurrence of the fall.

4.5.2 Stumble

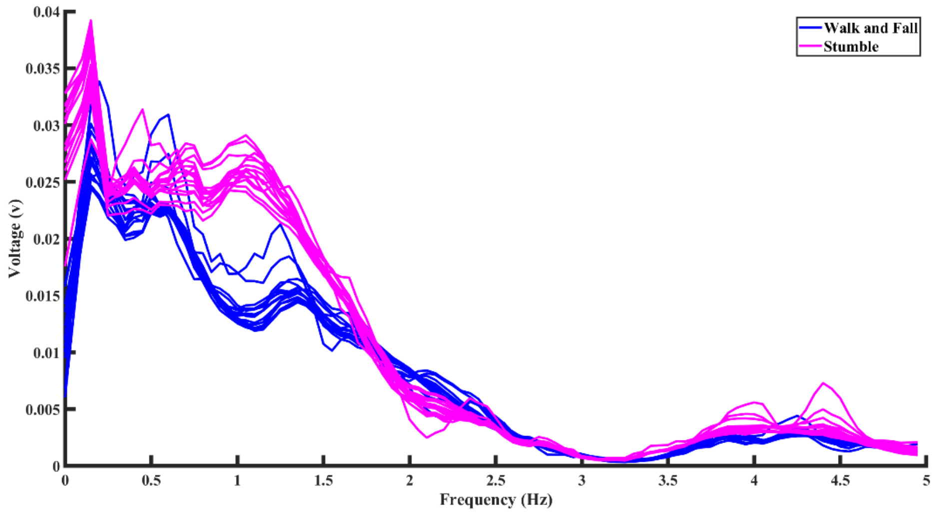

Figure 4.16 Fourier spectrum Walk and Fall vs Stumble for Single person scenario

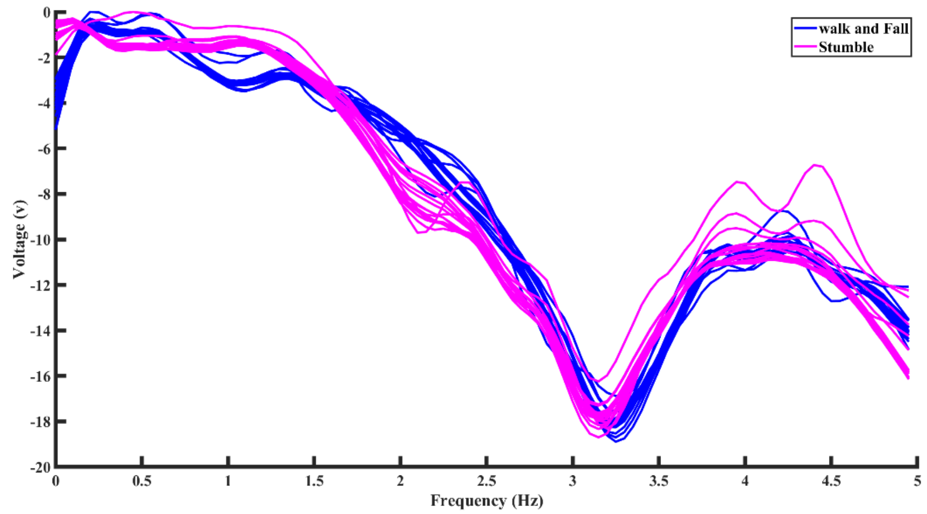

Figure 4.17 Power Spectrum Walk and Fall vs Stumble for Single person scenario

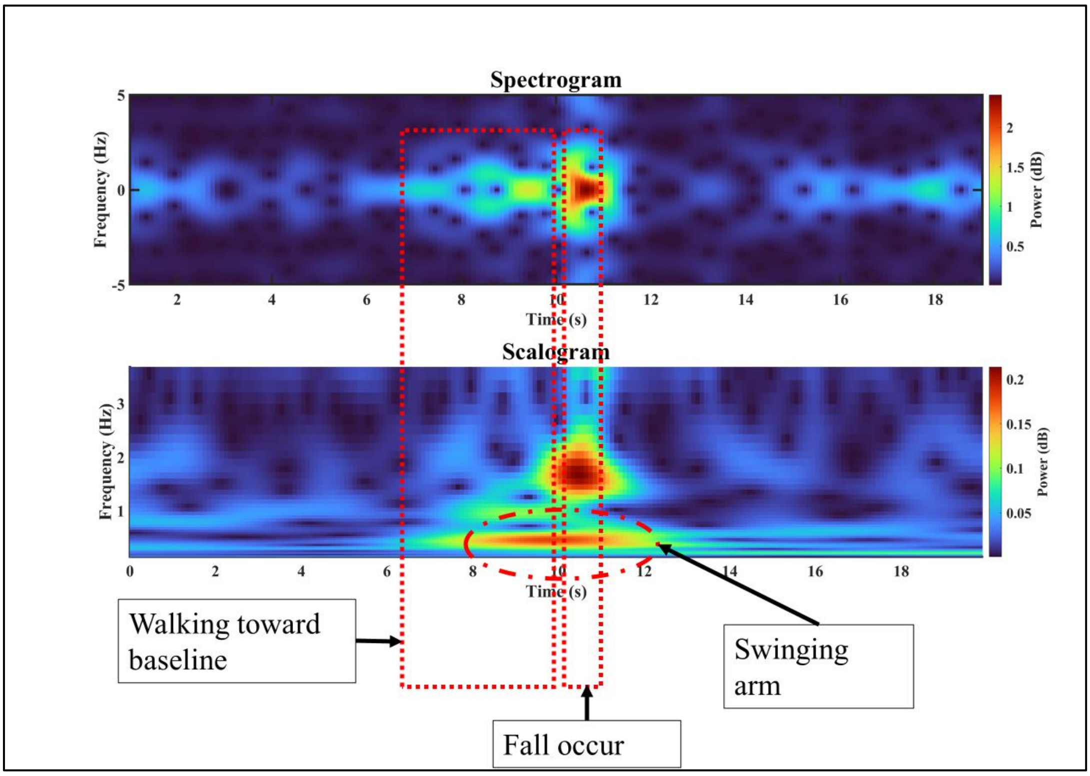

Figure 4.18 Stumble image features (Single person scenario)

On the contrary, stumbling, a type of fall activity characterized by a forward motion similar to walking and falling, exhibits an almost identical signature to walking and falling activities. This similarity can be observed in Figure 4.16 and 4.17, where the Fourier and power spectrum for walking and falling can be observed. However, stumbling activities display comparable patterns, particularly in the frequency range of 0.7 to 1.5 Hz. Within this range, the amplitude in both the Fourier and power spectra flattens at a high level, attributable to the unique biomechanics of stumbling. During stumbling, individuals may attempt to regain balance by employing arm movements, resulting in rhythmic motions that influence the frequency components within this range.

In stumbling, the subject is walking towards the baseline and then suddenly falls, akin to stumbling on a hard object on the ground. The key difference lies in the fact that during the fall in stumbling, there is a high intensity of power in the variation of frequency components, similar to human walking such present in Figure 4.18. This occurs because, during stumbling, the subject swings their arms in a manner similar to how people typically react to balance their body weight and prevent a fall. Stumbling, as a fall that occurs due to external factors such as uneven terrain, shares similarities with the activity of walk and fall. Despite their similarities, a significant difference in the involved frequency components can be observed in both the spectrogram and scalogram.

4.5.3 Slip and Fall

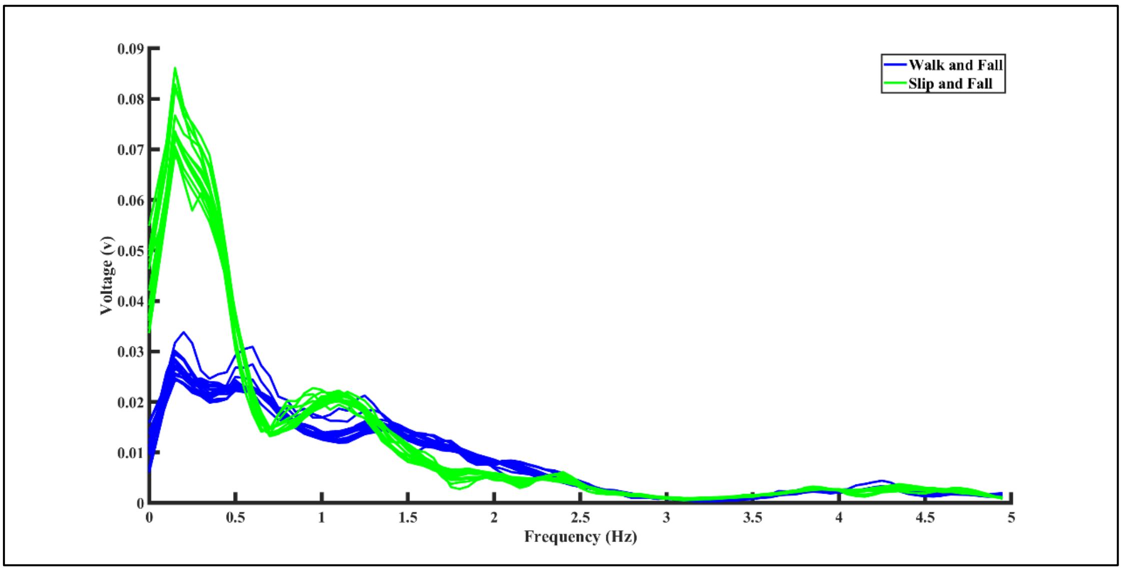

Figure 4.19 Fourier spectrum Walk and Fall vs Slip and Fall for Single person scenario

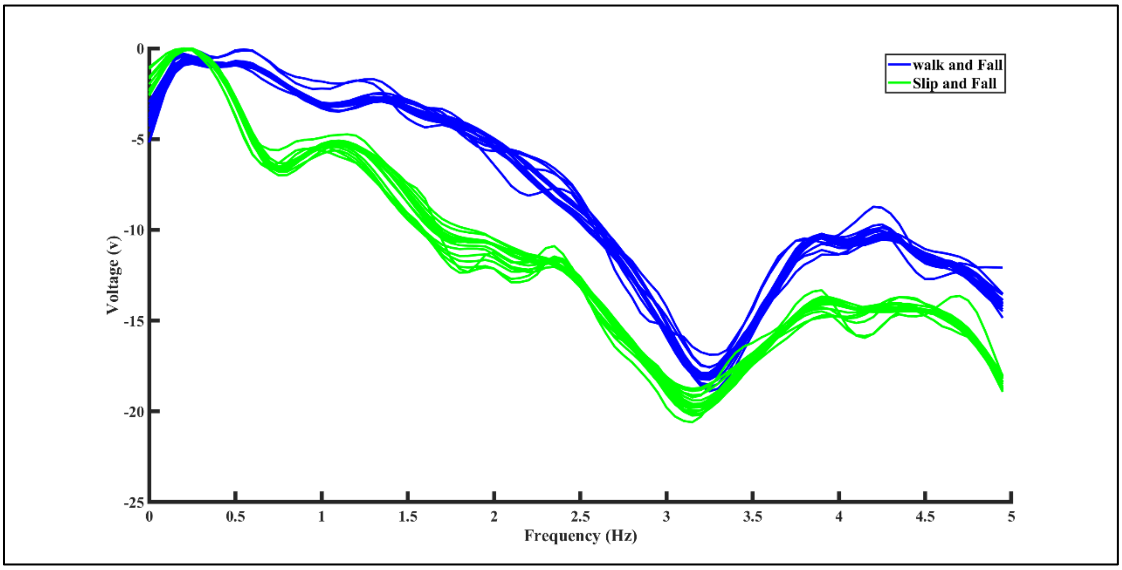

Figure 4.20 Power Spectrum Walk and Fall vs Slip and Fall for Single person scenario

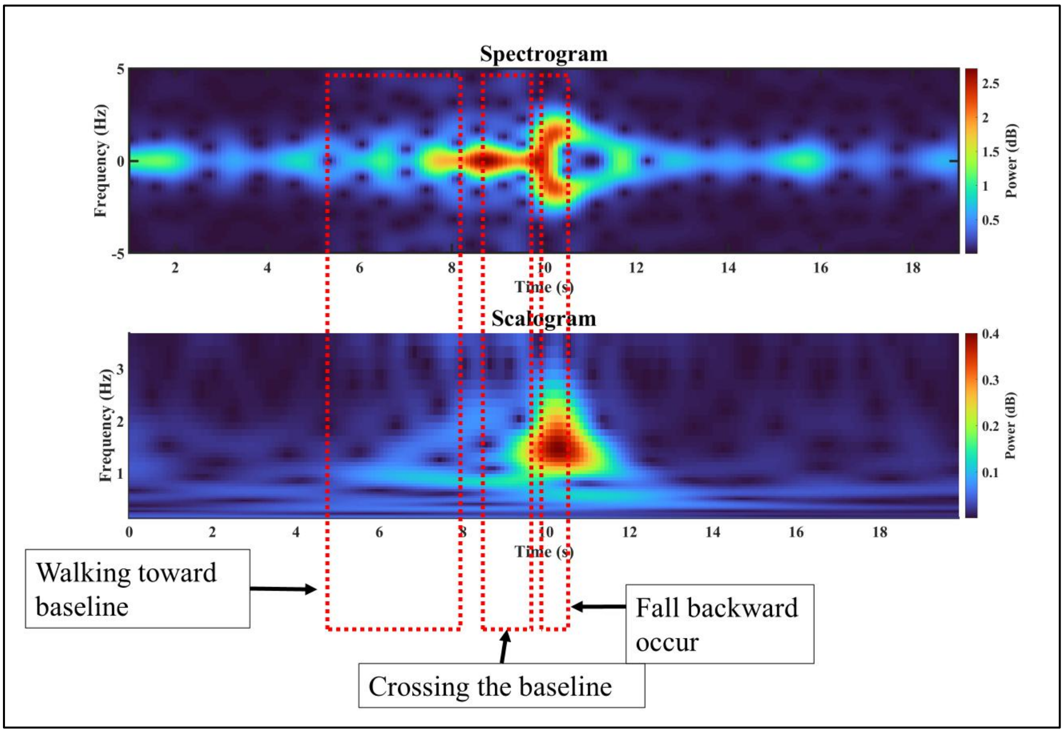

Figure 4.21 Slip and Fall image features (Single person scenario)

Meanwhile, slip and fall events exhibit distinct trajectories compared to walking, falling, and stumbling activities. Slip and fall incidents involve a different sequence of movements, where a walking motion is initially performed at the baseline before the fall occurs in a backward direction. In Figure 4.19 and 4.20, significant differences in Fourier and power spectrum in between walking and falling and slip and falling activities are evident, particularly range of 0.6 to 0.7 and 1.3 to 2.2 Hz, the signal patterns of slip and fall events resemble those of stumbling motions, characterized by higher amplitudes compared to walking and falling activities.

In range of 0.6 and 0.7 Hz discrepancy can be attributed to the swinging arm movements employed during walking activities when crossing the baseline. The major drop of amplitude can clearly be observed due to the angle of walking was passing the 180 degrees of θ_b. Furthermore, the backward fall trajectory in slip and fall events is discernible in the signal's amplitude drop in the frequency component range of 1.3 to 2.2Hz, which occurs more abruptly compared to walking and falling activities. This distinction underscores the unique characteristics of slip and fall events where the fall occur after a major amplitude drop, thus a sudden peak observe at this range indicates that the sudden shifts in body weight or rapid movements made to regain balance.

Moreover, in Figure 4.21. This similarity arises from a shared factor in the fall, namely external elements such as walking or stepping on slippery surfaces. Consequently, subjects experiencing this type of fall will swing their arms to maintain balance. However, distinctions in the pre-fall phase are observable, where before the fall occurs, the subject has already crossed the baseline. Additionally, the subject commits to a backward fall, altering the post-fall power intensity in comparison to the stumble activity.

4.5.4 Sit and Fall

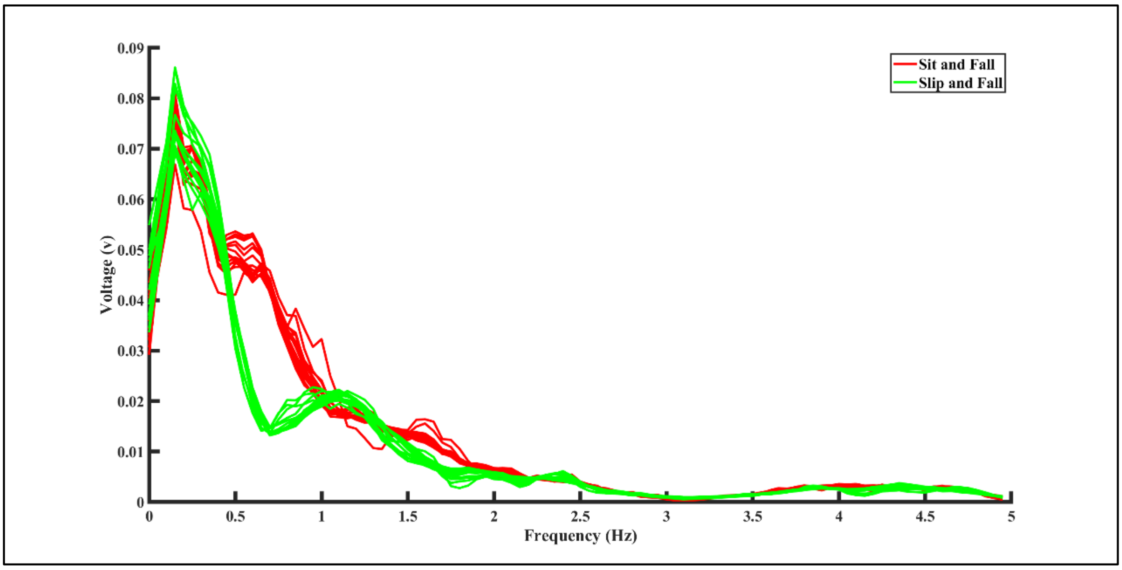

Figure 4.22 Fourier spectrum Walk and Fall vs Sit and Fall for Single person scenario

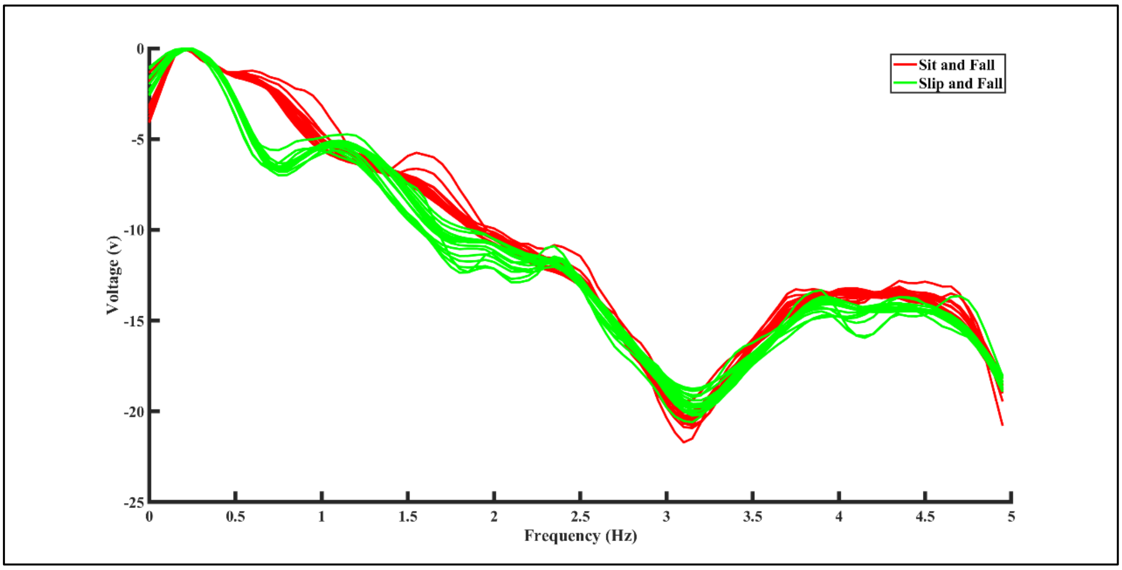

Figure 4.23 Power Spectrum Walk and Fall vs Sit and Fall for Single person scenario

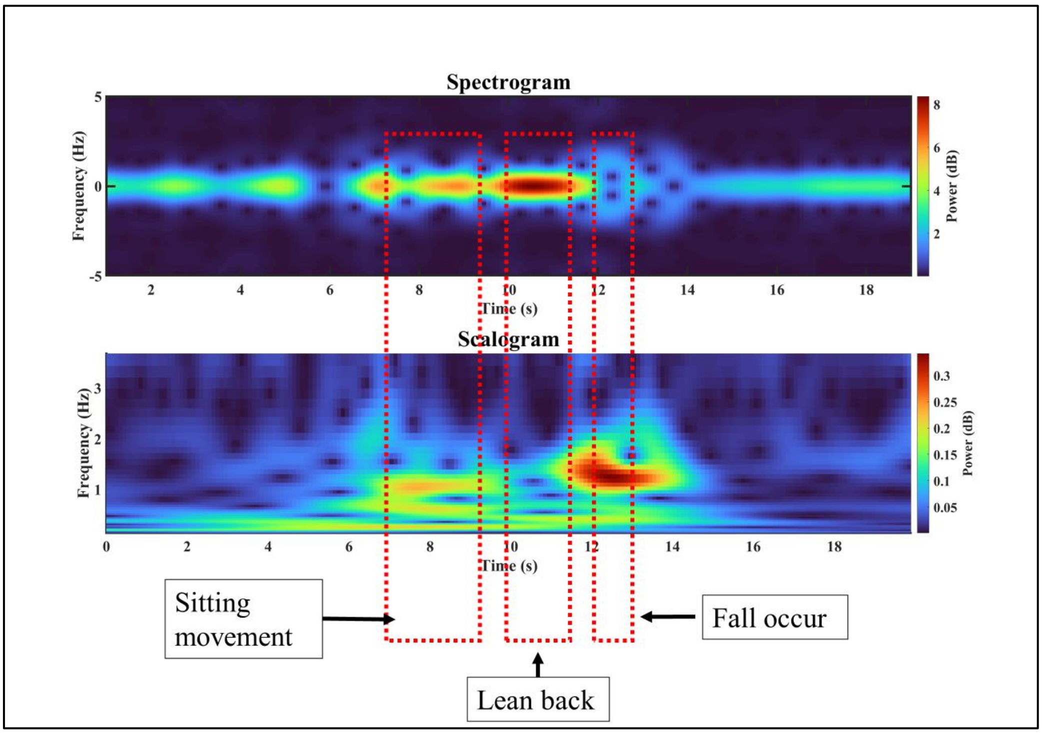

Figure 4.24 Sit and Fall image features (Single person scenario)

Figure 4.22 and 4.23illustrates the comparison between slip and fall and sit and fall Fourier and power spectrums, revealing pattern differences between the 0.5 Hz and 1 Hz frequency components. In this frequency range, the slip and fall pattern exhibits a significant amplitude drop, whereas the sit and fall pattern shows a flattening from the 0.5 to 0.7 Hz frequency component before gradually decreasing until 1 Hz. This disparity may indicate the separation of sitting and walking movements at the baseline, with sitting movements involving more varied actions such as sitting down, leaning backward, and getting up. These movements require lower rhythmic cycles which involve slower torso movements, which play a vital role in this frequency range. Additionally, in the frequency component range of 1-2 Hz, the voltage drops in the sit and fall pattern occurs more gradually compared to slip and fall. This difference may be attributed to the direction of fall in sit and fall activities, where the fall movement occurs sideways, resulting in a smoother decline in voltage.

Furthermore, the seat and fall activity follows a trajectory distinct from walk and fall and stumble, as it involves falling after the person rises from a sitting position. The image features illustrated in Figure 4.24 reveal three significant pieces of information in the spectrogram and scalogram. In both the spectrogram and scalogram, it is evident that the sitting movement has a high-power intensity, as the chair is placed on the baseline. Therefore, for a subject to place their body on the chair, they must cross the baseline. In the lean-back position, the subject also crosses the baseline, but with not as much power intensity as the sitting movement, as it only involves torso movement. However, for the fall movement, the scalogram does not provide much information about power intensity, while the spectrogram clearly shows high power, albeit for a slightly longer duration compared to walk and fall. This is because the fall activity in seat and fall occurs sideways and is not a high-speed movement, as the person still has the armrest to distribute their body weight for balancing before committing to a fall. Thus, this type of fall also having their unique signature that can be distinguished from other types due to its distinctive pre-fall motion.

4.5.5 Faint

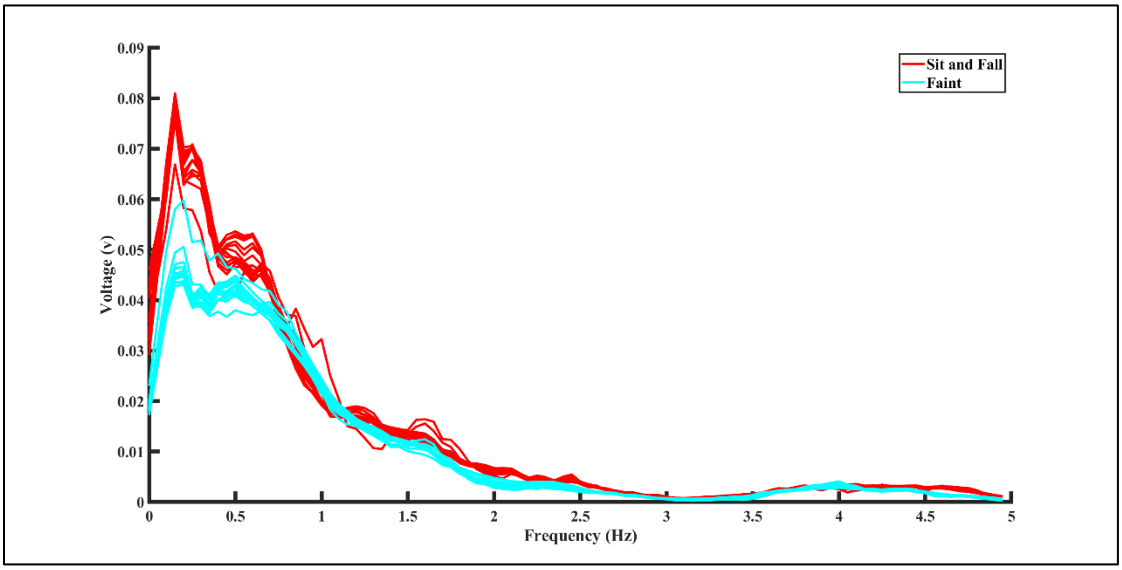

Figure 4.25 Fourier spectrum Sit and Fall vs Faint for Single person scenario

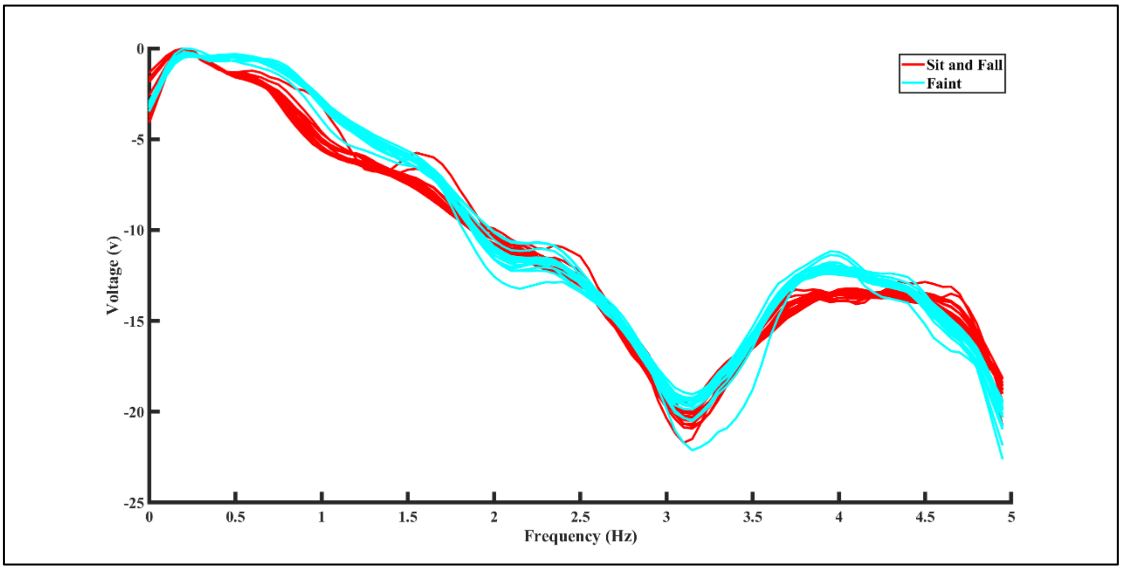

Figure 4.26 Power Spectrum sit and Fall vs Faint for Single person scenario

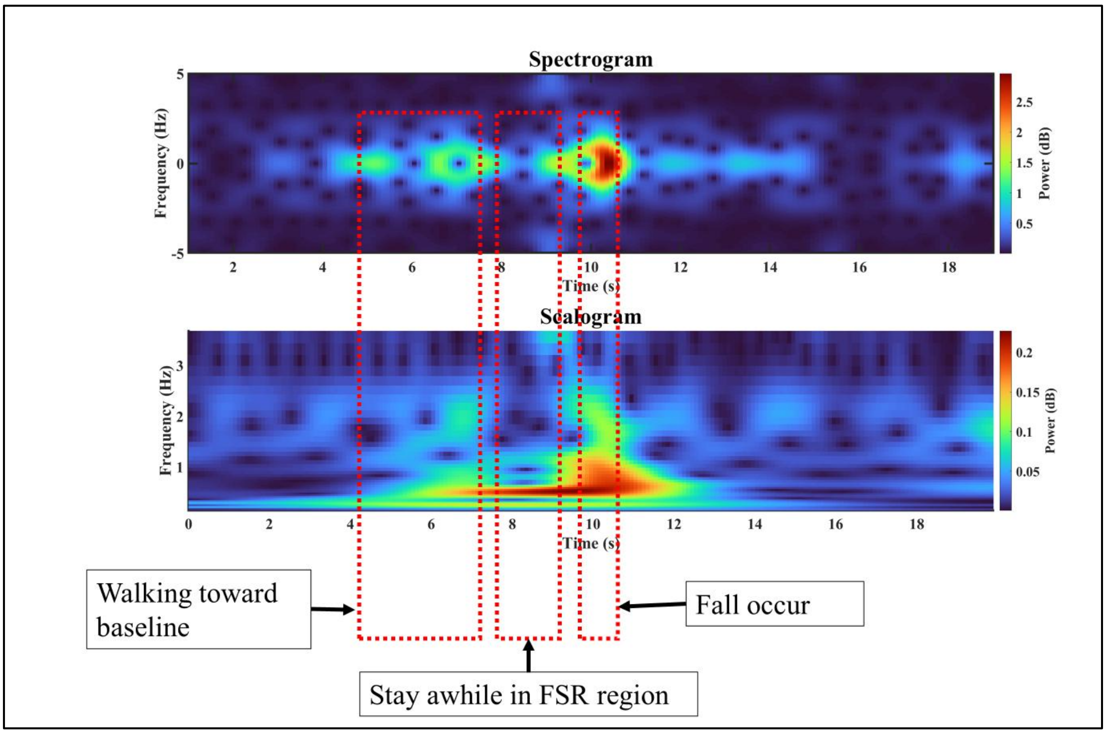

Figure 4.27 Faint image features (Single person scenario)

Fainting, as a type of fall activity, involves a lateral fall similar to sit and fall. This occurrence is typically triggered by dizziness. During this fall activity, the subject momentarily halts on the baseline, simulating a sensation of imbalance or dizziness, and then gradually descends in a sideways motion. Unlike high-speed falls such as walk and fall or stumble, fainting initiates from the lower body, resulting in a loss of control over body parts.

Fainting, a type of fall that occurs in the same direction as sit and fall, is compared in Figure 4.25. The figure reveals similar patterns between these two fall types. However, for faint activity, the amplitude is lower compared to fall activity. This difference can be attributed to the fact that during fainting, the individual remains still due to dizziness, whereas in sit and fall, there is a higher degree of movement trajectories observed. In Figure 4.26, the power spectrum of both activities exhibits a similar pattern but with different power drop levels. Fainting activity appears at a lower power level, indicating that remaining stationary at the baseline does not significantly impact the power change in the frequency range of 0.5 to 1.5 Hz.

The distinctive characteristics of this scenario are vividly illustrated in Figure 4.27. While the subject is crossing and remaining in the FSR region, there is a noticeable presence of high-intensity power with a low-frequency component. When the collapse unfolds, the frequency component with high power intensity experiences an increase, albeit for a slightly prolonged duration compared to other activities like walk and fall and stumble.

4.5.6 Fall-Like

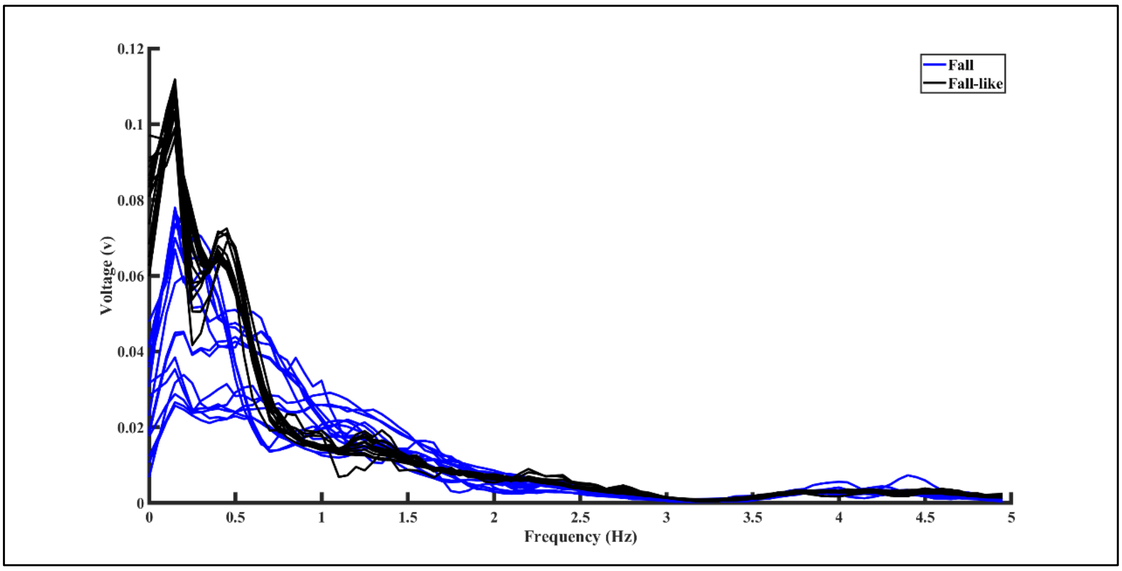

Figure 4.28 Fourier spectrum Fall vs Fall-Like for Single person scenario

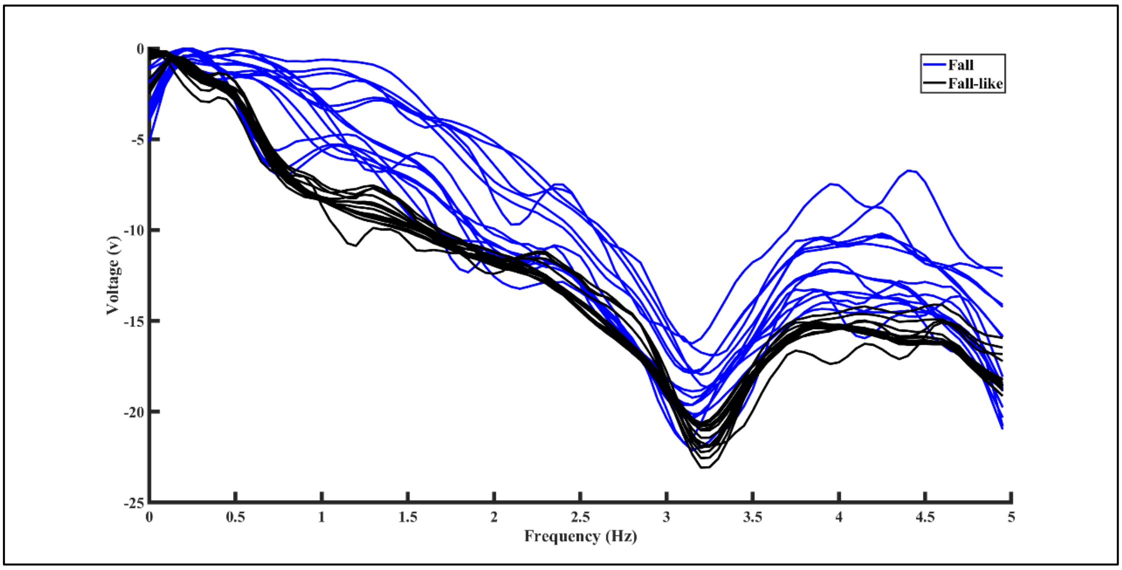

Figure 4.29 Power Spectrum Fall vs Fall-Like for Single person scenario

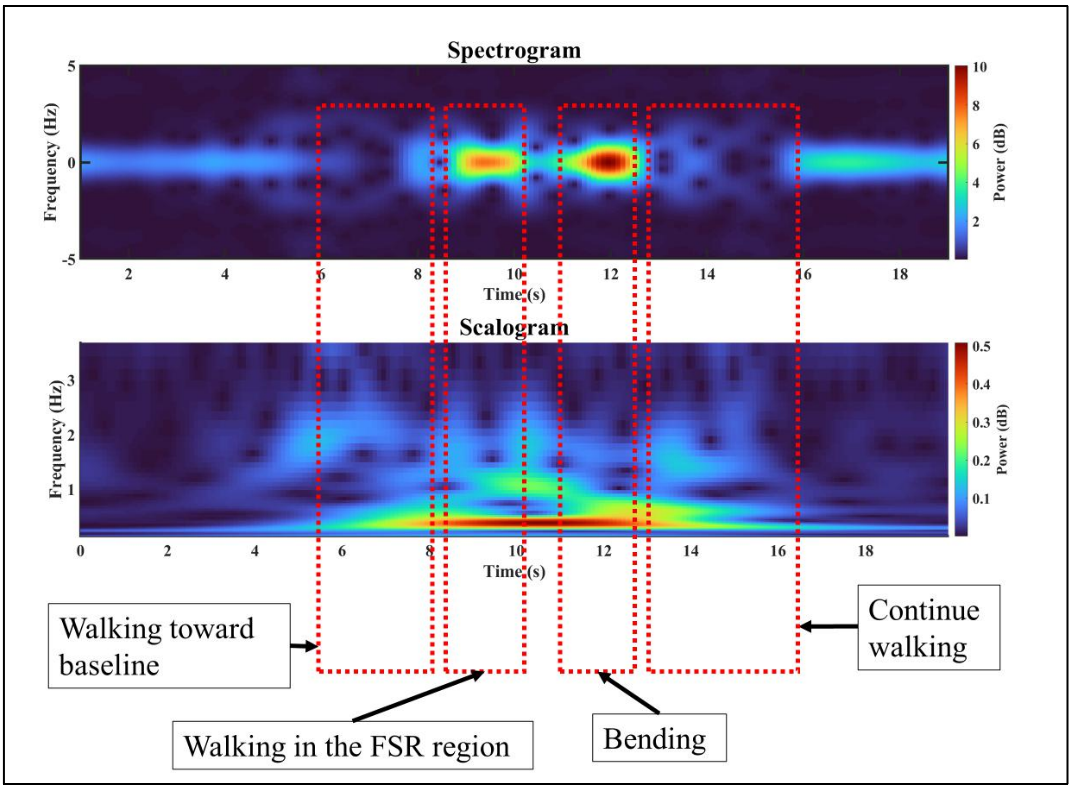

Figure 4.30 Bending image features (Single person scenario)

Fall-like movements serve as a significant distinction between fall and non-fall activities. However, Figure 4.28 clearly illustrates differences between fall-like movements and actual falls. The main peak of fall-like movements is notably higher compared to other types of falls, indicating a prominent rhythmic motion captured on two distinct sudden drops observed: the first drop from 0.11 V to 0.6 V, and the second drop from 0.07 V to 0.02 V, occurring at 0.5 Hz and 0.7 Hz frequency components, respectively. This insight suggests that fall-like activities, despite involving lowering of the upper body part, exhibit rhythmic movements that differentiate them from falls. This distinction is particularly evident in the frequency component range below 1 Hz, where the robustness of fall movements is discernible.

Furthermore, Figure 4.29illustrates that one type of fall-like movement exhibits a signature similar to other types of falls, with noticeable pattern similarities. However, differences in the declination of the spectrum between 0.5 to 1 Hz frequency components are observed, where the fall-like movement displays a steeper slope compared to fall activities. Consequently, at 1 Hz and above, the patterns appear similar, but due to the steeper slope in the 0.5-1 Hz range for fall-like movements, the power level is slightly lower compared to fall activities.

In contrast to falls, bending is a kind fall-like movement that involves the upper body moving toward the ground but is not random and lacks the high-speed motion characteristic of a fall. This distinction is evident in Figure 4.30, where the bending activity still produces high power intensity but in a low-frequency component and takes a longer duration to complete. A notable comparison is the time frame: fall signatures typically occur between 0.5 seconds to 1.5 seconds, while bending takes more than 2 seconds to be performed. This clear distinction highlights that falls are non-rhythmic with high-speed motion, even though the direction of body movement may be similar to fall-like motions.

4.5.7 Multiple person scenario

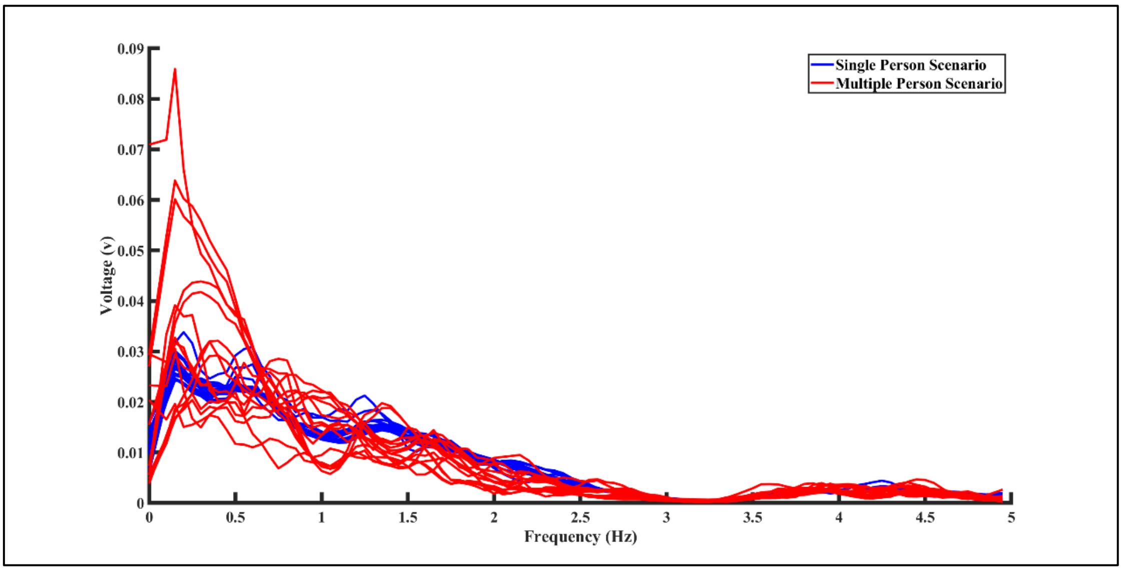

Figure 4.31 Fourier spectrum for single vs multiple person scenario based on walk and fall

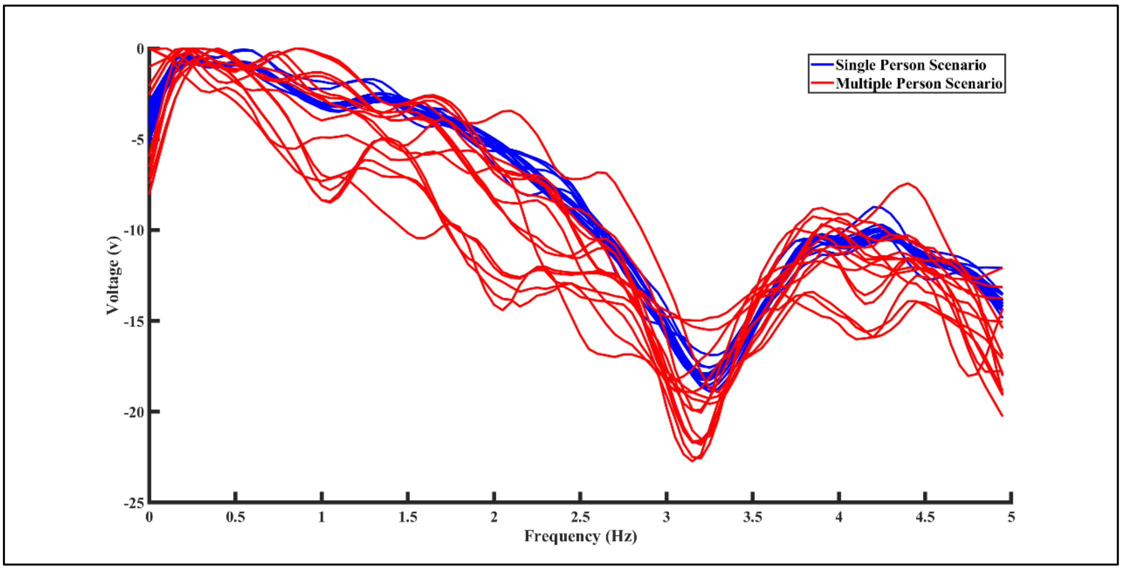

Figure 4.32 Power spectrum for single vs multiple person scenario based on walk and fall

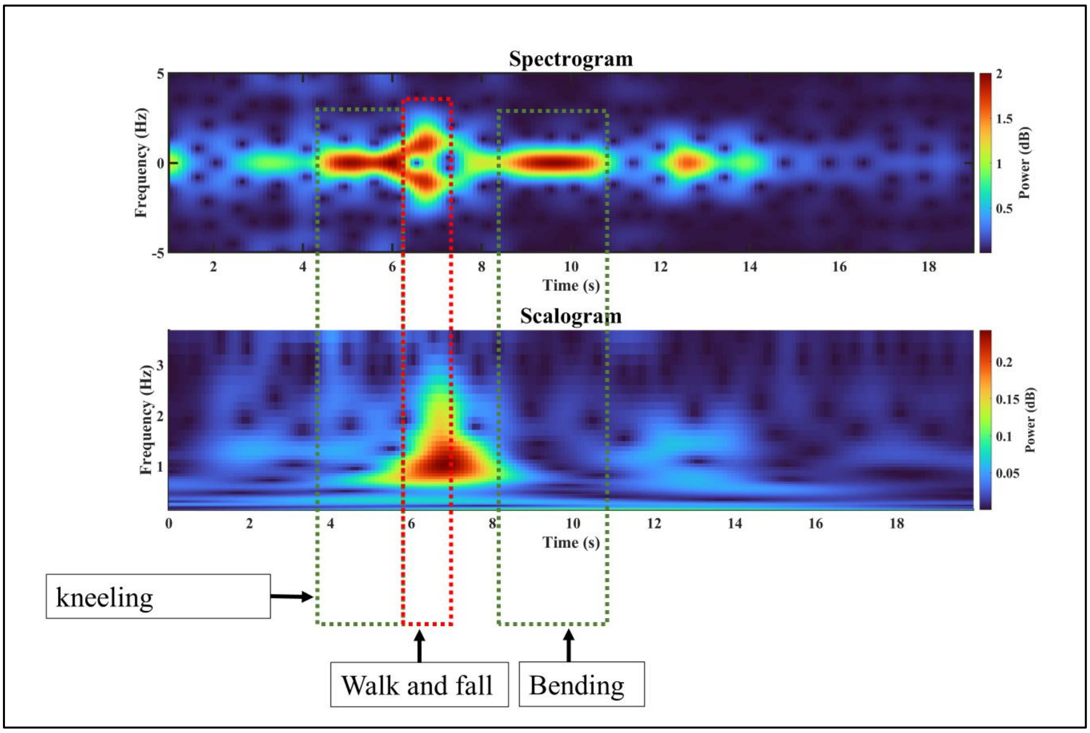

Figure 4.33 Walk and Fall image features (Triple person scenario)

As known, multiple person scenario involves a complex activity due to the simultaneous performance of fall and fall-like movements. As depicted in Figures 4.31 and 4.32, both the Fourier and power spectrum of multiple person scenario fail to distinguish each type of activity. Both spectrums offer information about the frequency content of a signal but do not capture the temporal dynamics or the time evolution of the signal. Given that it is a frequency-domain analysis technique, it may not adequately represent the nuanced temporal aspects of complex human motion. The technique assumes that the signal is stationary, which may not hold true for dynamic and evolving human movements. Consequently, it may not accurately project a proper signature on complex signal trajectories.

Moreover, a highly complex activity, such as multiple person scenario, proves to be considerably more intricate compared to single person scenario, as illustrated in Figure 4.33. The figure depicts a triple target detection involving walk and fall, kneeling, and bending activities. In the image, the kneeling activity is discernible but exhibits low power volume. This is attributed to the kneeling being performed at location 3, outside the FSR region and farther from the transmitter. On the other hand, the bending activity is more evident with better power volume, as it is performed closer to the Wi-Fi router. Despite these simultaneous activities, the fall movement remains dominant in this scenario, displaying the highest power intensity along with high frequency component. This dominance is facilitated by the specific window size chosen for detecting the fall movement, set at 1 second. This window size is suitable for capturing the catastrophic nature and high-speed movement associated with falls. Therefore, even amidst multiple movements performed simultaneously, the significant features of the fall movement can still be analysed through spectrogram and scalogram analyses.

4.6 Summary

In summary, the results demonstrate the effectiveness of the enveloping algorithm in characterizing each type of movement across both the time-domain and transformed signal representations. The preprocessing algorithm successfully preserved the amplitude modulation signature by applying threshold-based noise reduction in conjunction with the enveloping technique. Furthermore, a comparative analysis with a CW radar setup confirmed the reliability of the proposed method, as it consistently retained the amplitude modulation signatures. This alignment with the CW radar setup underscores the robustness of the developed approach in maintaining signal integrity, which is essential for accurate classification and detection in fall detection systems.

The analysis further demonstrates the signal's capability to effectively characterize movements through the Fourier spectrum, power spectrum, spectrogram, and scalogram. The distinction between different types of falls is further evident in the 0.3–0.8 Hz range, representing higher-frequency components associated with preparatory movements. These components may correspond to swaying torso motions or interactions between limbs and the ground during navigation. In particular, "walk-and-fall" and "stumbling" movements exhibit gradual declines in this frequency range, with the latter showing slightly sloped patterns indicative of rapid hand movements for balance correction. In contrast, for slip and fall events, high-amplitude peaks within this range indicate that the subject initially obstructs the signal, followed by a sudden drop reflecting the rapid occurrence of the fall. This pattern is distinguishable from slower falls, such as "sit-and-fall" and "fainting." In "sit-and-fall" scenarios, the fall occurs as the subject attempts to rise from a chair, with less height involved, resulting in a more gradual decline in signal amplitude. Similarly, in "fainting" cases, the subject’s unconscious movements serve to mitigate the impact of the fall, producing slower signal variations. The separation between fall and fall-like movements is also observable in the 0.8–1.3 Hz range, where the amplitude decline in fall-like movements is more gradual, reflecting smoother transitions. This difference arises from the subtle, controlled nature of movements, such as sitting or bending, in comparison to the abrupt changes seen during falls.

The spectrogram and scalogram further demonstrate excellent time-frequency resolution for the task of characterizing movements. This is evident in the visualization, where prominent movements are represented by darker red regions, indicating higher power concentration within specific frequency ranges at given moments. The type of fall can be effectively distinguished by analysing the pre-fall signatures, which manifest in distinct patterns unique to each movement type. For example, in walk and fall and stumble movements, the darker red colour associated with the fall appears over short durations, indicating the rapid nature of these events. However, a key distinction between these two movements lies in the presence of red patterns corresponding to arm swinging in the "stumble" scenario. This suggests that the subject's attempt to regain balance is reflected in the extended frequency components related to limb motion. Moreover, the separation between fall and fall-like movements is clearly discernible through the temporal distribution of power. In fall-like movements, the prominent red regions appear over longer periods, indicating smoother, sustained activities such as sitting or bending. This temporal contrast, where fall-like movements exhibit longer durations of high power compared to the abrupt and short bursts observed in falls, enhances the system’s ability to accurately classify and differentiate between these events. These insights emphasize the effectiveness of time-frequency analysis for improving the precision of fall detection systems.

The inclusion of second and third movements to simulate real-world scenarios successfully increased the complexity and noise within the collected signals. This complexity is evident in the Fourier spectrum, power spectrum, spectrogram, and scalogram, where multiple overlapping signatures are plotted. However, even under these conditions, the application of the same frequency ranges used in the single-person scenario allows for the segregation of fall, post-fall, and fall-like movements. Despite the success in distinguishing these events, the overlapping of signal signatures poses a significant challenge for manual classification without the assistance of ML and DL models. The intricacy of real-world movements and their overlapping features highlights the importance of advanced classification algorithms to ensure accurate detection. In conclusion, these results fulfil the first research objective by successfully developing a preprocessing method for pulse-based PWR signals that captures amplitude modulation signatures. Furthermore, the extracted key features demonstrate the ability to effectively characterize and differentiate fall movements from fall-like movements, validating the robustness of the proposed approach.

CHAPTER 5
CLASSIFICATION AND COMPARATIVE ANALYSIS RESULS

5.1 Introduction

This chapter presents a comprehensive discussion of the outcomes derived from the applied methodologies, directly addressing research objectives 2 and 3. These objectives were accomplished through the implementation of the methodologies outlined in sections 3.5 and 3.6 and 3.7.

In Section 5.2, the focus will be on the algorithms applied to each transformed signal, highlighting their roles in mapping features that will be fed into classifiers. This includes the application of PCA for feature dimension reduction, as well as the utilization of AlexNet feature layers that convert images into numerical values that can serve as features for the classifiers.

In Section 5.3, an in-depth performance analysis will be conducted on three distinct classifiers. These classifiers will be paired with six different sets of features. The analysis will encompass the optimization of parameters for each classifier algorithm, with the objective of attaining optimum accuracy while mitigating any signs of overfitting.

Finally, in Section 4.5, the optimized classifiers resulting from the preceding analysis will undergo a comprehensive comparison. This section will discuss the outcomes and ultimately identify the pair of feature sets with an optimized classifier, exhibiting the highest accuracy and F1 score.

5.2 Feature Selection

Subsequently, these transformed signals underwent features extraction and selection. For the Fourier spectrum and power domain, which are already in numerical features, this domain was directly assigned as features. Additionally, PCA was applied as a selection method, reducing the dimensionality of features based on the most variant components. As for the spectrogram and scalogram, being in image form, both were extracted using the AlexNet feature extraction layers, yielding numerical features.

5.2.1 Principal Component Analysis

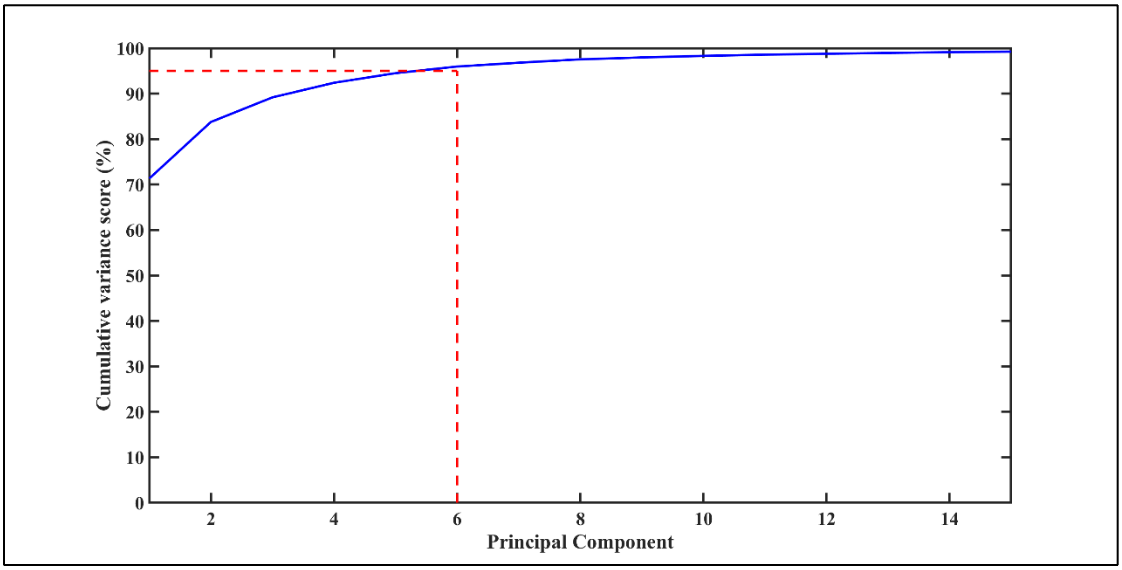

Figure 5.1 PCA cumulative variance of Fourier spectrum (Single person scenario)

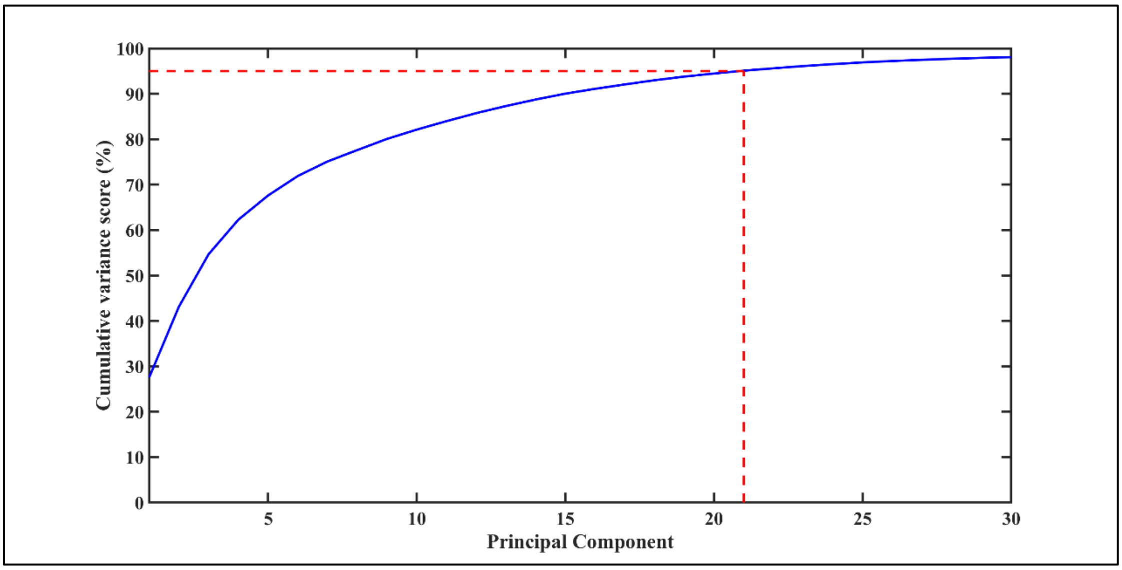

Figure 5.2 PCA cumulative variance of Power Spectrum (Single person scenario)

The PCA application was selected based on the most variant features that achieved a 95% cumulative variance score for the Fourier and power spectrum, as presented in Figures 5.1 and 5.2, respectively. Each number of PC represents the new transformed features obtained by projecting the original data onto orthogonal directions that capture the most variance. In Figure 5.1, it is evident that a 95% score is achieved on PC6, while in Figure 5.2, it is achieved on PC21. Each PC is associated with a set of coefficients, and the combination of these coefficients determines the amplitude and phase relationships between the frequency components. Therefore, the information about the amplitudes of different frequency components is distributed across the selected PCs. This observation suggests that the Fourier spectrum might require fewer dimensions to capture a significant portion of the variance compared to power spectrum. This implies that the Fourier spectrum only requires 6 dimensions of features for segregating each class, while the power spectrum needs 21 dimensions to achieve the same. As result. the dimensionality of the Fourier and power spectrum has been reduced from 100 to 6 and 21, respectively.

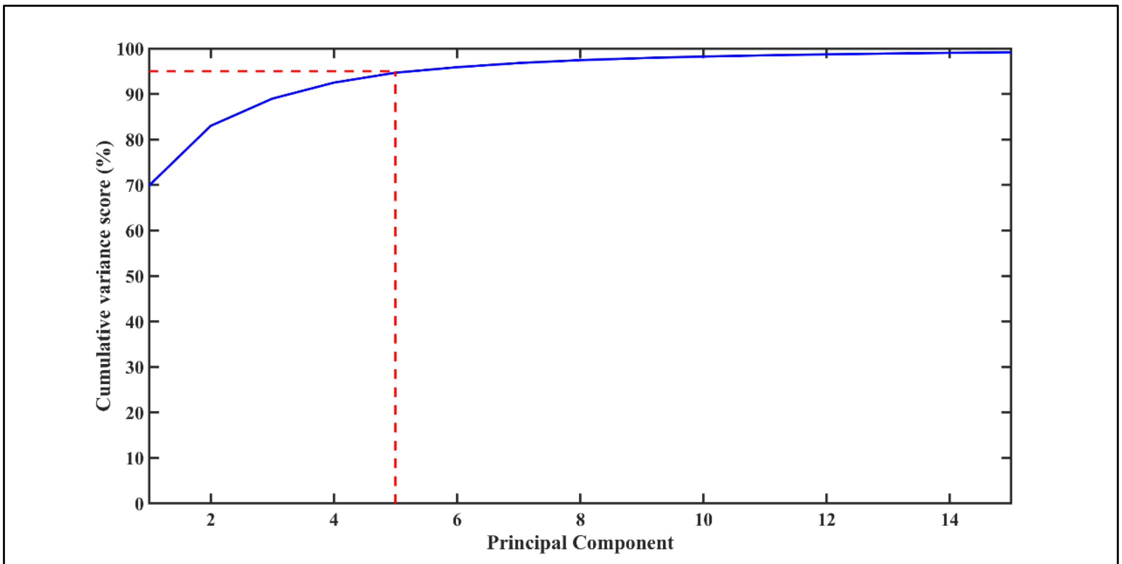

Figure 5.3 PCA cumulative variance of Fourier spectrum (Multiple person scenario)

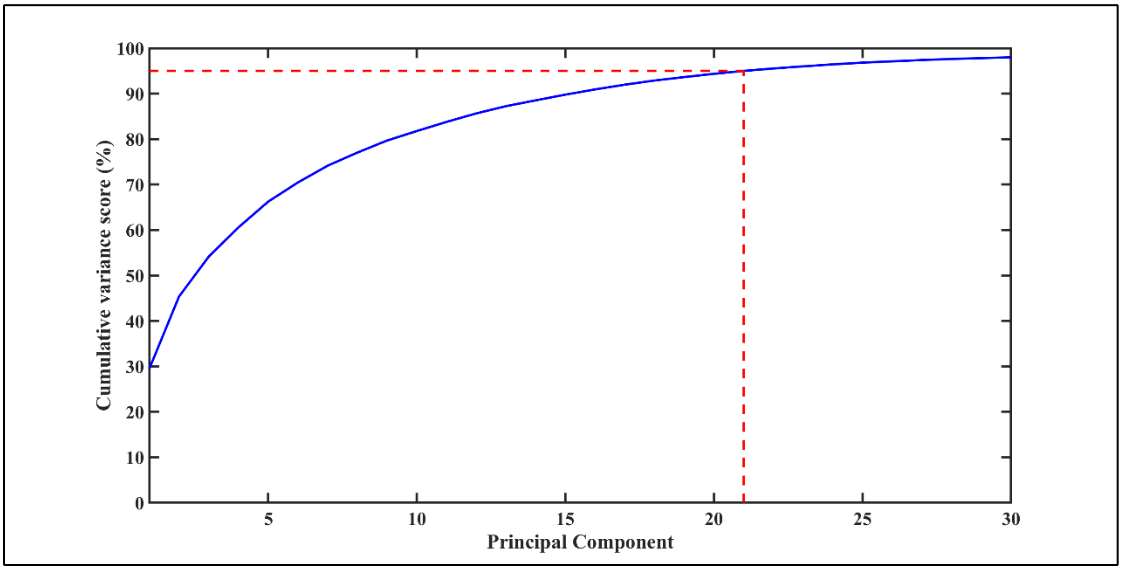

Figure 5.4 PCA cumulative variance of Power Spectrum (Multiple person scenario)

Furthermore, when analysing high-complexity data for multiple person scenario, the PCA application on the Fourier spectrum has a low dimension, achieving a 95% cumulative score on PC5, compared to single person scenario, as presented in Figure 5.3. This indicates that PCA is a meaningful method in capturing the variance of the feature set because even with the complex nature of multiple person scenario and the inability of the Fourier spectrum alone to segregate between each class through raw observation, PCA is able to capture the variance and achieve a 95% score on PC5. This also suggests that PCA is effective in capturing variance in large datasets, as single person scenario only has 540 data points, while multiple person scenario has a dataset of 1440 points. However, for the power spectrum, features are needed up to PC21 to achieve a 95% score, as illustrated in Figure 5.4. This figure reinforces the notion that the power spectrum does not significantly capture the signature of human movement or fall activities for PWR signals, even with a large dataset.

5.2.2 AlexNet Feature Layers

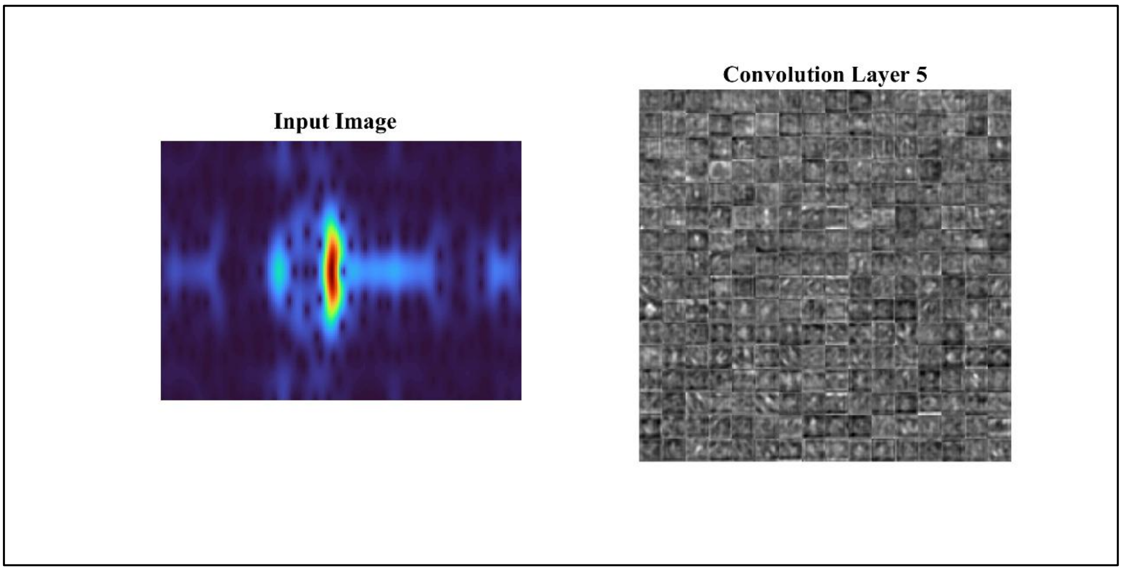

Figure 5.5 Feature map on spectrogram-AlexNet feature layers

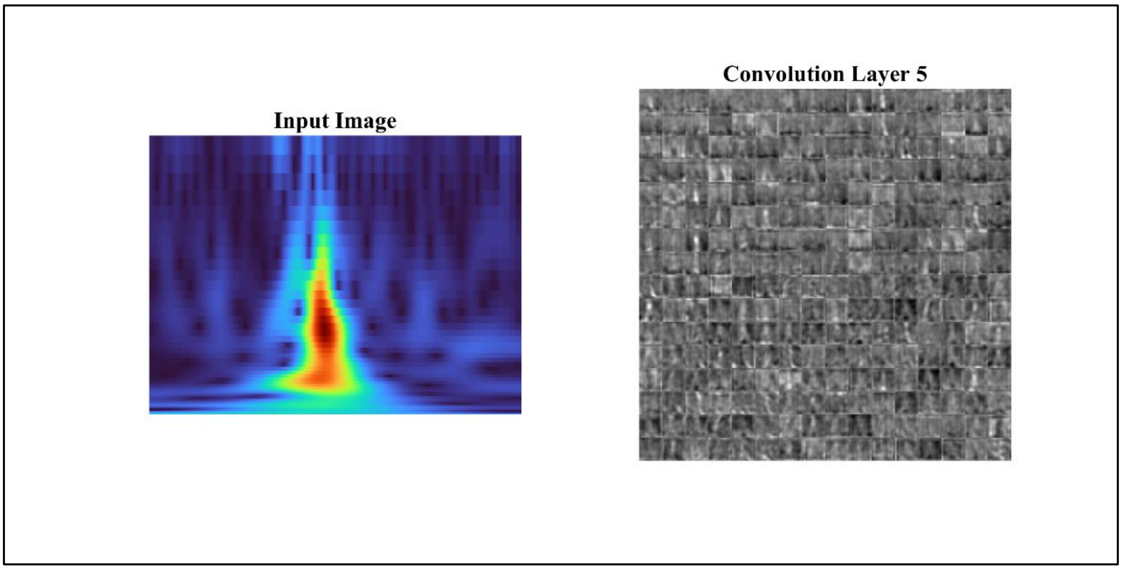

Figure 5.6 Feature map on scalogram-AlexNet feature layers

Continuing with the analysis, the next step involves feeding the features extracted from the AlexNet feature layers into traditional ML models such as SVM and RF to create hybrid classifiers. This approach leverages the power of deep learning in feature extraction from image data and combines it with the interpretability and effectiveness of traditional machine learning algorithms. The AlexNet feature layers, comprising 5 convolutional layers, transform the input image such as spectrogram and scalogram into feature maps, as illustrated in Figure 5.5 and 5.6, respectively. In this example, Convolutional Layer 5 (CL5) represents the final features extracted from the original image. The size of the result at CL5 is 6x6x256, and these features are then flattened into numerical features, resulting in a size of 9216 features being selected for further analysis. This hybrid approach aims to capitalize on the strengths of both deep learning and traditional machine learning algorithms for improved performance in classifying human movements and fall activities.

In summary, this section involved the transformation of time-domain signals into four different domains: Fourier spectrum, power spectrum, spectrogram, and scalogram. These domains then underwent feature selection, where Fourier and power spectrum features were directly assigned and subjected to PCA algorithm. On the other hand, the spectrogram and scalogram features were selected using the AlexNet feature layer. Consequently, this section resulted in six features for both single detection and multiple person scenario, as summarized in Table 5.1. This comprehensive approach aimed to capture diverse aspects of the signal and leverage different representations for effective classification of human movements and fall activities.

Table 5.1
Size of each feature

Features	**Size (Single Person Scenario)**	**Size (Multiple Person Scenario)**
Fourier spectrum	540 x 100	1440 x 100
Power Spectrum	540 x 100	1440 x 100
Fourier spectrum-PCA	540 x 6	1440 x 5
Power Spectrum-PCA	540 x 21	1440 x 21
Spectrogram-AlexNet	540 x 9216	1440 x 9216
Scalogram-AlexNet	540 x 9216	1440 x 9216

5.3 Optimizing Intelligence Classier

Optimizing the AI-based classifiers is a crucial step in this study, as the outcomes of this section hold substantial implications for various stages of the research process. It sheds light on the efficiency of the data collection trajectories, the effectiveness of the enveloping algorithm in preserving the Amplitude modulation signature, the impact of signal transformation, and the significance of each selected feature in delineating different classes of movement. Furthermore, this section yields optimized parameters for each classifier, providing insights into how the classifiers adapt to the complexity of the features provided. The classifiers employed in this study include FFNN, AlexNet, SVM, AlexNet-SVM, RF and AlexNet-RF. The optimization process plays a pivotal role in enhancing the overall performance and accuracy of the classification models.

5.3.1 Feed Forward Neural Network

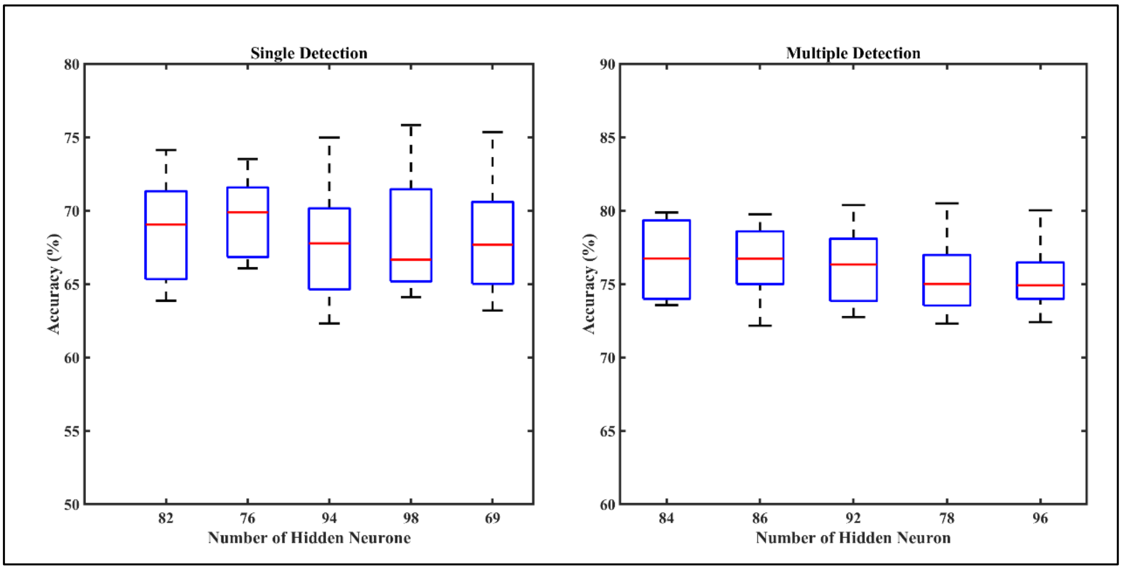

Figure 5.7 Validation accuracy for 10 consecutive repetitions for Fourier spectrum-FFNN

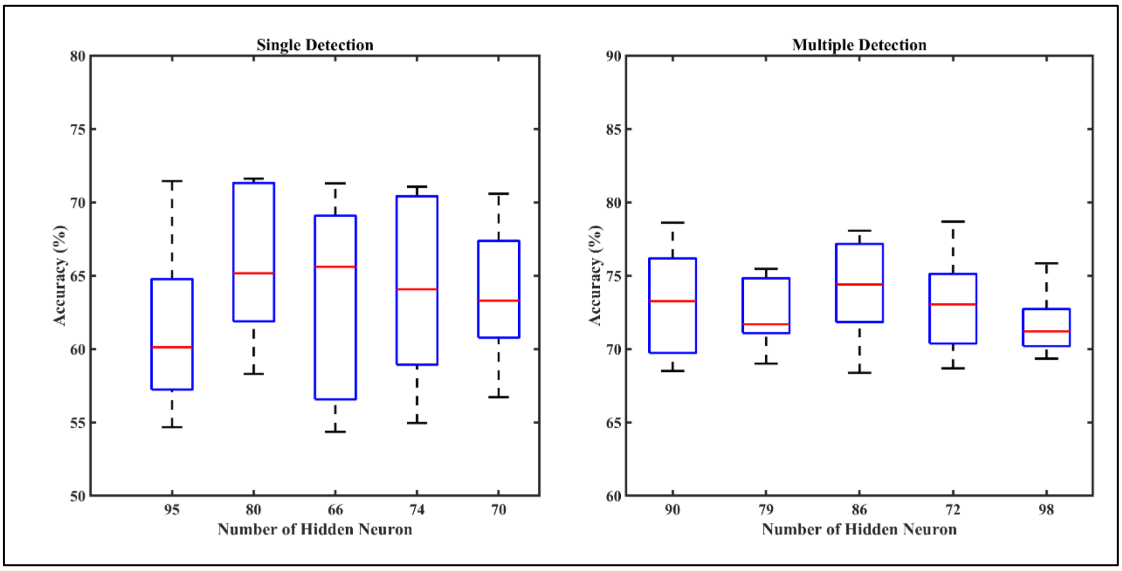

Figure 5.8 Validation accuracy for 10 consecutive repetitions for Power spectrum-FFNN

The analysis of the FFNN algorithm, an optimization process was executed, encompassing the testing of 100 different numbers of hidden neurons ranging from 1 to 100 with a step size of 1. Similar to other classifier algorithms, the FFNN received input features derived from the Fourier spectrum, power spectrum, and PCA outcomes on each domain. The outcomes, elucidated in Figures 5.7-5.10, delineate validation accuracy levels corresponding to the top five highest accuracies aligned with varying numbers of hidden neurons. Figure 5.7 illustrates the validation accuracy levels for the top five FFNN algorithm optimum hidden neuron counts, demonstrating bounds within the range of 60-75% for single person scenario and 68-80% for multiple person scenario. This suggests that the FFNN model exhibits improved performance with a substantial dataset, even when employing the same type of features. In comparison, the highest average validation accuracy level for single person scenario reached 69.45% with 82 hidden neurons, while for multiple person scenario, it attained 76.72% with 84 hidden neurons. On the other hand, Figure 5.8 presents the validation accuracy levels for features derived from the power spectrum. While the range of the top five validation accuracy levels for the algorithm's optimum hidden neurons did not exhibit significant differences, a closer examination of each average validation accuracy reveals a slight decline in results for the power spectrum feature set. For single person scenario, the highest validation accuracy reached 65.95% with 74 hidden neurons, and for multiple person scenario, it achieved 74.06% with 90 hidden neurons.

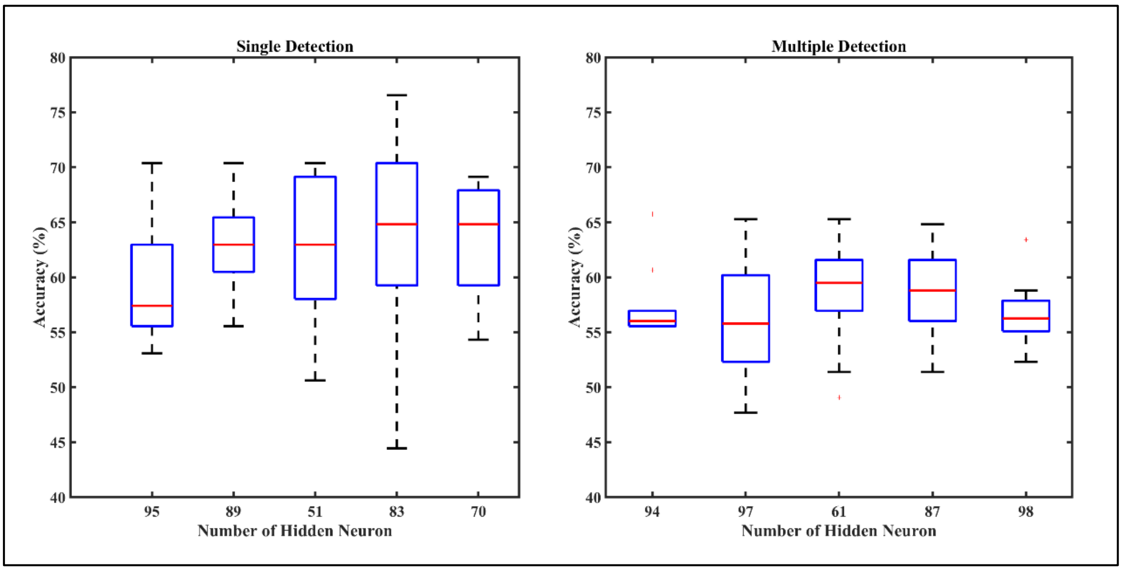

Figure 5.9 Validation accuracy for 10 consecutive repetitions for Fourier spectrum-PCA-FFNN

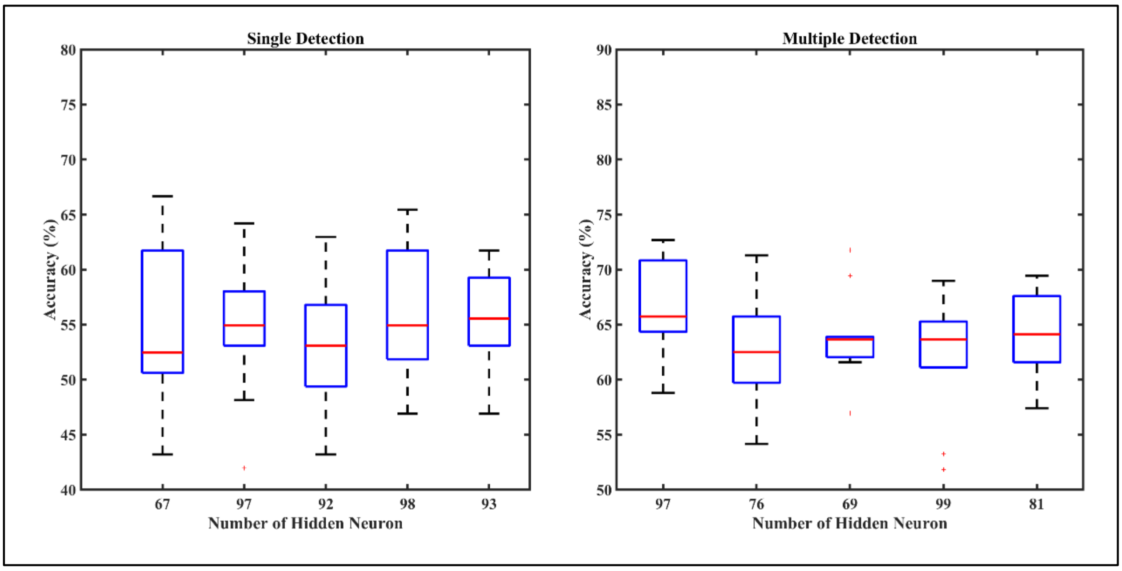

Figure 5.10 Validation accuracy for 10 consecutive repetitions for Power spectrum-PCA-FFNN

Moreover, the presence of PCA does not yield comparable improvements in the validation accuracy of features derived from the Fourier spectrum or power spectrum. This observation is distinctly evident in Figures 5.9 and 5.10. Figure 5.9 depicts the FFNN algorithm utilizing input features from the Fourier spectrum with PCA preprocessing. In this context, the range of the top five highest validation accuracy levels spans from 45% to 70% for single-target detection and from 55% to 75% for multiple-target detection. Notably, this validation accuracy range mirror that of the FFNN algorithm fed with power spectrum-PCA features, as illustrated in Figure 5.10. However, the highest average validation accuracy levels for features derived from the Fourier spectrum with PCA were superior to those derived from the power spectrum with PCA, registering at 64.44% (with 95 hidden neurons) compared to 58.88% (with 67 hidden neurons) for single-target detection. Conversely, in the case of multiple-target detection, the highest average validation accuracy level was achieved with power spectrum-PCA at 66.16% (with 97 hidden neurons), while Fourier spectrum-PCA yielded an average validation accuracy level of 58.8% (with 94 hidden neurons). Analysis based on the highest validation accuracy level for each model reveals that all FFNN models employing the four feature sets exhibited underfitting. The neural network algorithm exhibited limitations in comprehending and adapting to the feature map patterns associated with human fall detection, both in single and multiple detection trajectories.

5.3.2 AlexNet

The primary optimizable parameters include the choice of optimizer, either SGDM, traditionally used, or ADAM, a more potent optimizer introduced after the inception of AlexNet. Additionally, the optimizable parameters of AlexNet encompass their initial learning rates. This study conducted tests with three different initial learning rates which are $1e^{-3}$, $1e^{-4}$ and $1e^{-5}$.

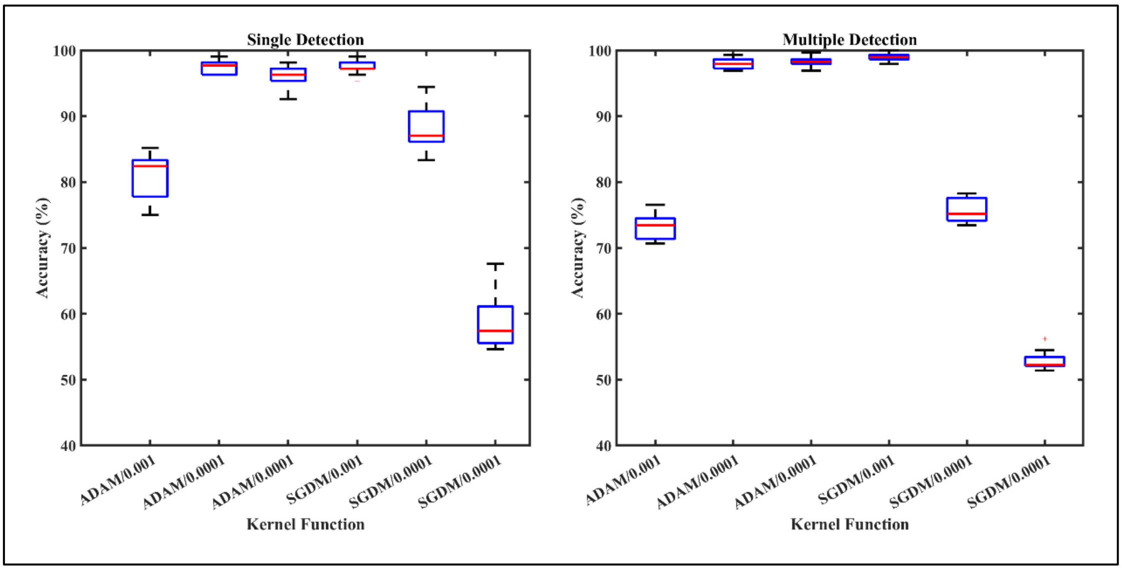

Figure 5.11 Validation accuracy for 10 consecutive repetitions for Spectrogram-AlexNet

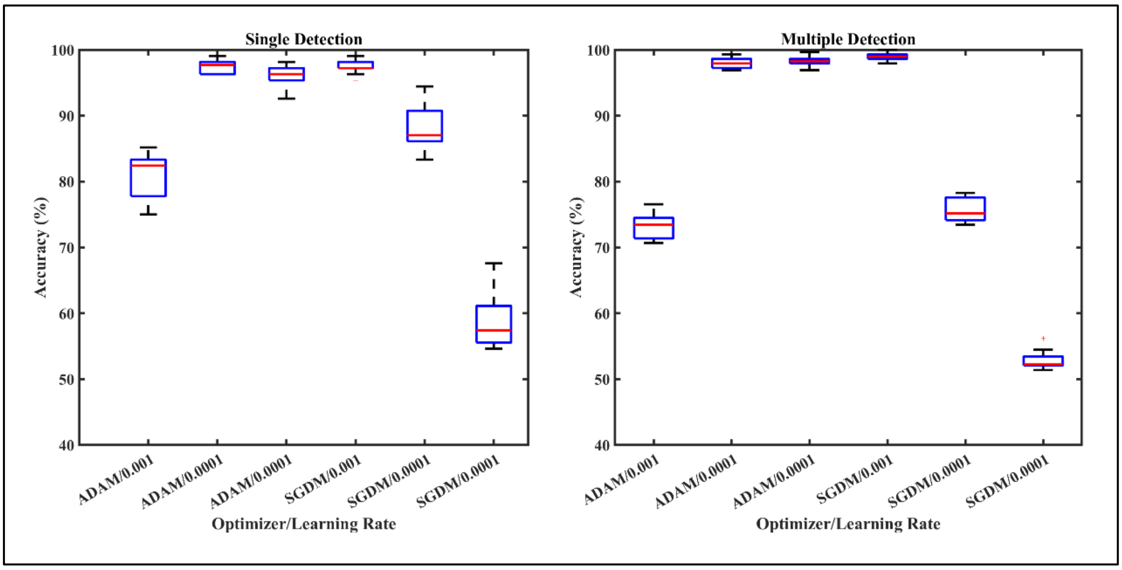

Figure 5.12Validation accuracy for 10 consecutive repetitions for Scalogram-AlexNet

Figure 5.11 illustrates the validation accuracy levels for AlexNet with input from spectrogram using six different optimizable parameters. In single person scenario, the validation accuracy levels exceeded 50%, with the highest achieved when employing the ADAM optimizer and a $1e^{-4}$ initial learning rate, resulting in a 97.59% average validation accuracy level. For multiple person scenario, the validation accuracy levels ranged between 20% and 100%, with the highest observed when utilizing the ADAM optimizer and a $1e^{-5}$ initial learning rate with validation accuracy level of 97.97%. This signifies that applying spectrogram feature images to the AlexNet algorithm yielded excellent results, particularly in single person scenario, surpassing the performance of hybrid SVM and RF classifiers. The distinction in optimized initial learning rates for single and multiple person scenario suggests that, in single data collection, the feature mapping occurs in a less complex manner. With a larger initial learning rate, the algorithm remains capable of tuning until achieving the optimized values for W and B.

Meanwhile, concerning Scalogram input features, Figure 5.12 reveals a lack of significant differences compared to Spectrogram input features. The validation accuracy ranges for both single and multiple detection fall within the same range for all optimizable parameters. However, upon analysing average validation accuracy, Scalogram input images exhibit a slightly lower performance. For single person scenario, the highest average validation accuracy was 97.14%, achieved by the one employing the ADAM optimizer with a $1e^{-4}$ initial learning rate. In the case of multiple person scenario, the average validation accuracy was 97.31% for the one utilizing the ADAM optimizer with a $1e^{-4}$initial learning rate. Consequently, this indicates that Spectrogram input features provide more informative data on human fall and fall-like movements, both in single and multiple person scenario for PWR signals.

5.3.3 Support Vector Machine

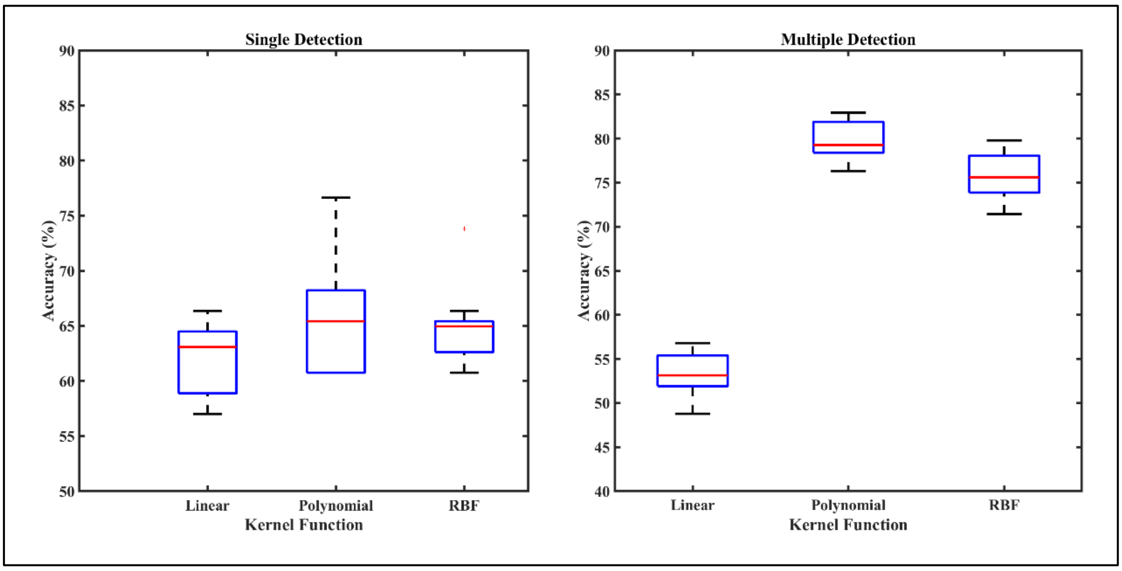

Figure 5.13 Validation accuracy for 10 consecutive repetitions for Fourier spectrum-SVM

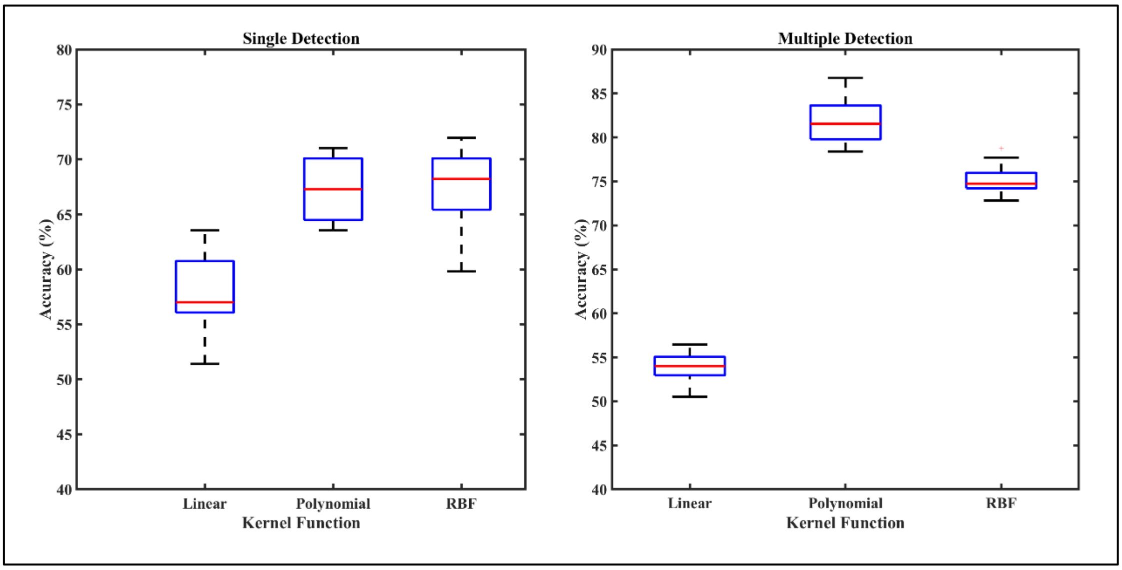

Figure 5.14 Validation accuracy for 10 consecutive repetitions for Power spectrum-SVM

The optimization of SVM involves tuning parameters such as the kernel function, including linear, polynomial, or RBF. Figure 5.13 illustrates the validation accuracy results of SVM with these three different kernel functions when using features from direct feeding of Fourier spectrum for both single and multiple person scenario. The model was deployed 10 times for each kernel function used. For single person scenario, all three kernel functions exhibit almost similar performances, with accuracies ranging between 55-80% with highest average validation accuracy was the polynomial kernel function with validation accuracy level of 67.48%. However, this validation accuracy level may be considered non-acceptable. Similarly, for multiple person scenario, the validation accuracy levels range between 50-80%, with highest average validation accuracy was the polynomial kernel function with validation accuracy level of 79.72% and the linear kernel function performs the worst, achieving only between 50-60% validation accuracy. This indicates that multiple person scenario involves highly complex trajectories, and the linear kernel function struggles to adapt. The results suggest that SVM with a linear function might provide inaccurate results in the context of the multiple person scenario.

Meanwhile, in the optimization of SVM with features from the power spectrum domain for both single and multiple person scenario, the validation accuracy results are depicted in Figure 5.14. As an example, the SVM algorithm utilizing polynomial kernel functions achieved the highest validation accuracy level in single person scenario, attaining an average validation accuracy of 65.98%. Conversely, in multiple person scenario, a slightly elevated validation accuracy level of 81.85% was observed when applying the polynomial kernel function. However, this validation accuracy level still indicates a non-acceptable result, with accuracies below 85%. Notably, the linear function underperforms significantly compared to the other kernel functions in the context of single and multiple person scenario using power spectrum features. This observation suggests that the power spectrum features project a highly complex set of characteristics, making it challenging for SVM, particularly with a linear kernel function, to effectively segregate between different classes.

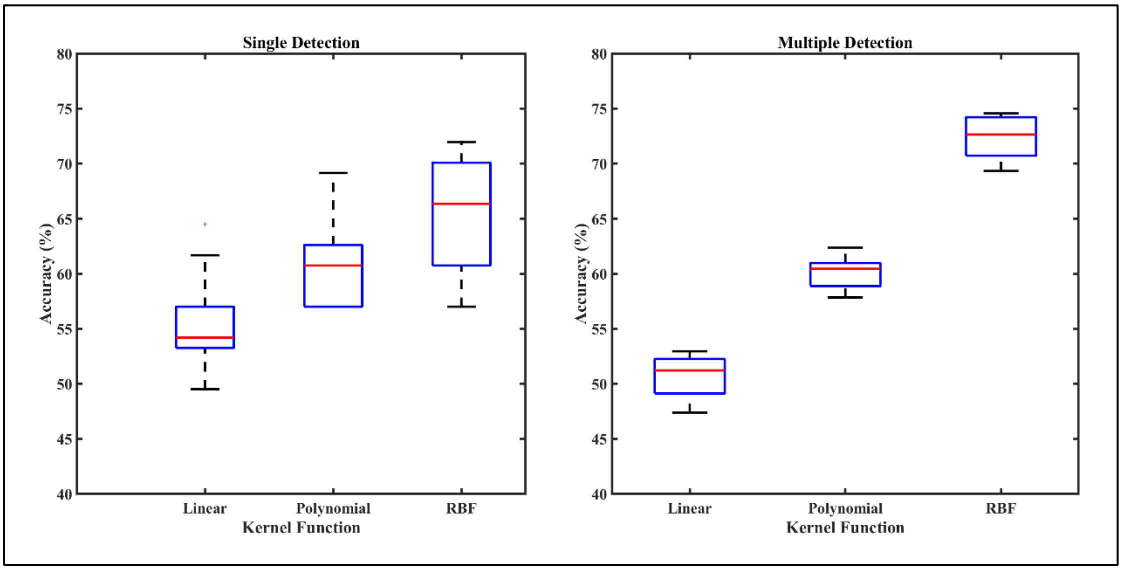

Figure 5.15 Validation accuracy for 10 consecutive repetitions for Fourier spectrum-PCA-SVM

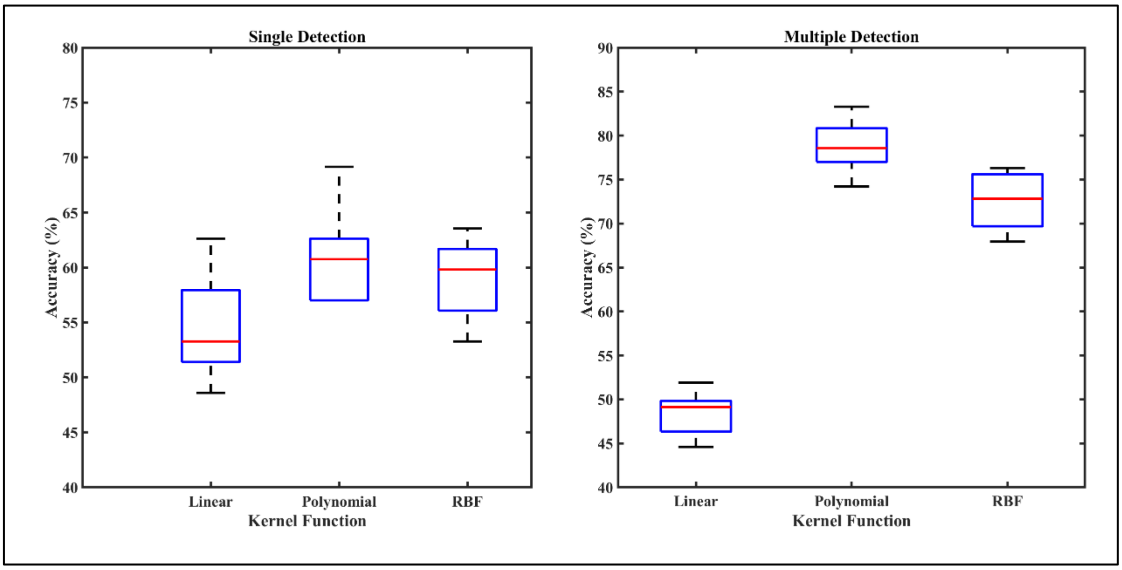

Figure 5.16 Validation accuracy for 10 consecutive repetitions for Power spectrum-PCA-SVM

The optimization of SVM with features from the reduced dimension of the Fourier and power spectrum using PCA is presented in Figure 5.15 and 5.16, respectively. Despite the dimension reduction, the SVM still struggles to adapt to the complexity of human movement in PWR signals. The diminished dimensionality of Fourier spectrum features, as revealed by the PCA algorithm, manifests a decline in validation accuracy levels for both single and multiple person scenario in comparison to the utilization of direct feeding features. The highest average validation accuracy achieved was 65.61% for single person scenario and 72.37% for multiple person scenario, both observed with the application of RBF kernel function in the SVM algorithm.

Similar to the influence observed with PCA application on Fourier spectrum features, the diminished dimensionality of power spectrum features results in a reduction in validation accuracy levels. The highest validation accuracy achieved for single person scenario was 61.12%, while for multiple person scenario, it reached 78.89% with the application of a polynomial kernel function. This decline in validation accuracy levels, even with dimension reduction, implies that the SVM algorithm encounters difficulties in effectively generalizing and adapting to the classification problem posed by the low-dimensional features provided.

5.3.4 AlexNet-SVM Hybrid Model

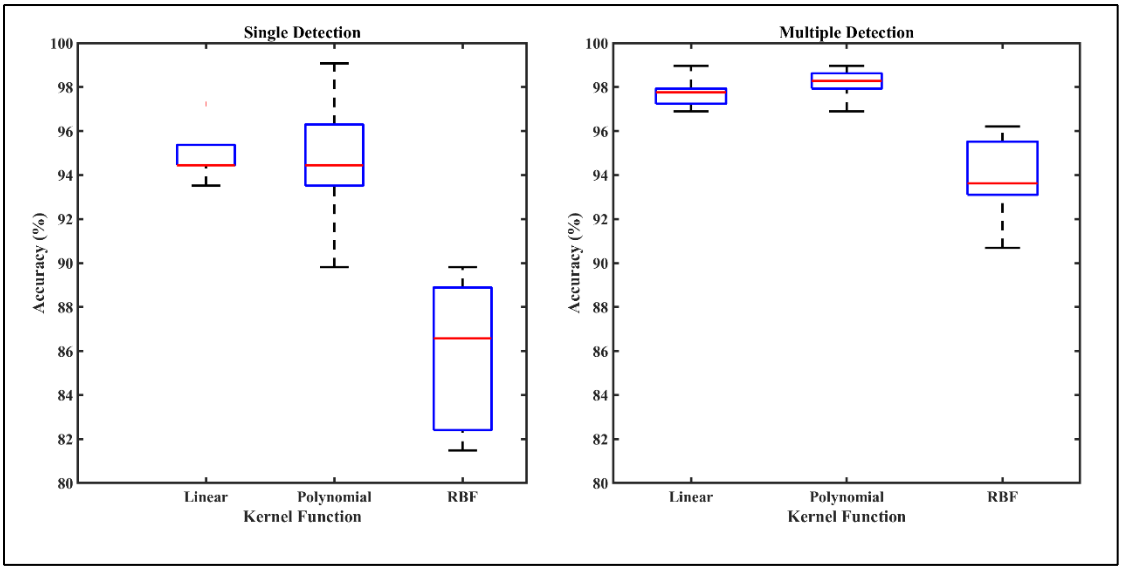

Figure 5.17 Validation accuracy for 10 consecutive repetitions for Spectrogram-AlexNet-SVM

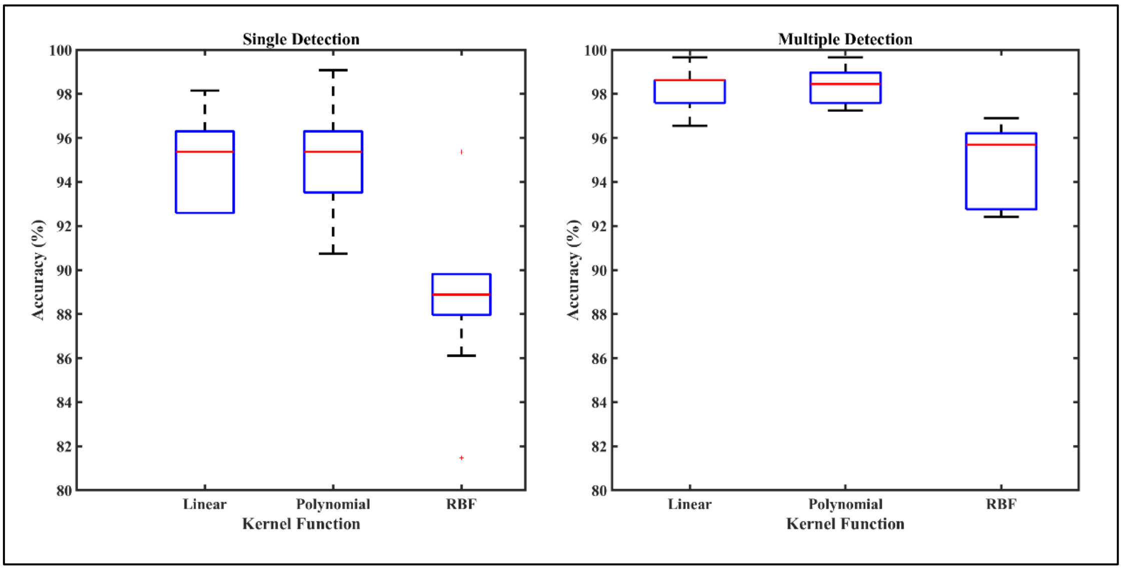

Figure 5.18 Validation accuracy for 10 consecutive repetitions for Scalogram-AlexNet-SVM

Conversely, the utilization of features from the AlexNet feature layers, incorporating spectrogram and scalogram, has demonstrated exemplary performance, as depicted in Figures 5.17 and 5.18, respectively. Both figures illustrate that, for single person scenario, the attained validation accuracy levels consistently surpass 90%, and for multiple person scenario, validation accuracy exceeds 95% across all kernel functions, including the linear variant. in the context of single person scenario for features derived from spectrogram, the highest validation accuracy level was attained with the polynomial function, achieving 94.81% validation accuracy. Concurrently, for multiple person scenario, the polynomial function also yielded the highest validation accuracy level, standing at an average of 98.14%. Additionally, the features extracted from scalogram images demonstrated exceptional performance, with signal target detection achieving a 95% validation accuracy level and multiple person scenario achieving an average validation accuracy level of 98.38%, both utilizing the polynomial kernel function.

This substantiates that the features derived from AlexNet feature layers establish a notable segregation point, even when confronted with a substantial feature dimension and a dataset that is sufficiently representative and diverse to encapsulate underlying patterns. Furthermore, the competence of the AlexNet feature layer in learning images is evident, particularly when exposed to a substantial dataset. This observation also implies that the SVM algorithm exhibits adept adaptability when confronted with time-frequency image features layers, in contrast to frequency-domain features, whether in their original or reduced dimensions. The SVM successfully assimilates patterns and relationships within the data, thereby enabling precise predictive outcomes by creating a good segregation point of Hyperplane.

5.3.5 Random Forest

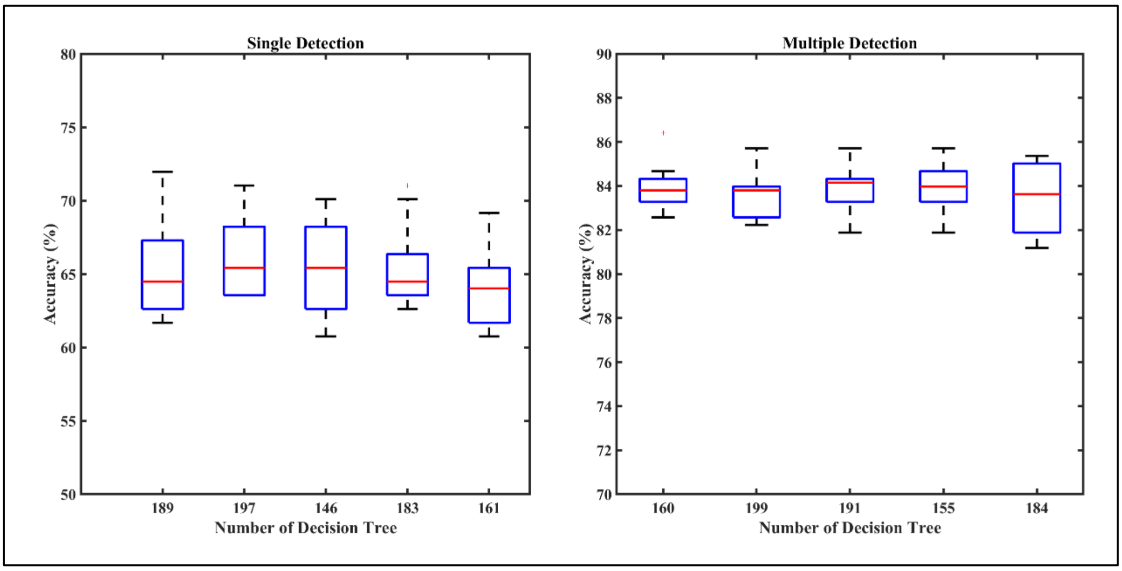

Figure 5.19 Validation accuracy for 10 consecutive repetitions for Fourier spectrum-RF

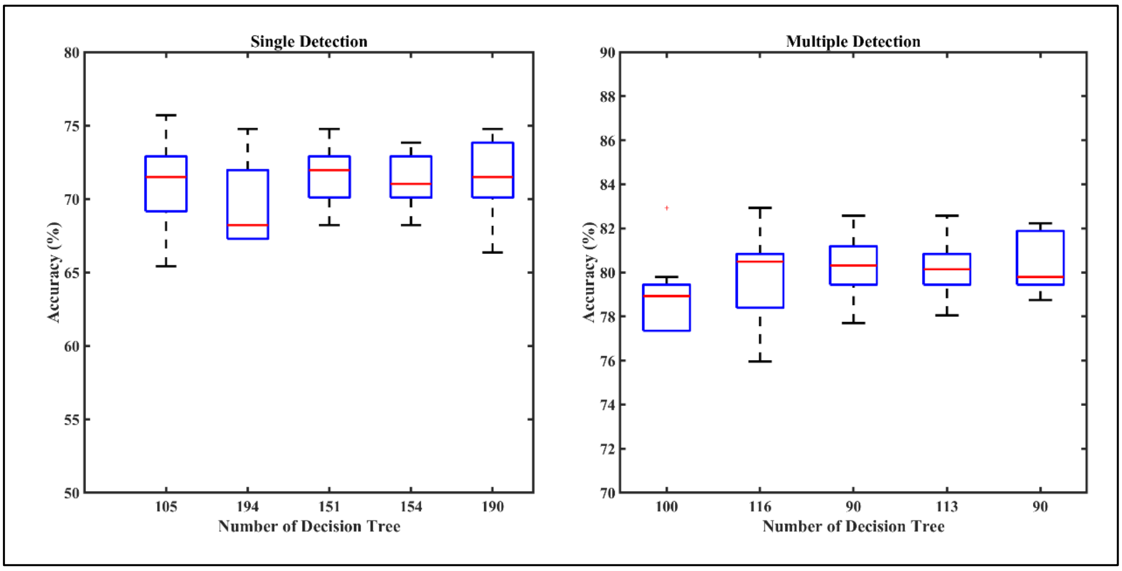

Figure 5.20 Validation accuracy for 10 consecutive repetitions for Power spectrum-RF

Subsequently, the analysis turned towards the RF algorithm, with a focus on optimizing the number of DT as a key parameter. The investigation involved exploring various quantities of DT, ranging from 1 to 200, with a step size of 1. Each configuration of DT was executed 10 times to ensure the robustness and consistency of predictions. Figures 5.19 and 5.20 illustrate the validation accuracy levels achieved by the RF algorithm when applied to Fourier and power spectrum features for single and multiple person scenario. Despite the examination of 200 distinct numbers of DT, the figures selectively highlight the top 5 configurations yielding the highest validation accuracy levels.

The outcomes from both figures align with the observations made in the SVM algorithm's performance on these feature types, indicating a challenge in achieving satisfactory validation accuracy levels. Notably, a discrepancy arises in the single person scenario, where the RF model exhibits superior performance with power spectrum features which achieved validation accuracy kevel of 70% - 80%. The highest validation accuracy, 74.49%, is attained with 105 DT, compared to Fourier spectrum features which the validation accuracy level bound 62% - 72%, where the highest validation accuracy of 67.48% is observed with 189 DT. In multiple person scenario, the Fourier spectrum features outperform, yielding validation accuracy in the range of 83% - 86%, with the highest average validation accuracy of 84.43% achieved with 160 DT. Meanwhile, power spectrum features exhibit validation accuracy in the range of 78% - 83%, with the highest average validation accuracy of 81.08% observed with 100 DT.

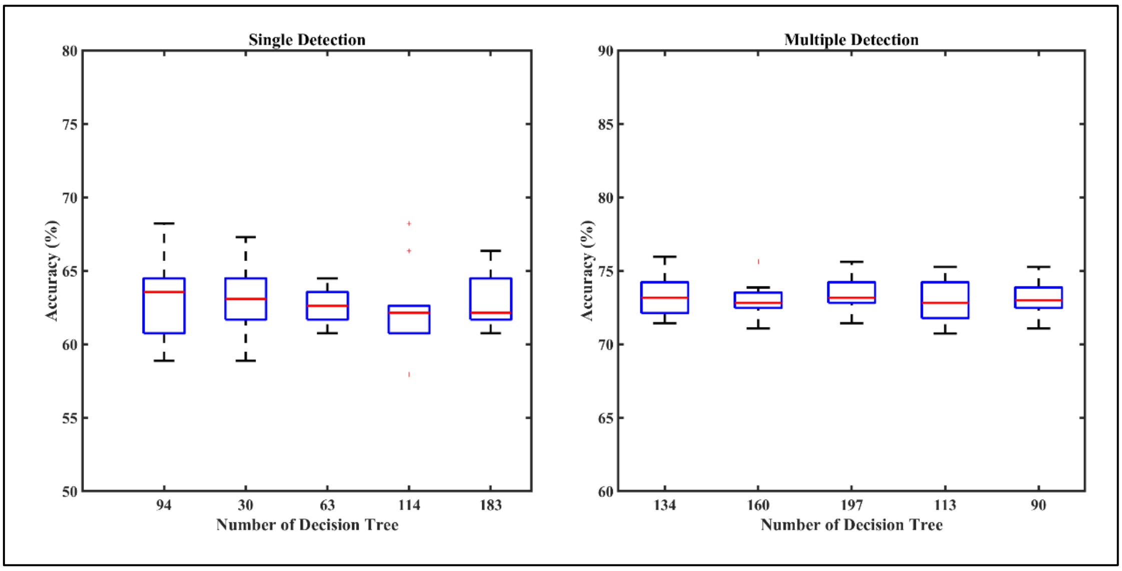

Figure 5.21 Validation accuracy for 10 consecutive repetitions for Fourier spectrum-PCA-RF

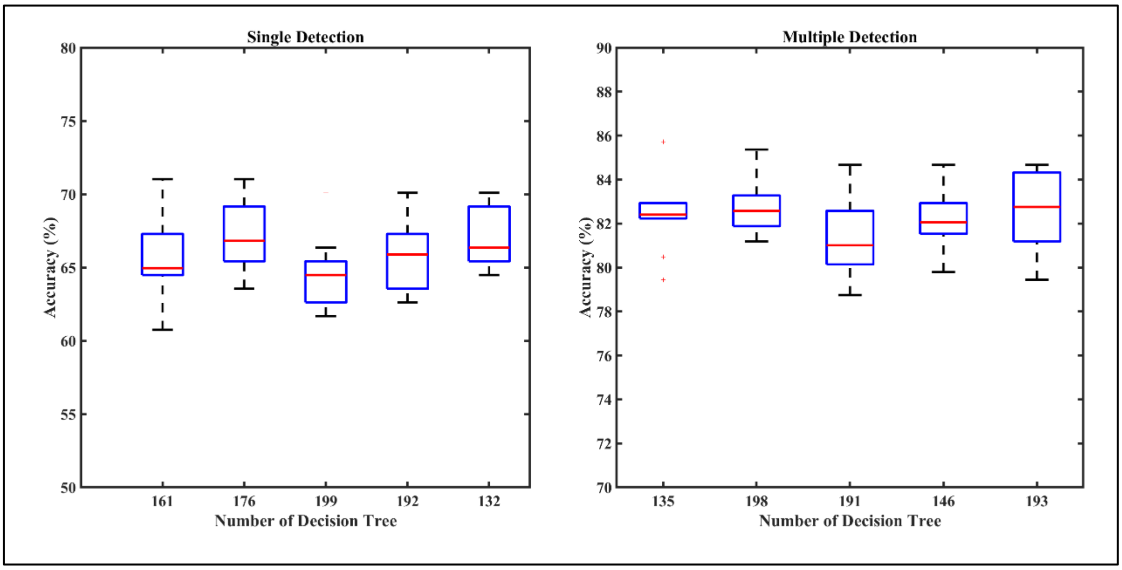

Figure 5.22 Validation accuracy for 10 consecutive repetitions for Power spectrum-PCA-RF

Subsequently, the introduction of PCA algorithms once again demonstrates a detrimental impact on validation accuracy levels when applied to Fourier and power spectrum features. As depicted in Figure 5.21, the top 5 validation accuracy levels for reduced dimension Fourier spectrum features with RF ranged between 58% and 70%, with the highest recorded at 94 DT. In the context of multiple person scenario, the top 5 validation accuracy levels ranged from 70% to 78%, with the highest at 74.15% achieved with 134 DT. These validation accuracy levels signal that these features may not be sufficiently indicative of human movement detection for PWR signals.

Conversely, the RF algorithm also exhibits limited adaptability to features derived from the reduced dimension of power spectrum, as illustrated in Figure 5.22. Particularly in single person scenario, the top 5 validation accuracy levels ranged from 62% to 72%, with the highest average validation accuracy level recorded at 67.29%. In multiple person scenario, notable improvement is observed, with all top 5 validation accuracy levels falling within the range of 80% to 86%. Despite some instances where certain numbers of DT achieved acceptable validation accuracy levels, overall consistency is lacking. For instance, the validation accuracy level of the RF algorithm with 193 DT reached 85.52% in the 5th iteration, while the remaining iterations consistently exhibit lower validation accuracy levels, fluctuating between 81% and 83%. Therefore, the most consistent and highest average validation accuracy level for the RF algorithm with reduced dimension power spectrum in multiple person scenario was observed with 135 DT, recording an average validation accuracy level of 83.45%.

5.3.6 AlexNet-RF Hybrid Model

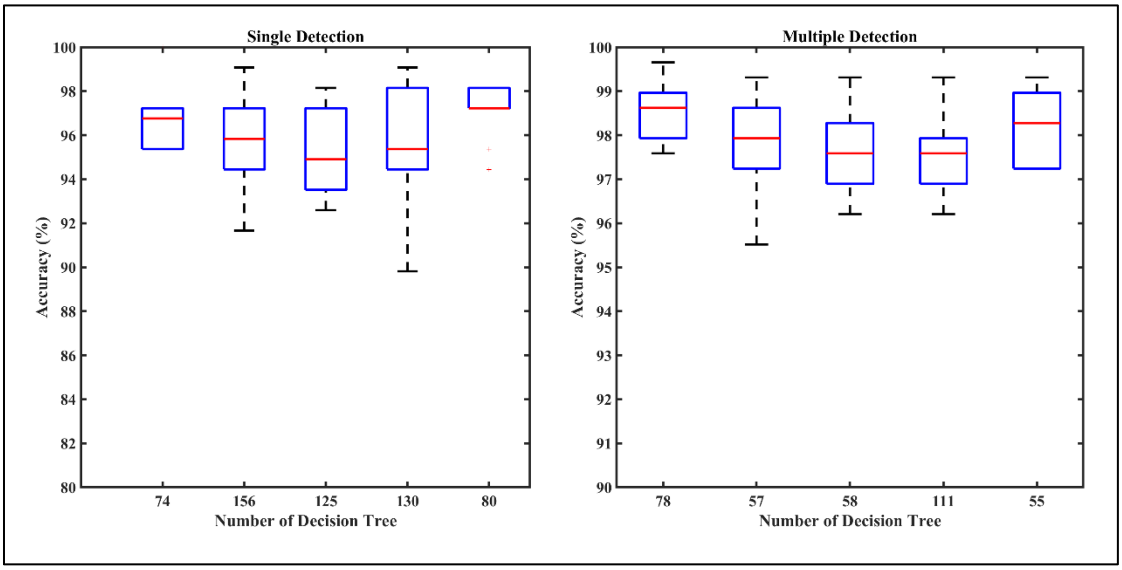

Figure 5.23 Validation accuracy for 10 consecutive repetitions for Spectrogram-AlexNet-RF

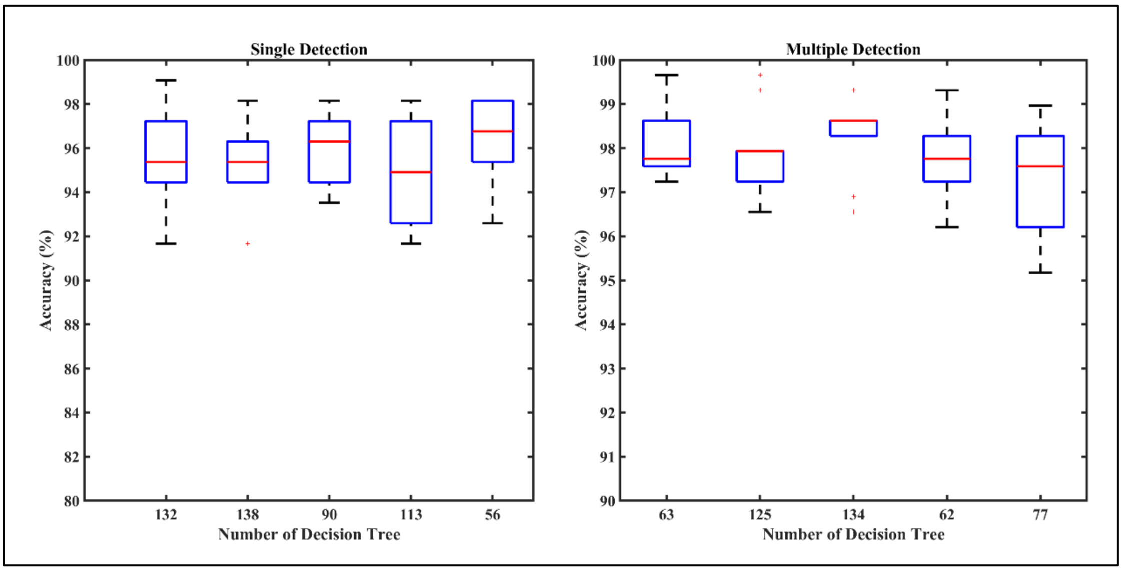

Figure 5.24 Validation accuracy for 10 consecutive repetitions for Scalogram-AlexNet-RF

Furthermore, the amalgamation of features from AlexNet feature layers with the RF algorithm exhibited notable performance, surpassing that of SVM. According to Figure 5.23, the spectrogram feature images demonstrated outstanding results, with validation accuracy levels ranging from 92% to 100% for single person scenario and 97% to 100% for multiple person scenario. The highest average validation accuracy for single person scenario was achieved with 74 DT at 97.5%, and for multiple person scenario, it reached 98.52% with 78 DT. In comparison to the spectrogram image features, the hybrid version with the input of scalogram image features, as illustrated in Figure 5.24, exhibited a similar range of validation accuracy levels for the top 5 optimized numbers of DT. However, the average validation accuracy levels for the most optimized parameters for single and multiple person scenario were slightly lower than those with spectrogram image input. For instance, the highest average validation accuracy for single person scenario was 97.35% with 132 DT, and for multiple person scenario, it was 98.34% with 62 DT.

The presented results indicate that the RF algorithm exhibits capability in effectively classifying human movement and fall activities within PWR signals, specifically when paired with hybrid algorithms and not with traditional manual feature extraction methods. This influence can be attributed to two primary factors. Firstly, the hybrid algorithms leverage excellent feature extraction and selection, effectively delineating each type of movement within time-frequency image features. Secondly, the RF algorithm showcases adeptness in learning and adapting to the distinctive patterns inherent in each feature. These findings further affirm that the bootstrapping, decision-making by DT, and the voting process employed by the RF algorithm contribute successfully to the classification of human movement signals in the context of PWR.

As summary, this section had scrutinized the impact of variation of optimizable parameters for each type classifiers paired with each type of features set and was tabulate in Table 5.2 and 5.3 for single and multiple person scenario, respectively. From both tables, it obviously shows that the signal transformation by FFT either in Fourier spectrum or power spectrum had not enough significant information in denoting each type of data collected using PWR signal and can claimed that the Hybrid classifier and DL algorithms was preform far better than the traditional ML algorithms.

Next, by analyse on each type of classifiers algorithms such done on SVM, the polynomial kernel function was perform well understanding the pattern of most type of feature set. meanwhile the features set that most suit with SVM algorithm in creating the hyperplane was features from AlexNet feature layer that extracted from scalogram images. As result, the hybrid SVM classifier with spectrogram-AlexNet feature layer achieve the highest validation accuracy result which were 95% and 98.38% for single and multiple person scenario, respectively.

Besides, the number of DT in RF algorithms shows that the Hybrid algorithms having a smaller number of DT but having high validation accuracy. This mean that the with good features set that provide separation point of data, it does not acquire large amount of DT for making decision and giving their votes for each class. As result, the highest validation accuracy on RF algorithm was achieve when the model being fed by spectrogram-AlexNet feature set with 74 number of DT on single person scenario and 78 DT for multiple person scenario.

Finally, the NN result shows that the AlexNet with spectrogram images perform well with ADAM optimizer due to its adaptive learning rate mechanism and momentum optimization where the validation accuracy level was 97.87% and 98.97% for single and multiple person scenario, respectively. Adam dynamically adjusts the learning rates for each parameter, allowing it to handle sparse gradients effectively and converge faster. Additionally, it incorporates momentum-like features, preventing it from getting stuck in local minima and providing better stability during training. The adaptive nature of Adam, which combines the benefits of both learning rate adaptation and momentum, makes it a popular choice for optimizing a wide range of deep learning models, contributing to its overall effectiveness compared to traditional SGDM.

Table 5.2
Result on optimized parameter for each classifier with each set of features (Single person scenario)

Classifiers	**Features**	**Optimizable parameters**	**Average Accuracy level (%)**
NN	Fourier spectrum	Number of hidden neurons:82	69.48
	Power Spectrum	Number of hidden neurons:74	65.92
	Fourier spectrum-PCA	Number of hidden neurons:95	64.44
	Power Spectrum-PCA	Number of hidden neurons:67	56.79
AlexNet	Spectrogram	Optimizer: ADAM Initial learning rate:1e-4	97.87
AlexNet	Scalogram	Optimizer: ADAM Initial learning rate:1e-4	97.59
SVM	Fourier spectrum	Kernel function: Polynomial	67.29
	Power Spectrum	Kernel function: Polynomial	65.98
	Fourier spectrum-PCA	Kernel function: RBF	65.61
	Power Spectrum-PCA	Kernel function: Polynomial	61.12
AlexNet-SVM	Spectrogram	Kernel function: Polynomial	94.81
AlexNet-SVM	Scalogram	Kernel function: Polynomial	95
RF	Fourier spectrum	Number of DT: 189	67.48
	Power Spectrum	Number of DT: 105	74.49
	Fourier spectrum-PCA	Number of DT: 94	64.30
	Power Spectrum-PCA	Number of DT: 161	67.29
AlexNet-RF	Spectrogram	Number of DT: 74	97.50
AlexNet-RF	Scalogram	Number of DT: 93	97.13

Table 5.3
Result on optimized parameter for each classifier with each set of features (Multiple person scenario)

Classifiers	**Features**	**Optimizable parameters**	**Average Accuracy level (%)**
NN	Fourier spectrum	Number of hidden neurons:84	76.72
	Power Spectrum	Number of hidden neurons:90	74.06
	Fourier spectrum-PCA	Number of hidden neurons:94	58.80
	Power Spectrum-PCA	Number of hidden neurons:97	66.16
AlexNet	Spectrogram	Optimizer: ADAM Initial learning rate: 1e-5	98.97
AlexNet	Scalogram	Optimizer: ADAM Initial learning rate: 1e-5	98.24
SVM	Fourier spectrum	Kernel function: Polynomial	79.72
	Power Spectrum	Kernel function: Polynomial	81.85
	Fourier spectrum-PCA	Kernel function: RBF	72.37
	Power Spectrum-PCA	Kernel function: Polynomial	78.89
AlexNet-SVM	Spectrogram	Kernel function: Polynomial	98.14
AlexNet-SVM	Scalogram	Kernel function: Polynomial	98.38
RF	Fourier spectrum	Number of DT: 160	84.83
	Power Spectrum	Number of DT: 100	81.08
	Fourier spectrum-PCA	Number of DT: 134	74.15
	Power Spectrum-PCA	Number of DT: 135	83.45
AlexNet-RF	Spectrogram	Number of DT: 78	98.52
AlexNet-RF	Scalogram	Number of DT: 63	98.34

5.4 Comparative Analysis

This investigation extends beyond a mere examination of accuracy levels, a more comprehensive analysis of each classifier model attaining the highest accuracy level is conducted in this section. The highlighted models in this context are those featured in Table 5.5 and 5.6, specifically SVM with scalogram-AlexNet features, RF with spectrogram-AlexNet features, and spectrogram-AlexNet for both single and multiple person scenario.

The outcomes of this evaluation have been organized in Table 5.4, specifically for single-target detection. The average recall, a metric gauging a classifier's proficiency in accurately identifying positive instances, assumes significance in scenarios where the consequences of false negatives carry substantial costs. Within the presented findings, SVM with Scalogram-AlexNet exhibits commendable performance with an average recall of 0.9544, indicative of a high sensitivity to positive instances. This notable performance can be attributed to the utilization of a polynomial kernel function, which appears effective in capturing intricate relationships within the dataset. Random Forest with Spectrogram-AlexNet also showcases robust recall at 0.9684, underscoring its capacity to mitigate false negatives. Following closely, Spectrogram-AlexNet with the ADAM optimizer attains a recall of 0.9744, underscoring the potential impact of optimizer selection on the model's efficacy in capturing positive instances.

Subsequently, the average precision, a metric assessing the accuracy of positive predictions, assumes particular significance in applications where precision is of paramount importance. Both SVM with Scalogram-AlexNet and Random Forest with Spectrogram-AlexNet excel in achieving high average precision values, recording 0.9474 and 0.9872, respectively. The precision exhibited by SVM can be attributed to the efficacy of its polynomial kernel in capturing intricate patterns within the data. Conversely, the ensemble nature of Random Forest, coupled with a substantial number of decision trees, contributes to its precision. In contrast, Spectrogram-AlexNet with the ADAM optimizer, while still achieving a respectable precision of 0.9524, lags slightly behind. This discrepancy suggests that the choice of optimizer may exert influence over the precision-oriented aspects of the model.

Moreover, the F1-score, which strikes a balance between precision and recall, offers a holistic assessment of classifier performance. SVM with Scalogram-AlexNet attains a robust F1-score of 0.9714, indicating a well-balanced trade-off between precision and recall. Following closely, Random Forest with Spectrogram-AlexNet achieves an F1-score of 0.981, underscoring its efficacy in achieving a harmonious amalgamation of precision and recall. Despite a slightly lower F1-score of 0.9648, Spectrogram-AlexNet with the ADAM optimizer still maintains a commendable equilibrium between precision and recall. This metric accentuates the significance of considering both false positives and false negatives in the comprehensive evaluation of classifier performance.

Proceeding to multiple person scenario, as presented in Table 5.5, SVM with Scalogram-AlexNet attains a recall of 0.9913, indicative of its high sensitivity to positive instances. The discernible contribution of the polynomial kernel function to this elevated recall underscores its effectiveness in capturing intricate patterns within the data. Following closely, RF with Spectrogram-AlexNet achieves a recall of 0.9888, emphasizing its efficacy in minimizing false negatives. Spectrogram-AlexNet with the ADAM optimizer, while exhibiting a slightly lower recall of 0.9744, still manifests the model's proficiency in capturing positive instances with the selected optimizer and learning rate.

Furthermore, the emphasis on average precision, highlighting the accuracy of positive predictions, is noteworthy for all classifiers. SVM with Scalogram-AlexNet achieves a precision of 0.9828, underscoring its capability to make accurate positive predictions. Surpassing this, RF with Spectrogram-AlexNet attains a precision of 0.9914, showcasing the ensemble's effectiveness in minimizing false positive predictions. Subsequently, Spectrogram-AlexNet with the ADAM optimizer follows with a precision of 0.9828, implying that the choice of optimizer and learning rate significantly influences the precision-oriented aspects of the model.

Moreover, the F1-scores provide a balanced assessment of precision and recall. SVM with Scalogram-AlexNet achieves an impressive F1-score of 0.9831, showcasing a harmonious blend of precision and recall. Following closely, RF with Spectrogram-AlexNet attains an F1-score of 0.9888, emphasizing its balanced performance.

Spectrogram-AlexNet with the ADAM optimizer achieves a respectable F1-score of 0.9661, indicating a balanced trade-off between precision and recall, albeit slightly lower than the other classifiers.

For validation purposes, this study also compares its findings with results from prior works, as summarized in Table 5.4. The study presented in [115] demonstrates superior performance, utilizing Passive IoT Radar (PIoTR) by combining Wi-Fi signals with RF energy harvesting data, which are transformed into Doppler spectrograms. Their approach achieved an accuracy of 91.3% using LSTM networks, showcasing the potential of integrating IoT infrastructure for activity recognition. Similarly, the work in [116] employed a PWR setup with a reference channel and further compared its performance with CSI data. This approach achieved a maximum accuracy of 79.8%, highlighting the benefits of combining CSI data with PWR signals for enhanced classification. Furthermore, the study in [117] focused on CSI-based human activity recognition using LSTM, Bi-LSTM, and 2D-CNN models. The best results were obtained with the 2D-CNN, achieving an accuracy of 95%, demonstrating the effectiveness of CNN architectures for extracting spatial-temporal patterns from CSI data. These comparative results emphasize the importance of advanced signal processing and model selection in achieving high-performance classification. This study builds upon and extends these prior works by demonstrating that hybrid classifiers and deep learning models using AlexNet features from spectrograms and scalograms can achieve even higher accuracy reaching up to 98.5% in multiple-person scenarios. This highlights the impact of combining feature extraction techniques with optimized classification models, establishing a new benchmark for fall detection systems in complex environments.

In summary, the selected models performed commendably, with each exhibiting distinct strengths and limitations. Notably, no significant differences emerged among the classifiers. However, if compelled to make a selection, the hybrid RF algorithm employing the spectrogram-AlexNet feature set showcased optimal results. It demonstrated high accuracy, precision, and recall, while also mitigating concerns related to overfitting. Additionally, the model presented less mathematical complexity, addressing potential issues associated with elapsed time during training. This collective performance makes the hybrid RF algorithm with spectrogram-AlexNet features a promising choice for the considered application.

Table 5.4
Comparative analysis with other approaches

Approach	Features extracted	Classifiers	Accuracy level (%)
Enveloping on PWR signal	Spectrogram	AlexNet-RF	98.5
CSI	Normalized CSI plot	2D-CNN	95
Multi-channel PWR and CSI	Spectrogram	2D-CNN	79.8
PIoTR	Spectrogram	LSTM	91.3

Table 5.5
Assessment result for each classifier model (single person scenario)

Classifiers	**Features**	**Optimized parameters**	**Average Accuracy (%)**	**Average recall**	**Average precision**	**Average F1-score**
AlexNet	Spectrogram	Optimizer: ADAM Initial learning rate: 1e-4	98.97	0.9744	0.9524	0.9648
AlexNet-SVM	Scalogram-	Kernel function: Polynomial	98.34	0.9544	0.9474	0.9714
AlexNet-RF	Spectrogram	Number of DT: 74	98.52	0.9684	0.9872	0.981

Table 5.6
Assessment result for each classifier model (multiple person scenario)

Classifiers	**Features**	**Optimized parameters**	**Average Accuracy (%)**	**Average recall**	**Average precision**	**Average F1-score**
AlexNet	Spectrogram	Optimizer: ADAM Initial learning rate: 1e-5	97.87	0.9828	0.9661	0.9744
AlexNet-SVM	Scalogram	Kernel function: Polynomial	95	0.9828	0.9831	0.9913
AlexNet-RF	Spectrogram	Number of DT: 78	98.50	0.9786	0.9914	0.9888

5.5 Summary

The application of feature selection and classification techniques successfully segregated different types of falls and distinguished fall movements from fall-like movements in both single and multiple-person scenarios. Principal Component Analysis (PCA) effectively reduced the feature dimensions, achieving a reduction from 100 to 6 features for the Fourier spectrum and from 100 to 21 features for the power spectrum, while maintaining 95% of the cumulative variance. These optimized feature sets were subsequently fed into ML classifiers for further analysis. For image-based features, the transformation process was also successful, converting images into numerical feature sets with a dimension of 9216. These features were utilized by AlexNet, where the classifier layer employed NN. Additionally, these image-based features were integrated into a hybrid model, where the classification layer used either SVM or RF to enhance performance. This dual approach of feature selection and classifier optimization ensured robust detection and classification of falls, meeting the requirements for accurate and efficient fall detection across varying conditions.

The results of optimizing the classifiers based on feature inputs were comprehensively presented in this chapter. The findings reveal that signal transformation using FFT, whether through the Fourier or power spectrum, lacked sufficient discriminatory information to effectively classify PWR signals. In contrast, hybrid classifiers and DL algorithms demonstrated superior performance over traditional ML methods. Specifically, the SVM classifier with a polynomial kernel exhibited strong pattern recognition across most feature sets, with the AlexNet feature layer extracted from scalogram images proving to be the most effective in constructing hyperplanes. As a result, the hybrid SVM classifier utilizing spectrogram-AlexNet feature sets achieved the highest validation accuracies, with 95% for single-person scenarios and 98.38% for multiple-person scenarios. Similarly, the RF algorithm demonstrated that hybrid models required fewer DT to maintain high accuracy. The optimal feature sets provided clear decision boundaries, enabling the RF classifier to achieve peak performance with 74 DT for single-person scenarios and 78 DT for multiple-person scenarios. Moreover, NN models achieved outstanding results when utilizing the Adam optimizer with AlexNet features derived from spectrogram images.

These models yielded validation accuracies of 97.87% for single-person scenarios and 98.97% for multiple-person scenarios. Adam's adaptive learning rate and momentum-based optimization facilitated efficient convergence, robustly handling sparse gradients, and minimizing the risk of getting trapped in local minima. This demonstrated the effectiveness of Adam compared to traditional SGDM, further enhancing the reliability and accuracy of the classification system.

Despite the success of DL and hybrid models, these models underwent a detailed comparative analysis using precision, recall, and F1-score to provide deeper insights into their performance. The SVM with Scalogram-AlexNet achieved high recall and precision, attributed to its polynomial kernel's ability to capture intricate patterns, while RF with Spectrogram-AlexNet excelled in precision due to its ensemble structure, minimizing false positives. Spectrogram-AlexNet with the ADAM optimizer, though slightly behind, maintained solid results across recall, precision, and F1-score, highlighting the optimizer's influence on model performance. In multiple-person scenarios, all classifiers achieved high sensitivity and precision, with RF and SVM showing particularly balanced performance. Among the models, the hybrid RF algorithm with Spectrogram-AlexNet stood out, achieving optimal results with high accuracy, precision, and recall, while maintaining low mathematical complexity and addressing overfitting risks. This makes it a robust and efficient choice for the application, ensuring reliable performance with minimal training overhead.

In summary, this chapter had project a meaningful result in achieving second and third objective where the development and assessment types of classifier algorithm based on extracted features for the task of classify each type of fall and segregate from fall-like in controlled and realistic environment been achieved together with evaluating and validating analysis for the capability between the traditional ML, DL and hybrid algorithm in term of accuracy, efficiency, robustness and capability of the algorithm to adapt on the high complex signal data.

CHAPTER 6
CONCLUSION

6.1 Conclusion

In conclusion, this study has demonstrated notable success in effectively executing the classification task for human fall detection, encompassing both single and multiple detection scenarios, while proficiently distinguishing falls from fall-like movements. This achievement carries significant societal impact, particularly in contributing to the improvement of elderly individuals' quality of life. Moreover, it aligns with Malaysia's strategic direction towards becoming an aging nation by 2030, highlighting the crucial importance of elderly care as emphasized in the RMK-12. The study's outcomes not only advance the field of assistive living technologies but also address pressing societal needs, reinforcing the importance of research in promoting the well-being of the elderly population. The motivation driving this study was to accomplish four main goals which are formulating preprocessing methods for pulse based PWR signals, characterising salient and image features, developing classifier algorithms, and evaluating traditional ML, DL, and hybrid algorithms.

The PWR system has proven its efficacy in supplying Amplitude modulation signatures for the detection of human falls and movements, despite being initially designed for communication and packet data transfer. The implementation of an enveloping algorithm on the beacon signal has successfully preserved time-domain patterns formed by signal trajectories. This achievement addresses previous challenges, including concerns related to the comfort of wearable devices among the elderly, privacy issues associated with vision-based sensors, and electromagnetic radiation exposure from conventional radar systems. Moreover, the PWR system has demonstrated effectiveness in overcoming limitations related to the detection of multiple persons and addressing false alarms triggered by fall-like movements. These outcomes collectively position the PWR system as a promising technology for mitigating various challenges associated with fall detection, thereby contributing to advancements in the field of ALT.

Furthermore, the effectiveness of the PWR system in providing relevant information is evident in the application of post-signal transformation algorithms. The Fourier spectrum analysis reveals distinct segregation patterns between different types of falls, indicating the significant relevance of the extracted information to human fall and movement detection. Additionally, detailed analyses of time-frequency images further support the evidence of the PWR system's capability in the human fall detection system. The examination of power intensity, specific to duration and frequency components, within time-frequency images proves to be instrumental in distinguishing between various types of falls and discerning differences between falls and fall-like movements. This nuanced analysis underscores the robustness and specificity of the information obtained through the PWR system, contributing to its efficacy in enhancing the precision and accuracy of human fall detection.

Furthermore, the integration of AI classifiers in this study proved instrumental in discerning the effectiveness of the PWR system by identifying optimal features for the classification task. The features utilized in this investigation were derived from the transformed signal, incorporating direct input, PCA, and a feature set obtained from the layers of the AlexNet algorithm. The classifiers designed in this study encompassed 6 models such FFNN, AlexNet, SVM, AlexNet-SVM, RF and AlexNet-RF algorithm. The feature sets were employed in traditional ML by feeding the ML models with direct input and PCA applications. For DL, the time-frequency features were utilized in the AlexNet algorithm, while a hybrid classifier emerged from combining features from AlexNet feature layers with ML algorithms. This comprehensive approach allowed for a nuanced evaluation of the synergies between different feature extraction methods and classifiers, enhancing the overall effectiveness of the fall detection system.

Based on the outcomes of the classification task, this study draws the conclusion that, for human fall and movement detection utilizing the PWR system, the time-frequency features stand out as the crucial elements holding significant information for each collected dataset, both in single and multiple person scenario scenarios. This observation underscores the PWR system's notable ability to detect and project complex movement signals with an excellent capture of pertinent movement information. Moreover, the comparative analysis reveals that, with well-mapped features derived from PWR capturing trajectories, a relatively straightforward ML model such as RF can effectively make decisions through algorithms that function akin to conditional logic (if-else statements). This simplicity in ML model implementation, coupled with the robust information extracted from the PWR system, highlights the efficiency and effectiveness of the proposed approach in human fall and movement detection.

Overall, this study has demonstrated significant progress in the domain of human fall detection, particularly through the application of PWR technology. The research findings showcase the system's effectiveness in accurately detecting falls and distinguishing them from fall-like movements, presenting promising solutions for enhancing the safety and well-being of the elderly population. Through the integration of preprocessing methods, feature extraction techniques, and classifier algorithms, this study has not only advanced ALT but also addressed pressing societal needs. The adaptability and efficacy of the PWR system in overcoming challenges related to comfort, privacy, and accuracy underscore its potential to revolutionize fall detection systems. Furthermore, the study highlights the synergy between artificial intelligence and traditional machine learning approaches, emphasizing the importance of nuanced feature extraction and model simplicity. This synergy enhances the reliability and efficiency of the system, paving the way for further advancements in the field of fall detection and elderly care.

6.2 Future Works

While the present study has achieved success in delving into the development of an elderly fall detection system utilizing PWR, it is important to note that its scope has been confined to the detection of falls within the FSR region. Moving forward, there is a notable opportunity to broaden the scope of this investigation by extending it to include bistatic areas rather than limiting the focus solely to the FSR region. By expanding the study's reach beyond the confines of FSR, it would be possible to create a more comprehensive fall detection system that can leverage the entirety of indoor spaces for detecting falls among the elderly. This proposed extension could potentially enhance the system's capabilities and contribute to a more robust and versatile solution for elderly fall detection, thereby addressing a wider range of scenarios within indoor environments.

Additionally, exploring different sensor placements could significantly improve the efficacy and reliability of the fall detection system. The current study primarily focuses on a fixed sensor configuration, but varying the positions of the sensors could yield valuable insights into optimizing detection accuracy. For instance, strategically placing sensors at different heights, angles, and locations within a room might uncover the most effective configurations for capturing fall incidents. Experimenting with these variables could lead to an optimized sensor network that maximizes coverage and minimizes blind spots, thereby enhancing the overall performance of the system.

Furthermore, conducting experiments in environments of varying sizes and layouts is crucial for assessing the scalability and adaptability of the fall detection system. The current study's experiments are limited to a specific space, which may not reflect the diversity of real-world indoor settings. By testing the system in larger and more complex areas, such as multi-room apartments or larger communal spaces, researchers can evaluate how well the system performs under different spatial conditions. This approach will help identify any limitations or necessary adjustments required for different indoor environments, ultimately contributing to a more flexible and widely applicable fall detection solution for the elderly.

Moreover, the same experimental setup can be extended to different environmental conditions, such as varying temperatures, humidity levels, and atmospheric pressures, to evaluate the consistency and reliability of the collected signals. Environmental factors may introduce subtle variations in signal propagation, reflection, and absorption, which could affect the classifier's performance and robustness. Conducting experiments under controlled variations of these parameters will provide insights into how well the hybrid classifiers and deep learning algorithms generalize across diverse conditions. This investigation can help refine feature extraction techniques and improve model adaptability, ensuring the system's stability and accuracy in real-world applications where environmental dynamics are unavoidable.

REFERENCES

[1] J. Wang, Z. Chen, and Y. Song, "Falls in aged people of the Chinese mainland: Epidemiology, risk factors and clinical strategies," Nov. 2010. doi: 10.1016/j.arr.2010.07.002.

[2] World Health Organization, "PAGE 1 AGEinG And LifE CoursE, fAmiLy And Community HEALtH WHo Global report on falls Prevention in older Age," 2007.

[3] M. Montero-Odasso *et al.*, "World guidelines for falls prevention and management for older adults: a global initiative," Sep. 01, 2022, *Oxford University Press*. doi: 10.1093/ageing/afac205.

[4] R. Kakara, G. Bergen, E. Burns, and M. Stevens, "Morbidity and Mortality Weekly Report Nonfatal and Fatal Falls Among Adults Aged ≥65 Years-United States, 2020-2021," 2023. [Online]. Available: https://www.cdc.gov/mmwr/mmwr_continuingEducation.html

[5] Department of Statistic Malaysia, "POPULATION BY SEX Males outnumbered females," 2022.

[6] A. Keogh, J. F. Dorn, L. Walsh, F. Calvo, and B. Caulfield, "Comparing the usability and acceptability of wearable sensors among older Irish adults in a real-world context: Observational study," *JMIR Mhealth Uhealth*, vol. 8, no. 4, 2020, doi: 10.2196/15704.

[7] A. Putra Adhitama *et al.*, "Technology for Patient's Fall Detection System in Hospital Settings: A Systematic Literature Review," *Health and Technology Journal (HTechJ)*, vol. 1, no. 1, 2023, doi: 10.53713/htechj.v1i1.21.

[8] N. T. Newaz and E. Hanada, "The Methods of Fall Detection: A Literature Review," 2023. doi: 10.3390/s23115212.

[9] A. Naser, A. Lotfi, M. D. Mwanje, and J. Zhong, "Privacy-Preserving, Thermal Vision With Human in the Loop Fall Detection Alert System," *IEEE Trans Hum Mach Syst*, vol. 53, no. 1, 2023, doi: 10.1109/THMS.2022.3203021.

[10] E. Ramanujam, L. Rasikannan, and A. Balasubramanian, "Coupling of Dimensionality Reduction and Stacking Ensemble Learning for Smartphone-Based Human Activity Recognition," *International Journal of E-Services and Mobile Applications*, vol. 14, no. 1, 2022, doi: 10.4018/ijesma.300267.

[11] S. Kim, M. A. Nussbaum, and F. Lure, "Use Of Linear-Polarization Doppler Radar System to Detect Falls: Results From a Simulated Living Environment," *Proceedings of the Human Factors and Ergonomics Society Annual Meeting*, vol. 64, no. 1, 2020,

doi: 10.1177/1071181320641003.

[12] N. N. Ismail, N. E. A. Rashid, M. N. F. Nasarudin, W. M. W. Mohamed, S. Zainuddin, and Z. I. Khan, "VEHICLE DETECTION AND CLASSIFICATION USING FORWARD SCATTER RADAR (FSR) FOR TRAFFIC MANAGEMENT USING CONVOLUTIONAL NEURAL NETWORK," *Planning Malaysia*, vol. 21, no. 4, 2023, doi: 10.21837/pm.v21i28.1312.

[13] W. Jiang, Y. Ren, Y. Liu, and J. Leng, "Artificial Neural Networks and Deep Learning Techniques Applied to Radar Target Detection: A Review," 2022. doi: 10.3390/electronics11010156.

[14] P. S. Diao, T. Alves, B. Poussot, and S. Azarian, "A review of Radar Detection Fundamentals," *IEEE Aerospace and Electronic Systems Magazine*, 2022, doi: 10.1109/MAES.2022.3177395.

[15] G. Ziegelberger *et al.*, "Guidelines for limiting exposure to electromagnetic fields (100 kHz to 300 GHz)," May 01, 2020, *Lippincott Williams and Wilkins*. doi: 10.1097/HP.0000000000001210.

[16] Jabatan Perangkaan Malaysia, "LAPORAN SURVEI PENGGUNAAN DAN CAPAIAN ICT OLEH INDIVIDU DAN ISI RUMAH ICT USE AND ACCESS BY INDIVIDUALS AND HOUSEHOLDS SURVEY REPORT," 2020. [Online]. Available: https://www.dosm.gov.my

[17] World Health Organization, *WHO POLICY BRIEF Ageism in artificial intelligence for health: WHO policy brief*. 2022. [Online]. Available: http://apps.who.int/bookorders.

[18] A. Nayarisseri, "Artificial Intelligence, Big Data and Machine Learning Approaches in Precision Medicine & Drug Discovery," *Curr Drug Targets*, vol. 22, no. 6, 2022, doi: 10.2174/18735592mtezsmdmnz.

[19] W. Nai, X. Zhang, X. Lei, Y. Chen, and D. Dong, "Soft decision strategy design for signal demodulation in IEEE 802.11 protocol suite based wireless communication process," in *Proceedings of the IEEE International Conference on Software Engineering and Service Sciences, ICSESS*, 2017. doi: 10.1109/ICSESS.2017.8343009.

[20] L. Ren and Y. Peng, "Research of fall detection and fall prevention technologies: A systematic review," 2019. doi: 10.1109/ACCESS.2019.2922708.

[21] K. Z. Rajab, B. Wu, P. Alizadeh, and A. Alomainy, "Multi-target tracking and activity classification with millimeter-wave radar," *Appl Phys Lett*, vol. 119, no. 3, 2021, doi: 10.1063/5.0055641.

[22] A. Sarkar and D. Ghosh, "Accurate sensing of multiple humans buried under rubble

using IR-UWB SISO radar during search and rescue," *Sens Actuators A Phys*, vol. 348, 2022, doi: 10.1016/j.sna.2022.113975.

[23] Unit Perancang Ekonomi Jabatan Perdana Menteri Malaysia, "Rancangan Malaysia Kedua Belas, 2021-2025," 2021. [Online]. Available: https://www.epu.gov.my

[24] R. Koris *et al.*, "The cost of healthcare among Malaysian community-dwelling elderly," *Jurnal Ekonomi Malaysia*, vol. 53, no. 1, 2019, doi: 10.17576/JEM-2019-5301-8.

[25] N. Safian *et al.*, "Factors associated with the need for assistance among the elderly in Malaysia," *Int J Environ Res Public Health*, vol. 18, no. 2, 2021, doi: 10.3390/ijerph18020730.

[26] S. Noor, F. Md. Isa, and L. Mohd Nor, "Ageing Care Centre Women Entrepreneur: A Silver Bullet for Ageing Tsunami in Malaysia," *Sains Humanika*, vol. 12, no. 1, 2019, doi: 10.11113/sh.v12n1.1600.

[27] F. Md Isa, S. Noor, G. Wei Wei, S. D. B. Syed Hussain, H. Mohamad Ibrahim, and M. A. S. Ahmdon, "Exploring the facet of elderly care centre in multiethnic Malaysia," *PSU Research Review*, vol. 6, no. 1, 2022, doi: 10.1108/PRR-05-2020-0013.

[28] Z. Zahari, M. F. Abd Rahim, M. Justine, and Sulfandi, "Environmental Hazards and Falls among Elderly with Low Back Pain," *Environment-Behaviour Proceedings Journal*, vol. 7, no. 20, 2022, doi: 10.21834/ebpj.v7i20.3497.

[29] J. Jagnoor *et al.*, "Fall related injuries: A retrospective medical review study in North India," *Injury*, vol. 43, no. 12, 2012, doi: 10.1016/j.injury.2011.08.004.

[30] N. Maneeprom, S. Taneepanichskul, and A. Panza, "Falls among physically active elderly in senior housings, Bangkok, Thailand: Situations and perceptions," *Clin Interv Aging*, vol. 13, 2018, doi: 10.2147/CIA.S175896.

[31] A. Ungar *et al.*, "Fall prevention in the elderly," 2013. doi: 10.11138/ccmbm/2013.10.2.091.

[32] A. Geetha, M. Aravindan, J. Anandjahan, and S. Aravindh, "CNN based fall detection and health monitoring system using IoT," *International Journal of Advanced Science and Technology*, vol. 29, no. 3, 2020.

[33] J. lin Yuan *et al.*, "Prevalence/potential risk factors for motoric cognitive risk and its relationship to falls in elderly Chinese people: a cross-sectional study," *Eur J Neurol*, vol. 28, no. 8, 2021, doi: 10.1111/ene.14884.

[34] L. Marchini and V. Allareddy, "Epidemiology of facial fractures among older adults: A retrospective analysis of a nationwide emergency department database," *Dental Traumatology*, vol. 35, no. 2, 2019, doi: 10.1111/edt.12459.

[35] S. Chaieb, A. Ben Mrad, and B. Hnich, “Obsolete personal information update system: towards the prevention of falls in the elderly,” *Applied Intelligence*, vol. 53, no. 14, 2023, doi: 10.1007/s10489-022-04289-3.

[36] A. A. Z. Abu Bakar, A. A. Kadir, N. S. Idris, and S. N. M. Nawi, “Older adults with hypertension: Prevalence of falls and their associated factors,” *Int J Environ Res Public Health*, vol. 18, no. 16, 2021, doi: 10.3390/ijerph18168257.

[37] D. Yi, S. Jang, and J. Yim, “Relationship between Associated Neuropsychological Factors and Fall Risk Factors in Community-Dwelling Elderly,” *Healthcare (Switzerland)*, vol. 10, no. 4, 2022, doi: 10.3390/healthcare10040728.

[38] A. J. Garbin and B. E. Fisher, “The Interplay Between Fear of Falling, Balance Performance, and Future Falls: Data From the National Health and Aging Trends Study,” *Journal of Geriatric Physical Therapy*, vol. 46, no. 2, 2023, doi: 10.1519/JPT.0000000000000324.

[39] A. C. de Sena, A. M. Alvarez, S. F. L. Nunes, and N. P. da Costa, “Nursing care related to fall prevention among hospitalized elderly people: an integrative review,” 2021. doi: 10.1590/0034-7167-2020-0904.

[40] D. K. da S. Teixeira, L. M. Andrade, J. L. P. Santos, and E. S. Caires, “Falls among the elderly: environmental limitations and functional losses,” *Revista Brasileira de Geriatria e Gerontologia*, vol. 22, no. 3, 2019, doi: 10.1590/1981-22562019022.180229.

[41] Z. Hong *et al.*, “The relationship between self-rated economic status and falls among the elderly in Shandong province, China,” *Int J Environ Res Public Health*, vol. 17, no. 6, 2020, doi: 10.3390/ijerph17062150.

[42] C. L. Baixinho, M. D. A. Dixe, C. Madeira, S. Alves, and M. A. Henriques, “Falls in institutionalized elderly with and without cognitive decline: A study of some factors,” *Dementia e Neuropsychologia*, vol. 13, no. 1, 2019, doi: 10.1590/1980-57642018dn13-010014.

[43] S. ELDEMİR, K. ELDEMİR, Ç. ÖZKUL, and A. GÜÇLÜ GÜNDÜZ, “The Effects of Spinomed Orthosis on Balance and Walking Performance in Elderly People with Thoracic Hyperkyphosis,” *Gazi Sağlık Bilimleri Dergisi*, vol. 7, no. 3, 2022, doi: 10.52881/gsbdergi.1199930.

[44] M. Al Majali, M. Sunnaa, and P. Chand, “Emerging Pharmacotherapies for Motor Symptoms in Parkinson’s Disease,” 2021. doi: 10.1177/08919887211018275.

[45] M. Hippi, M. Kangas, R. Ruuhela, J. Ruotsalainen, and S. Hartonen, “RoadSurf-

Pedestrian: a sidewalk condition model to predict risk for wintertime slipping injuries," *Meteorological Applications*, vol. 27, no. 5, 2020, doi: 10.1002/met.1955.

[46] J. L. Vincenzo *et al.*, "Older Adults' Perceptions Regarding the Role of Physical Therapists in Fall Prevention: A Qualitative Investigation," *Journal of Geriatric Physical Therapy*, vol. 45, no. 3, 2022, doi: 10.1519/JPT.0000000000000304.

[47] A. Fujii, K. Murao, and N. Matsuhisa, "Pulse Wave Generation Method for PPG by Using Display," *IEEE Access*, vol. 11, 2023, doi: 10.1109/ACCESS.2023.3260862.

[48] A. de Souza Dias, L. Naves Dias Alves, A. Santos Freitas, J. Santos dos Reis, and E. Naves Dias, "ACCIDENTS CAUSED BY FALLS IN THE ELDERLY PEOPLE: A PUBLIC HEALTH PROBLEM," *Journal Health and Technology - JHT*, vol. 1, no. 1, 2022, doi: 10.47820/jht.v1i1.7.

[49] N. Mohamed Hassan Saleh, A.-H. El-Gilany, H. Noshy Abd El-Aziz Mohamed, and N. Mahmoud Elsakhy, "Effect of Matter of Balance program on improving balance and reducing fear of falls among community-dwelling older adults," *Egyptian Journal of Health Care*, vol. 13, no. 1, 2022, doi: 10.21608/ejhc.2022.233175.

[50] V. Fatmawati, N. M. Rukmana, W. Septianto, and D. E. Yuniarsih, "The effect of core stability exercise in reducing the risk of falling in the elderly at the work area of Kasian 1 public health center," *International Journal of Health Science and Technology*, vol. 3, no. 1, 2021, doi: 10.31101/ijhst.v3i1.1910.

[51] S. M. Kiik, A. R. Vanchapo, M. F. Elfrida, M. S. Nuwa, and S. Sakinah, "Effectiveness of Otago Exercise on Health Status and Risk of Fall Among Elderly with Chronic Illness," *Jurnal Keperawatan Indonesia*, vol. 23, no. 1, 2020, doi: 10.7454/jki.v23i1.900.

[52] Y. Takeuchi, "'Characteristics of Head Center of Mass Sway and Neck Flexor Activity During Compensatory Backward Stepping in the Elderly,'" *Biomed J Sci Tech Res*, vol. 38, no. 3, 2021, doi: 10.26717/bjstr.2021.38.006157.

[53] V. F. da Silva *et al.*, "Physical Training Coupled with Non-Invasive Brain Stimulation Modulates Cortical Waves Decreasing the Likelihood of Falls in Adults Elderly with Fragility," *International Journal of Advanced Engineering Research and Science*, vol. 6, no. 5, 2019, doi: 10.22161/ijaers.6.5.41.

[54] K. Seibert *et al.*, "Application Scenarios for Artificial Intelligence in Nursing Care: Rapid Review," 2021. doi: 10.2196/26522.

[55] S. Ashry, T. Ogawa, and W. Gomaa, "CHARM-Deep: Continuous Human Activity Recognition Model Based on Deep Neural Network Using IMU Sensors of

Smartwatch," *IEEE Sens J*, vol. 20, no. 15, 2020, doi: 10.1109/JSEN.2020.2985374.

[56] A. Poulose and D. S. Han, "Hybrid indoor localization using IMU sensors and smartphone camera," *Sensors (Switzerland)*, vol. 19, no. 23, 2019, doi: 10.3390/s19235084.

[57] C. L. Lin, W. C. Chiu, F. H. Chen, Y. H. Ho, T. C. Chu, and P. H. Hsieh, "Fall Monitoring for the Elderly Using Wearable Inertial Measurement Sensors on Eyeglasses," *IEEE Sens Lett*, vol. 4, no. 6, 2020, doi: 10.1109/LSENS.2020.2996746.

[58] K. Bharathkumar, C. Paolini, and M. Sarkar, "FPGA-based Edge Inferencing for Fall Detection," in *2020 IEEE Global Humanitarian Technology Conference, GHTC 2020*, 2020. doi: 10.1109/GHTC46280.2020.9342948.

[59] H. C. Lin, M. J. Chen, C. H. Lee, L. C. Kung, and J. T. Huang, "Fall Recognition Based on an IMU Wearable Device and Fall Verification through a Smart Speaker and the IoT," *Sensors*, vol. 23, no. 12, 2023, doi: 10.3390/s23125472.

[60] M. Bastico, V. Ruiz Bejerano, and A. Belmonte-Hernández, "Simultaneous Real-Time Human Fall Detection and Reidentification Based on Multisensors Data," in *ACM International Conference Proceeding Series*, 2022. doi: 10.1145/3529190.3534728.

[61] K. M. Esquivel *et al.*, "Factors Influencing Continued Wearable Device Use in Older Adult Populations: Quantitative Study," *JMIR Aging*, vol. 6, 2023, doi: 10.2196/36807.

[62] K. Moore *et al.*, "Older adults' experiences with using wearable devices: Qualitative systematic review and meta-synthesis," 2021. doi: 10.2196/23832.

[63] M. Menolotto, D. S. Komaris, S. Tedesco, B. O'flynn, and M. Walsh, "Motion capture technology in industrial applications: A systematic review," 2020. doi: 10.3390/s20195687.

[64] A. Kashevnik, W. Othman, I. Ryabchikov, and N. Shilov, "Estimation of motion and respiratory characteristics during the meditation practice based on video analysis," *Sensors*, vol. 21, no. 11, 2021, doi: 10.3390/s21113771.

[65] G. Anitha and S. B. Priya, "Vision Based Real Time Monitoring System for Elderly Fall Event Detection Using Deep Learning," *Computer Systems Science and Engineering*, vol. 42, no. 1, 2022, doi: 10.32604/CSSE.2022.020361.

[66] T. Alanazi, K. Babutain, and G. Muhammad, "A Robust and Automated Vision-Based Human Fall Detection System Using 3D Multi-Stream CNNs with an Image Fusion Technique," *Applied Sciences (Switzerland)*, vol. 13, no. 12, 2023, doi: 10.3390/app13126916.

[67] S. Li *et al.*, "A Fall Detection Network by 2D/3D Spatio-temporal Joint Models with

Tensor Compression on Edge," *ACM Transactions on Embedded Computing Systems*, vol. 21, no. 6, 2022, doi: 10.1145/3531004.

[68] L. Gong *et al.*, "A novel computer vision-based data driven modelling approach for person specific fall detection," *J Ambient Intell Smart Environ*, vol. 13, no. 5, 2021, doi: 10.3233/AIS-210611.

[69] C. T. Nguyen, T. D. Phan, M. T. Duong, V. B. Nguyen, H. T. Pham, and M. H. Le, "Vision-based Fall Detection System: Novel Methodology and Comprehensive Experiments," in *Proceedings of 2023 International Conference on System Science and Engineering, ICSSE 2023*, 2023. doi: 10.1109/ICSSE58758.2023.10227233.

[70] Z. Guan *et al.*, "A Video-based Fall Detection Network by Spatio-temporal Joint-point Model on Edge Devices," in *Proceedings -Design, Automation and Test in Europe, DATE*, 2021. doi: 10.23919/DATE51398.2021.9474206.

[71] Suruhanjaya Komunikasi dan Multimedia Malysia, "Video_Surveillance_Public_Spaces_compressed," *2018*.

[72] A. Alboksmaty, N. Solomons, S. Gul, A. Neves, and P. Aylin, "Remote patient monitoring at home using ambient sensors: a systematic review," *Eur J Public Health*, vol. 32, no. Supplement_3, 2022, doi: 10.1093/eurpub/ckac130.065.

[73] R. Parmar and S. Trapasiya, "A Comprehensive Survey of Various Approaches on Human Fall Detection for Elderly People," *Wirel Pers Commun*, vol. 126, no. 2, 2022, doi: 10.1007/s11277-022-09816-6.

[74] J. S. R. Alex, M. Abai Kumar, and D. V. Swathy, "Deep Learning Approaches for Fall Detection Using Acoustic Information," in *Lecture Notes in Electrical Engineering*, 2021. doi: 10.1007/978-981-15-7241-8_35.

[75] J. Lian, X. Yuan, M. Li, and N. F. Tzeng, "Fall Detection via Inaudible Acoustic Sensing," *Proc ACM Interact Mob Wearable Ubiquitous Technol*, vol. 5, no. 3, 2021, doi: 10.1145/3478094.

[76] D. Droghini, S. Squartini, E. Principi, L. Gabrielli, and F. Piazza, "Audio Metric Learning by Using Siamese Autoencoders for One-Shot Human Fall Detection," *IEEE Trans Emerg Top Comput Intell*, vol. 5, no. 1, 2021, doi: 10.1109/TETCI.2019.2948151.

[77] K. Fang, Z. Xu, Y. Li, and J. Pan, "A Fall Detection using Sound Technology Based on TinyML," in *Proceedings - 11th International Conference on Information Technology in Medicine and Education, ITME 2021*, 2021. doi: 10.1109/ITME53901.2021.00053.

[78] F. Muheidat and L. A. Tawalbeh, "In-home floor based sensor system-smart carpet- To

facilitate healthy aging in place (AIP)," *IEEE Access*, vol. 8, 2020, doi: 10.1109/ACCESS.2020.3027535.

[79] V. R. Chawan, M. Huber, N. Burns, and K. Daniel, "Person Identification And Tinetti Score Prediction Using Balance Parameters : A Machine Learning Approach To Determine Fall Risk," in *ACM International Conference Proceeding Series*, 2022. doi: 10.1145/3529190.3529223.

[80] L. and W. B. Wang Lu and Weng, "Design of Magnetic Tactile Sensor Arrays for Intelligent Floorboard Based on the Demand of Older People," in *Proceedings of 2023 Chinese Intelligent Automation Conference*, Z. Deng, Ed., Singapore: Springer Nature Singapore, 2023, pp. 618–625.

[81] J. Clemente, F. Li, M. Valero, and W. Song, "Smart Seismic Sensing for Indoor Fall Detection, Location, and Notification," *IEEE J Biomed Health Inform*, vol. 24, no. 2, 2020, doi: 10.1109/JBHI.2019.2907498.

[82] K. Wu, Y. Huang, M. Qiu, Z. Peng, and L. Wang, "Toward Device-free and User-independent Fall Detection Using Floor Vibration," *ACM Trans Sens Netw*, vol. 19, no. 1, 2023, doi: 10.1145/3519302.

[83] Y. Shao, X. Wang, W. Song, S. Ilyas, H. Guo, and W. S. Chang, "Feasibility of using floor vibration to detect human falls," *Int J Environ Res Public Health*, vol. 18, no. 1, 2021, doi: 10.3390/ijerph18010200.

[84] C. H. Li, Z. Huang, J. Lin, T. Hou, Y. Zi, and J. Li, "Excellent-Moisture-Resistance Fluorinated Polyimide Composite Film and Self-Powered Acoustic Sensing," *ACS Appl Mater Interfaces*, vol. 15, no. 29, 2023, doi: 10.1021/acsami.3c05154.

[85] X. Chen, S. Jiang, and B. Lo, "Subject-Independent Slow Fall Detection with Wearable Sensors via Deep Learning," in *Proceedings of IEEE Sensors*, 2020. doi: 10.1109/SENSORS47125.2020.9278625.

[86] C. Gu, "Short-range noncontact sensors for healthcare and other emerging applications: A review," 2016. doi: 10.3390/s16081169.

[87] X. Qiao, Y. Feng, S. Liu, T. Shan, and R. Tao, "Radar Point Clouds Processing for Human Activity Classification Using Convolutional Multilinear Subspace Learning," *IEEE Transactions on Geoscience and Remote Sensing*, vol. 60, 2022, doi: 10.1109/TGRS.2022.3230977.

[88] K. Saho, S. Hayashi, M. Tsuyama, L. Meng, and M. Masugi, "Machine Learning-Based Classification of Human Behaviors and Falls in Restroom via Dual Doppler Radar Measurements," *Sensors*, vol. 22, no. 5, 2022, doi: 10.3390/s22051721.

[89] B. Y. Su, K. C. Ho, M. Rantz, and M. Skubic, “Radar placement for fall detection: Signature and performance,” *J Ambient Intell Smart Environ*, vol. 10, no. 1, 2018, doi: 10.3233/AIS-170469.

[90] Y. Yao *et al.*, “Fall Detection System Using Millimeter-Wave Radar Based on Neural Network and Information Fusion,” *IEEE Internet Things J*, vol. 9, no. 21, 2022, doi: 10.1109/JIOT.2022.3175894.

[91] B. Wang, Z. Zheng, and Y. X. Guo, “Millimeter-Wave Frequency Modulated Continuous Wave Radar-Based Soft Fall Detection Using Pattern Contour-Confined Doppler-Time Maps,” *IEEE Sens J*, vol. 22, no. 10, 2022, doi: 10.1109/JSEN.2022.3165188.

[92] B. Wang, H. Zhang, and Y. X. Guo, “Radar-Based Soft Fall Detection Using Pattern Contour Vector,” *IEEE Internet Things J*, vol. 10, no. 3, 2023, doi: 10.1109/JIOT.2022.3213693.

[93] C. Song, K. Ma, J. He, and Y. Jia, “Fall Detection Based on HOG Features for Millimeter Wave Radar,” in *Proceedings - 2022 2nd International Conference on Frontiers of Electronics, Information and Computation Technologies, ICFEICT 2022*, 2022. doi: 10.1109/ICFEICT57213.2022.00064.

[94] A. Dey, S. Rajan, G. Xiao, and J. Lu, “Radar-Based Fall Event Detection Using Histogram of Oriented Gradients of Binary-Encoded Radar Signatures,” *IEEE Sens Lett*, vol. 7, no. 11, pp. 1–4, 2023, doi: 10.1109/LSENS.2023.3323903.

[95] X. Jiang, L. Zhang, and L. Li, “Multi-Task Learning Radar Transformer (MLRT): A Personal Identification and Fall Detection Network Based on IR-UWB Radar,” *Sensors*, vol. 23, no. 12, 2023, doi: 10.3390/s23125632.

[96] C. Ding, H. Zhao, Y. Ma, H. Hong, and X. Zhu, “Soft Fall Detection With a Height-Tracking Method Based on MIMO Radar System,” *IEEE Geoscience and Remote Sensing Letters*, vol. 20, 2023, doi: 10.1109/LGRS.2023.3268654.

[97] S. Waqar, M. Muaaz, and M. Patzold, “Direction-Independent Human Activity Recognition Using a Distributed MIMO Radar System and Deep Learning,” *IEEE Sens J*, vol. 23, no. 20, 2023, doi: 10.1109/JSEN.2023.3310620.

[98] M. Muaaz, S. Waqar, and M. Pätzold, “Orientation-Independent Human Activity Recognition Using Complementary Radio Frequency Sensing,” *Sensors*, vol. 23, no. 13, 2023, doi: 10.3390/s23135810.

[99] M. Shen, K. L. Tsui, M. A. Nussbaum, S. Kim, and F. Lure, “An Indoor Fall Monitoring System: Robust, Multistatic Radar Sensing and Explainable, Feature-Resonated Deep

Neural Network," *IEEE J Biomed Health Inform*, vol. 27, no. 4, 2023, doi: 10.1109/JBHI.2023.3237077.

[100] L. Anishchenko, A. Zhuravlev, and M. Chizh, "Fall detection using multiple bioradars and convolutional neural networks," *Sensors (Switzerland)*, vol. 19, no. 24, 2019, doi: 10.3390/s19245569.

[101] L. Martínez-Villaseñor, H. Ponce, J. Brieva, E. Moya-Albor, J. Núñez-Martínez, and C. Peñafort-Asturiano, "Up-fall detection dataset: A multimodal approach," *Sensors (Switzerland)*, vol. 19, no. 9, 2019, doi: 10.3390/s19091988.

[102] A. Taha, M. M. A. Taha, B. Barakat, W. Taylor, Q. H. Abbasi, and M. Ali Imran, "AI-Based Fall Detection Using Contactless Sensing," in *Proceedings of IEEE Sensors*, 2021. doi: 10.1109/SENSORS47087.2021.9639715.

[103] I. Ullmann, R. G. Guendel, N. C. Kruse, F. Fioranelli, and A. Yarovoy, "A Survey on Radar-Based Continuous Human Activity Recognition," *IEEE Journal of Microwaves*, vol. 3, no. 3, 2023, doi: 10.1109/jmw.2023.3264494.

[104] X. Chen and X. Ni, "Noncontact Sleeping Heartrate Monitoring Method Using Continuous-Wave Doppler Radar Based on the Difference Quadratic Sum Demodulation and Search Algorithm," *Sensors*, vol. 22, no. 19, 2022, doi: 10.3390/s22197646.

[105] F. Fereidouni, S. T. Mohammadi, V. F. Shahraki, and F. Jahantigh, "Human Health Risk Assessment of 4-12 GHz Radar Waves using CST STUDIO SUITE Software," *J Biomed Phys Eng*, vol. 12, no. 3, 2022, doi: 10.31661/jbpe.v0i0.1272.

[106] F. Santi, D. Pastina, and M. Bucciarelli, "Experimental demonstration of ship target detection in GNSS-based passive radar combining target motion compensation and track-before-detect strategies," *Sensors (Switzerland)*, vol. 20, no. 3, 2020, doi: 10.3390/s20030599.

[107] J. Wang, H. Fu, B. Wang, and L. Liu, "Spatial resolution analysis of passive bistatic radar using low-orbit navigation augmented signals," in *Journal of Physics: Conference Series*, 2022. doi: 10.1088/1742-6596/2369/1/012062.

[108] R. S. Thoma *et al.*, "Cooperative Passive Coherent Location: A Promising 5G Service to Support Road Safety," *IEEE Communications Magazine*, vol. 57, no. 9, 2019, doi: 10.1109/MCOM.001.1800242.

[109] B. Gabard, V. Wasik, O. Rabaste, T. Deloues, D. Poullin, and H. Jeuland, "Airborne Targets Detection by UAV-Embedded Passive Radar," in *EuRAD 2020 - 2020 17th European Radar Conference*, 2021. doi: 10.1109/EuRAD48048.2021.00095.

[110] G. Mazurek, K. Kulpa, M. Malanowski, and A. Droszcz, “Experimental seaborne passive radar,” *Sensors*, vol. 21, no. 6, 2021, doi: 10.3390/s21062171.

[111] A. Asif and S. Kandeepan, “Cooperative fusion based passive multistatic radar detection,” *Sensors*, vol. 21, no. 9, 2021, doi: 10.3390/s21093209.

[112] S. A. Musa, R. S. A. R. Abdullah, A. Sali, A. Ismail, and N. E. A. Rashid, “Low-slow-small (LSS) target detection based on micro doppler analysis in forward scattering radar geometry,” *Sensors (Switzerland)*, vol. 19, no. 15, 2019, doi: 10.3390/s19153332.

[113] J. Wang, Z. Qin, F. Gao, and S. Wei, “An approximate maximum likelihood algorithm for target localization in multistatic passive radar,” *Chinese Journal of Electronics*, vol. 28, no. 1, 2019, doi: 10.1049/cje.2018.02.018.

[114] S. Dongus, H. Jalilian, D. Schürmann, and M. Röösli, “Health effects of WiFi radiation: a review based on systematic quality evaluation,” 2022. doi: 10.1080/10643389.2021.1951549.

[115] W. Li, S. Vishwakarma, C. Tang, K. Woodbridge, R. J. Piechocki, and K. Chetty, “Using RF Transmissions from IoT Devices for Occupancy Detection and Activity Recognition,” *IEEE Sens J*, vol. 22, no. 3, 2022, doi: 10.1109/JSEN.2021.3134895.

[116] W. Li, M. J. Bocus, C. Tang, R. J. Piechocki, K. Woodbridge, and K. Chetty, “On CSI and Passive Wi-Fi Radar for Opportunistic Physical Activity Recognition,” *IEEE Trans Wirel Commun*, vol. 21, no. 1, 2022, doi: 10.1109/TWC.2021.3098526.

[117] P. Fard Moshiri, R. Shahbazian, M. Nabati, and S. A. Ghorashi, “A CSI-Based Human Activity Recognition Using Deep Learning,” *Sensors (Basel)*, vol. 21, no. 21, 2021, doi: 10.3390/s21217225.

[118] L. Guan *et al.*, “Multi-Person Breathing Detection with Switching Antenna Array Based on WiFi Signal,” *IEEE J Transl Eng Health Med*, vol. 11, 2023, doi: 10.1109/JTEHM.2022.3218638.

[119] Y. Deng, W. Li, S. Zhang, F. Wang, W. Xiao, and Z. Cui, “Clutter suppression method for off-grid effects mitigation in airborne passive radars with contaminated reference signals,” *Sensors*, vol. 21, no. 19, 2021, doi: 10.3390/s21196339.

[120] F. Abuhoureyah, W. Yan Chiew, A. S. Bin Mohd Isira, and M. Al-Andoli, “Free device location independent WiFi-based localisation using received signal strength indicator and channel state information,” *IET Wireless Sensor Systems*, vol. 13, no. 5, 2023, doi: 10.1049/wss2.12065.

[121] M. N. F. Nasarudin *et al.*, “A Comparative Study on Human Movement Classification Using Wi-Fi Based Passive Forward Scattering Radar,” *TEM Journal*, vol. 12, no. 3,

2023, doi: 10.18421/TEM123-13.

[122] M. S. I. Sagar *et al.*, "Application of machine learning in electromagnetics: Mini-review," 2021. doi: 10.3390/electronics10222752.

[123] O. Valgaev, F. Kupzog, and H. Schmeck, "Adequacy of neural networks for wide-scale day-ahead load forecasts on buildings and distribution systems using smart meter data," *Energy Informatics*, vol. 3, no. 1, 2020, doi: 10.1186/s42162-020-00132-6.

[124] O. I. Chumachenko, S. V. Shymkov, and A. T. Kot, "TWO-LEVEL SYSTEM FOR TUNING PARAMETERS OF ARTIFICIAL NEURAL NETWORKS," *Electronics and Control Systems*, vol. 1, no. 63, 2020, doi: 10.18372/1990-5548.63.14517.

[125] K. Kalari *et al.*, "Optimization of the remediation of oil-drilling cuttings by combining artificial neural networks with knowledge-based models," in *IOP Conference Series: Earth and Environmental Science*, 2022. doi: 10.1088/1755-1315/1123/1/012080.

[126] M. Madhiarasan, M. Louzazni, and B. Belmahdi, "Statistical Analysis of Novel Ensemble Recursive Radial Basis Function Neural Network Performance on Global Solar Irradiance Forecasting," *Journal of Electrical and Computer Engineering*, vol. 2023, 2023, doi: 10.1155/2023/2554355.

[127] Z. Wu, A. Tran, D. Rincon, and P. D. Christofides, "Machine learning-based predictive control of nonlinear processes. Part I: Theory," *AIChE Journal*, vol. 65, no. 11, 2019, doi: 10.1002/aic.16729.

[128] Z. Wu and P. D. Christofides, "Economic machine-learning-based predictive control of nonlinear systems," *Mathematics*, vol. 7, no. 6, 2019, doi: 10.3390/math7060494.

[129] S. Jaeger, "The Golden Ratio in Machine Learning," in *Proceedings - Applied Imagery Pattern Recognition Workshop*, 2021. doi: 10.1109/AIPR52630.2021.9762080.

[130] A. Jahagirdar and R. Phalnikar, "Comparison of feed forward and cascade forward neural networks for human action recognition," *Indonesian Journal of Electrical Engineering and Computer Science*, vol. 25, no. 2, 2022, doi: 10.11591/ijeecs.v25.i2.pp892-899.

[131] R. Sapna, S. N. Sheshappa, P. Vijayakarthik, and S. P. Raja, "Global Pattern Feedforward Neural Network Structure with Bacterial Foraging Optimization towards Medicinal Plant Leaf Identification and Classification," *International Journal of Advanced Computer Science and Applications*, vol. 13, no. 12, 2022, doi: 10.14569/IJACSA.2022.0131209.

[132] A. Salim *et al.*, "Classification of Coffee Roast Levels using Multi-Layer Perceptron on MNDT s-Parameters," in *IEEE Symposium on Wireless Technology and Applications,*

ISWTA, 2022. doi: 10.1109/ISWTA55313.2022.9942782.

[133] Y. Yao *et al.*, “mmSignature: Semi-supervised human identification system based on millimeter wave radar,” *Eng Appl Artif Intell*, vol. 126, 2023, doi: 10.1016/j.engappai.2023.106939.

[134] J. J. Valdes, Z. Baird, S. Rajan, and M. Bolic, “Radar-based Noncontact Human Activity Classification Using Genetic Programming,” in *2020 IEEE Congress on Evolutionary Computation, CEC 2020 - Conference Proceedings*, 2020. doi: 10.1109/CEC48606.2020.9185814.

[135] O. Okwuashi and C. E. Ndehedehe, “Deep support vector machine for hyperspectral image classification,” *Pattern Recognit*, vol. 103, 2020, doi: 10.1016/j.patcog.2020.107298.

[136] B. Peng, H. Yan, R. Lin, and G. Yin, “Application of Surface-Enhanced Raman Spectroscopy in the Screening of Pulmonary Adenocarcinoma Nodules,” *Biomed Res Int*, vol. 2022, 2022, doi: 10.1155/2022/4368928.

[137] Q. Liu, W. Zhu, Z. Ma, and S. Report, “Multi-task support vector machine with generalized huber loss,” 2022, doi: 10.21203/rs.3.rs-2286985/v1.

[138] J. Shao, X. Liu, and W. He, “Kernel based data-adaptive support vector machines for multi-class classification,” *Mathematics*, vol. 9, no. 9, 2021, doi: 10.3390/math9090936.

[139] S. Shin, M. Kang, J. Jung, and Y. T. Kim, “Development of miniaturized wearable wristband type surface emg measurement system for biometric authentication,” *Electronics (Switzerland)*, vol. 10, no. 8, 2021, doi: 10.3390/electronics10080923.

[140] X. YANG, “POWER GRID FAULT PREDICTION METHOD BASED ON FEATURE SELECTION AND CLASSIFICATION ALGORITHM,” *International Journal of Electronics Engineering and Applications*, vol. IX, no. II, 2021, doi: 10.30696/ijeea.ix.ii.2021.34-44.

[141] C. Yang, A. Fa-you, Y.-F. Wu, S. Yan, C. Zhu, and H. Zhang, “Impact of Parameter Tuning with Genetic Algorithm, Particle Swarm Optimization, and Bat Algorithm on Accuracy of the SVM Model in Landslide Susceptibility Evaluation,” *Math Probl Eng*, vol. 2023, 2023, doi: 10.1155/2023/1393142.

[142] M. Aljanabi, M. A. Ismail, and A. H. Ali, “Intrusion detection systems, issues, challenges, and needs,” *International Journal of Computational Intelligence Systems*, vol. 14, no. 1, 2021, doi: 10.2991/ijcis.d.210105.001.

[143] P. Bendiek, A. Taha, Q. H. Abbasi, and B. Barakat, “Solar Irradiance Forecasting Using

a Data-Driven Algorithm and Contextual Optimisation," *Applied Sciences (Switzerland)*, vol. 12, no. 1, 2022, doi: 10.3390/app12010134.

[144] L. Bloch and C. M. Friedrich, "Machine Learning Workflow to Explain Black-Box Models for Early Alzheimer's Disease Classification Evaluated for Multiple Datasets," *SN Comput Sci*, vol. 3, no. 6, 2022, doi: 10.1007/s42979-022-01371-y.

[145] T. Zhongda, "Kernel principal component analysis-based least squares support vector machine optimized by improved grey wolf optimization algorithm and application in dynamic liquid level forecasting of beam pump," *Transactions of the Institute of Measurement and Control*, vol. 42, no. 6, 2020, doi: 10.1177/0142331219885273.

[146] A. Salim *et al.*, "ECOC-SVM Classification of Coffee Roast Levels based on MNDT s-Parameters," in *2022 IEEE 10th Conference on Systems, Process and Control, ICSPC 2022 - Proceedings*, 2022. doi: 10.1109/ICSPC55597.2022.10001741.

[147] A. Alnaeb, R. S. A. R. Abdullah, A. A. Salah, A. Sali, N. E. A. Rashid, and I. Pasya, "Detection and classification real-time of fall events from the daily activities of human using forward scattering radar," in *Proceedings International Radar Symposium*, 2019. doi: 10.23919/IRS.2019.8768130.

[148] K. Hanifi and M. E. Karsligil, "Elderly Fall Detection with Vital Signs Monitoring Using CW Doppler Radar," *IEEE Sens J*, vol. 21, no. 15, 2021, doi: 10.1109/JSEN.2021.3079835.

[149] F. Luo, S. Poslad, and E. Bodanese, "Human Activity Detection and Coarse Localization Outdoors Using Micro-Doppler Signatures," *IEEE Sens J*, vol. 19, no. 18, 2019, doi: 10.1109/JSEN.2019.2917375.

[150] Z. Zhao *et al.*, "Point Cloud Features-Based Kernel SVM for Human-Vehicle Classification in Millimeter Wave Radar," *IEEE Access*, vol. 8, 2020, doi: 10.1109/ACCESS.2020.2970533.

[151] Q. Yang *et al.*, "Beyond one-against-all (OAA) and one-against-one (OAO): An exhaustive and parallel half-against-half (HAH) strategy for multi-class classification and applications to metabolomics," *Chemometrics and Intelligent Laboratory Systems*, vol. 204, 2020, doi: 10.1016/j.chemolab.2020.104107.

[152] D. C. Toledo-Pérez, J. Rodríguez-Reséndiz, R. A. Gómez-Loenzo, and J. C. Jauregui-Correa, "Support Vector Machine-based EMG signal classification techniques: A review," 2019. doi: 10.3390/app9204402.

[153] Z. Wang, A. Ren, Q. Zhang, A. Zahid, and Q. H. Abbasi, "Recognition of Approximate Motions of Human Based on Micro-Doppler Features," *IEEE Sens J*, vol. 23, no. 11,

2023, doi: 10.1109/JSEN.2023.3267820.

[154] T. H. Lee, A. Ullah, and R. Wang, “Bootstrap Aggregating and Random Forest,” in *Advanced Studies in Theoretical and Applied Econometrics*, vol. 52, 2020. doi: 10.1007/978-3-030-31150-6_13.

[155] G. Audemard, S. Bellart, L. Bounia, F. Koriche, J. M. Lagniez, and P. Marquis, “Trading Complexity for Sparsity in Random Forest Explanations,” in *Proceedings of the 36th AAAI Conference on Artificial Intelligence, AAAI 2022*, 2022. doi: 10.1609/aaai.v36i5.20484.

[156] X. Fu, Y. Chen, J. Yan, Y. Chen, and F. Xu, “BGRF: A broad granular random forest algorithm,” *Journal of Intelligent and Fuzzy Systems*, vol. 44, no. 5, 2023, doi: 10.3233/JIFS-223960.

[157] J. Sun, H. Yu, G. Zhong, J. Dong, S. Zhang, and H. Yu, “Random Shapley Forests: Cooperative Game-Based Random Forests With Consistency,” *IEEE Trans Cybern*, vol. 52, no. 1, 2022, doi: 10.1109/TCYB.2020.2972956.

[158] D. Jia and H. Zhao, “Optimization of Entrepreneurship Education for College Students Based on Improved Random Forest Algorithm,” *Mobile Information Systems*, vol. 2022, 2022, doi: 10.1155/2022/3682194.

[159] M. Jiang, T. Cheng, K. Dong, S. Xu, and Y. Geng, “Fault diagnosis method of submersible screw pump based on random forest,” *PLoS One*, vol. 15, no. 11 November, 2020, doi: 10.1371/journal.pone.0242458.

[160] P. Schratz, J. Muenchow, E. Iturritxa, J. Richter, and A. Brenning, “Hyperparameter tuning and performance assessment of statistical and machine-learning algorithms using spatial data,” *Ecol Modell*, vol. 406, 2019, doi: 10.1016/j.ecolmodel.2019.06.002.

[161] P. Probst, M. N. Wright, and A. L. Boulesteix, “Hyperparameters and tuning strategies for random forest,” 2019. doi: 10.1002/widm.1301.

[162] P. Amutha and R. Priya, “An optimized random forest for multi class classification to classify the students using machine learning approaches,” *Int J Health Sci (Qassim)*, 2022, doi: 10.53730/ijhs.v6ns7.13116.

[163] S. van Gaal, A. Alimohammadi, A. Y. X. Yu, M. E. Karim, W. Zhang, and J. M. Sutherland, “Accurate classification of carotid endarterectomy indication using physician claims and hospital discharge data,” *BMC Health Serv Res*, vol. 22, no. 1, 2022, doi: 10.1186/s12913-022-07614-1.

[164] I. D. Raji, H. Bello-Salau, I. J. Umoh, A. J. Onumanyi, M. A. Adegboye, and A. T. Salawudeen, “Simple Deterministic Selection-Based Genetic Algorithm for

Hyperparameter Tuning of Machine Learning Models," *Applied Sciences (Switzerland)*, vol. 12, no. 3, 2022, doi: 10.3390/app12031186.

[165] K. Bouchard, J. Maitre, C. Bertuglia, and S. Gaboury, "Activity Recognition in Smart Homes using UWB Radars," in *Procedia Computer Science*, 2020. doi: 10.1016/j.procs.2020.03.004.

[166] Y. Zhao, V. Sark, M. Krstic, and E. Grass, "Synthetic Training Data Generator for Hand Gesture Recognition Based on FMCW RADAR," in *Proceedings International Radar Symposium*, 2022. doi: 10.23919/irs54158.2022.9904997.

[167] A. Rezaei *et al.*, "Unobtrusive Human Fall Detection System Using mmWave Radar and Data Driven Methods," *IEEE Sens J*, vol. 23, no. 7, 2023, doi: 10.1109/JSEN.2023.3245063.

[168] J. Xue, L. Tang, X. Zhang, L. Jin, M. Hao, and Y. Gui, "Feature evaluation and comparison in radar emitter recognition based on sahp," *Electronics (Switzerland)*, vol. 10, no. 11, 2021, doi: 10.3390/electronics10111274.

[169] F. Sadeghi, A. Larijani, O. Rostami, D. Martín, and P. Hajirahimi, "A Novel Multi-Objective Binary Chimp Optimization Algorithm for Optimal Feature Selection: Application of Deep-Learning-Based Approaches for SAR Image Classification," *Sensors*, vol. 23, no. 3, 2023, doi: 10.3390/s23031180.

[170] A. Sherstinsky, "Fundamentals of Recurrent Neural Network (RNN) and Long Short-Term Memory (LSTM) network," *Physica D*, vol. 404, 2020, doi: 10.1016/j.physd.2019.132306.

[171] H. Zhao, Z. Chen, H. Jiang, W. Jing, L. Sun, and M. Feng, "Evaluation of three deep learning models for early crop classification using Sentinel-1A imagery time series-a case study in Zhanjiang, China," *Remote Sens (Basel)*, vol. 11, no. 22, 2019, doi: 10.3390/rs11222673.

[172] J. Zhu, H. Chen, and W. Ye, "A Hybrid CNN-LSTM Network for the Classification of Human Activities Based on Micro-Doppler Radar," *IEEE Access*, vol. 8, 2020, doi: 10.1109/ACCESS.2020.2971064.

[173] X. Wang, P. Zhang, W. Gao, Y. Li, Y. Wang, and H. Pang, "Misfire Detection Using Crank Speed and Long Short-Term Memory Recurrent Neural Network," *Energies (Basel)*, vol. 15, no. 1, 2022, doi: 10.3390/en15010300.

[174] N. Matsunaga, Y. Ohtani, and T. Hirahara, "Loss Function Considering Temporal Sequence for Feed-Forward Neural Network–Fundamental Frequency Case," 2019. doi: 10.21437/ssw.2019-26.

[175] J. D. Cardenas, C. A. Gutierrez, and R. Aguilar-Ponce, "Deep Learning Multi-Class Approach for Human Fall Detection Based on Doppler Signatures," *Int J Environ Res Public Health*, vol. 20, no. 2, 2023, doi: 10.3390/ijerph20021123.

[176] T. Imamura, V. G. Moshnyaga, and K. Hashimoto, "Fall detection with a single Doppler radar sensor and LSTM recurrent neural network," in *Midwest Symposium on Circuits and Systems*, 2022. doi: 10.1109/MWSCAS54063.2022.9859430.

[177] C. Kittiyanpunya, P. Chomdee, A. Boonpoonga, and D. Torrungrueng, "Millimeter-Wave Radar-Based Elderly Fall Detection Fed by One-Dimensional Point Cloud and Doppler," *IEEE Access*, vol. 11, 2023, doi: 10.1109/ACCESS.2023.3297512.

[178] H. Li, A. Mehul, J. Le Kernec, S. Z. Gurbuz, and F. Fioranelli, "Sequential Human Gait Classification with Distributed Radar Sensor Fusion," *IEEE Sens J*, vol. 21, no. 6, 2021, doi: 10.1109/JSEN.2020.3046991.

[179] H. Li, A. Shrestha, H. Heidari, J. Le Kernec, and F. Fioranelli, "Bi-LSTM Network for Multimodal Continuous Human Activity Recognition and Fall Detection," *IEEE Sens J*, vol. 20, no. 3, 2020, doi: 10.1109/JSEN.2019.2946095.

[180] A. Shewalkar, D. nyavanandi, and S. A. Ludwig, "Performance Evaluation of Deep neural networks Applied to Speech Recognition: Rnn, LSTM and GRU," *Journal of Artificial Intelligence and Soft Computing Research*, vol. 9, no. 4, 2019, doi: 10.2478/jaiscr-2019-0006.

[181] G. A. Oguntala, Y. F. Hu, A. A. S. Alabdullah, R. A. Abd-Alhameed, M. Ali, and D. K. Luong, "Passive RFID Module with LSTM Recurrent Neural Network Activity Classification Algorithm for Ambient-Assisted Living," *IEEE Internet Things J*, vol. 8, no. 13, 2021, doi: 10.1109/JIOT.2021.3051247.

[182] M. Yin, S. Liao, X. Y. Liu, X. Wang, and B. Yuan, "Towards extremely compact rnns for video recognition with fully decomposed hierarchical tucker structure," in *Proceedings of the IEEE Computer Society Conference on Computer Vision and Pattern Recognition*, 2021. doi: 10.1109/CVPR46437.2021.01191.

[183] J. Chen, W. Li, P. Yang, S. Li, and B. Chen, "Fault Diagnosis of Electric Submersible Pumps Using a Three-Stage Multiscale Feature Transformation Combined with CNN–SVM," *Energy Technology*, vol. 11, no. 10, 2023, doi: 10.1002/ente.202201033.

[184] I. Sajedian, J. Kim, and J. Rho, "Finding the optical properties of plasmonic structures by image processing using a combination of convolutional neural networks and recurrent neural networks," *Microsyst Nanoeng*, vol. 5, no. 1, 2019, doi: 10.1038/s41378-019-0069-y.

[185] H. T. Nguyen, C. T. Nguyen, T. Ino, B. Indurkhya, and M. Nakagawa, "Text-independent writer identification using convolutional neural network," *Pattern Recognit Lett*, vol. 121, 2019, doi: 10.1016/j.patrec.2018.07.022.

[186] X. Chen and X. Yang, "Image Semantic Recognition Algorithm of Colorimetric Sensor Array Based on Deep Convolutional Neural Network," *Advances in Multimedia*, vol. 2022, 2022, doi: 10.1155/2022/4325117.

[187] H. Yu, D. Zhu, Q. Zhang, and W. Wang, "Intelligent monitoring small target detection algorithm based on improved faster R-CNN," 2023. doi: 10.1117/12.2680509.

[188] W. Gomez-Flores, J. J. Garza-Saldana, and S. E. Varela-Fuentes, "A Huanglongbing Detection Method for Orange Trees Based on Deep Neural Networks and Transfer Learning," *IEEE Access*, vol. 10, 2022, doi: 10.1109/ACCESS.2022.3219481.

[189] B. Wang, L. Guo, H. Zhang, and Y. X. Guo, "A Millimetre-Wave Radar-Based Fall Detection Method Using Line Kernel Convolutional Neural Network," *IEEE Sens J*, vol. 20, no. 22, 2020, doi: 10.1109/JSEN.2020.3006918.

[190] W. Taylor, K. Dashtipour, S. A. Shah, A. Hussain, Q. H. Abbasi, and M. A. Imran, "Radar sensing for activity classification in elderly people exploiting micro-doppler signatures using machine learning," *Sensors*, vol. 21, no. 11, 2021, doi: 10.3390/s21113881.

[191] X. Zheng, L. Wang, and H. Zhou, "Image Feature Extraction and Retrieval Optimization of Book Pages Based on Convolutional Neural Network," *Traitement du Signal*, vol. 39, no. 3, 2022, doi: 10.18280/ts.390312.

[192] J. Li, X. Chen, G. Yu, X. Wu, and J. Guan, "HIGH-PRECISION HUMAN ACTIVITY CLASSIFICATION VIA RADAR MICRO-DOPPLER SIGNATURES BASED ON DEEP NEURAL NETWORK," in *IET Conference Proceedings*, 2020. doi: 10.1049/icp.2021.0651.

[193] R. Khanna, D. Oh, and Y. Kim, "Through-Wall Remote Human Voice Recognition Using Doppler Radar With Transfer Learning," *IEEE Sens J*, vol. 19, no. 12, 2019, doi: 10.1109/JSEN.2019.2901271.

[194] S. A. Shah and F. Fioranelli, "Human Activity Recognition: Preliminary Results for Dataset Portability using FMCW Radar," in *2019 International Radar Conference, RADAR 2019*, 2019. doi: 10.1109/RADAR41533.2019.171307.

[195] V. Lobanova, D. Bezdetnyy, and L. Anishchenko, "Human Activity Recognition Based on Radar and Video Surveillance Sensor Fusion," in *Proceedings - 2023 IEEE Ural-Siberian Conference on Biomedical Engineering, Radioelectronics and Information*

Technology, USBEREIT 2023, 2023. doi: 10.1109/USBEREIT58508.2023.10158846.

[196] E. L. Chuma and Y. Iano, "Human Movement Recognition System Using CW Doppler Radar Sensor with FFT and Convolutional Neural Network," in *2020 IEEE MTT-S Latin America Microwave Conference, LAMC 2020*, 2020. doi: 10.1109/LAMC50424.2021.9602484.

[197] A. Çınar and S. A. Tuncer, "Classification of lymphocytes, monocytes, eosinophils, and neutrophils on white blood cells using hybrid Alexnet-GoogleNet-SVM," *SN Appl Sci*, vol. 3, no. 4, 2021, doi: 10.1007/s42452-021-04485-9.

[198] B. A. Mohammed *et al.*, "Hybrid Techniques of Analyzing MRI Images for Early Diagnosis of Brain Tumours Based on Hybrid Features," *Processes*, vol. 11, no. 1, 2023, doi: 10.3390/pr11010212.

[199] E. M. Senan, M. E. Jadhav, T. H. Rassem, A. S. Aljaloud, B. A. Mohammed, and Z. G. Al-Mekhlafi, "Early Diagnosis of Brain Tumour MRI Images Using Hybrid Techniques between Deep and Machine Learning," *Comput Math Methods Med*, vol. 2022, 2022, doi: 10.1155/2022/8330833.

[200] D. U. K. Putri, D. N. Pratomo, and Azhari, "Hybrid convolutional neural networks-support vector machine classifier with dropout for Javanese character recognition," *Telkomnika (Telecommunication Computing Electronics and Control)*, vol. 21, no. 2, 2023, doi: 10.12928/TELKOMNIKA.v21i2.24266.

[201] A. Çınar and Ş. Şenler Yıldırım, "A HYBRID DEEP LEARNING BASED CLASSIFICATION FOR SOME BASIC MOVEMENTS IN PHYSICAL REHABILITATION," *NWSA Academic Journals*, vol. 17, no. 2, 2022, doi: 10.12739/nwsa.2022.17.2.1a0478.

[202] Djazila Souhila Korti and Zohra Slimane, "Advanced Human Activity Recognition through Data Augmentation and Feature Concatenation of Micro-Doppler Signatures 893 Original Scientific Paper," 2023.

[203] M. Hassan, *Wireless and Mobile Networking*. 2022. doi: 10.1201/9781003042600.

[204] S. Sand, A. Dammann, and C. Mensing, *Positioning in Wireless Communications Systems*, vol. 9780470770641. 2014. doi: 10.1002/9781118694114.

[205] N. Samama, *Indoor positioning: Technologies and performance*. 2019. doi: 10.1002/9781119421887.

[206] V. C. Chen, D. Tahmoush, and W. J. Miceli, *Radar micro-doppler signatures: Processing and applications*. 2014. doi: 10.1049/PBRA034E.

[207] F. Fioranelli, H. Griffiths, M. Ritchie, and A. Balleri, *Micro-doppler radar and its*

applications. 2020. doi: 10.1049/SBRA531E.

[208] M. Cherniakov, *Bistatic Radar: Principles and Practice*. 2007. doi: 10.1002/9780470035085.

[209] Kementerian Wilayah Persekutuan Malaysia, “GARIS PANDUAN PERANCANGAN FIZIKAL BAGI WARGA EMAS,” 2019. [Online]. Available: https://www.townplan.gov.my

[210] C. Van Loan, *Computational Frameworks for the Fast Fourier Transform*. 1992. doi: 10.1137/1.9781611970999.

[211] O. Özhan, *Basic Transforms for Electrical Engineering*. 2022. doi: 10.1007/978-3-030-98846-3.

[212] G. Manfredi, J.-P. Ovarlez, and L. Thirion-Lefevre, “Features Extraction of the Doppler frequency signature of a human walking at 1 GHz”, doi: 10.1109/IGARSS.2019.8897817ï.

[213] Y. U. Jo and D. C. Oh, “Real-Time Hand Gesture Classification Using Crnn with Scale Average Wavelet Transform,” *J Mech Med Biol*, vol. 20, no. 10, 2020, doi: 10.1142/S021951942040028X.

[214] X. Yu *et al.*, “Transacting Multiple Mother Wavelets in Continuous Wavelet Transform for Epilepsy EEG Classification via CNN,” in *2021 IEEE 9th International Conference on Information, Communication and Networks, ICICN 2021*, 2021. doi: 10.1109/ICICN52636.2021.9673990.

[215] A. Al-Saegh, “Identifying a Suitable Signal Processing Technique for MI EEG Data,” *Tikrit Journal of Engineering Sciences*, vol. 30, no. 3, 2023, doi: 10.25130/tjes.30.3.14.

[216] Q. Wang, C. Meng, and C. Wang, “Analog Continuous-Time Filter Designing for Morlet Wavelet Transform Using Constrained L2-Norm Approximation,” *IEEE Access*, vol. 8, 2020, doi: 10.1109/ACCESS.2020.3007254.

[217] L. Li, H. Cai, and Q. Jiang, “Adaptive synchrosqueezing transform with a time-varying parameter for non-stationary signal separation,” *Appl Comput Harmon Anal*, vol. 49, no. 3, 2020, doi: 10.1016/j.acha.2019.06.002.

[218] M. Finžgar and P. Podržaj, “A wavelet-based decomposition method for a robust extraction of pulse rate from video recordings,” *PeerJ*, vol. 2018, no. 11, 2018, doi: 10.7717/peerj.5859.

[219] M. P. Wachowiak, R. Wachowiak-Smolíková, M. J. Johnson, D. C. Hay, K. E. Power, and F. M. Williams-Bell, “Quantitative feature analysis of continuous analytic wavelet transforms of electrocardiography and electromyography,” *Philosophical Transactions*

of the Royal Society A: Mathematical, Physical and Engineering Sciences, vol. 376, no. 2126, 2018, doi: 10.1098/rsta.2017.0250.

[220] P. Wang and J. Gao, "A robust method for the extraction of instantaneous attributes from seismic data," in *International Geoscience and Remote Sensing Symposium (IGARSS)*, 2012. doi: 10.1109/IGARSS.2012.6350370.

[221] E. A. Martinez-Rios, B. B. Rogelio, N. T. Sergio, and P. M. Hector, "Applications of the Generalized Morse Wavelets: A Review," 2023. doi: 10.1109/ACCESS.2022.3232729.

[222] M. S. Nixon and A. S. Aguado, *Feature extraction and image processing for computer vision*. 2019. doi: 10.1016/C2017-0-02153-5.

[223] A. Subasi, *Chapter 2 - Data preprocessing*. 2020.

[224] B. Ghojogh, M. Crowley, F. Karray, and A. Ghodsi, *Elements of Dimensionality Reduction and Manifold Learning*. 2023. doi: 10.1007/978-3-031-10602-6.

[225] R. Bro and A. K. Smilde, "Principal component analysis," 2014. doi: 10.1039/c3ay41907j.

[226] J. R. Beattie and F. W. L. Esmonde-White, "Exploration of Principal Component Analysis: Deriving Principal Component Analysis Visually Using Spectra," 2021. doi: 10.1177/0003702820987847.

[227] *Advances in Principal Component Analysis*. 2022. doi: 10.5772/intechopen.97992.

[228] J. K. Mandal, Sanjay, J. S. Banerjee, and S. Nayak, *Applications of Machine Intelligence in Engineering*. 2022. doi: 10.1201/9781003269793.

[229] U. Michelucci, *Advanced applied deep learning: Convolutional neural networks and object detection*. 2019. doi: 10.1007/978-1-4842-4976-5.

[230] C. C. Aggarwal, *Neural Networks and Deep Learning: A Textbook*. 2023. doi: 10.1007/978-3-031-29642-0.

[231] T. Wasserman and L. D. Wasserman, *Apraxia: The Neural Network Model*. 2023. doi: 10.1007/978-3-031-24105-5.

[232] *Computational Optimizations for Machine Learning*. 2022. doi: 10.3390/books978-3-0365-3187-8.

[233] *Applied Machine Learning*. 2023. doi: 10.3390/books978-3-0365-7907-8.

[234] L. Yang, G. Li, M. Ritchie, F. Fioranelli, and H. Griffiths, "Gait classification based on micro-Doppler features," in *2016 CIE International Conference on Radar, RADAR 2016*, 2017. doi: 10.1109/RADAR.2016.8059301.

APPENDICES

APPENDIX A

UITM Ethics Committee Approval

www.uitm.edu.my

UNIVERSITI TEKNOLOGI MARA

Pejabat
Timbalan Naib Canselor
(Penyelidikan dan Inovasi)

Reference : 600-TNCPI (5/1/6)
Our reference : REC/03/2022 (FB/15)
Date : 27 June 2022

Assoc. Prof. Ir Ts Dr Nur Emileen Abdul Rashid
Microwave Research Institution
Universiti Teknologi MARA
40450 Shah Alam,
SELANGOR

Dear Assoc. Prof. Ir Ts Dr Nur Emileen,

APPROVAL LETTER - UiTM RESEARCH ETHICS COMMITTEE

Thank you for submitting your research proposal to the Research Ethics Committee (REC). After reviewing the list of documents as attached the Committee approved your proposal titled "Automatic Elderly Fall Detection Alert System" at the Microwave Research Institute, UiTM Shah Alam.

Details of the approval are as follows:

Approval number:	REC/06/2022 (ST/FB/9)
Approval Period:	27 June 2022 until 30 September 2023
Authorised personnel: 1. Assoc. Prof. Ir Ts Dr Nur Emileen Abdul Rashid 2. Dr Megat Syahirul Amin Megat Ali 3. Ir Dr Nor Ayu Zalina Zakaria 4. Muhammad Nazrin Farhan Nasarudin 5. Hidayatusherlina Razali	6. Assoc. Prof. Ir Dr Zuhani Ismail Khan 7. Assoc. Prof. Ts Dr Idnin Pasya Ibrahim 8. Dr Siti Amalina Enche Ab Rahim 9. Assoc. Prof. Dr Norziaton Ismail Khan 10. Assoc. Prof Ts Dr Rizal Effendy Mohd Nasir 11. Professor Raja Syamsul Azmir Raja Abdullah

The UiTM Research Ethics Committee operates in accordance to the ICH Good Clinical Practice Guidelines, Malaysian Good Clinical Practice Guidelines and the Declaration of Helsinki. The approval of this project is conditional upon your continuing compliance with these guidelines and declaration.

Failure to submit reports will result in withdrawal of consent for the project to proceed. Amendments, if any, to the study documents are to be submitted to the REC for approval.

If you require further information, please contact the REC Secretariat at 03-55448069/03-55442794 or email at recsecretariat@uitm.edu.my.

Yours sincerely,

EMERITUS PROFESSOR DATO' DR RAYMOND AZMAN ALI
Chairman
UiTM Research Ethics Committee

c.c.: Director, Accounting Research Institute (ARI), UiTM

Universiti Teknologi MARA
Aras 3, Bangunan Wawasan
40450 Shah Alam, Selangor, MALAYSIA
Tel: (+603) 5544 2004/2255
Faks: (+603) 5544 2070

ISO 9001:2015 No. Sijil: 10120156

UiTM di hatiku

APPENDIX B

Example of the MATLAB Codes for enveloping, signal transformation and feature selection

```
clear,close all
clc

load(['filename',num2str(i),'.mat']);
fs=5000;
time=0:1/fs:20-1/fs;
duration=length(A)/fs;
numbpeaks=10.*duration;

%% Remove Noise
k=movvar(A,variance_window);
k=detrend(k);
idx=find(k>A);
A(idx)=0;

%% envelopping algorith
[pks,ipk,w,p]=findpeaks(A,'MinPeakDistance',total_number_of_peaks);
fs=10;
t=0:1/fs:20-1/fs;

%% Signal Transformation
nfft=length(pks);
fs=10;
F=fft(pks);
F=abs(F)/nfft; %fourier spectrum
F=F(1:length(F)/2);
pxx=10*log10(F); %power spectrum
[s,f,t1]=stft(pks,10,window,Overlap_size,FFTLength); %spectrogram
[cfs,frq]=cwt(pks,10,'amor'); %scalogram

%% feature selection

%pca
[coeff_fdomain, score_fdomain,explained_fdomain] = pca(fdomain); %Fourier spectrum-PCA
[coeff_pspectrum, score_pspectrum,explained_pspectrum] = pca(abs(pspectrum)); %Power spectrum-PCA

%AlexNet Feature Layer
load("optimized_alexnet") %load ALexnet trainewd with spectrogram or sclaogram
imds = imageDatastore('filename', ...
    'IncludeSubfolders',true, ...
    'LabelSource','foldernames'); % load image
inputSize = optimizedNet.Layers(1).InputSize %extract input size
augimds = augmentedImageDatastore(inputSize(1:3),imds); % change the image size fit into Alexnet
Trainingfeatures = activations(netTransfer, augimdsTrain, 'flatten'); %extract the features

```

APPENDIX C

Example of the MATLAB Codes for the classification and F1-score ananlysis

```
%% Classifiers

%%FFNN

net= feedforwardnet(hiddenlayer_size);
net.trainParam.epochs = 30;
net.layers{1}.transferFcn='logsig'; %trasnfer function from input to hidden
net.layers{2}.transferFcn='purelin'; %trasnfer function from hidden to output
net = configure(net, features, expectedoutput);
net.trainFcn = 'trainlm'; %optimizer
[net,tv] = train(net,features,expectedoutput); %training FFNN

pred = net(features); %classify the trained FFNN


%AlexNet

imds = imageDatastore('filename',true, ...
    'LabelSource','foldernames'); %input image either scalogram or spectrogram

net = alexnet %call pre-trained alexnet
        inputSize = net.Layers(1).InputSize %extract input size
        layersTransfer = net.Layers(1:end-3); %remove the outputlayer
        numClasses = numel(categories(imdsTrain.Labels)) % set output size

        layers = [
            layersTransfer
            flattenLayer()
            fullyConnectedLayer(numClasses,'WeightLearnRateFactor',20, ...
            'BiasLearnRateFactor',20)
            softmaxLayer
            classificationLayer('Name', 'classoutput')]; %modify the pre-trained-Alexnet

        options = trainingOptions(optimizer, ...
            'MiniBatchSize',Mini_batch_size, ...
            'MaxEpochs',100, ...
            'InitialLearnRate',initial_learning_rate, ...
            'Shuffle','every-epoch', ...
            'ValidationData',augimdsValidation, ...
            'ValidationFrequency',3, ...
            'Verbose',false, ...
            'Plots','training-progress'); %set the AlexNet optimize parameter

[netTransfer,info] = trainNetwork(augimdsTrain,layers,options); %train the Alexnet
[YPred,scores] = classify(netTransfer,validation_dataset); %classify the Alexnet

```

```
%SVM

t=templateSVM('KernelFunction',kernel,'KernelScale','auto', ...
    'Standardize',true,'OutlierFraction',0.02); %set the optimize parameter
SVMModel = fitcecoc(Trainingfeatures',imdsTrain.Labels,'Learners',t); %train SVM model
[label,score] = predict(SVMModel,features); % classify

% Random Forest

Mdl = TreeBagger(numTrees, Trainingfeatures,Trainingexpectedoutput);%set the optimize parameter
[label,score] = predict(Mdl, features);%classify

%% precision, recall and F1score

C = confusionmat(expected_output, classification_result); %extract the confusion matrix

for i = 1:numClasses
    TP = C(i, i);
    FP = sum(C(:, i)) - TP;
    FN = sum(C(i, :)) - TP;

    precision(i) = TP / (TP + FP);
    recall(i) = TP / (TP + FN);
end

F1_score = 2 * (precision .* recall) ./ (precision + recall);
```

AUTHOR'S PROFILE

Muhammad Nazrin Farhan Nasarudin obtained his Bachelor of Engineering (Hons.) in Electronics in 2021 from Universiti Teknologi MARA (UiTM), Shah Alam, where he is currently pursuing a Ph.D. in Electronics Engineering. His doctoral research focuses on radar-based human movement detection, involving advanced techniques in signal processing, feature extraction, and classification algorithms. His work includes experimentation with Convolutional Neural Networks (CNNs) and hybrid classifiers to improve the accuracy and robustness of movement detection systems.

In parallel with his academic journey, Nazrin is an experienced Industrial AI Engineer, with a strong focus on building and fine-tuning AI systems for real-world applications. His work centres around Retrieval-Augmented Generation (RAG) pipelines for chatbots, where he integrates Natural Language Processing (NLP), Large Language Models (LLMs), and vector-based semantic search to deliver intelligent, context-aware responses. He also leads the development of AI-powered solutions for document understanding—including image-to-text pipelines, OCR enhancement, and AI-assisted form automation tools for administrative workflows.

His multidisciplinary expertise bridges academia and industry, combining low-level signal analytics with high-level machine learning applications, making him proficient in both research innovation and AI system deployment at scale.

LIST OF PUBLICATIONS:

[1] M. N. F. Nasarudin *et al.*, “A Comparative Study on Human Movement Classification Using Wi-Fi Based Passive Forward Scattering Radar,” *TEM Journal*, vol. 12, no. 3, 2023, doi: 10.18421/TEM123-13.

[2] M. N. F. Nasarudin *et al.*, “Characterization of Physical Movement Signatures from WiFi-based Passive Forward Scattering Radar,” *International Journal of Emerging Technology and Advanced Engineering*, vol. 12, no. 11, 2022, doi: 10.46338/ijetae1122_03.

[3] N. E. A. Rashid, H. Razali, N. L. Saleh, M. N. F. Nasarudin, M. A. A. K. Azmi, and A. Ahmed, “Passive Wi-Fi Radar Fall And Non-Fall Motion Classification Using Hybrid PCA-SVM Classifier,” in *IEEE Symposium on Wireless Technology and Applications, ISWTA*, 2023. doi: 10.1109/ISWTA58588.2023.10250116.

[4] H. Razali, N. E. Abd. Rashid, M. N. F. Nasarudin, N. N. Ismail, Z. Ismail Khan, and S. A. Enche Ab Rahim, “A review: radar-based fall detection sensor,” *Journal of Electrical & Electronic Systems Research*, vol. 24, no. Apr2024, pp. 1–11, Apr. 2024, doi: 10.24191/jeesr.v24i1.001.

[5] Razali, H., Abd Rashid, N. E., Nasarudin, M. N. F., Ismail, N. N., Ismail Khan, Z., Enche Ab Rahim, S. A., Megat Ali, M. S. A., & Zakaria, N. A. Z. (2024). Human movement detection and classification capabilities using passive Wi-Fi based radar. International Journal of Electrical and Computer Engineering (IJECE), 14(3), 3545. https://doi.org/10.11591/ijece.v14i3.pp3545-3556

[6] H. Razali, N. E. Abd Rashid, A. B. Azman, M. N. F. Nasarudin, Z. I. Khan and S. A. Che Ab Rahim, "Threshold-Based Fall Detection System Utilizing Passive Wi-Fi Radar Technology," 2024 IEEE Symposium on Wireless Technology & Applications (ISWTA), Kuala Lumpur, Malaysia, 2024, pp. 157-161, doi: 0.1109/ISWTA62130.2024.10651725.

LIST OF AWARDS:

[1] Gold Medal Award - International Virtual Expo of Innovation Product and System Design 2023 (INVIDE)

[2] Silver Medal Award - Invention, Innovation & Design Exposition 2023 (IIDE)

LIST OF INTELLECTUAL PROPERTIES:

[1] UKCS - Passive Forward Scattering Radar Fall Detection Sensor: System Block Diagram and Architecture

[2] MyIPO - Type of Fall Classification Algorithm